INTERACTION OF HALOARCHAEA WITH Fe^{2+} AND Mn^{2+} IONS

THESIS SUBMITTED TO

GOA UNIVERSITY

FOR THE AWARD OF DEGREE OF

DOCTOR OF PHILOSOPHY

IN

MICROBIOLOGY

BY

Ms. N. SANIKA SHIVDAS, M.Sc.

DEPARTMENT OF MICROBIOLOGY

GOA UNIVERSITY

JUNE, 2014

INTERACTION OF HALOARCHAEA WITH Fe^{2+} AND Mn^{2+} IONS

THESIS SUBMITTED TO

GOA UNIVERSITY

FOR THE AWARD OF DEGREE OF

DOCTOR OF PHILOSOPHY

IN

MICROBIOLOGY

BY

Ms. N. SANIKA SHIVDAS, M.Sc.

Research Guide

Prof. IRENE J. FURTADO, M.Sc., Ph.D.

DEPARTMENT OF MICROBIOLOGY

GOA UNIVERSITY

JUNE, 2014

CERTIFICATE

This is to certify that **MISS. N. SANIKA SHIVDAS** has satisfactorily completed the thesis entitled **"INTERACTION OF HALOARCHAEA WITH Fe^{2+} AND Mn^{2+} IONS"** submitted to Goa University for the award of the degree of **DOCTOR OF PHILOSOPHY IN MICROBIOLOGY** is a record of original and independent work carried out during the period of October 2009 - June 2014 in DEPARTMENT OF MICROBIOLOGY, GOA UNIVERSITY under my supervision and that it has not previously formed the basis for the award of any Degree, Diploma, Associate-ship or Fellowship or any other similar title to any candidate of this or any other University.

I affirm that the thesis submitted by MISS N. SANIKA SHIVDAS is completely independent research work carried by her under my supervision.

SIGNATURE OF GUIDE

DECLARATION

It is hereby declared that this thesis entitled **"INTERACTION OF HALOARCHAEA WITH Fe^{2+}AND Mn^{2+} IONS"** submitted to the Goa University, for the award of the degree of **DOCTOR OF PHILOSOPHY IN MICROBIOLOGY** is a record of original and independent work carried out by me during October 2009 - June 2014, in the **DEPARTMENT OF MICROBIOLOGY, GOA UNIVERSITY** under the supervision of **Dr. IRENE J. FURTADO**, Professor, Department of Microbiology, Goa University and that it has not previously formed the basis for the award of any Degree, Diploma, Associate-ship or Fellowship or any other similar title to any candidate of this or any other University.

SIGNATURE OF STUDENT **SIGNATURE OF GUIDE**

(SANIKA N SHIVDAS) **(Prof. IRENE FURTADO)**

Acknowledgment

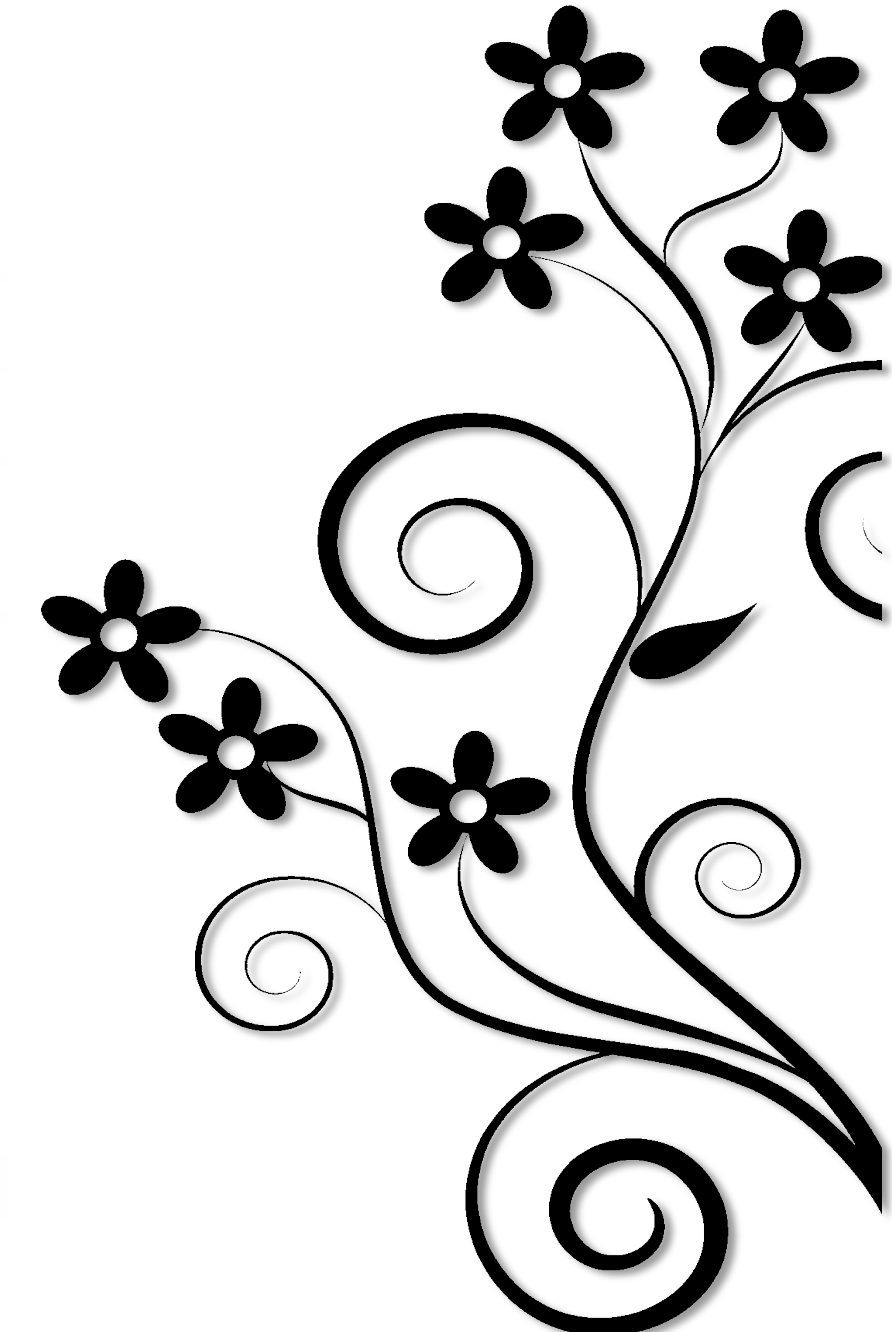

Dedicated to my mummy and papa

Love you both ...

INDEX

ABBREVIATIONS

A : Absorbance

APS : Ammonium per sulfate

bp: boiling point

° C : Degree centigrade

Ca^{2+} : Calcium ions

EDTA: Ethylene diamine tetraacetic acid

G: Gram (s)

h : hour (h)

HCI: Hydrochloric acid

HNO_3: nitric acid

IU: International units

K^+ : Pottasium ions

KDa: Kilo daltons

L : liter

Lbs: pounds

M: Molar

mAmps: Milli amperes

Mg^{2+} : Magnesium ions

Min: minutes

mL : millilitre

mM: Milli molar

mm: millimeter

NaCI: Sodium chloride

NADPH : Nicotinamide adenine dinucleotide posphate(reduced)

NGSM: NaCI glucose synthetic medium

NASM: NaCI Acetate synthetic medium

nm : nanometer

NTYE: NaCI tryptone yeast extract medium

OD: Optical Density

o: ortho

PAGE: Polyacrylamide gel electrophoresis

R_f : Resolution factor

rpm : revolutions per minute

RT (room temperature): (2 8 - 30 ◦C) ± 3 ◦C

SDS: Sodium dodecyl sulfate

Sec: seconds

SEM: Scanning electron microscopy

Spp. : species

TEM: Transmission electron microscopy

TEMED: Tetra methyl ethylene diamine

TLC: Thin layer chromatography

UV: ultra violet

V : volts

v/v : volume / volume

w/v : weight / volume

% : percentage

µ: micron

λ: wavelength

µg: microgram

µl: microliter

Chapter 1

Environmental Significance of Fe^{2+} and Mn^{2+} ions and its interaction with Haloarchaea.

INTRODUCTION

Since the beginning of the Industrial Age, metals are being emitted and deposited in the environment (Mosley 2009). In some cases, metals have accumulated in both terrestrial and aquatic environments in high concentrations and caused harm to animals and humans via ingestion of soil and/or dust, food, and water; inhalation of polluted air; and absorption via the skin from polluted soil, water, and air (Yaman 2012). As the world's population and economies continue to grow, especially in developing countries, the need for metals will increase and so will the potential for soil and water contamination. This will have serious implications on environmental quality and human health.

Industrial operations like mining, add metal ions globally to the soil (Kavitha *et al*. 2013). Such mining waste incorporates into the soil, and its metal contents are eventually absorbed by plants, not only leading to their toxification but transferring the same to its fruits or grains like millets, rice, wheat etc. Hence, building up the silent epidemic of environmental poisoning. Plants and their products contaminated by metals when consumed either as tool of medicine or food by man or as forage by animals, over a period of time get accumulated and interfere with physiological and biochemical functioning of body system which often times are reflected in terms of health problems ranging from cancer to heart diseases. (Yaman 2012; Jimoh 2006).

1.1 Global distribution of Fe^{2+} ions in geosphere

1.1.1 Rocks

Iron is a lustrous, ductile, malleable, silver-gray metal, grouped in VIII of the Periodic Table (Emsley 2011). Iron is a member of the first row transition series of elements, consisting of

scandium (Sc), titanium (Ti), vanadium (V), chromium (Cr), manganese (Mn), iron (Fe), cobalt (Co), nickel (Ni), copper (Cu) and zinc (Zn), along with ruthenium (Ru) and osmium (Os). The element has an atomic number of 26, an atomic mass of 56, two main oxidation states (+2 and +3) and four naturally occurring isotopes (^{54}Fe, ^{56}Fe, ^{57}Fe and ^{58}Fe). ^{56}Fe is the major isotope forming 92% of the total mass (Beard and Johnson 2004).

In the lithosphere, iron is the fourth most abundant element at a mean concentration of 5 % by weight (Chime 2013) forming several common minerals, including pyrite FeS_2, magnetite Fe_3O_4, haematite Fe_2O_3 and siderite $FeCO_3$. It is also present in many rock-forming minerals, including mica, garnet, amphibole, pyroxene and olivine and as Fe^{3+} in iron oxides and hydroxides, as the result of weathering (Hazen *et al.* 2008). Iron is common in igneous, metamorphic and sedimentary rocks. Most of the igneous and metamorphic rocks consist of ferrous form than the ferric while the reverse is true for the sedimentary rocks. Most of the iron in igneous rocks is found in ferromagnesian silicates the most of which are mica, garnet, amphibole, pyroxene and olivine. Important iron rich accessory minerals are magnetite (Fe_3O_4), ilemnite ($FeTiO_3$) and pyrite (FeS_2). The weathering of igneous rocks oxidizes most ferrous to the ferric state. The ferric iron is then incorporated in the clay minerals or hydrolyzed to ferric oxyhydroxide. During deposition and diagenesis of sediments derived from the weathering products iron is often reduced and precipitated as sulfides (Raiswell and Canfeild 1998). Banded iron formations (BIFs; oxidized deposits of Pre-Cambrian age) are the largest accumulations of iron in the lithosphere (Hedrich *et al*. 2011), containing about 28% (by weight) iron. Iron is an essential nutrient for all known life forms, with the seeming exception of *Lactobacillus* spp. (Nairz *et al.* 2010). It is usually required only in trace amounts (i.e. it is a micronutrient), although in some exceptional cases such as the

magnetotactic bacteria, cellular iron contents are up to 11.5-fold greater than in more 'typical' bacteria which requires 10^{-7} to 10^{-5} M for optimal growth (Chavadar and Bajekal, 2008; Andrew *et al*. 2003). In nature, the occurrence of iron species that predominates depends greatly on physicochemical parameters, such as pH, oxygen concentration and redox potential of that environment (Oshiki *et al*. 2013). Ferrous iron, althogh stable in anoxic environments, is susceptible to spontaneous chemical oxidation by molecular oxygen (**Fig. 1.1**). The rate of occurrence of which depends on ferrous iron, dissolved oxygen, concentrations of protons (hydronium ions), temperature and pH. In most environments, rates of spontaneous chemical oxidation of ferrous iron are very low corresponding to 8.4×10^{-7} μg min^{-1}at pH 2, though these become appreciably greater at higher pH values such as pH 7 which corresponds to 8.4 mg min^{-1} (Johnson *et al*. 2012). Ferric iron is thermodynamically stable in aerated waters. Its strong tendency to hydrolyse (react with water) means that it is present at extremely low concentrations in most water bodies, though in the presence of complexing agents (e.g. chelating organic acids and humic colloids), concentrations of soluble ferric iron can be significantly greater. However, the solubility of non-complexed ferric iron is also pH-related, and extremely acidic waters (pH of ~2.5 or less) may contain highly elevated concentrations of this ionic species (140 mg L^{-1}), which is a powerful oxidizing agent (Hedrich *et al*. 2011).

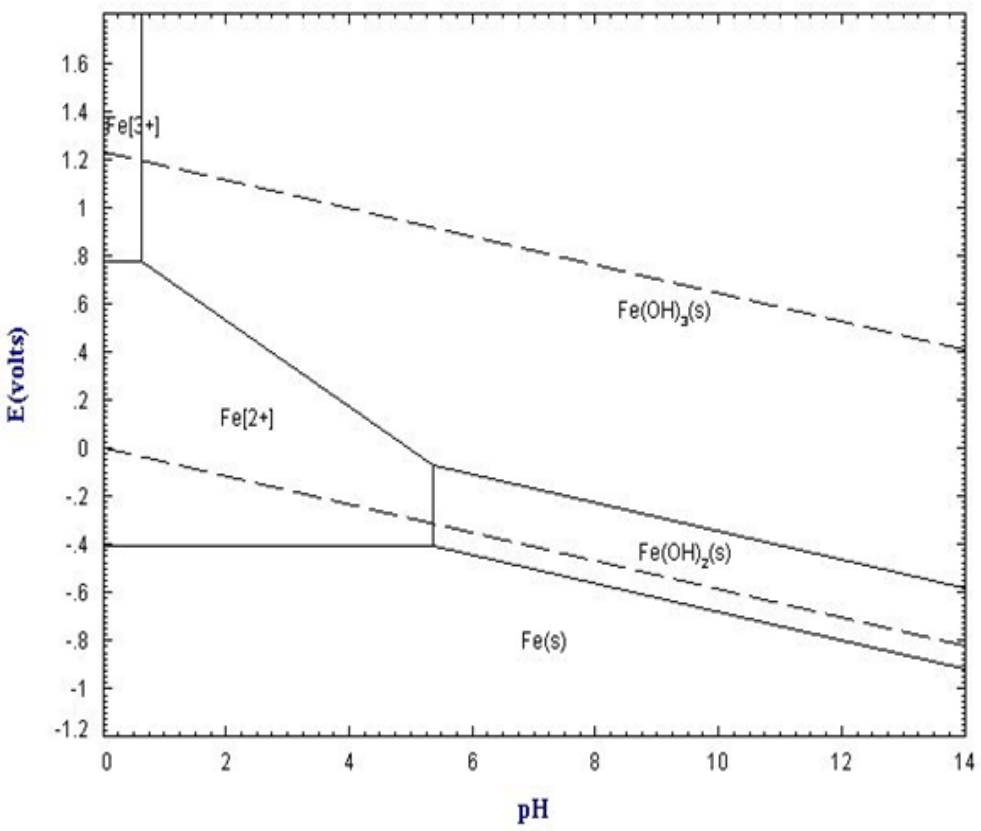

Fig. 1.1 Spontaneous chemical oxidation by molecular oxygen (Eh-pH profile of Fe) (Takeno 2005)

1.1.2 Soil

Soil contains 1-5 % of total iron or 20000-100,000 lb a^{-1} in the plow layer. Most of the iron in soil is found in silicate minerals or iron oxides and hydroxides, forms that are not readily available for plant use. The iron oxides and hydroxides impart red or yellow color to the soil. Iron in soil exists in ferrous (Fe^{2+}) and ferric forms (Fe^{3+}) depending on the soil pH and the aeration status of the soil. The concentration of iron decreases sharply as the soil pH increases with a minimum of pH 7.5- 8.5, the range at which iron deficiency occur in most

cases (Schulte 2004). Organic matter can improve iron availability by combining with iron thereby reducing precipitation as oxide/ hydroxides. Consequently, this results in higher concentration of iron remaining in the soil solution available for root absorption. When microbes decompose organic matter, iron tied up in organic matter is released in the form available for uptake by plants (Schulte 2004).

1.1.3 Sea water

Iron occurs in seawater in particulate and dissolved, organic and inorganic forms, over a wide range of physical size classes. Particulate iron (Fe^{3+}), commonly defined as that fraction removed by filtration through 0.2 or 0.4 mm pore size filters, is contained in particles of alumino-silicate clays, the intact cells of marine microorganisms, and a variety of biogenic detritus, ranging in size from submicron to 0.1 mm in diameter (Bruland and Rue 2001). Dissolved iron (Fe^{2+}) (0.2–0.4 mm) consists largely of iron complexed with organic molecules, including several classes of organic chelators, cell lysis products, and humic compounds (Gledhill and Buck 2012). A significant portion of operationally defined "dissolved Fe" actually consists of small (0.02–0.45 μm) colloidal particles, ranging from, 10% of total dissolved Fe in open ocean samples to 90% in coastal waters (Wu *et al*. 2001). Measured dissolved iron concentrations in the ocean range over six orders of magnitude, from as low as 0.03 nM in the surface waters of open ocean HNLC (high nutrient low chlorophyll) regions to 3 mM in hydrothermal vent fluids (**Table 1.1**). External sources of iron to the ocean include atmospheric dust deposition, river input, hydrothermal vents, and release from marine sediments via reductive dissolution and resuspension.

Table 1.1 Dissolved Iron concentration in water bodies

Water body	Fe^{2+} Concentration
Surface waters (HNLC regions)	0.03 nM
Hydrothermal vent fluids	3 mM
Open Ocean	40 nM

1.1.4 Air

Atmospheric deposition of continentally-derived particles ("aerosols", "dust") is a major external input of iron to the oceans. In some open ocean areas, including the iron-limited subarctic Pacific, dust deposition is the dominant iron source to the surface layer. The atmospheric iron source is composed largely of aluminosilicate minerals derived from arid and semi-arid mid-latitude regions in the Northern Hemisphere (Ito and Xu 2013); the exception to this rule is downwind of heavily populated areas, where a significant fraction of aerosol iron may originate from anthropogenic sources (Kumar and Sarin 2010). Aerosol production rates vary in response to precipitation amount and wind strength (Trenberth 2011). Typically particles of 1–100 mm diameter become entrained in the atmosphere. The largest atmospheric particles are deposited quickly via gravitational settling near the source area, but smaller size classes (10 mm) reach high altitudes and can be transported hundreds or thousands of kilometers before being deposited (Prospero and Lamb 2003; Maring *et al.* 2003). Deposition occurs through either the direct "dry" settling of particles or the

entrainment of particles in rainfall, termed "wet" deposition. During wet deposition, entrained aerosol iron is exposed to more neutral conditions, first in rainwater (pH 4–7) and then upon mixing with seawater (pH. 8), after which an estimated 0.3– 6.8% of the aerosol iron remains in the dissolved phase. In contrast to wet deposited iron, the solubility of dry deposited iron in seawater is generally low (<<1 %) (Baker and Croot 2010). Jickells and Spokes (2001) combine these observations to estimate an overall solubility of atmospheric iron in seawater of 0.8–2.1 % of the total iron deposition flux, resulting in a soluble, bioavailable iron flux to the oceans of 13–67 $x10^{10}$ g $year^{-1}$.The fraction of iron in soils and rocks at the Earth's surface varies, but generally falls between 2.9 % and 4.8 %, with a widely-used average of 3.5 % (Jickells and Spokes 2001). Most aerosol particles in the atmosphere are exposed to low pH conditions (pH 1–5.5) during cycles of cloud formation and evaporation, which may enhance the release of dissolved iron species from the particles and facilitate high rates of photoreductive dissolution of particulate and colloidal Fe^{3+} (Kumar and Sarin 2010).

1.1.5 Rivers and streams

The world discharge of the rivers and streams, on average, $37x10^{12}$ m^3 $year^{-1}$ of water, carrying $4.6x10^{15}$ g $year^{-1}$ of dissolved constituents and $20x10^{15}$ g $year^{-1}$ of suspended sediment. As with aerosol flux, river discharge is highly seasonal and geographically uneven. A large fraction of the global discharge is to the central Atlantic Ocean due to the action of very large rivers like Amazon, Orinoco, Congo and Mississippi; most of the global sediment load is borne by rivers draining the Himalayas (Gupta *et al*. 2012). Measured values of dissolved iron in rivers vary widely, as illustrated by the Amazon and Danube, which have concentrations of 800–1000 and 21–156 nM, respectively (Wu *et al*. 2001). 90 % of the

"dissolved" fraction actually consists of small colloid particles (0.4 mm) that tend to flocculate with organic matter to form larger particles when brought into contact with seawater, and are efficiently removed during estuarine mixing (Wells *et al*. 2000). As a result, the dissolved Fe concentration of water that actually reaches the ocean is closer to 40 nM, yielding a global flux of only $1.5x10^{9}$ mol Fe $year^{-1}$ (Baar and Jong 2001). Likewise, most of the large riverine load of particulate iron ($13x10^{12}$ mol $year^{-1}$) is deposited in deltas and estuaries. Fluids released from hydrothermal vents at mid-ocean ridges and in back-arc basins contain high concentrations of reduced iron acquired via reductive dissolution during circulation through basaltic rocks at high temperatures (350–400 ºC) and pressures (300–400 bar). Typical concentrations of dissolved Fe are 1–3 mmol L^{-1}, and at least at certain vents the Fe flux is dominated by Fe^{3+} oxyhydroxides. Though the gross hydrothermal input of iron to the deep ocean is large, an estimated $30–90x10^{9}$ mol $year^{-1}$ (Baar and Jong 2001), most of the reduced iron species in vent fluids are rapidly oxidized and precipitated upon mixing with cold ambient bottom water (~2 ^{o}C). The net result is large ferromanganese deposits close to venting sites but a negligible flux of iron to deep ocean water (Dick *et al*. 2013). Relative to crustal abundances, both deep marine clays and coastal and shelf muds are enriched in iron with average iron contents of 6 % (Baar and Jong 2001). Roughly half of this iron exists in forms susceptible to reductive dissolution (oxide coatings, organics) and includes a component exported from overlying waters (Berelson *et al*. 2003). Diagenetic alteration of these iron-rich sediments releases high concentrations (10–100 mM) of Fe^{2+} into sediment pore waters. (Bennette *et al*. 2012). The vast majority of dissolved pore water iron diffusing through the sediment column will be immobilized, either through oxidation to insoluble Fe^{3+} species in oxic sediment layers or through sulfide mineral precipitation under anoxic

conditions (Bennette *et al*. 2012) . The small fraction that reaches the sediment–water interface is nonetheless enough to increase dissolved Fe concentrations at this boundary to 1–100 nM, well above the mean oceanic value. Much of this remaining dissolved Fe^{2+} is then reprecipitated as Fe^{3+}or scavenged onto particles upon mixing with bottom water (Koretsky *et al.* 2006), with the remainder contributing to the dissolved iron inventory of deep waters (Baar and Jong 2001). The importance of the benthic flux as a source of iron to surface waters has been demonstrated for several parts of the ocean, especially along continental shelves (Elrod 2004).

Concentrations of dissolved iron in the coastal ocean, shallow seas overlying the continental shelves, and semi-enclosed basins are typically several orders of magnitude higher (1–100 nM) than in the open ocean. The distribution of non-colloidal particulate iron (0.4 nM) in the surface ocean is similar to that of dissolved iron, with strong increasing gradients moving towards the coast and continental shelf. Particulate concentrations are often several orders of magnitude greater than dissolved concentrations, ranging from extreme lows of 0.1 nM in the remote gyres to 100–800 nM in coastal areas (Baar and Jong 2001). A majority of particulate iron (50–90 %) is considered refractory, while the remainder (10–50 %) is leachable with dilute acid, and may be more easily converted to bioavailable forms (Baar and Jong 2001). Processes such as photoreduction and zooplankton/ microbe-mediated dissolution of biogenic may result in daily or episodic variations in particulate Fe abundance in the euphotic zone (Sunda 2012) (**Fig. 1.2**).

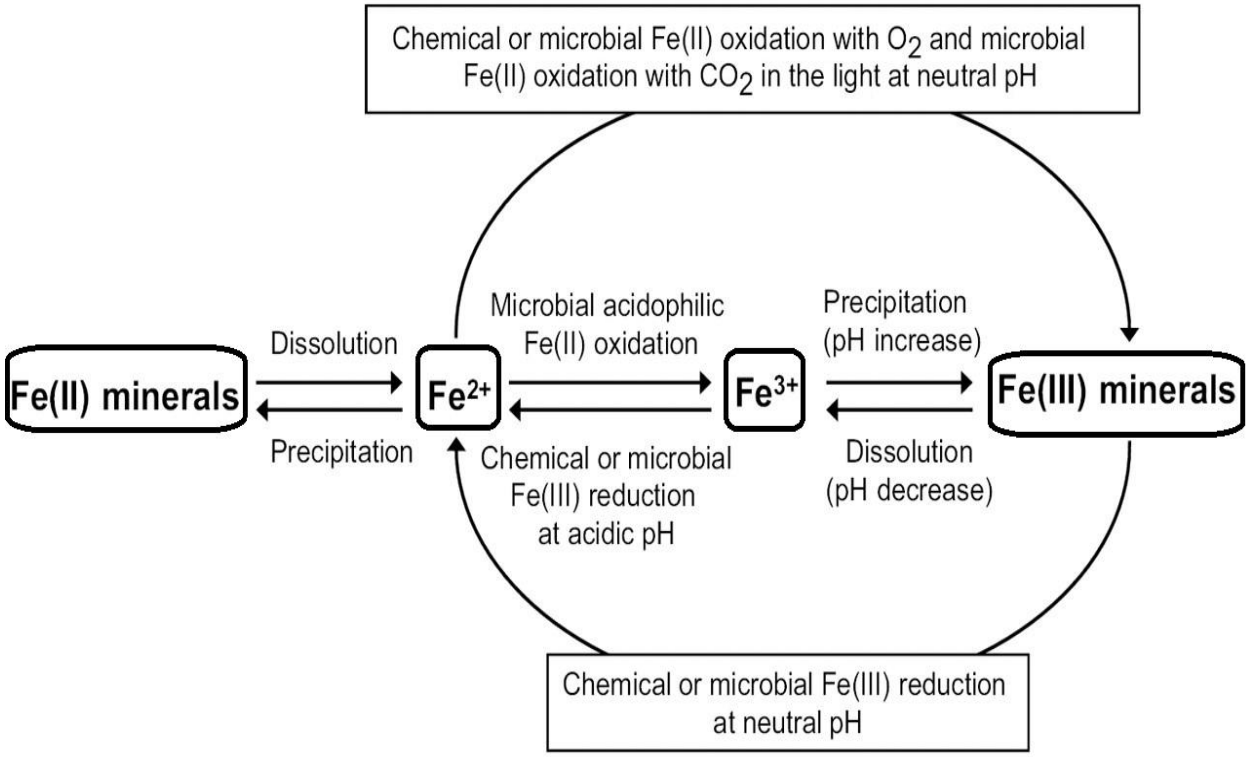

Fig. 1.2 Biogeochemical cycle of iron (Kappler and Straub 2005)

1.2 Global distribution of Mn^{2+} in geosphere

1.2.1 Soil

Manganese (Mn) is the twelfth most abundant element in the earth's crust and is naturally present in rocks, soil, water, and food. Manganese is one of the most abundant and widely distributed metals in nature. The Earth's crust consists of 0.1 % of manganese. As constituent of the soil, its concentrations range from 40 to 900 mg kg^{-1}. Manganese is present in soil as a result of mineral weathering and atmospheric deposition, originating from both natural and anthropogenic sources. There are three possible oxidation states of manganese in soil, namely

Mn^{2+}, Mn^{3+} and Mn^{4+}. The divalent ion is the only form that is stable in soil solution, while Mn^{3+} and $Mn^{4+}$are only stable in the solid phase of soil (Lin *et al.* 2011). Manganese mobility in soil is extremely sensitive to soil conditions such as acidity, wetness, organic matter content, biological activity etc. The solubility of soil manganese is thus controlled by redox potential and soil pH, where low pH or low redox potential favour the reduction of insoluble manganese oxides resulting in increased manganese mobility. At soil pH above 6, manganese forms bonds with organic matter, oxides and silicates whereby its solubility decreases. The solubility of manganese is also high in anaerobic conditions at pH above 6, as well as in aerobic conditions at pH below 5.5 (McBride 1994; Kabata and Pendias 2001). The natural presence of manganese in rock and soil provides a source of manganese that may dissolve in ground and surface waters or may erode and deposit as sediment, with the subsequent potential for dissolution.

1.2.2 Water bodies

In aquatic systems manganese solubility increases at low pH as well as under low oxidation-reduction potential, and is most commonly in the $Mn^{2+}$and Mn^{4+} oxidation states. The presence of high concentrations of chlorides, nitrates and sulphates may increase manganese solubility, raising both aqueous mobility and uptake by plants (Dubinin and Korsakova 2011). Concentrations of manganese in open seawater range from 0.4 to 10 µg dm^{-3}. Concentrations of dissolved manganese in natural waters that are essentially free of anthropogenic sources can range from 10 to > 10000 µg dm^{-3}, while tap water can typically contain > 1 mg dm^{-3}. However, manganese concentrations in natural surface waters rarely exceed 1000 µg dm^{-3} and are usually less than 200 µg dm^{-3} (**Table 1.2**). Average levels in drinking water are 4 µg dm^{-3} (Howe *et al*. 2004; Pearson and Greenway 2005). The marine

environmental chemistry of manganese is largely governed by pH, oxygen concentration of the solution and redox conditions (**Fig. 1.3**). In fact, manganese oxidation increases with the decrease in acidity of the medium. The redox cycle of manganese in the oceans occurs at the oxic-anoxic boundary, which is often located at the sediment-water interface (**Fig. 1.4**). Manganese oxides are present on the ocean floor as concretions, crusts and fine disseminations in sediments. It is well known, for example, that the soft bottom sediments of the oceans are particularly rich in manganese aggregates in the form of nodules (Bonatti and Nayudu 1965; Wang *et al*. 2011). Free manganese ions are released in the water by means of the photochemical and chemical reduction of manganese oxides coming from the organic matter (Sunda and Huntsman, 1998; De Schamphelaire *et al*., 2007). The process is initialised after the increase in temperature, the decrease in oxygen concentrations and the upward movement of the redox-cline (Hunt, 1983). The transport of the dissolved manganese ions is governed by molecular diffusion in the water pores and it follows a manganese concentration gradient (the gradient decreases towards the oxic zone). In the marine environment, in absence of micro-organisms or mineral particles, manganese oxidation is a slow process (Wehrli *et al*., 1995). A reduced dissolved oxygen condition (called hypoxia) causes the rise of the ionic flux of manganese, which goes from the sediment to the overlying waters, where it reaches concentrations 1,000-folds higher than those normally occurring in seawater (up to 22 mg L^{-1}) (Aller, 1994). Concentrations of manganese found in tissues of marine and freshwater fish tend to range from < 0:2 to 19 mg kg^{-1} dry weight.

Pure manganese is a silver-stained metal; however, it does not occur in the environment in a pure form. Rather, it occurs in manganese-compounds, combined with other elements such as

oxygen, sulphur, carbon, silicon and chlorine. These forms of manganese are solid and some of them can dissolve in water or be suspended in the air as small particles.

Table 1.2. Manganese concentrations in soil and water

Source	Manganese concentrations
Soil	500-900 mg kg^{-1}
Natural waters	< 1- 130 µg L^{-1}
Sea waters	0.03-0.8 µg L^{-1}
Tap water	Upto 1 mg L^{-1}

The small dust particles in the air usually settle at the bottom within a few days, depending on their size, weight, density and weather conditions. Manganese can exist in 11 oxidation states, ranging from –3 to +7, but the most common ones are: +2 (e.g., $MnCl_2$) and +4 (e.g., MnO_2) (Pinsino *et al.* 2012). There are inorganic and organic Mn compounds, with the inorganic forms being the most common in the environment. Ocean spray, forest fires, vegetation, crustal rock and volcanic activity are the major natural atmospheric sources of manganese (Concise International Chemical Assessment Document [CICAD] 63, 2004). Concentrations of manganese in terrestrial plants tend to range from 1 to 700 mg kg^{-1} (Gerber 2002).

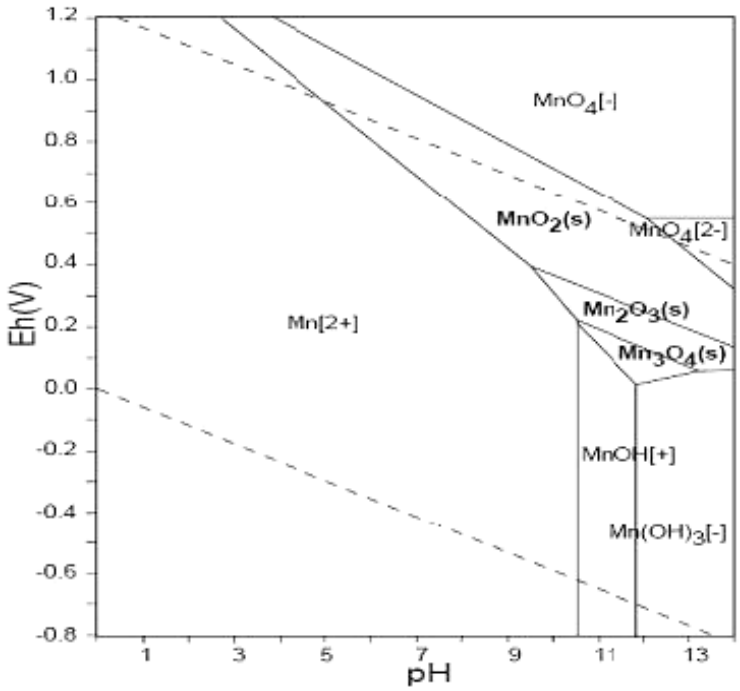

Fig. 1.3 Eh-pH profile of manganese (Takeno 2005)

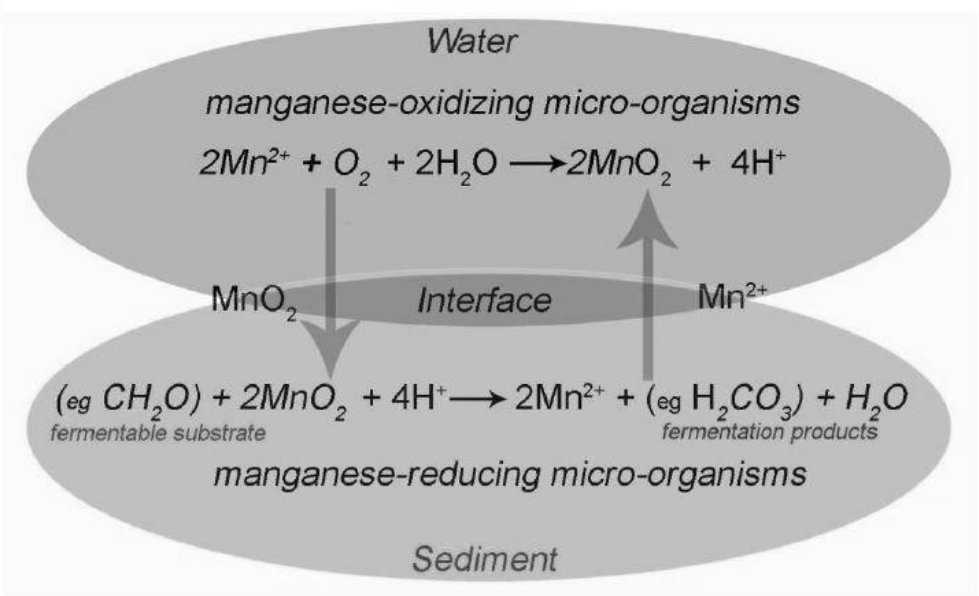

Fig. 1.4 The redox cycle of manganese in the oceans (Pinsino *et al*. 2012)

1.3 Global anthropogenic sources of Fe^{2+}

Anthropogenic sources of iron include the iron and steel industry, sewage and dust from iron mining (Reimann and de Caritat 1998). World production of new iron is over 500 million tonnes a year, and recycled iron adds other 300 million tonnes. Economically workable reserves of iron ores exceed 100 billion tonnes. The main mining areas are China, Brazil, Australia, Russia and Ukraine (**Fig. 1.5**), with sizeable amounts mined in the USA, Canada, Venezuela, Sweden and India. The amount varies strongly, and is different in the Atlantic and the Pacific Ocean (US Geological Survey 2011). Iron–steel industry is one of the main sources of the metals in the environment, because large amounts of dust are produced during the crushing, screening, and dumping of ores, while considerable quantities of particulate metals, including fine dusts (approximately 0.3 μm), are also emitted by metallurgical factories during the production of ferrous and non-ferrous metals and foundry byproducts. In addition, large amounts of particulate metals are emitted from accessory processes such as coke plants or electric power generators (Uyar *et al*. 2008). Iron as iron sulphate is used as fertiliser and herbicide (Reimann *et al.* 2003). The agricultural drainage water containing pesticides and fertilizers and effluents of industrial activities and runoffs in addition to sewage effluents supply the water bodies and sediment with huge quantities of inorganic anions including iron (European Commission Directorate General ECDG, 2002).

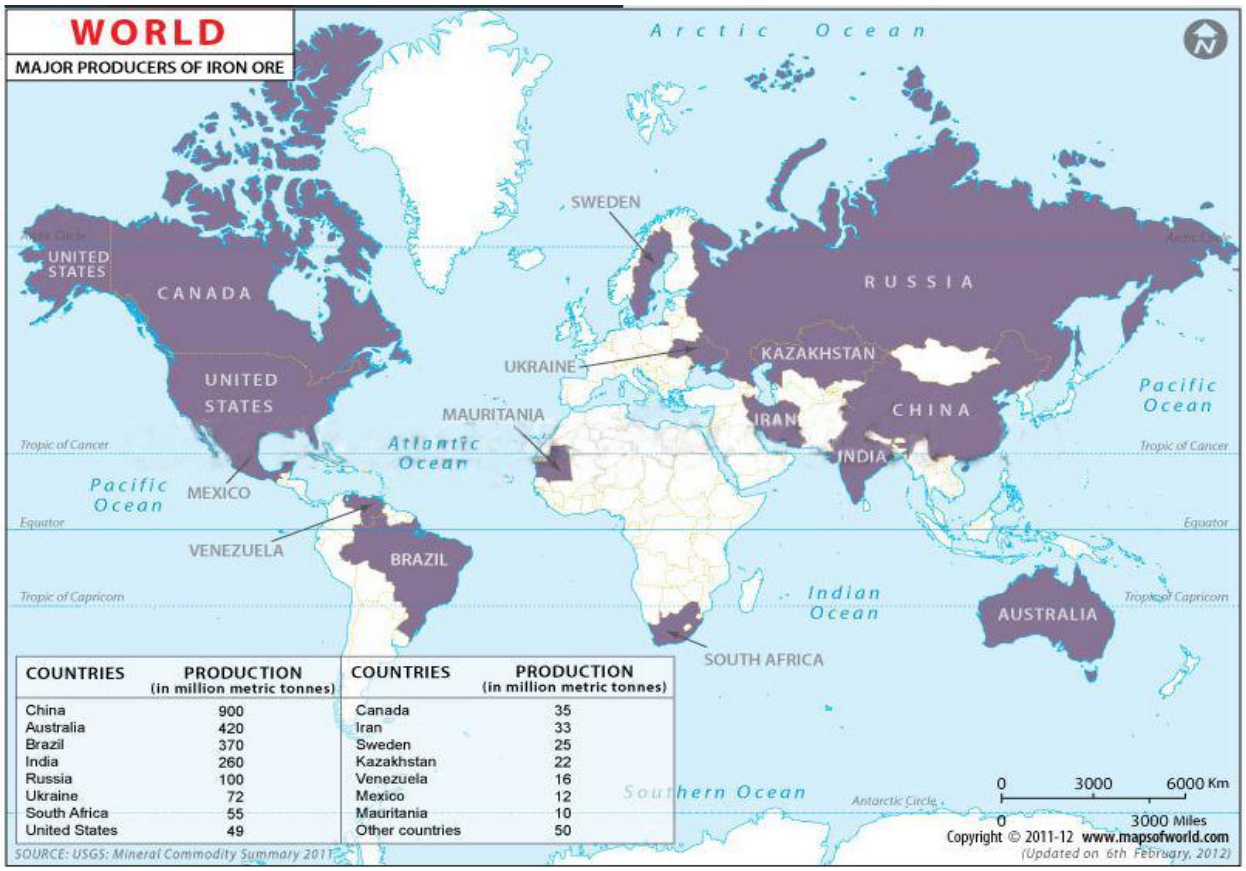

COUNTRIES	PRODUCTION (in million metric tonnes)	COUNTRIES	PRODUCTION (in million metric tonnes)
China	900	Canada	35
Australia	420	Iran	33
Brazil	370	Sweden	25
India	260	Kazakhstan	22
Russia	100	Venezuela	16
Ukraine	72	Mexico	12
South Africa	55	Mauritania	10
United States	49	Other countries	50

Fig. 1.5 World map of major producers of iron ore (US Geological Survey 2011)

1.4 Global anthropogenic sources of Mn^{2+}

The major anthropogenic sources of environmental manganese include municipal wastewater discharges, sewage sludge, mining and mineral processing (particularly nickel), emissions from ferroalloy-, steel-, and iron production as well as combustion of fossil fuels (Hronec 2010). Atmospheric concentrations of manganese in the general environment vary widely from less than 0:1 µg dm^{-3} up to 10 µg dm^{-3} or more near steel, iron or alloy plants (Gerber 2002). The emissions of manganese from combustion of fuel additives are generally of lower importance Special problems concerning air pollution, especially dust and smoke containing manganese dioxide and manganese tetroxide (Mn_3O_4), arise during the mining, crushing, and

smelting of ores as well as during steel production. Approximately 2 tonnes of manganese ore are required to make 1 tonne of ferromanganese alloy (Williams *et al*. 2012; Howe *et al*. 2004). The main mining areas are China, South Africa, Brazil, Australia, Russia, Ukraine, India, Gabon (**Fig 1.6**) (US Geological Survey 2011). Steel emissions were found to be the predominant source of manganese in urban particulate matter (Sweet *et al.* 1993). Manganese can also be released to the air during other human activities/processes, such as welding and fungicide application. Atmospheric manganese has also been associated with exploitation of automobiles. In regions where the anti-clock fuel additive methylcyclopentadienyl manganese tricarbonyl (MMT) is used in automobile engines; manganese is a component of automobile exhaust (Majestic *et al.* 2007). One of the principal sources of inorganic manganese as a pollutant in the urban atmosphere is the combustion of MMT, particularly in areas of high traffic density (Sierra *et al*. 1998). Combustion of MMT leads to the emission of manganese phosphates and manganese sulphate, with manganese oxides such as manganese tetroxide a minor component. The size of particles emitted to the atmosphere varies from 0.1 to 0.45 μm (Howe *et al*. 2004). Manganese can be released to water by discharge from industrial facilities or as leachate from landfills and soils. Land disposal of manganese-containing wastes is the principal source of manganese releases to soil (Howe *et al.* 2004). Sea disposal of mine tailings and liquor is reported to be significant source of manganese to the marine environment (Florence *et al*.1994).

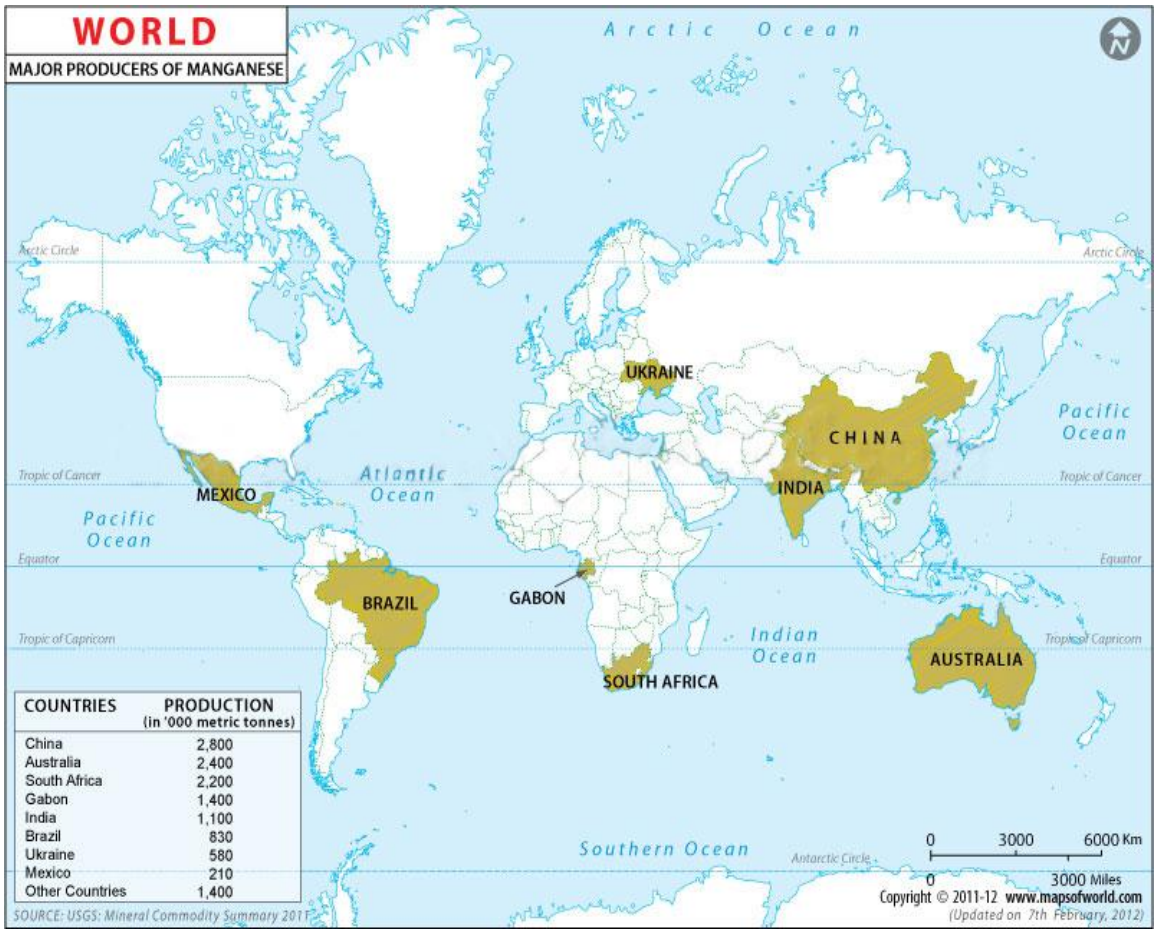

COUNTRIES	PRODUCTION (in '000 metric tonnes)
China	2,800
Australia	2,400
South Africa	2,200
Gabon	1,400
India	1,100
Brazil	830
Ukraine	580
Mexico	210
Other Countries	1,400

Fig. 1.6 World major producers of manganese (US Geological Survey 2011)

1.5 Bioclinical aspect of Iron

1.5.1 Daily iron intake and its significance

The total amount of iron in the human body is approximately 4 g, of which 70% is present in red blood coloring agents. Iron is a dietary requirement for humans, just as it is for many other organisms. Men require approximately 7 mg iron on a daily basis, whereas women require 11 mg. The body absorbs approximately 25% of all iron present in food (Muhammad *et al* 2013).

All living organisms on earth have an absolute requirement for iron to survive and to thrive. Several essential and highly conserved enzymes, such as the ribonucleotide reductases that produce deoxyribonucleic acids (DNA), require iron to carry out their function (Aisen *et al*. 2001). Other well known proteins such as hemoglobin and myoglobin utilize the same element to bind and transport oxygen in blood and muscle cells, respectively. As part of the cytochrome and cytochrome oxidase systems, iron also plays a major role in the generation of energy by mitochondria and bacterial cells. When it is bound to a protein the iron can be incorporated in prosthetic groups such as iron-sulfur clusters or the characteristic heme group, while other proteins such as transferrin can bind the metal ion directly. In the body iron is strongly bound to transferrin, which enables exchange of the metal between cells (Crichton 2009).

1.5.2 Deleterious effects of iron

Healthy people are generally not affected by iron overdose, which is also generally rare. It may occur when one drinks water with iron concentrations over 200 ppm (Ravenscroft *et al.* 2013).

When iron exceeds the required amount, it is stored in the liver. The bone marrow contains high amounts of iron, as it produces haemoglobin. High intakes of cobalt, zinc, cadmium, copper and manganese interfere with iron absorption in the human body, which can lead to anaemia (Muhammad *et al* 2013). Iron compounds may have a more serious effect upon health than the relatively harmless element itself. Water soluble binary iron compounds such as $FeCl_2$ and $FeSO_4$ may cause toxic effects upon concentrations exceeding 200 mg, and are lethal for adults upon doses of 10-50 g. A number of iron chelates may be toxic, and the

nerve toxin iron penta carbonyl is known for its strong toxic mechanism. Iron may cause conjunctivitis, choroiditis, and retinitis if it contacts and remains in the tissues. Chronic inhalation of excessive concentrations of iron oxide fumes or dusts may result in development of a benign pneumoconiosis, called siderosis, which is observable as an x-ray change. No physical impairment of lung function has been associated with siderosis. Inhalation of excessive concentrations of iron oxide may enhance the risk of lung cancer development in workers exposed to pulmonary carcinogens. LD_{50} (oral, rat) =30 gm kg^{-1}. High levels of free iron may damage or destroy the natural resistance. It catalyzes the formation of highly reactive compounds, such as hydroxyl radicals, that cause damage to the macromolecular components of the cells, including DNA and proteins. (Aisen *et al*. 2001; Lobo *et al*. 2010). The high frequency of infections, reported in hemodialysis patients, when receiving intravenous (IV) iron preparations, revealed that IV iron administration is associated with time-dependent increases of the intracellular oxidative stress in many immunocompetent cell populations, resulting in dysfunctional cellular immunity. The CD4+ lymphocytes are mainly affected, with a statistically significant reduction in their survival after incubation with all doses of iron preparations. IV iron products induce also various deleterious effects on CD16+ lymphocyte populations, which may also be mediated by intracellular ROS formation (Gupta et al 2010). Iron plays a major role in the generation and perpetuation of inflammatory processes. Many chronic inflammatory diseases are directly influenced by the intracellular and extracellular iron concentrations. Disease activity, and particularly the manifestation of serositris and various hematological disturbances in rheumatoid arthritis, systemic lupus erythematosous, Still's disease, dermatomyositis, and other collagen diseases are strongly correlated with serum and tissue ferritin levels (Yildirim

et al. 2004; Lim *et al.* 2004). Ferritin and iron homeostasis are implicated in the pathogenesis of many other disorders, including atherosclerosis, Parkinson's disease, Alzheimer disease, and restless leg syndrome (Rashmi *et al.* 2012).

Iron deficits lead to anemia, causing tiredness, headaches and loss of concentration. The immune system is also affected. In young children this negatively affects mental development, leads to irritability, and causes concentration disorder. Young children, pregnant women and adult women are often treated with Fe^{2+} salts upon iron deficits.

During iron deficiency its intake may be increased by means of vitamin C tablets, because this vitamin reduces tertiary iron to binary iron. When high concentrations of iron are absorbed, for example by haemochromatose patients, iron is stored in the pancreas, the liver, the spleen and the heart. Thus, exerting an adverse effect on these vital organs (Nadadur *et al*. 2008).

1.6 Bioclinical aspect of manganese

Manganese is an essential element for humans, animals, and plants, and is required for growth, development, and maintenance of health. Daily intakes range from 2-9 mg day^{-1} for adult human and approximately 3-5 per cent is absorbed from the gastrointestinal tract (Agency for Toxic Substances and Disease Registry [ASTDR] 2000). In addition, vitamin and mineral supplements may contain 1 to 20 mg Mn/ tablet (Aschner 2005). Absorption of Mn from the diet occurs in the divalent and tetravalent state (Barceloux 1999). Chronic inhalation exposure to relatively high levels of Mn has been associated with adverse neurological effects and a few studies have reported the same following the ingestion of high levels or chronic exposure to Mn in drinking water (ASTDR 2000, WHO 2004). Clinical Mn

neurotoxicity has been reported in patients receiving long-term parenteral nutrition and in patients with chronic liver dysfunction or renal failure, as a result of their inability to eliminate and clear Mn from the blood (Nagatomo *et al.* 1999; Ikeda 2000; Pal 1999).

Manganese is necessary for a variety of metabolic functions including those involved in skeletal system development, energy metabolism, activation of certain enzymes, nervous system function, immunological system function, and reproductive hormone function, and is an antioxidant that protects cells from damage due to free radicals (Institute of Medicine [IOM] 2001). Mn also plays an essential role in regulation of cellular energy, bone and connective tissue growth and blood clotting (Erikson 2003). In human beings, chronic manganese excess (10 mg d^{-1}) affects the central nervous system, with the symptoms resembling those of Parkinson's disease (Santamaria 2008). In the brain, Mn is an important cofactor for a variety of enzymes, including the antioxidant enzyme superoxide dismutase, as well as enzymes involved in neurotransmitter synthesis and metabolism (Aschner *et al*. 2007). Manganese has three primary metabolic functions: (*i*) it acts as an activator of the gluconeogenic enzymes pyruvate carboxylase and isocitrate dehydrogenase, (*ii*) it is involved in protecting mitochondria1 membranes through superoxide dismutase; and (*iii*) it activates glycosyl transferase, which is involved in mucopolysaccharide synthesis. In humans, manganese excess is renowned for its role in neurotoxicity, associated with a characteristic syndrome called 'manganese madness' or 'Parkinson-like' diseases (Perl & Olanow, 2007). This neurodegenerative disorder is due to the accumulation of manganese inside intracellular compartments, such as the Golgi apparatus and mitochondria. In mammals, prenatal and postnatal exposure to manganese is associated with embryo-toxicity, fetal-toxicity, and decreased postnatal growth (Sanchez *et al*., 1993; Colomina *et al*., 1996). Few instances of

Mn deficiencies have been reported in humans, with symptoms including dermatitis, slowed growth of hair and nails, decreased serum cholesterol levels, and decreased levels of clotting proteins (ASTDR 2000; Finley 2003). In addition, several diseases have been reported to be characterized by low blood Mn concentrations, including epilepsy, mseleni disease, and Down's syndrome, osteoporosis, and Perthest disease (Avila *et al*. 2013). Manganese deficiency has also been cited as a possible aetiologic factor for some congenital malformations and several inborn errors of metabolism have been associated with poor Mn status (*e.g*., phenylketonuria, maple syrup urine disease) (Avila *et al*. 2013).

1.7 Involvement of microbes in biogeochemical cycling of Fe^{2+} and Mn^{2+}

The oxidation reduction processes of metals by microorganism often lead to accumulation or precipitation of insoluble metal oxides which act as byproduct of these reactions. *Geobacter metallireducans* a freshwater isolate contains a membrane bound Fe^{3+} reductase, reported to reduce Fe^{3+} using acetate as oxidizing agent. Similarly *Shewanella putrefaciens* can couple oxidation of organic compounds such as pyruvate and lactate to carbon dioxide and acetate during Fe^{3+} reduction process (Loveley *et al*. 2004). *Acidithiobacillus ferrooxidans* contains enzymes that can reduce soluble Fe^{3+} under acidic conditions and could be involved in dissimilatory Fe^{3+} reduction with reduced sulfur compounds as the electron donor. Dissimilatory metal reduction is a process utilized by microorganisms to conserve energy through oxidizing organic or inorganic electron donor and reducing a metal or metalloid. Furthermore, when these byproducts react with ions or compounds in environment results in deposition of mineral particles such as magnetite (Bharde *et al*. 2008), siderite (Parmar *et al*. 2000), vivianite (Zegeye *et al*. 2007), greigite (Bazilynski and Frankel 2000). This synthesis of minerals by microorganism is termed as biologically induced mineralization (Bazilynski

and Frankel 2000). Biogenic iron and manganese minerals are particularly common products (**Table 1.3**) of BIM processes because of the relatively high concentrations of these elements in the earth's crust (4th and the 12th most abundant elements, respectively). Biologically induced mineralization (BIM) occurs when an organism modifies its local microenvironment creating conditions such that there is extracellular chemical precipitation of mineral phases (Bazylinski and Schubbe 2007; Dupraz *et al*. 2009). Oxidative and reductive reactions mediated by microbes play important roles in the iron cycle, and the formation of some sedimentary iron deposits has been attributed directly to microbial iron oxidation. Bacterial iron reduction has been associated with the formation of magnetite (Fe_3O_4), siderite ($FeCO_3$), rhodochrosite ($MnCO_3$) and sodium carbonate (natron, $Na_2CO_3.10H_2O$) (Gadd 2010). The bacteria that reduce manganese enzymically often do so as a form of respiration where oxidized manganese serves as a terminal electron acceptor and is reduced to Mn^{2+} (Lovley, 2000). Metal sulfides are subject to oxidation by bacteria such as *Acidithiobacillus ferrooxidans, Leptospirillum ferrooxidans, Sulfolobus spp. and Acidianus brierleyi*. The bacterial action may involve direct oxidative attack of the crystal lattice of a metal sulfide or indirect oxidative attack by generation of acid ferric sulfate, which oxidizes the metal sulfide chemically. The indirect mechanism is of primary importance in the solubilization of uraninite (UO2). Microbial oxidation of metal sulfides is exploited industrially in extracting metals from low-grade metal sulfide ores and uraninite (Jerez 2009; Gadd 2010).

Table 1.3 Induction of Iron and Manganese Mineral formation by various microorganisms

Mineral name	**Chemical formula**	**Microorganism involved**	**References**
Ferric oxyhydroxide	$Fe(OH)_3$	*Fe-oxidizing bacteria*	Chan *et al.* 2011; Yoshida *et al*. 2008
Green rust	$2Fe(OH)_3 \cdot Fe(OH)_2$ (approx.)	*Shewanella putrifaciens*	Kukkadapu *et al*. 2004; O'Loughlin 2008
Goethite	α-FeO(OH)	*Gallionella ferruginea;* Sulfolobales str. MK5.	Hallberg and Ferris 2004; Kozubal *et al.*2012
Lepidocrocite	γ- FeO(OH)	Marine bacteriophage (PWH3a-P1)*; Bacillus subtilis*	Daughney *et al.*2004; Chatellier *et al*. 2001
Ferrihydrite	$5Fe_2O_3 \cdot 9H_2O$	*Gallionella ferruginea, Leptothrix ochracea, Bacillus subtilis*	Hallberg and Ferris 2004; Kennedy *et al.* 2004
Magnetite	Fe_3O_4	*Shewanella putrefaciens* (Fe^{3+} reducing bacteria), magnetotactic bacteria. *(Eg. Magnetospirillum magnetotacticum).;* SRB*(Desulfovibrio magneticus), F. oxysporum, Verticillium, Shewanella alga; M. magneticum* AMB-1	Bazilynski and Frankel 2000, Faivre Schuler 2008; Bharde *et al.* 2006; Roh *et al.* 2003; Baumgartner *et al*. 2013.
Hematite	Fe_2O_3	*Gallionella ferruginea; Metallosphaera yellowstonensis* str. MK1.	Hallberg and Ferris 2004; Kozubal *et al.* 2012

Maghemite	γ-Fe_2O_3	*Actinobacter* sp. thermophilic iron reducing bacteria	Zhang *et al*. 1997; Bharde *et al*. 2008
Siderite	$FeCO_3$	*Shewanella alga,Thermoanaerobacter ethanolicus;* thermophilic iron reducing bacteria	Zhang *et al.* 1997; Parmar *et al*. 2000; Roh *et al*. 2003
Hydrous Ferric Phosphate	$FePO_4 \cdot nH_2O$	*Acidovorax* sp.	Miot *et al*. 2009
Vivianite	$Fe_3(PO_4)2 \cdot 2H_2O$	*Shewanella putrefaciens, Desulfovibrio alaskensis (SRB),Alkaliphilus metalliredigens*	Kukkadapu *et al*. 2004, Zegeye *et al.* 2007; Roh *et al.* 2007
Cubic FeS (Sphalerite-type)	FeS	*Magnetotactic bacteria.*	Posfai *et al.* 1998a, b.
Mackinawite (tetragonal FeS)	FeS	*Magnetotactic bacteria, Desulfovibrio desulfuricans*	Posfai *et al*. 1998a, b.
Greigite	Fe_3S_4	*Magnetotactic bacteria, Actinobacter* sp.	Bharde *et al.* 2008; Faivre Schuler2008
Pyrrhotite	$Fe_{1-x}S$	*Magnetotactic bacteria,*	Farina *et al.* 1990
Pyrite	FeS_2	*Magnetotactic bacteria, SRB*	Bazilinski 1996; Donald and Southam 1999

Jarosite	$KFe_3(SO_{4)2}(OH)_6$	*Sulfobacillus thermosulfidooxidans; Acidithiobacillus ferroxidans; Metallosphaera yellowstonenesis* str. MK1, *Sulfolobales* str. MK5.	Ding *et al*. 2007; Daoud and Karamanev 2006; Kozubal *et al.* 2012
Schwertmanite	$Fe_8O_8SO_4(OH)_6$	*Acidithiobacillus ferroxidans*	Egal *et al.* 2009
Melanterite	$FeSO_4 \cdot 7H_2O$	*Thiobacillus* sp., *SRB*	Fortin *et al.* 1996
Rhodochrosite	$MnCO_3$	*Leptothrix discophora, Pyrobaculum islandicum*	Zhang *et al.* 2002; Kashefi *et al.* 2000.
Manganese oxides	MnO_2	*Pseudomonas* sp., *Leptothrix discophora, Bacillus* sp., *Acremonium strain KR21-2*	Tebo *et al.* 2004; Villalobos *et al.* 2003; Brouwers *et al.* 2000; Miyata *et al.* 2004
Bixbyite	Mn_2O_3	*Acinetobacter* sp.	Hosseinkhani and Emtiazi 2011
Todorokite	$Mn_4O_7 \cdot H_2O$	*Pseudomonas putida* strain GB-1.	Feng *et al.* 2010
Birnessite	$Na_4Mn_{14}O_{27} \cdot 9H_2O$	*Pseudomonas putida*, *Paraconiothyrium* sp.	Villalobos *et al.* 2003; sasaki *et al*. 2006

1.8 Effects of Iron and Manganese on microorganisms.

The iron content of *E.coli* ranges from ~10^5 to 10^6 atoms per cell, depending on growth conditions (Abdul-Tehrani *et al*. 1999). Based on this, at high cell densities (10^9 cells ml^{-1}), each generation would be expected to consume up to 10^{18} iron atoms per litre (Braun *et al*. 1998). Unfortunately, ferric ion has a solubility of just 10^{-17} M at pH 7 providing a mere

$6x10^6$ iron atoms per litre and indeed bacteria such as *E. coli* generally require iron at around 10^{-7} to 10^{-5} M to achieve optimal growth (Andrew *et al*. 2003). Iron is one of the metals where the toxicity is based on the ability of Fe^{2+} to catalyze the formation of highly reactive hydroxyl radical from hydrogen peroxide or lipid peroxides. Reactive oxygen species are partially reduced derivatives of molecular oxygen that are produced as a natural consequence of aerobic metabolism (Andrew *et al.* 2003). The one- and two-electron-reduction products of oxygen, namely superoxide and hydrogen peroxide, are only mildly reactive physiologically. However, iron interacts with these species to generate the highly reactive and extremely damaging hydroxyl radical. The key reactions are shown below:

Iron reduction, $O_2^- + Fe^{3+} \longrightarrow Fe^{2+} + O_2$ (1)

Fenton reaction (Fenton 1894): $Fe^{2+} + H_2O_2 \longrightarrow Fe^{3+} + OH^- + HO$ (2)

Haber Weiss reaction (Haber and Weiss 1932) : (1) + (2)

$O_2^- + H_2O_2 \xrightarrow{\text{Fe catalysis}} HO + OH^- + O_2$ (3)

In vivo superoxide concentrations are considered to be too low (at ~ 10^{-10} M) to cause iron reduction (Eq. 1) but can be sufficiently high to damage the exposed [4Fe-4S] clusters of dehydratase-lyase family members (e.g. aconitase and α, β - dihydroxyacid dehydratase) which in turn leads to release of free iron (Andrew *et al*. 2003).

The analogous reaction with Mn^{2+} does not occur. The critical difference between the two being the reduction potential of the reaction $Mn^{3+} \longrightarrow Mn^{2+} + e^-$ > $Fe^{3+} \longrightarrow Fe^{2+} + e^-$ (+1.55V & +0.77 V respectively). The high redox potential of Mn^{2+} renders the free Mn^{2+} innocuous under conditions (in an aerobic environment) where free Fe^{2+} would actively

generate toxic free radicals. Cells can thus tolerate very high cytoplasmic concentrations of Mn^{2+}. The intracellular Mn^{2+} levels in most cell types are low, of the order of 10 µM. During expression of Mn^{2+} uptake systems, de novo $^{54}Mn^{2+}$ uptake alone routinely yields cytoplasmic $^{54}Mn^{2+}$ levels of > 300 µM in both *E. coli* and *S. enteric* typhimurium (Kehres and Maguire 2003). Manganese affects the expression of iron regulatory genes in *B. japonicum* and the cellular iron status (Puri *et al.* 2010). Mn^{2+} ions are reported to cause cell surface alteration in *Salmonella* by decrease in membrane fluidity and increase in the cell membrane permeability (Liu *et al.* 2011).

1.9 Types of interaction of microbes with metals

1.9.1 Metal resistance Mechanisms in Prokaryotes and Eukaryotes:

Survival of microorganisms in the presence of the toxic metals depends on intrinsic biochemical and structural properties, physiological and /genetic makeup of the microorganism and its ability for adaptation, environmental modification of metal speciation, availability and toxicity. A cell acquires metal resistance by preventing the access of metals to sensitive cellular components or altering them to reduce their sensitivity. The mechanisms generally proposed for resistance to metal toxicity in bacteria and other microorganisms (**Fig 1.7**) are:

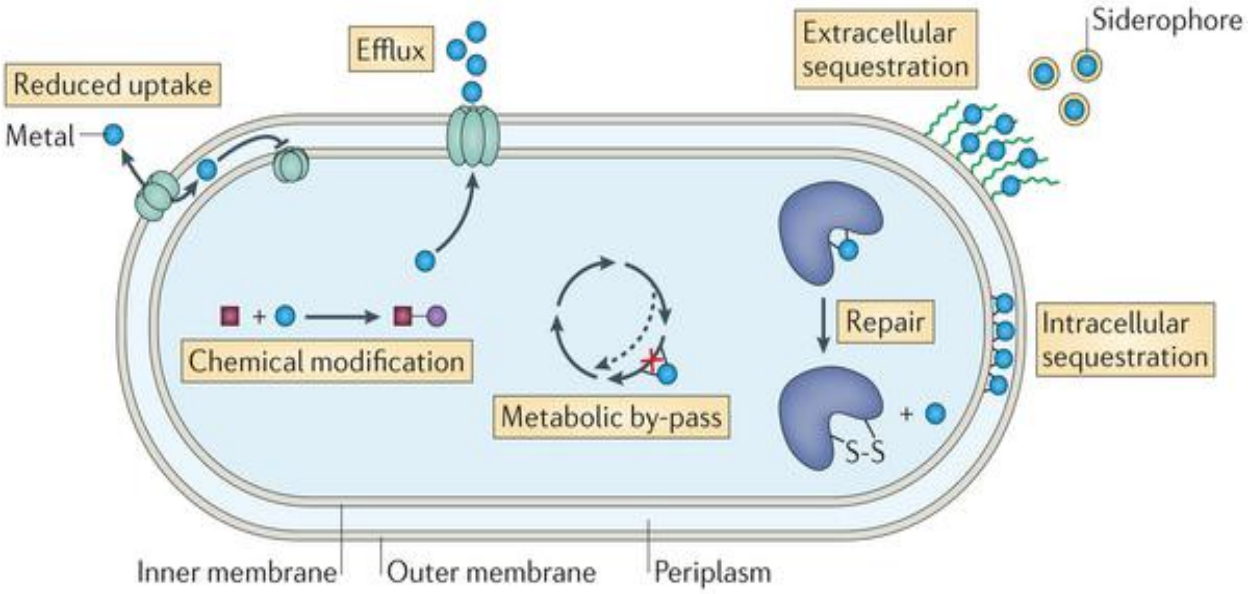

Fig. 1.7 Metal resistance mechanisms in eubacteria (Lemire 2013)

1.9.1.1. Exclusion of the metal by a permeability barrier

Bacterial surfaces such as cell wall, or polymeric materials (exopolymers) exuded by bacteria, including slimes, sheaths, or biofilms, and even dormant spores, can act as important sites for the adsorption of ions and mineral nucleation and growth (Bazylinski and Frankel 2004). When S layers are present, they are the outermost layer of the cell facing the surrounding environment. S layers are acidic and possess a net negative charge thereby having an affinity for metal cations (Southam 2000). The cell surface functional groups such as carboxyl, hydroxyl, phosphate, sulfate being negatively charged are attracted towards the positively charged cations such as Fe^{2+}, Mn^{2+}, Zn^{2+}, Ni^{2+}, Co^{2+} hence restricting their entry inside the cell (Volesky 2007). This mode of immobilization sequesters metal ions extracellularly and is independent of energy or cell metabolism (Gadd, 2009). Difference in cell wall composition among different group of microorganisms viz. algae contain alginic

acid, fucoidan and cellulose, those of red algae contain agar, carrageenan, xylans, pectins and cellulose. The cell wall of green algae contains pectic substances and cellulose (Kuyucak and Volesky 1990; Davis *et al.* 2003). The cell wall of yeast contain large number of complex organic compounds and their polymers such as glucans, mannan, proteins, lipids, chitin and chitosan; The carboxyl group of the peptidoglycan serves as main metal binding site at the cell wall of gram positive bacteria, whereas phosphate groups contribute significantly in case of gram negative bacteria (Gadd and White, 1993). Thus, cause significant differences in the type and amount of metal sorbed. Besides bacteria, biomass of fungi, algae, yeast are also widely used as biosorbents of various metal ions (**Table 1.4**). Ability of Haloarchaeal members to adsorb metal ions reported thus far pertains to zinc, cadmium, arsenic, nickel, aluminium and mercury by Prakash et al. (2012 a, b).

Table 1.4 Microorganisms used as potential adsorbents of various metal ions.

Metal ions	**Microbial Sorbent**	**Adsorbed metal (mg g^{-1})**	**References**
Pb^{2+}	*Bacillus* sp.	92.3	Tunali *et al*. 2006
Pb^{2+}	*Bacillus firmus*	467	Salehizadeh and Shojaosadati 2003
Pb^{2+}	*Enterobacter* sp.	50.9	Lu *et al*. 2006
Pb^{2+}	*Pseudomonas aeruginosa*	79.5	Chang *et al*. 1997
Pb^{2+}	*Pseudomonas putida*	56.2	Pardo *et al*. 2003
Pb^{2+}	*Streptomyces rimosus*	135	Selatnia *et al*. 2004a
Pb^{2+}	*Saccharomyces cerevisiae*	79.2	Al-Saraj *et al*. 1999
Pb^{2+}	*Penicillium canescens*	213.2	Say *et al*. 2003

Pb^{2+}	*Penicillium chrysogenum*	116	Niu *et al.* 1993
Pb^{2+}	*Penicillium digitatum*	5.5	Veglio and Beolchini 1997
Pb^{2+}	*Aspergillus niger*	93	Spanelova *et al*. 2003
Pb^{2+}	*Cystoseira trinodis*	49.08	Salehi *et al.* 2013
Pb^{2+}	*Chlorella vulgaris*	178.5	Edris *et al*. 2014
Pb^{2+}	*Haloferax* sp. TL5	5	Popescu and Dumitru 2009
Zn^{2+}	*Streptomyces rimosus*	30	Mameri *et al.* 1999
Zn^{2+}	*Bacillus firmus*	418	Salehizadeh and Shojaosadati 2003
Zn^{2+}	*Pseudomonas putida*	6.9	Pardo *et al.* 2003
Zn^{2+}	*Streptoverticillium cinnamoneum*	21.3	Puranik and Paknikar 1997
Zn^{2+}	*Thiobacillus ferroxidans*	172.4	Liu *et al*. 2004
Zn^{2+}	*Saccharomyces cerevisiae*	23.4	Al- Saraj *et al.* 1999
Zn^{2+}	*Penicillium chrysogenum*	13	Skowronski *et al*. 2001
Zn^{2+}	*Penicillium spinulosum*	1.3	Kapoor and Viraraghavan 1995
Zn^{2+}	*Mucor racemosus*	57.67	El-Morsy *et al* 2013
Zn^{2+}	*Haloferax* sp. TL 5	0.8	Popescu and Dumitru 2009
Cu^{2+}	*Bacillus* sp.	16.3	Tunali *et al*. 2006
Cu^{2+}	*Enterobacter* sp.	32.5	Lu *et al*. 2006
Cu^{2+}	*Micrococcus luteus*	33.5	Nakajima *et al*. 2001

Cu^{2+}	*Pseudomonas putida*	96.9	Uslu and Tanyol 2006
Cu^{2+}	*Thiobacillus ferroxidans*	39.8	Liu *et al*. 2004
Cu^{2+}	*Pseudomonas stutzeri*	22.9	Nakajima *et al.* 2001
Cu^{2+}	*Saccharomyces cerevisiae*	6.4	Al-Saraj *et al*. 1999
Cu^{2+}	*Penicillium chrysogenum*	92	Deng and Ting 2005
Cu^{2+}	*Penicillium italicum*	0.4 - 2	Ahluwalia and Goyal 2007
Cu^{2+}	*Aspergillus versicolor*	13.15	Gazem and Nazareth 2012
Cu^{2+}	*Chlorella miniata*	0.366	Romera *et al*.2006
Fe^{3+}	*Streptomyces rimosus*	122	Selatnia *et al.* 2004
Fe^{3+}	*Saccharomyces cerevisiae*	16.8	Bustard and McHale 1998
Fe^{3+}	*Chlorella vulgaris*	0.439	Romera *et al*. 2006
Fe^{3+}	Sulfate reducing bacteria	88.29	Quan *et al*. 2013
Fe^{2+}	*Synechocystis* sp. E35.	32.5	Sevgi *et al*. 2009
Mn^{2+}	*Saccharomyces cerevisiae*	18.95	Parvathi *et al*. 2007
Mn^{2+}	*Nostoc*	14.98	Mane *et al.* 2010
Mn^{2+}	*Spirogyra*	15.73	Mane *et al*. 2010
Mn^{2+}	*Aspergillus niger*	19.34	Parvathi *et al.* 2007
Mn^{2+}	*Pseudomonas aeruginosa* AT18	22.39	Silva *et al*. 2009
Cr^{4+}	*Bacillus coagulans*	39.9	Srinath *et al*. 2002
Cr^{4+}	*Bacillus licheniformis*	69.4	Zhou *et al*. 2007

Cr^{4+}	*Pseudomonas sp.*	95.0	Ziagova *et al*. 2007
Cr^{4+}	*Zoogloea ramigera*	2	Nourbakhsh *et al.* 1994
Cr^{4+}	*Haloferax* sp. TL 15	0.8	Popescu and Dumitru 2009
Cr^{6+}	*Saccharomyces cerevisiae*	32.6	Ozer and Ozer 2003
Cr^{6+}	*Candida tropicalis*	29.1	Bahafid *et al*. 2013
Cr^{3+}	*Penicillium chrysogenum*	18.6	Tan and Cheng 2003
Cr^{6+}	*Chlorella vulgaris*	1.525	Romera *et al.* 2006
Cr^{6+}	*Sargassum* sp.	1.327	Romera *et al*. 2006
Ni^{2+}	*Bacillus thuringensis*	45.9	Ozturk 2007
Ni^{2+}	*Streptomyces rimosus*	32.6	Selatnia *et al*.2004
Ni^{2+}	*Saccharomyces cerevisiae*	46.3	Ozer and Ozer 2003
Ni^{2+}	*Penicillium chrysogenum*	56.2	Deng and Ting 2005
Ni^{2+}	*Aspergillus niger*	0.96	Kapoor *et al*. 1999
Ni^{2+}	*Aspergillus tereus*	19.6	Dias *et al*.2002
Ni^{2+}	*Chlorella vulgaris*	0.2-1.017	Romera *et al*. 2006
Ni^{2+}	*Haloferax* sp. TL 15	0.2	Popescu and Dumitru 2009
Ni^{2+}	*Cystoseira trinodis*	14.58	Salehi *et al*. 2013

1.9.1.2 Efflux pump

In this process, metal ion that enters the cell are excluded by means of transport systems for cations such as Mg^{2+}, Na^{+}, K^{+}. In bacteria efflux pumping is the basic of most toxic ion resistance systems involving transporters such as P type ATPases or cation/ H+ antiporters. P-type ATPases belong to the family of transmembrane transporters responsible for movements of ions and small organic molecules in and out of the cell membranes. The subfamily of transmembrane transporters which includes Pm-type ATPases regulates efflux of toxic heavy metals outside the cell membranes and prevents the over accumulation of highly reactive and toxic soft-metals thus play an important role in heavy metal resistance (Coombs and Barkay 2005). The first bacterial ferrous iron transporter discovered was in *E.coli* and is encoded by the anaerobically induced, and iron-repressed, feoAB genes. These genes are conserved in many bacteria (although feoB is often found without feoA) (Andrew *et al*. 2003). Another type of bacterial iron transporter is the metal transporting binding-protein-dependent ABC systems that have specificity for iron. Such systems include the SfuABC, SitABCD, YfeABCD, FbpABC and FutABC transporters of *Serratia marcescens*, *Salmonella typhimurium*, *Yersinia pestis*, *Neisseria gonorrhoeae and Synechocystis* PCC 6803(Andrew *et al.* 2003). The Sit system is encoded by genes within the *Salmonella* pathogenicity island and is required for mouse infection. However, it appears that this system has much greater affinity for Mn^{2+} than Fe^{2+} (and cannot transport Fe^{3+}), and so may not function primarily in iron transport (Kehres *et al.* 2002). The Yfe system of *Y. pestis* is repressed by iron and manganese, and is required for full virulence and for normal growth under iron-restricted conditions. The Fut system of *Synechocystis* is also iron-repressed and

involved in ferric iron uptake. The Sfu and Fbp systems seem to be involved in transporting iron, delivered by transferrin and lactoferrin, across the CM.

In *S. cerevisiae*, two members of the Nramp family of metal transporters (Smf1p and Smf2p) act in the uptake and intracellular trafficking of manganese. Nramp (for natural resistance-associated macrophage protein) represents a large family of metal ion transporters that are widely conserved from bacteria to humans. These are metal-proton symporters that act on a broad range of divalent metals, including manganese, iron, cadmium, and copper. In eukaryotes, these transporters are localized at the cell surface or at intracellular sites, but in all cases, the metal is transported in the direction of the cytosol. Smf1p is a high-affinity transporter for manganese (Cullota *et al*. 2005). As with other members of the Nramp family, a range of divalent metals can act as substrates for Smf1p. When over expressed in yeast, Smf1p can increase cellular accumulation of manganese, copper, cadmium, and iron. And when expressed in oocytes, the metals manganese, copper, iron, zinc, and cadmium are all transported by Smf1p in a proton-dependent manner. Smf1p has been observed to localize to the plasma membrane of *S. cerevisiae* cells (Cullota *et al*. 2005). Smf1p is not to be the only source of cellular manganese, and other cell surface transporters for manganese are operative under physiological conditions. These might include high affinity transporters for other metals, such as iron, copper, or zinc, which can also transport manganese at low affinity. Alternatively, manganese can enter the cell via phosphate transporters, and one or more of the phosphate uptake systems in yeast (Xiang *et al*. 2005) may contribute to manganese accumulation. The second Nramp transporter for manganese is Smf2p. Smf2p has a profound impact on manganese accumulation and bioavailability, even under manganese-replete physiological conditions. PHO84 encodes a cell surface inorganic phosphate transporter that

is a major source of phosphate for *S. cerevisiae* (Xiang *et al*. 2005). Pho84p also acts as a low-affinity manganese transporter. When cells are exposed to high manganese concentrations (in excess of 10 μM), they accumulate the metal in a linear fashion, and a deletion in pho84 eliminates the uptake of excess manganese (Jensen *et al*. 2003). As such, Pho84p appears to be the major source of toxic manganese for the cell. It is therefore conceivable that when yeast cells are exposed to very high levels of manganese, the manganese-phosphate complexes that form in the environment are readily taken up via the Pho84p transporter (**Fig**. **1.8**). Unlike Smf1p and Smf2p, there is no known down-regulation of Pho84p in response to manganese; therefore, the cell becomes quite vulnerable to manganese toxicity. Fortunately, much of the accumulated manganese is eliminated from the cell via the action of Pmr1p. Pmr1p is the major route for eliminating toxic manganese from the cell. Mutants lacking Pmr1p are exquisitely sensitive to manganese toxicity and accumulate very high levels of the metal, largely in the cytosol (Ton *et al*. 2002). Presumably, the excess manganese pumped into the Golgi by Pmr1p proceeds to exit the cell via secretory pathway vesicles that merge with the cell surface and release the manganese contents back into the extracellular environment.

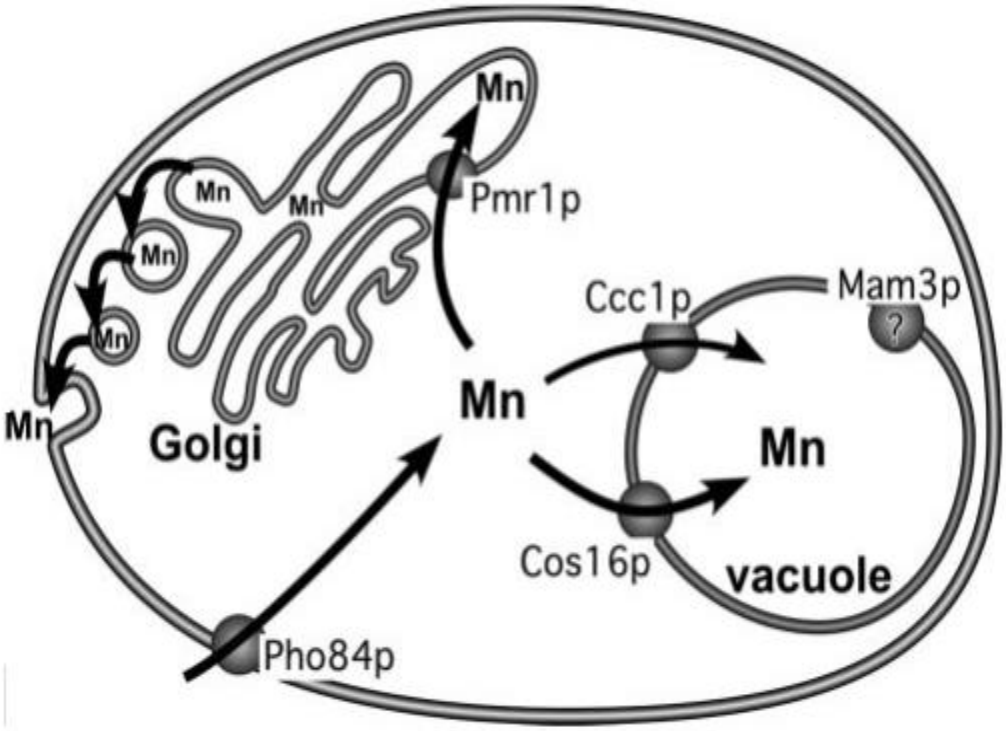

Fig. 1.8 Manganese transport under manganese surplus or toxicity conditions in *S. cerevisiae* (Cullota *et al*. 2005)

1.9.1.3 Enzymatic detoxification

In enzymatic detoxification of harmful metals and metalloids a toxic metal species may be converted to a less toxic or nontoxic entity by enzymatic oxidation or reduction. The bacterial oxidation of AsO^{-2} to AsO_4^{-3} by a strain of *Alcaligenes faecalis* and reduction of CrO_4^{2-} to Cr $(OH)_3$ by *Ps. fluorescens* LB300 or *Enterobacter cloacae* are examples of such redox reactions. (Silver and Phung 2005) Still other detoxification processes involve enzymatic or nonenzymatic methylation of metals and metalloids such as Sn, Hg, Pb, As, and Se. (Bentley and Thomas 2002). The *mer* operon that confers mercury resistance to bacteria is widely distributed in mercury resistant bacterial population (Osborn *et al*., 1997; Barkey *et*

al., 2003). The *merA* encodes mercury reductase enzymes which detoxify mercury by reducing Hg^{2+} to volatile Hg° (De *et al*., 2008). A deep sea sedimentary manganese-oxidizing bacterium, *Brachybacterium* sp. strain Mn 32, posess high Mn^{2+} resistance (MIC 55 mM) and Mn^{2+}- oxidizing/removing abilities. This bacterial strain is reported to remove Mn^{2+} employing a simple pathway involving oxidation of soluble Mn^{2+} to insoluble biogenic Mn oxides (Wang *et al*., 2009). The most well-characterized Mn^{2+}oxidizing bacteria are *Bacillus* sp. strain SG-1, *Leptothrix discophora* strain SS-1, and *Pseudomonas putida* strains MnB1 and GB-1 (Waasbergen *et al*. 1996; Nelson 2006; Brouwers 1999). Although distantly related phylogenetically, enzymes related to multicopper oxidases appear to be involved in Mn^{2+}oxidation in all of these organisms. Multicopper oxidases, MnxG (eg. Laccase, ceruloplsamin, ascorbate oxidase) are a diverse family of proteins that utilize multiple copper ions as cofactors in the oxidation of a wide variety of substrates (Solomon *et al*. 1996). *Pseudomonas* sp. G1DM21 isolated from Cr^{6+} contaminated industrial landfill reduce Cr^{6+} to Cr^{3+} through chromate reductase activity (Desai *et al*., 2008).

Ferric reductases catalyze the reduction of ferric iron (Fe^{3+}) to ferrous iron (Fe^{2+}). Many bacterial ferric iron reductases have been described from a variety of different bacteria including *Azotobacter vinelandii* (Bevers and Theil 2011), *Bacillus megaterium*, *Bacillus subtilis*, *Escherichia coli*, *Legionella pneumophila* (Balska and Lipiak 2013). The majority use NADH or NADPH as the electron donor for ferric iron reduction. Dependent on the bacterial species and the strategy for iron uptake, ferric reductases have been identified in the cell's cytoplasm, periplasm and cytoplasmic membrane. Extracellular ferric reductases are secreted in culture medium and serves as means of acquiring iron. The activity was dependent on the presence of NADH, catalytic amounts of FMN and Mg^{2+}.

L. monocytogenes is a best example of possessing this type of reductases. Membrane bound ferric reductase activities were reported from *Spirillum itersonii, E. coli,* and *Staphylococcus aureus* (Schroder *et al*. 2003). These ferric reductases were suggested to be part of a membrane-bound electron transport chain that uses NADH, succinate, glycerol-3 phosphate, or L-lactate as the donor to reduce ferric iron.

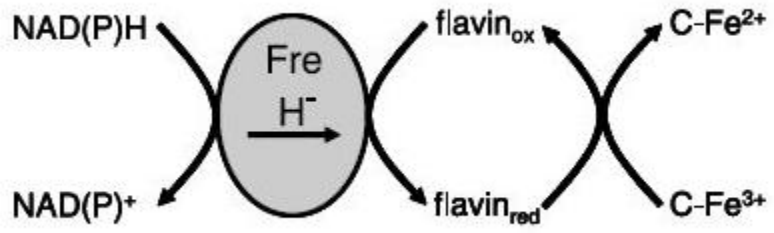

Fig.1.9. Reaction catalysed by bacterial flavin reductases that act by forming a ternary complex between the reductant NAD(P)H and free flavin. The reduced flavin then dissociates from the enzyme that may serve as direct chemical reductant of complexed ferric iron (C- Fe^{3+}) (Schroder *et al*. 2003).

1.9.1.4 Metal Binding Metabolites

Microorganisms release a diverse range of specific and non specific metal binding compounds into environment which can act to ameliorate the presence of toxic metal and or mediate uptake. Microbially produced macromolecules can bind significant amounts of potentially toxic metals. These include humic and fulvic acid arising from lignocellulose degradation and extracellular polymeric substances a mixture of polysaccharides, mucopolysaccharides and proteins produced by bacteria, algae and fungi. (Schreiber *et al*. 1990, Beech and Cheung 1995; Spark *et al*. 1997). These exopolysaccharides are chemically diverse and are mostly acidic heteropolysaccharides with functional groups viz. hydroxyl,

carboxyl, amides and phosphoryl which exhibit high affinity towards heavy metals(Bhaskar and Bhosle, 2006; Bramhachari *et al.,* 2007; Braissant *et al*., 2007). Bacterial EPS play a key role in initial attachment of cells to different substrata, cell-to-cell aggregation, protection against desiccation and resistance to harmful exogenous materials (Decho, 1990; Iyer *et al*., 2004; Pal and Paul, 2008). Various microbial biopolymers have been shown to possess potential to bind heavy metals with different degree of specificity and affinity (Bhaskar and Bhosle, 2006; De *et al.* 2008; Pal and Paul, 2008). *Klebsiella oxytoca BAS-10* is a Gram-negative micro-organism capable of producing large amounts of an iron-binding exopolysaccharide that, in the presence of metallic cations, precipitates as a dense gel. The polysaccharides that specifically bind to Fe^{3+} have been discovered, including the capsular polysaccharide from *Bacillus licheniformis* and the acidic exopolysaccharide from *Bradyrhizobium japonicum* (Leone *et al*. 2007).

1.9.1.5 Extracellular/ Intracellular Metal Sequestration

Microorganisms are also known to produce extracellular specific metal binding compounds like siderophores. Bacteria elaborate and secrete high-affinity extracellular ferric chelators, called siderophores (iron carriers), to solubilise iron prior to transport (Andrew *et al.* 2003). Gram-negative bacteria (*E.coli*) take up ferri-siderophore complexes via specific outer membrane (OM) receptors in a process that is driven by the cytosolic membrane (CM) potential and mediated by the energy-transducing TonB-ExbB-ExbD system. Periplasmic binding proteins shuttle ferri-siderophores from the OM receptors to CM ATP-binding cassette (ABC) transporters that, in turn, deliver the ferri-siderophores to the cytosol (**Fig**. **1.10A**) where the complexes are probably dissociated by reduction. Bacteria, such as Gram-positives, that lack an OM require neither OM receptors nor TonBExbB- ExbD systems (**Fig**.

1.10B). To allow ferri-siderophores to traverse their CM, they use binding-protein-dependent ABC permeases that are analogous to those employed by Gram-negatives except that the binding protein is generally a lipoprotein tethered to the external surface of the CM. Siderophores are of low molecular mass (61000 Da) and are characterised by their high specificity and affinity (K_{aff} $>10^{30}$) towards ferric iron. They are generally synthesised and secreted by bacteria (and fungi and monocotyledonous plants) in response to iron restriction although some, such as the mycobactins of mycobacteria, remain associated with the cell envelope (Ratledge and Dover 2010). Siderophores can reach extremely high concentrations up to 200 mg L^{-1} can be achieved for aerobactin produced by some *E.coli* strains. Siderophores usually form hexadentate octahedral complexes with ferric iron and typically employ hydroxamates, K-hydroxycarboxylates and catechols as extremely effective Fe^{3+} ligands. Common precursors for siderophore biosynthesis include citrate, amino acids, dihydroxybenzoate and N5-acyl-N5-hydroxyornithine (Kell 2009). Post synthesis, siderophores are secreted across the cell membrane.

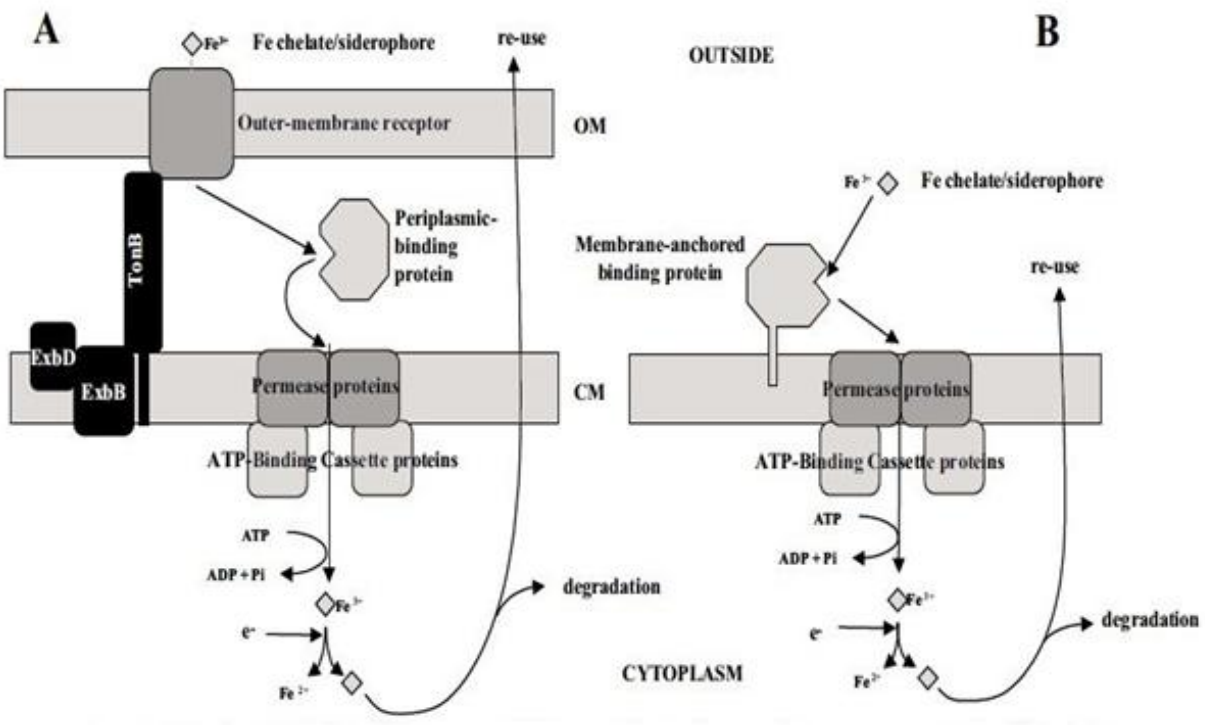

Fig. 1.10 Siderophore mediated iron uptake in Gram negative (A) and Gram positive (B) bacteria (Andrews *et al*. 2003).

Many bacteria deposit intracellular reserves of iron within iron storage proteins. These iron stores can then be used to enhance growth when external iron supplies are restricted. Three types of iron storage protein are recognised in bacteria: the archetypal ferritins which are also found in eukaryotes, the haem containing bacterioferritins found only in eubacteria and the smaller Dps proteins present in prokaryotes. Iron storage proteins take up iron in the soluble ferrous form, but iron is deposited in the central cavity in the oxidised ferric form. The first Dps protein discovered was from *E.coli*. This protein was found to be DNA-binding protein with a role in protecting DNA from redox stress produced by reaction between ferrous iron and hydrogen peroxide (Nair and Finkel 2004).

Further, in the prokaryotic cyanobacteria metal ion sequestration within the cell is performed by the class II metallothioneins. Class II metallothioneins are sulfhydryl containing cystein rich metal binding proteins which range from 3.5 kDa to 14 kDa that sequester metal, thus preventing accumulation of potentially toxic forms of metal ions within the cell. (Ybarra and Webb 1999). Metal ion binding occurs through the interaction of the ions with the sulfhydryl groups of cystein residues. Metallothioneins play an important role in immobilization of toxic heavy metals thereby protecting bacterial metabolic processes catalysed by enzymes (Blindauer *et al*., 2002; Liu *et al*., 2003). Several cyanobacterial and bacterial strains have been reported to encode metallothioneins for maintaining cytosolic metal homeostasis viz. *Synechococcus* PCC 7942 (SmtA), *Anabaena* PCC 7120 (SmtA), *Oscillatoria brevis* (BmtA), *Pseudomonas aeruginosa* (BmtA) and *Pseudomonas putida* (BmtA) (Turner *et al*., 1996; Blindauer *et al*., 2002; Liu *et al.,* 2003). Two copper-inducible supernatant proteins viz. CuBPI and CuBP2 with molecular mass 21 kDa and 19 kDa were identified in marine bacterium, *Vibrio alginolyticus* which were 25-46 times amplified in the supernatant of copper-challenged culture as compared with control. Thus these proteins facilitated copper accumulation and homeostasis (Harwood-Sears and Gordo, 1990).

1.9.2 Metal Resistance in Haloarchaea

1.9.2.1 Intracellular Proteins

Haloarchaea are reported to have γ- glutamylcysteine (γ-GC) that is analogous to glutathione (GSH) and involved in maintaining a reducing environment within the cell, overcomimg oxidative and disulfide stress. The thiol group of cysteine in γ-GC can chelate the toxic metal ions thereby conferring resistance. The multimeric nonhaem ferritin DpsA-like protein of

Halobacterium salinarum is found to sequester iron in response to the oxidative stress exerted by excess iron (Reindel *et al.* 2005). This protein was down regulated under iron deficient conditions. It exhibits the features of nonhaem bacterial ferritins that are expressed to sequester the excess iron. Their expression is repressed under conditions of iron starvation. Among haloarchaea, *Halococcus saccharolyticus, Halogeometricum sp., Halorubrum saccharovorum, Haloterrigena terkmenica* are reported to produce carboxylate type siderophores (Dave *et al.* 2006). Overexpression of siderophores in haloarchaea increase chelation in case of iron deficiency. On the other hand, repression of the siderophores in presence of excess iron may avoid uptake (Malki *et al*. 2009; Dave *et al.* 2006). Kaur *et al* (2006) have proposed that chelation of Fe^{2+} by the ferritin DpsA is a mechanism for detoxifying Fe^{2+} in *Halobacterium* sp. strain NRC-1. Transcription of DpsA is up-regulated by Fe^{2+}, Co^{2+}, and Zn^{2+} and down-regulated by $Mn^{2+}$and Fe deficiency conditions; the transcription regulator(s) for this mechanism have not been identified.

1.9.2.2 Metabolites

Haloarchaea synthesize EPS as a protective mechanism for survival under adverse conditions such as nutrient starvation, temperature fluctuation, and presence of toxic compounds (Poli *et al.* 2011). Kawakami *et al.* (2007), has reported that *Halobacterium salinarum* CCM 2090 has a Ca^{2+}-dependent aggregation system, where the Ca^{2+} binds to certain aggregation factors present on the cell surface and induces ionic crossbridging between the EPS resulting in aggregation of the haloarchaeal cells. The presence of certain receptor proteins on the cell surface that interact with Ca^{2+} to form cell aggregates/flocs has also been demonstrated. Four haloarchaeal genomes, *Haloquadratum walsbyi, Haloarcula marismortui, Haloterrigena turkmenica, and Halobacterium* sp. strain NRC-1, have been annotated with cbp encoding

the cell surface calcium binding acidic-repeat protein (Bolhuis *et al.* 2006) that has been proposed to be the factor involved in Ca^{2+}-dependent aggregation, although its role in this process remains to be demonstrated. As explained by Kawakami et al. (2007) $Ca^{2+}$is the twentieth element found in the fourth row of the periodic table, which could be replaced by other transition metal ions such as Mn^{2+}, Cr^{2+}, Fe^{2+}, Co^{2+}, Ni^{2+}, Cu^{2+}, and Zn^{2+}, belonging to the same row. The distinctive electronic configuration of these metals may be responsible for these metals substituting Ca^{2+}during aggregate formation. Thus, tolerance to these metals may be mediated through binding with EPS. This was also supported by the observation that there is no aggregation in presence of certain other metals lacking this electronic configuration, such as Mg^{2+} and Sr^{2+} (alkali earth metals), Mo^{2+}, $Cd^{2+}$and Sn^{2+} (fifth period), and $Hg^{2+}$and Pb^{2+} (sixth period). Iron uptake studied in *Halobacterium salinarum* by Hubmatcher *et al.* (2007) revealed the role of xenosiderophores (triacetylfusarinin) for iron uptake that is an energy dependant process either dependent on the respiratory chain or on the existence of the membrane potential. Iron transport across the cell membrane was proposed to include a reductive step that is located at the cell surface or existence of a ligand exchange mechanism at the cell wall or at the membrane.

1.9.2.3 Efflux pumps

Efflux pumps (**Fig 1.11**) are one of the most common mechanisms of resistance to inorganic ions in microbes including archaea.

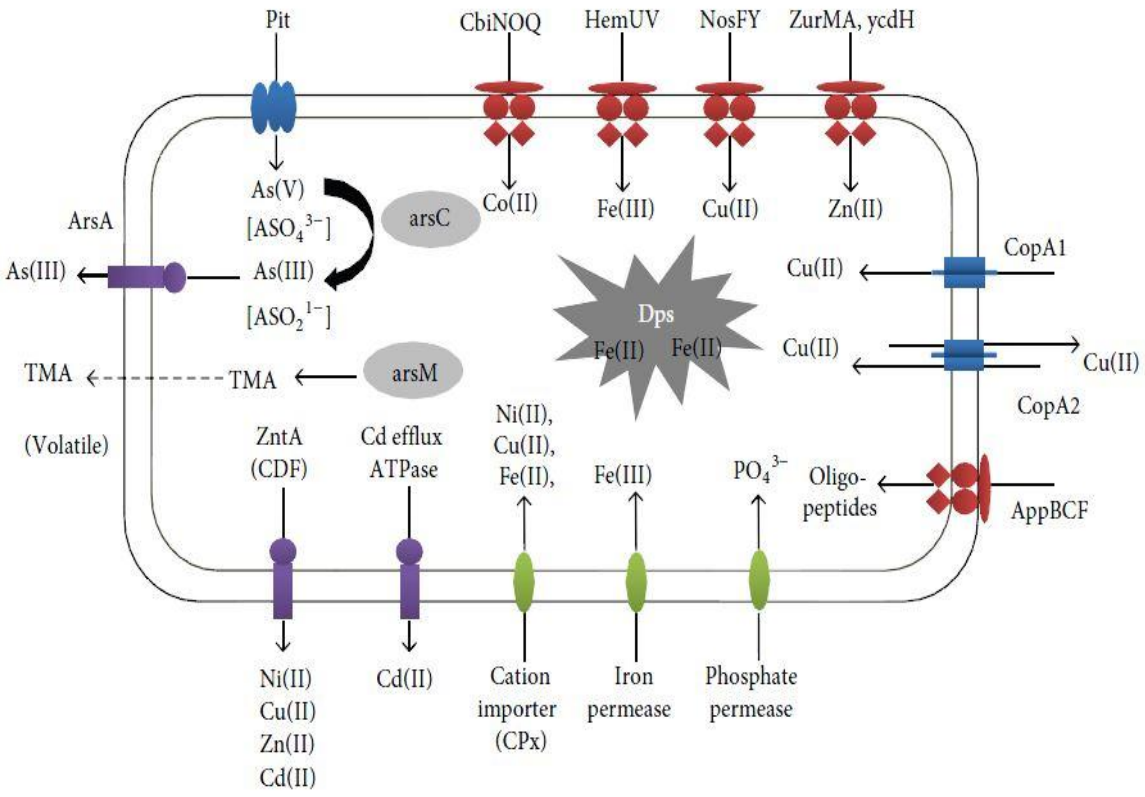

Fig. 1.11. Various metal transporters reported in *Halobacterium* sp. strain NRC-1 (DasSarma *et al*. 2006)

1.9.2.3.1 P_{1B}- Type ATPases

The P_{1B}-type ATPases are a large family of integral membrane proteins driven by ATP hydrolysis (Fagan and Saier 1994). Metal ions such as Mg^{2+}, Ca^{2+}, Cu^{2+}, Ag^{2+}, Zn^{2+}, and Cd^{2+}act as substrates to these ATPases (Saeir 1994). These transporters serve the purpose of uptake of essential elements and efflux of toxic elements, thus conferring resistance to the expelled metal ion (Snavely *et al*. 1989; Neis 2003). In a system level analysis of *Halobacterium* sp. strain *NRC-1,* the functionality and role of such transporters in metal resistance exhibited upregulation of *yvgX*, a P1B-typeATPase, in response to $Cu^{2+}$and Zn^{2+}metal stress (Kaur *et al.* 2006). In bacteria, the *yvgX* family is known to encode two

kinds of CopA proteins, CopA1 and CopA2 (Klein and Lewinson 2011). CopA1 is essential for copper influx and tolerance, while CopA2 is involved in the influx/efflux of Cu and its transport to Cu-containing enzyme cytochrome oxidase c (Klein and Lewinson 2011; Raimunda *et al*. 2011). Archaea is reported to prefer CopA2 over CopA1 (Coombs and Barkay 2005). The *yvgX* of *Halobacterium* sp. strain *NRC-1* was found to be more specific for Cu^{2+} efflux family as the Δ*yvgX* strain was susceptible to Cu^{2+} and not to Zn^{2+}or $Co^{2+}$and therefore belongs to the CopA2 family of proteins. CopA2 is also found in other haloarchaea like *Haloarcula marismortui, Haloarcula hispanica,* and *Haloquadratum walsbyi* (Orell *et al*. 2012). Cu-CPx-type ATPases have also been shown to be involved in uptake of copper to meet cellular demands (Tottey 2001; Solioz and Stoyanov 2003). The *cpx* gene that encodes CPx P1B-type ATPases was found to be down regulated by Fe^{2+}, Cu^{2+}, and Ni^{2+} to avoid influx in *Halobacterium* sp. strain *NRC-1* (Kaur *et al.* 2006). This mechanism of resistance involving the down regulation of uptake systems avoids toxic metal upsurge within the cell.

1.9.2.3.2 Cation diffusion facilitators (CDF) metal transporters

The CDF family of transport proteins is ubiquitously present in all three domains of life (Paulsen and Saier Jr., 1997). CDF function as homo-dimeric antiporters, transporting metal ions against concentration gradients using H^+/K^+ to create electrochemical gradient. Based upon their substrate specificity, CDFs have been classified as Zn^{2+}-CDF, Fe/Zn-CDF, and Mn-CDF (Montanini *et al*. 2007). They usually possess six transmembrane domains (TMDs) with a cytoplasmic N- and C-terminal and a histidine loop of variable length between TMD IV and V (Haney *et al*. 22005; Anton *et al*. 1999). The amphipathic domains TMD I, II, V, and VI are involved in metal transfer and are the most conserved, while the hydrophobic TMDIII and IVare critical for zinc specificity and mutations within these domains alter

substrate specificity (Montanini *et al.* 2007). The genome of *Halobacterium* sp. strain *NRC-1* was annotated with putative CDF Cd $^{2+}$transporter *ZntX*, which confers resistance against Ni^{2+}, Cu^{2+}, and Zn^{2+}besides Cd^{2+} (Kaur *et al.* 2006). The upregulation of *ZntA* in response to heavy metals (Cu and/or Zn) and poor growth of Δ*zntA* strain in presence of Ni^{2+}, Cu^{2+}, Zn^{2+}, and Cd^{2+} have confirmed the role of this transporter in metal resistance (Kaur *et al*.2006). *Haloarcula hispanica* and *Haloarcula marismortui* have also been annotated with *Znt*A for Zn^{2+}transport. A putative CDF family protein has also been found on the chromosome of *Natrialba magadii* for inorganic metal ion transport (Orell *et al.* 2012).

1.9.2.3.3 ATP-Binding Cassette (ABC) transporters

ABC transporters are ubiquitously present in all living forms from bacteria to eukaryotes including archaea. They are involved in various functions such as nutrient uptake (Stumpe and Bakker 1997), oligopeptide and protein transport (Tame et al. 1994), metal extrusion (Salt and Wagner 1993; Rea *et al.* 1998), and drug efflux (Van Veen *et al*. 2000). ABC transporters for sugar and polypeptide have been found in *Haloferax volcanii* (Hartman *et al*. 2010), *Haloarcula marismortui* (Baliga *et al.* 2004), *Halobacterium* sp. *NRC- 1* (Kaur *et al.* 2006), *Natronomonas pharaonis* (Falb *et al*. 2005), and *Haloquadratum walsbyi* (Bolhuis 2006). Many of the ABC transporters are metal ion transporters in *Halobacterium* sp. such as *cbiNOQ* for Co^{2+}transport (Roth *et al.* 1993), *hemUV* for iron uptake (Faraldo-G´omez and Sansom 2003; Schneider and Paoli 2005) , *nosFY* for copper (Zumft *et al.* 1990), and *zurMA* for zinc transport (**Table 1.5**).

1.9.2.4 Metal resistance operons

Most haloarchaea have large plasmids in addition to their genomes (chromosomes) known as minichromosomes/ megaplasmids. These minichromosomes harbor genes for antibiotic resistance or metal resistance that may be essential for haloarchaeal survival (DasSarma *et al.* 2009). The pNRC100, one of the two mini chromosomes of model organism *Halobacterium* sp. strain *NRC-1,* harbors the *arsADRC* gene cluster, responsible for conferring arsenate (As^{5+}) and arsenite (As^{3+})/antimonite (Sb^{3+}) resistance (Kaur *et al.* 2006). As^{5+}can be taken up by the cells through phosphate transporters (pit/pst) and As^{3+} by aquaglycerophorins (glycerophorin membrane transport proteins) (Mukhopadhyay *et al.* 2002) or hexose transporters (Suzuki and Matsushita 1968). $As^{5+}$is then converted to $As^{3+}$by arsenate reductase encoded by *arsC arsA* codes for P1B-type ATPase transporters that help in extrusion of As^{3+}/Sb^{3+} from the cell. *arsR* and *arsD* encode trans-acting repressors of the operon. ArsR and ArsD bind to As^{3+}/Sb^{3+} resulting in expression of the *arsA* and *arsC*.Arsenate reductase encoded by *arsC* is expressed weakly in *Halobacterium* sp. strain *NRC-1,* and therefore deletion of *arsC* and *arsADRC* was found to be ineffective in conferring arsenate sensitivity. The operon *arsADRC* was found to be inducible by arsenite and antimonite. *Halobacterium* sp. strain NRC-1 also harbors both arsA in ars operon on the megaplasmid pNRC100 and arsB on the main chromosome. However, arsB was found to play no role in arsenic resistance in this organism. Thus, it has been proposed that *Halobacterium* sp. strain *NRC*-1 harbors a novel transporter unrelated to with a similar function (Wang *et al.* 2004). In *Halobacterium* sp. strain *NRC-1,* a second arsenite resistance operon, *arsR2M,* is present upstream of *arsADRC* on pNRC100**,** where *arsR2* is constitutively expressed while As^{3+}/Sb^{3+} induce the expression of *arsM* (Wang *et al.* 2004).

The *arsR2* is analogous to *arsR* and *arsM* encodes a putative As^{3+}-methyltransferase very similar to human methyltransferases and S-adenosyl methioninedependent methyltransferases of *Magnetospirillum magnetotacticum.*

ArsM is involved in converting As^{3+} to methylated species like dimethylarsinate (DMA), trimethylarsine oxide (TMAO), or trimethylarsine (TMA) gas (Cullen and Bentley 2005). *arsM* exhibited as increased sensitivity to arsenite but not towards arsenate or antimonite (Wang *et al*. 2004). Thus, two possible mechanisms of As^{3+}resistance have been proposed to be conferred by *arsM*. First, the generation of a concentration gradient results in the movement of methylated arsenite (negatively charged/uncharged) out of the cell. Second, the volatile trimethylarsine formed diffuses out of the cell thus eliminating As^{3+} (Yuan 2008). In *Halobacterium* sp. strain *NRC-1,* the *arsM* gene is present as a part of the *arsR2M* operon involved in arsenite resistance (Wang *et al.* 2004). Mercury resistance in archaea and bacteria is conferred by the *mer* operon involved in detection, regulation, transport, and reduction of Hg^{2+} (Osborn *et al*. 1997).The *merRHAI* operon of thermoacidophilic archaeon *Sulfolobus solfataricus* is the best studied mercury resistance operons in Archaea. The operon is under the control of the regulator MerR, which represses the operon in absence of Hg^{2+} and enhances transcription in its presence. MerH is the metallochaperone with a TRASH (trafficking, resistance, and sensing of heavy metals) domain that binds Hg^{2+}, and MerA is the mercuric reductase for reduction and detoxification to volatile Hg(0) (Schelert *et al.* 2006). Some *mer* operons carry additional *mer* genes, notably *merB*, an organomercurial lyase, that cleaves theC-Hg bonds of organomercurials, and the released Hg^{2+} is reduced to Hg(0) by MerA .Only *Halobacterium* sp. strain *NRC-1* and *Haloterrigena turkmenica* have been annotated with *merA* and *merB* genes, respectively (Osborn *et al.*1997).

1.9.3 Transformations of metals by archaea

Archaeabacteria are reported to impact the mobility of metals in the environment by mode of oxidation or reduction of elements with the aim of energy conservation or detoxification, or indirectly by altering the pH or redox conditions of their environment, which in turn affects metal precipitation or solubilization (Bini 2010). Archaeal species are also able to transform metals into their insoluble forms in bio-mineralization processes that lead to the formation of mineral deposits of the corresponding metal ores. In hyperthermophilic habitats, the presence of magnetite and uraninite has been proposed to be due to the activity of *P. islandicum.* Cell cultures of *P. islandicum* are capable of Fe^{3+} oxide and U^{4+} mineral reduction, leading to the formation of ultrafine magnetite and UO_2, respectively (Kashefi *et al*., 2008a, b). Other metals, including Tc^{7+}, Cr^{6+}, Co^{3+}, Mn^{4+} (Kashefi & Lovley, 2000), and Au^{3+} (Kashefi *et al*., 2001), are also reduced by *P. islandicum* in the presence of hydrogen as the electron donor. *Pyrococcus furiosus* and the archaeal strain 234 are also able to reduce gold, as well as Fe^{3+}, in the presence of H_2 (Kashefi *et al*., 2001). Metal transformations leading to the formation of insoluble precipitates may also result from metabolic processes. For example, anaerobic oxidation of methane (AOM) can be carried out using different electron acceptors, including the metals manganese or iron (Beal *et al*., 2009). However, under such conditions, AOM proceeds at significantly slower rates than those observed for sulfate dependent AOM (Beal *et al.*, 2009).

Marine environments are the most thoroughly studied among aquatic ecosystems concerning archaeal diversity. Archaeal habitats are often encountered in shallow or deep sea anaerobic sediments including free living and endosymbiotic methanogens, hot springs or deep sea hydrothermal vents comprising the methanogens, sulfate reducers and extreme halophiles

and highly saline land locked seas (Silveira *et al*. 2013). The discovery of numerous archaeal species from metal rich environment that contributes to the highly oxidative environment such as mining sites, salterns and metal contaminated soils has enhanced the interest in studying metal resistance in these microbes (Maezato and Blum 2012).

Haloarchaea belonging to the domain Archaea comprises of 36 genera and 129 species identified (Oren 2012). The members of this family are predominant microflora of hypersaline environments such as solar salterns, soda lakes and salt deposits (Tabak *et al*. 2005). These environments serve as avenues for transformation of native microflora into potential metal resistant strains. The factual studies pertaining to haloarchaea and metal ions are limited to only minimum inhibitory concentrations (MIC). Haloarchaea exhibit a high degree of variation in the concentration of metals that they can tolerate (Sehgal and Gibbons 1960; Neito *et al.* 1987; Khandivalli and Furtado 1999). Interestingly, metals like Mn^{2+}, Fe^{2+}, Co^{2+}, Ni^{2+} and Zn^{2+} are found to enhance growth mostly being micronutrients for any biological cell at low concentrations (Kaur *et al.* 2006). However, the formation of metal complexes in the growth medium may determine the true soluble metal concentrations and indeed, the toxicity of some metals are attributed to a metal complex rather than a metal cation (Neito *et al*. 1987). The high chloride ion (Cl^-) content in the hypersaline environment or the growth medium for haloarchaea results in the formation of metal chlorocomplexes (Srivastava and Kowshik 2012). Besides, the toxicity of a metal to microorganism does not have a linear relationship with its concentration and it depends strongly upon chemical speciation (Blust *et al.* 1995). For example, Zn^{2+} and Cu^{2+}, complexation with chloride ions may result in precipitation at high salinities. Therefore, these complexes are not available to micro-organisms for uptake. However, metals such as Hg^{2+}, Ag^{2+}, Fe^{2+}, Co^{2+}, Ni^{2+}, and

Mn^{2+}either form lipophilic soluble chlorocomplexes or weak chloro complexes that dissociate easily and are thus available to organisms for uptake (Srivastava and Kowshik 2012). Hence, while studying metal resistance in haloarchaea, metal speciation and the bioavailability of metals are an indispensable factor that needs to be considered. Metal speciation depends on alkalinity, pH, hardness (presence of Ca/Mg), natural dissolved organic matter, redox potential, and salinity. The metal species determines the solubility, bio-availability, and membrane transport, besides influencing the phenomenon of adsorption, oxidation/reduction, and residence time (Brown *et al.* 2001). Moreover, in order to exert its toxicity, metals need to be imported inside the microbial cell. Cell membrane acts as a barrier for essential as well as for toxic metal ions. Indubitably, unlike eukaryotes, except for few eubacteria like *B. sphaericus*, haloarchaeal members are bestowed with unique cell envelope structure consisting of S-layers comprising protein or often glycoprotein subunits that form a self assembled two dimentional array enclosing the whole cell surface. Depending on species, the S-layers have a thickness between 5 and 25 nm and possess identical pores with 2–8 nm in diameter. S-layers consist of identical protein subunits arranged in monolayers of simple and repetitive hexagonal patterns. Type culture of *Haloferax,* namely *Haloferax volcanni* contain mannosyl- (β 1-4)- galactosyl phosphodolichol, with sulfated and/or phosphorylated dihexosyl phosphodolichol and dolichol phosphate bearing a tetra saccharide comprising of mannose, galactose , rhamnose and hexose with the glucans linked to C_{55} and/or C_{60} dolichol moieties. The monophosphorylated dolichol is observed to have neutral sugars, charge density, which is thought to stabilize the haloarchaeal proteins in the presence of high salt (Madern *et al.* 2000). The proteins and the glycolipids of S-layers possess carboxyl and hydroxyl groups

that are known to bind metal ions such as U, Ni^{2+}, Cu^{2+} and noble metals in *B. sphaericus* JG-A12 (Pollmann and Matys 2007). As far as archaea is concerned, only S –layers of *Methanococcus janaschii* is reported for binding of Fe^{3+}, Pb^{2+} along with EPS for binding of Cu^{2+}, Ca^{2+} and Zn^{2+} (Orange *et al*. 2011). Besides, all haloarchaeal have diphytanyl (C_{20} C_{20}) glycerol ether core lipids with some strains having additional phytanyls ester terpanyl (C_{20} C_{25}) glycerol ether core lipids in their membranes. The phosphoryl groups of the polar heads of the lipid molecules explained the metal fixation by cells of *M. janaschii*. Although the role of membrane transporters in the efflux of metal ions is annotated in haloarchaeal genome, the function of S-layers of haloarchaeal community in metal resistance or uptake is not known. Although as mentioned in earlier paragraphs iron uptake studies in *Halobacterium salinarum* is detailed with respect to its kinetics indicating an energy dependant process suggestive of reduction of Fe at membrane level (Hubmatcher *et al*. 2007), energy independent process/ passive uptake using dead biomass of haloarchaea is not explored. Sorption and biokinetics of metals such as As^{2+}, Zn^{2+}, Cd^{2+}, Ni^{2+}, Al^{3+} and Hg^{2+} by *Halobacterium* s*accharovorum, Hb. salinarium* and *Natronobacterium gregoryi* is investigated by Prakash *et al*. (2012 a,b) in live cells. The use of dead biomass in metal absorption in haloarchaea with unique cell surface properties remains to be explored in detail. Despite the fact that eubacteria and eukaryotes are used as good adsorbents of different metal ions, use of extremely halophilic bacteria has an advantage of being able to withstand salinities of 35 g L^{-1} where eubacterial proteins are known to be salted out (Aharon 2008) hence, making haloarchaeal community a prospective candidate for remediation of waters with high salinities. While examining the efficiency of any adsorbent to sorb metal ions it is important to predict the efficiency of adsorbent –adsorbate interaction. Mechanism of metal ion adsorption can be studied by use

of the mechanistic models which are able not only to represent but also to explain and predict the experimental behavior of adsorption (Pagnanelli *et al*. 2002; Volesky 2007). The Langmuir model (L type, based on monolayer adsorption of solute) and the Freundlich model (F type, developed for heterogeneous surfaces) are the most widely accepted and used in literatures (Volesky 2007). Numerous kinetic models have been suggested to describe the reaction order of adsorption systems based on solution concentration. Kinetic models based on the capacity of the adsorbent have also been presented, such as the Lagergren's first-order equation $\log (q_e - q_t) = \log q_e - k_1 / 2{:}303$ where, q is the amount of adsorbed metal ion on the biosorbent at time t; k_1 is the rate constant of Lagergren first-order biosorption and Ho's second-order expressiom $t/q_t = 1/k_2 q^2_e + t/q_e$ where q_e is the maximum adsorption capacity (mg g^{-1}) and k_2 is the equilibrium rate constant (g mg^{-1} min^{-1}) (Ho 2006). The first-order equation of Lagergren (Lagergren 1898) and the pseudo second-order equation are the most widely used kinetic models to describe the adsorption process in eubacteria and eukarya (Wang and Chen 2009). Thus, the knowledge of unrevealed mechanistic models and kinetic studies of haloarchaeal adsorbent will add the haloarchaeon under study to the list of bioadsorbent widely used.

Table 1.5 Transporters for various metals in haloarchaeal genomes. (Srivastava and Kowshik 2012)

	Cd^{2+} ***(Cd efflux ATPase)***	**Co^{2+}** ***(cbiNOQ)***	**Cu^{2+}** ***(yvgX)***	**Fe^{3+}** ***(hemUV)***	**Zn^{2+}** ***(zurMA)***	**AsO_4^{3-}** ***(arsABC)***	**Mn^{2+}** ***(ycdH)***	**Mo** ***(MoCo)***	**Ni^{2+}** ***(ZntX)***
Halobacterium NRC-1	+	+	+	+	+	+	-	-	-
Haloferax volcanii	-	+	-	+	+	+	+	+	-
Natronomonas pharaonis	+	+	+	+	+	-	+	-	-
Haloarcula marismortui	+	+	+	+	+	+	+	+	-
Haloquadtratum walsbyi	+	+	+	+	+	+	+	-	+
Halorubrum lacusprofundi	-	+	+	+	+	+	+	-	-
Halomicrobium mukohataei	-	+	+	+	+	+	-	-	-
Halorhabdus utahensis	-	+	+	+	+	+	-	-	-
Haloterrigena turkmenica	-	+	-	+	+	+	+	-	-
Haloalkalicoccus jeotgali	-	+	+	+	+	+	-	-	+
Natrialba magadii	+	+	+	+	+	+	+	-	+

AIMS AND SCOPE

Haloarchaea are predominant microflora of hypersaline econiches such as solar saltern, salt lakes, and salt deposits and so on (Zafrilla *et al*. 2010). Urbanisation and industrialisation including mining, agriculture, and waste disposal in coastal countries results in the discharge of effluents containing toxic metal ions into rivers and estuarine econiches (Pereira *et al*. 2012). Saltpans located along the estuary often serve as a sink of these metal toxicants (Chapman and Wang 2001). Moreover, solar salterns are sites where microorganisms thrive and where haloarchaea are predominant (Litchfield and Gillevet, 2002). Microbes are known to interact with metals in the environment, altering their physical and chemical state, with metals and minerals also able to affect microbial growth, activity and survival (Gadd 2010).

Eubacteria are widely studied for their metal resistance abilities such as detoxification, biosorption, bioaccumulation and bioprecipitation (Gadd 2010). However, these consortia of eubacterial microbes are unable to survive harsh environment such as high salinities, temperature, pH etc. the reason being that eubacterial molecules such as proteins are salted out by the presence of 35 g L^{-1} NaCl concentration (Oren 2008). Alternatively, haloarchaea have developed various mechanisms of resistance in order to thrive under metal stress (Kaur *et al.* 2006; Bini 2010). Haloarchaea exhibit a high degree of variation in the concentration of metals that they can tolerate namely Li^{+}, As^{5+}, As^{3+}, Hg^{2+} and Mn^{2+}, Ni^{2+}, Cu^{2+}, Fe^{2+} /Fe^{3+}, Zn^{2+} and Cd^{2+} (Neito *et al*. 1987; Khandivalli and Furtado 1999; Naik and Furtado 2009) Haloarchaeal members are bestowed with unique cell envelope structure consisting of S-layers comprising protein or often glycoprotein subunits that form a self assembled two dimentional array enclosing the whole cell surface and glycerol ether core lipids in their membranes (Asker *et al.* 2002). Hence, with respect to these unique cell envelope properties

of haloarchaea the study of interaction with metal ions such as Fe^{2+}/ Mn^{2+} ions would add to the knowledge of metal – haloarchaea interaction. With these backdrop and the fact that eubacteria and eukaryotes are widely studied for their metal resistance mechanisms with only scarce reports on haloarchaea to resist/tolerate metals, the research work was aimed to study the interaction of haloarchaea with metal ions namely, Fe^{2+} and Mn^{2+} ions.

In the light of the above, the present research study was directed at:

- Evaluating the response of the haloarchaea GUSF-1 and GUFF129 obtained from Haloarchaeal repository, Department of Microbiology, Goa University to metal ions of $Fe^{2+}$and Mn^{2+} in terms of growth, changes in cellular features of the haloarchaeon including the role of genome in metal tolerance
- Unveiling of the mechanism of metal-microbe interaction as sorption, uptake and accumulation
- Characterizing the products of interaction and the formulation of haloarchaeal adsorbent for bioremediation of Fe^{2+} and Mn^{2+} from saline systems.

Chapter 2

Response of Haloarchaea to Fe^{2+} and Mn^{2+} ions and molecular characterization of GUSF-1

Coastal regions are exposed to environmental stress due to increase in urbanization and industrialization (Alagarsamy 2006). Saltpans located along the coast are made by evaporation of estuarine waters entering them which are often vulnerable to metal ions such as Fe^{2+}, Mn^{2+}, Ni^{2+}, Zn^{2+}, Co^{2+}, Pb^{2+}etc., thus, acting as a sink of the metal toxicants. Microorganisms which thrive in this econiche are known for their tolerance or resistance to these metal ions (Pereira *et al.* 2012). However, reports pertaining to response of haloarchaea towards the metal ions iron and manganese and the effect of the physico-chemical factors such as temperature, pH, salinity of the environment which are known to be major parameters influencing the bioavailability of the metal ions to the organism thus, affecting their growth and physiology, are scarce (Kaur *et al.* 2006; Desai and Nayak 2009). The screening of 21 haloarchaeal cultures for their tolerance to Fe^{2+} and Mn^{2+} ions along with the response of selected haloarchaeons GUSF-1 and GUFF 129 to these metal ions and the speciation of same, form the basis of this chapter. The relevant similar methodologies are clubbed together while the results are presented under two sections Section A:- Response of haloarchaeon GUSF-1 and GUFF 129 to Fe^{2+} ions and Section B:- Response of haloarchaeon GUSF-1 and GUFF 129 to Mn^{2+} ions. Finally, this chapter ends with a discussion on the respective sections.

METHODOLOGY

2.1 Screening of haloarchaeal cultures for growth and tolerance to Fe^{2+} and Mn^{2+} in different growth media.

2.1.1 NTYE medium.

To evaluate the maximum tolerance concentration of Fe^{2+}/Mn^{2+} ions, 1 M stock solution of $FeSO_4.7H_2O$/ $MnCl_2.6H_2O$ was prepared separately in sterile distilled water. Aliquots of the stock solution was added to a set of boiling tubes containing 5 ml of NTYE, to a concentration of 0, 0.5, 1, 2, 3, 3.5, 4 mM of Fe^{2+}ions or 0, 1, 5,10, 20, 50, 80, 100, 200 mM of Mn^{2+}ions, respectively. Tubes were incubated on a rotary shaker (Remi, India) at 150 rpm, room temperature (28-30 ºC) and growth or no growth was observed by taking absorbance at A_{600nm} using uv-visible spectrophotometer (UV2401 Shimadzu- Japan) for 8 days.

2.1.2 NGSM medium

Response of haloarchaeal cultures to Fe^{2+} or Mn^{2+}ions was studied by adding aliquots of the metal stock solution to a set of tubes containing 5 ml of NGSM to a concentration of 0, 0.5, 1, 2, 3, 3.5, 4 mM of Fe^{2+} or 0, 1, 10, 20, 50, 80, 100 mM of Mn^{2+} ions, respectively. Tubes were incubated at room temperature (28-30 ºC), 150 rpm for 8 days. Growth or no growth was observed as mentioned in section 2.1.1.

2.2 Effect of physico-chemical factors on growth of select isolates in NGSM with Fe^{2+}/ Mn^{2+}.

2.2.1 Effect of pH on growth of GUSF-1 and GUFF129

Triplicate set of 5 flasks, each having 50 ml of NGSM medium adjusted to pH 3 / 5 / 6 / 7 / 8.5 with 1 N KOH/ 0.1 N HCl/ KH_2PO_4, were inoculated with 5 % v/v final inoculum of 4 d old cultures of GUSF-1 and GUFF129, respectively. Fe^{2+} ($FeSO_4.7H_2O$) /Mn^{2+} ($MnCl_2.6H_2O$) were incorporated to final concentration of 1 mM. Controls devoid of metal and without culture were also maintained.

2.2.2 Effect of % NaCl on growth of GUSF-1 and GUFF129

Triplicate set of 5 flasks, each having 50 ml of NGSM medium and having NaCl concentrations at 0 / 5 / 10 / 15 / 20 / 25 / 30 % adjusted to pH 6.0 with 1 N KOH were inoculated with 5 % v/v final inoculum of 4 d old cultures of GUSF-1and GUFF129, respectively. Fe^{2+} ($FeSO_4.7H_2O$) / Mn^{2+} ($MnCl_2.6H_2O$) were incorporated to final concentration of 1 mM. Controls devoid of metal and without culture were also maintained. Changes in absorbance at $A_{600\,nm}$ over 10 d were recorded.

2.2.3 Effect of temperature on growth

Triplicate sets of 150 ml conical flasks containing 50 ml of sterile NGSM medium were inoculated with 5 % v/v of 4 d old culture broth of GUSF-1/GUFF129 respectively. Fe^{2+} ($FeSO_4.7H_2O$) / Mn^{2+} ($MnCl_2.6H_20$) were incorporated to final concentration of 1 mM. Controls devoid of metal and without culture were also maintained. All the flasks were

incubated either at 30 / 37 / 42 / 55 ºC on a rotary incubator shaker at 150 rpm and monitored at $A_{600\ nm}$ for 10 d.

2.2.4 Detection of Fe^{2+} / Fe^{3+} in cell free culture broth and whole cells grown in Fe^{2+} / Fe^{3+} ($FeSO_4.7H_2O$ / $FeCl_3.6H_2O$)

Aliquot of cell free culture broth grown under optimum conditions of growth, were taken to estimate the amount of Fe^{2+} / Fe^{3+}. For detection in culture broth, the same was taken in 1 ml eppendorf tube and spun at 12000 rpm for 10 min at 4 ºC followed by separation of supernatant and the pellet. Metal inside the cells was checked by lysing the cells with distilled water and monitored colorimetrically by 1, 10- phenanthroline assay for iron. (Vogel 1986). The phenanthroline method was slightly modified by adding 1,10- phenanthroline reagent directly to the test sample solution and measuring the peak maxima at 510 nm for Fe^{2+} content while for Fe^{3+} content hydroxylamine was added followed by phenanthroline reagent to the test sample solution. Appropriate controls were also maintained with Fe^{2+} and without culture to check Fe^{3+} content due to auto oxidation. Quantification results were confirmed by AAS using standard iron solution prepared with 0.1 N nitric acid in the range of 0-10 ppm. Accumulation was also confirmed by determining the dry cell weight of culture grown with/ without Fe^{2+}/ Fe^{3+}.

2.2.5 Detection of Mn^{2+} in growing cells and in cell free culture broth

Aliquot of cell free culture broth grown under optimum conditions of growth was taken to estimate the amount of Mn^{2+}. For detection in culture broth, the same was taken in 1ml eppendorf tube and spun at 12000 rpm for 10 min at 4 ºC followed by separation of supernatant and the pellet. Metal inside the cells was checked by lysing the cells with

distilled water. The contents were then digested with nitric acid (HNO_3) and sulfuric acid (H_2SO_4) (2:1 v/v), separately and were estimated for Mn by AAS. Standard of manganese solution of known concentration for AAS was prepared in 0.1 N nitric acid in the range of 0-15 ppm to obtain the standard graph.

2.3 Evaluation of cellular changes during growth on Fe^{2+}/ Mn^{2+}.

2.3.1 Gram staining

Gram reaction for respective haloarchaeal cultures of both control and respective metal exposed cells was studied using modified Gram staining method for halophiles. (Dussault 1955) An even smear was made on clean grease free, dry, glass slide was air dried and fixed in 2 % acetic acid for 3 min. The fixed smear was air dried and flooded for 30 sec with 2 % crystal violet solution, followed with Gram's iodine for 30 sec. Thereafter, the smear was decolorized with 70 % absolute alcohol and exposed for 1 min to 0.5 % saffranine, washed and air dried. The slide was then observed under oil immersion lens using a phase contrast microscope (Olympus model BX 40).

2.3.2 Scanning Electron Microscopy

The stationary phase cells of both control and respective metal exposed cells were harvested (12000 rpm, 10 min, 4 ^{o}C), washed with 15 % NaCl and then fixed with (2 % v/v) gluteraldehyde prepared in 15 % NaCl for 24 h. The cells were dehydrated with acetone series of 30, 50, 70, 90 and 100 %. The coverslips were then coated and mounted on to gold stubs and observed under scanning electron microscope coupled with energy dispersive X-ray spectrometer (SEM-EDX) (JEOL JSM-5800LV).

2.3.3 Effect on Cell hydrophobicity

Hydrophobicity was determined by measuring the percent affinity to hydrocarbon as employed in the Microbial Adhesion to Hexadecane assay (MATH) of Rosenberg *et al.* (1991). Cultures grown with/without Fe^{2+}/Mn^{2+} were centrifuged at 12000 rpm, 4 ºC for 10 min and the respective pellet were suspended in 15 % saline. The absorbance A600 nm was adjusted to 1.0. The cell suspension was later layered with 0.3 ml of n-hexadecane, mixed thoroughly on a cyclomixer for 1 min and allowed to stand at room temperature for 30 min. On phase separation, the second absorbance was recorded and the percentage hydrophobicity was inferred.

2.3.4 Effect on pigment characteristics

Stationary phase cells of GUSF-1and GUFF129 grown with Fe^{2+}/ Mn^{2+} and without metal ions were harvested individually by centrifugation at 10,000 rpm (REMI, India), washed with 20 % NaCl. The cell pellet was then suspended in acetone and sonicated in a labsonic (Braun, USA) sonicator at 6 sec pulse for 3 min. The acetone fraction containing the pigment was collected by centrifugation and scanned between 300- 800 nm.

2.3.5 Whole cell proteins

2.3.5.1 Preparation of protein lysates

5-15 ml of respective haloarchaeal cultures grown with Fe^{2+}/ Mn^{2+} containing NGSM medium were centrifuged at 12000 rpm, 10 min at 4 ºC and the pellet were washed with 15 % NaCl followed by addition of 50 µl of 2X Laemmli buffer (Laemmli 1970) and boiled for

10 min. Finally 20 µl of dye solution was added and loaded into wells of a SDS polyacrylamide gel and electrophoresis was carried out at constant voltage of 80 volts.

2.3.5.2 Casting of gel for electrophoresis

Glass plates and spacers were cleaned with acetone swab. Teflon spacers were placed on three sides except on top and clipped with clamps. Molten agar (1 % w/v) was poured to seal the three sides from inside. Separating gel mixture was prepared according to Appendix. TEMED and APS were added last, solution swirled gently and poured into the glass plate sandwich to a level of about 4 cm from the top and overlaid with distilled water for uniform setting. After one hour, the water was drained. Stacking gel was prepared according to Appendix and poured on top of the separating gel. Teflon comb was inserted in the gel fluid immediately and allowed to set.

2.3.5.3 Electrophoresis

The comb was removed on setting of the gel, 30 µl of protein samples (30 µg ml^{-1}) were loaded into each well and the lower and upper tanks filled with the running buffer (Appendix). Power supply was set to a constant current of 30 m amps or 80 volts. When the tracking dye reached the bottom of the gel in about 4 h, power supply was turned off. Plates were separated carefully and gel was stained.

2.3.5.4 Staining and destaining

Gel was stained with coomassie blue (Appendix) for twelve hours and destained on a gel rocker using destain solution 1 (Appendix) for 1 h and then transferred into destaining solution 2 (Appendix) till clear bands appeared.

2.3.6 Lipid analysis

100 ml of respective haloarchaeal cultures grown in Fe^{2+}/ Mn^{2+} containing NGSM medium were centrifuged at 12000 rpm and the pellet were washed with 15 % NaCl followed by suspending the respective pellets in 2 ml of 4 M NaCl and extracting with 2:1 v/v of methanol: chloroform for 12 h. The individual extracts were collected by centrifugation and re-extracted with (2:1:0.8 v/v) of methanol:chloroform:water. To respective combined extracts 1:1 chloroform water was added. The chloroform phase was collected and dried in stream of nitrogen and redissolved in minimal amount of chloroform. The individual chloroform extracts of each culture were concentrated and spotted individually on Silica gel G coated glass plates. The plates were developed in solvent system containing (85:22.5:10:4 v/v) chloroform: methanol: acetic acid: water. Glycolipids were visualized by spraying the developed chromatogram with 0.5 % α-naphthol in 50 % methanol-water followed by 5 % H_2SO_4 in ethanol and heating the plates at 100 ºC. Phospholipids visualized using ammonium molybdate sulfuric acid spray.

2.3.7 Cell stability

Respective cultures grown in Fe^{2+}/ Mn^{2+} containing medium were harvested by centrifugation at 12000 rpm, 4 ºC and the cell pellet obtained was suspended in NaCl solution with 20, 15, 12 and 10 % concentration. The initial A_{600} nm was recorded and compared to that with final absorbance after 30 min time interval.

2.4 Evaluation of Siderophore production by haloarchaeal cultures

2.4.1 Estimation for siderophore production in medium without Fe^{2+}/ Mn^{2+}

NGSM medium was decontaminated of iron by adding 8-hydroxyquinoline dissolved in chloroform to ensure complete removal of Fe^{3+} (Schwyne and Neilands 1987). The two cultures were inoculated (5 % v/v) in NGSM medium and incubated at optimum growth conditions. Cultures GUSF-1 and GUFF129 (10-12 days old) were centrifuged at 10000 rpm for 15 min and the culture supernatant were examined for extracellular siderophore production by CAS aasay (Chrome Azurol Sulphonate). CAS assay is based on the fact that a strong chelator (siderophore) removes iron from CAS / iron / detergent complex indicated by change in color from blue to orange after 2-5 min on addition of 1 ml of CAS solution to 1 ml of culture supernatant. For quantative estimation, the percentage of siderophore units were estimated as proportion of CAS color shifted using formula % siderophore units (SU) = [(Ar-As)/Ar] x100 where Ar = A_{630} nm of reference (CAS assay solution + uninoculated media), As = A_{630} nm of test sample (CAS solution + culture supernatant) (Payne 1994).

2.4.2 Estimation for siderophore production in Fe^{2+}/ Mn^{2+} containing medium

Culture supernatant of GUSF-1 and GUFF129 grown in 1 mM of Fe^{2+}/ Mn^{2+} at optimum growth conditions was collected by centrifuging at 10,000 rpm for 15 min, and the culture supernatant were examined for extracellular siderophore production by CAS assay and quantified, respectively as detailed in 2.4.1.

2.5 Determining the role of plasmids in metal tolerance if any

2.5.1 Isolation of Plasmid DNA

Culture GUSF-1 and GUFF129 grown in presence of 1 mM of Fe^{2+}/ Mn^{2+} ions and that without metal were screened for the presence of plasmids. Plasmid mini preps were done, using alkaline lysis method (Birnboim and Doly, 1979; Sambrook *et al*., 1989). 1.5 ml of culture suspension (A_{600nm} = 1.8) was taken in an eppendorf microfuge tube and centrifuged at 10,000 rpm for 10 min at 4 °C. The supernatant was discarded leaving the cell pellet. The pellet was suspended in 100 µl ice-cold glucose EDTA tris-buffer (solution I) (appendix) by vortexing and microfuge tube was subsequently kept in ice for 10 min. 200 µl of freshly prepared solution II (appendix) was added and the contents were mixed by inverting the microfuge tubes rapidly 4-5 times. The microfuge tubes were stored on ice for 10 min. Then 150 µl of ice-cold solution III (appendix) was added and the microfuge tubes were gently vortexed to disperse solution III through the viscous cell lysate. The microfuge tubes were kept on ice for 3-5 min, followed by harvesting at 10,000 rpm for 10 min at 4 °C. The clean supernatant was transferred to a fresh microfuge tube. Plasmid DNA was precipitated with two volumes of cold ethanol at room temperature. The contents were gently mixed by inversion followed by incubation on ice for 2 min. The sample in microfuge tube was centrifuged at 10,000 rpm for 10 min at 4 °C. The supernatant was discarded and the pellet (plasmid DNA) was washed with 70 % (v/v) chilled ethanol at 4 °C. The supernatant was discarded again and the pellet was allowed to dry in air for 10 min by keeping microfuge tubes inverted on tissue paper. The dry pellet containing plasmid DNA was resuspended in appropriate volume (20-50 µl) of TE buffer (pH 8.0) containing DNase free RNase (20 µg ml^{-1}) and stored at -20 °C until needed for agarose gel electrophoresis analysis.

2.5.2 Agarose gel electrophoresis of DNA

Agarose gel electrophoretic analysis of plasmid DNA was performed using horizontal slab gels BG-100, 10x6 cms apparatus (Banglore Genei, Bangalore, India) and 0.8 % agarose (with 0.5 µg ml^{-1} ethidium bromide) prepared in 1X TAE buffer. Electrophoresis was performed using 1X TAE buffer (Appendix) as electrode buffer at constant voltage of 80 V for 90 min in the gel. DNA samples (5 µl) containing plasmid DNA [genomic DNA in case of section 2.6.2.] were mixed with 2 µl 6X DNA loading buffer (Appendix), briefly spun using eppendorf centrifuge and loaded into the wells of agarose gel flooded with 1X TAE buffer. The electrophoresis was done usually until the dye front has travelled 2/3 rd of the agarose gel. The gel was viewed and photographed using a gel documentation system (Alpha-Innotech, USA).

2.6 Identification of haloarchaeon GUSF-1 and GUFF 129

2.6.1 Biochemical characterization

Tentative identification of haloarchaeon GUSF-1 and GUFF129 was done based on biochemical characteristics following Bergey's Manual of Systematic Bacteriology Volume I (2^{nd} edition), The Prokaryotes: Volume IV (2^{nd} edition) (Tindall 1992) and (Hezayen *et al*. 2001) up to genus level.

2.6.2 Molecular characterization of haloarchaeon GUSF-1

2.6.2.1 Extraction of genomic DNA

Genomic DNA of GUSF-1 was extracted using CTAB-NaCl (hexadecyltrimethyl ammonium bromide) method with slight modification. 10-15 ml of culture GUSF-1 was grown in NTYE

medium till it reached A_{600nm}= 1.8. The culture broth was spun at 10,000 rpm at 4 ^{o}C for 10 min. To the pellet obtained, 270 µl of 1 % CTAB-NaCl was added followed by incubation at 37 ^{o}C on rotary shaker at 180 rpm for 30 min. To this 150 µl of 10 % SDS was added followed by incubation at 65 ^{o}C for 10 min. The contents were then centrifuged at 10,000 rpm at 15 ^{o}C for 20 min. The supernatant was collected in a clean eppendorf tube. To this 800 µl of chloroform: isoamyl alcohol (24:1) was added and centrifuged at 8000 rpm, 4 ^{o}C for 15 min. The supernatant was then collected in eppendorf tube followed by addition of 800 µl of phenol: chloroform: isoamyl alcohol. This mixture was again centrifuged at 8000 rpm, 4 ^{o}C for 15 min. The supernatant was collected in another eppendorf tube without disturbing the middle layer. 800 µl of phenol: chloroform: isoamylalcohol was again added followed by spinning at 8000 rpm, 4 ^{o}C for 15 min. The supernatant was collected without disturbing the middle layer. To this 560 µl chilled isopropanol was added and mixed gently by inverting the eppendorfs. The tubes were kept on ice for 15 min followed by centrifuging at 12000 rpm, 4 ^{o}C for 15 min to pellet down the genomic DNA. Isopropanol was carefully removed and tubes were blotted dry. The pellet was washed with 500 µl of chilled ethanol and kept overnight in freezer. The contents were then centrifuged at 12000 rpm, 4 ^{o}C for 15 min. Ethanol was removed by blot drying and the DNA was resuspended in 50 µl 0.1 X TE buffer (Appendix). The DNA was stored at 4 ^{o}C.

2.6.2.2 Agarose gel electrophoresis

Agarose gel electrophoresis of genomic DNA was carried out as described in section **2.5.2**

2.6.2.3 Amplification of genomic DNA by Polymerase Chain Reaction (PCR)

Genomic DNA was amplified using archaeal primers Arch165F 5' TCCGGTTGATCCTGCCAG3' and RPP2 5' CCAAGCTTCTAGACGGTACC TTGTTACGACTT 3'. Each PCR reaction contained 2 U Taq Polymerase, 10X Taq buffer, 2 mM $MgCl_2$, 10mM of dNTP's, 10 µM of each primer and 1 µl of template DNA. Final reaction was made up to 50 µl with ultra pure distilled water. The thermocycler was programmed to initial denaturation at 94 °C for 5 minutes and 10 cycles of denaturation at 94 °C for 1 minute, primer annealing at 56 °C and strand extension at 72 °C for 1 min, followed by 30 cycles of 94 °C for 1 min. This was followed by a final elongation step at 72 °C for 20 min.

The amplified DNA was purified using the PCR purification kit. The 16SrDNA amplicons corresponding to ~ 1.5 kb were then bi- directionally sequenced. The reactions were analysed through automated sequencer (Applied biosystems).

RESULTS

SECTION A: Response of haloarchaeal cultures to Fe^{2+} ions

2.7 Determination of maximum tolerance concentration of Fe^{2+} for haloarchaeal cultures

2.7.1 NTYE medium

Growth of all the cultures was affected by presence of Fe^{2+} ions. In nutrient rich medium, growth of all cultures is not sustained in 3.5 mM and 4 mM of Fe^{2+} except for GUSF-1, GUFF129 and BF5. 15 % growth of cultures is sustained at 3 mM of Fe^{2+} ions of these GUFF129 < GUSF-1 = GUFF168 < BF11 < GUFF 181< BF5 = BF15 = FLF20 (**Fig. 2.1**). With 1 mM increment of Fe^{2+} ions, the decrease in growth is 74.7 % to 52.6 % in case of GUSF-1 and 81.5 % to 47.4 % in case of GUFF129, respectively.

2.7.2 NGSM medium

In NGSM medium all the cultures were resistant to 2 mM of Fe^{2+} ions with growth of 18 % (**Fig. 2.2**). Cultures BF9, GUSF-1 and GUFF129 were resistant to 3 mM of Fe^{2+} with growth of 5 %, 10.5 % and 12.5 % respectively. With 1 mM increment of Fe^{2+} ions, the decrease in growth is 68.42 % to 52.6 % in case of GUSF-1 and 65.8 % to 48.4 % in case of GUFF129, respectively.

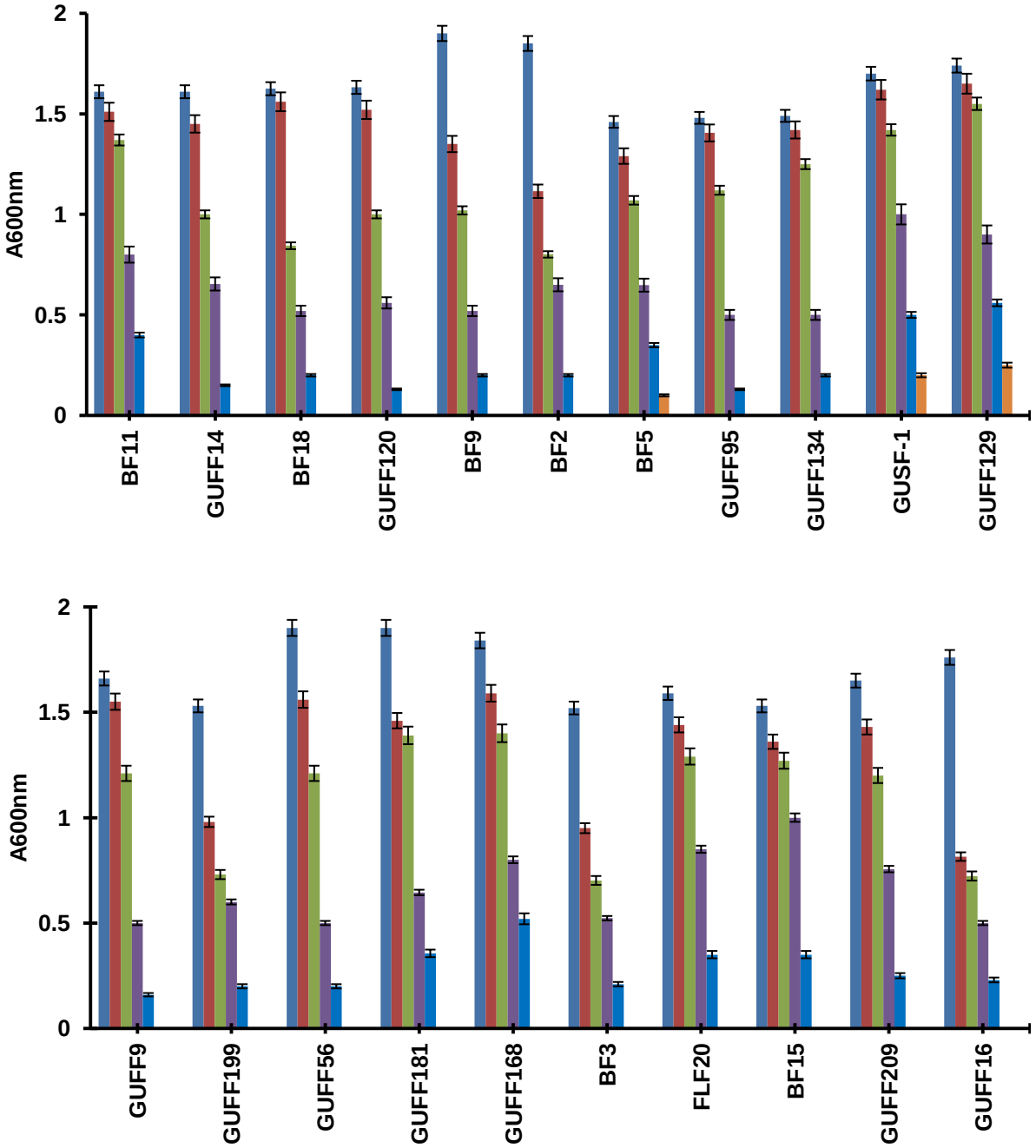

Fig. 2.1 Tolerance of haloarchaeal cultures to different concentrations of Fe^{2+} ions ($FeSO_4.7H_2O$) in NTYE

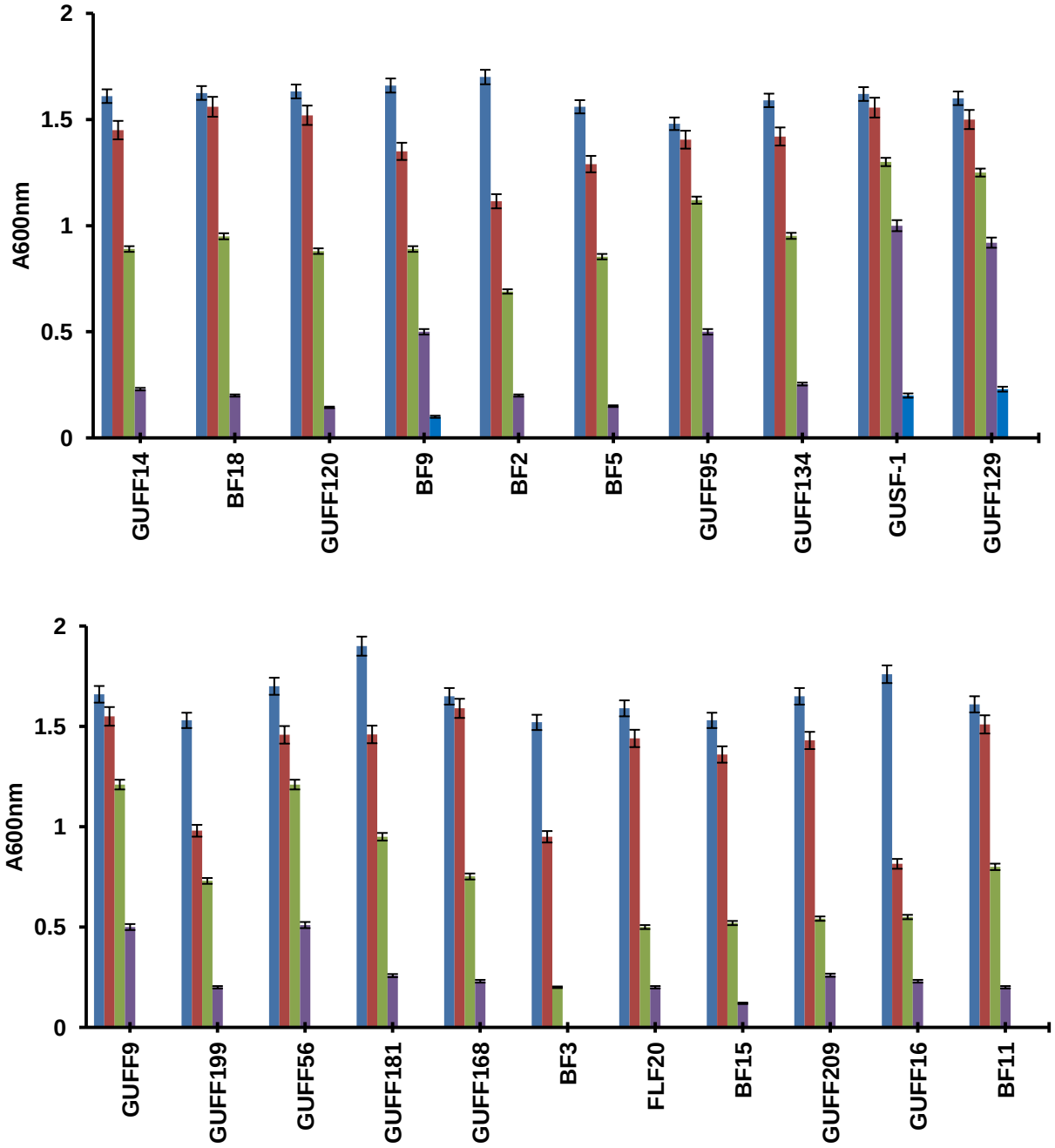

Fig. 2.2 Tolerance of haloarchaeal cultures to different concentrations of Fe^{2+}ions ($FeSO_4.7H_2O$) in NGSM

2.8 Effect of physico-chemical factors on growth of GUSF-1 and GUFF129 in NGSM with Fe^{2+}

2.8.1 Effect of pH on the growth of GUSF-1 and GUFF129

Culture GUSF-1 failed to grow at pH 3.0 and pH 10.0 (**Fig. 2.3a**). At pH 5.0 GUSF-1 grew with growth rate of $3.12x10^3$ gen h^{-1} with a doubling time of 320 min gen^{-1}. At pH 6.0, the growth rate was $2.94x10^2$ gen $h^{-1}$with a doubling time of 33.94 min gen^{-1}. At pH 7.0, the growth rate was 1.9 $x10^2$ gen $h^{-1}$with a doubling time of 51.06 min gen^{-1}. At pH 8.5 the growth rate was 7.65 x 10^3 gen $h^{-1}$with a doubling time of 130.6 min gen^{-1}.

In Fe^{2+}, containing medium GUSF-1 failed to grow at pH 3.0 and pH 10.0 (**Fig. 2.3b**). At pH 5.0 GUSF-1 grew with growth rate of 5.2 $x10^3$ gen h^{-1} with a doubling time of 192 min gen^{-1}. At pH 6.0, the growth rate was 2.08 $x10^2$ gen $h^{-1}$with a doubling time of 47.9 min gen-1. At pH 7.0, the growth rate was 2.79 $x10^2$ gen $h^{-1}$with a doubling time of 35.8 min gen^{-1}. At pH 8.5 the growth rate was 9 x 10^3 gen h^{-1} with a doubling time of 110.6 min gen^{-1}.

As depicted in **Fig. 2.4a** GUFF-129 failed to show prominent growth at pH 3.0 and pH 10.0 with turbidity of only 0.09, respectively. . At pH 5.0 GUFF-129 grew with growth rate of 7.27 $x10^3$ gen h^{-1} with a doubling time of 137.53 min gen^{-1}. At pH 6.0, the growth rate was 1.8 $x10^2$ with a doubling time of 52.82 min gen^{-1}. At pH 7.0, the growth rate was 1.88 $x10^2$ with a doubling time of 52.9 min gen^{-1}. At pH 8.5 the growth rate was 3.1x 10^2 with a doubling time of 110.6 min gen^{-1}.

As observed in **Fig. 2.4b** in Fe^{2+} containing medium, culture GUFF-129 failed to grow at pH 10.0 while at pH 3.0 showed a turbidity of only 0.2 and growth rate of $2.78x10^4$ gen h^{-1} with doubling time of 3600 min gen^{-1} . At pH 5.0, GUFF-129 grew with growth rate of $7.2x10^3$

gen h^{-1} with a doubling time of 137.5 min gen^{-1}. At pH 6.0, the growth rate was $6.94x10^3$ gen h^{-1} with a doubling time of 144.57 min gen^{-1}. At pH 7.0, the growth rate was $1.56 x10^2$ gen h^{-1} with a doubling time of 64 min gen^{-1}. At pH 8.5 the growth rate was 1.04×10^2 gen h^{-1} with a doubling time of 96 min gen^{-1}.

2.8.2 Effect of % NaCl on the growth of GUSF-1 and GUFF129

As seen in **Fig. 2.3c** GUSF-1 in fail to grow at 0 % salinity. In TYE with 5% salinity, it grew with a growth rate of $8.33x\ 10^4$ gen h^{-1} with a doubling time of 1200 min gen^{-1} while at 10 % salinity culture grew with a growth rate of $3x\ 10^3$ gen $h^{-1}$with a doubling time of 333.3 min gen^{-1}. At 15 % salinity GUSF-1 had a growth rate of 6×10^3 gen $h^{-1}$with a doubling time of 150 min gen^{-1}. At 20 % and 25 % salinity culture grew with growth rate 2.29×10^2 gen h^{-1} with a doubling time of 43.60 min gen^{-1} respectively. At 30 % salinity GUSF-1 had a growth rate of $1x\ 10^2$ gen h^{-1} with a doubling time of 97.64 min gen^{-1}.

In Fe^{2+} containing medium, GUSF-1 in fail to grow at 0 % and 5 % salinity **(Fig. 2.3d).** At 10 % salinity culture grew with a growth rate of 1.1×10^2 gen $h^{-1}$with a doubling time of 84.5 min gen^{-1}. At 15 % salinity GUSF-1 had a growth rate of 1.3×10^2 gen $h^{-1}$with a doubling time of 72 min gen^{-1}. At 20 % and 25 % salinity culture grew with growth rate 2.5×10^2 gen $h^{-1}$with a doubling time of 40 min $gen^{-1}$and 2.29×10^2 gen h^{-1} respectively. At 30 % salinity GUSF-1 had a growth rate of $9.4x\ 10^3$ gen h^{-1} with a doubling time of 106.35 min gen^{-1}.

GUFF-129 failed to grow at 0 % salinity (**Fig. 2.4c**). In TYE with 5% salinity, it grew with a growth rate of $5x\ 10^3$ gen h^{-1} with a doubling time of 200 min gen^{-1} while at 10 % salinity culture grew with a growth rate of 1.25×10^3 gen $h^{-1}$with a doubling time of 79.7 min gen^{-1}. At 15 % salinity GUFF-129 had a growth rate of 2.2×10^2 gen h^{-1} with a doubling time of

44.1 m gen^{-1}. At 20, 25 and 30 % salinity culture grew with growth rate 2.5 x 10^2 gen $h^{-1}$with a doubling time of 39.93 min gen^{-1} respectively.

In Fe^{2+} containing medium also GUFF-129 failed to grow at 0 % (**Fig. 2.4d**). At 5 % and 10 % salinity culture grew with a growth rate of 5.1 x 10^3 gen h^{-1} and 9.3x10^3 gen h^{-1} with a doubling time of 192.77 min gen^{-1} and 106.6 min gen^{-1}. At 15 % salinity GUFF-129 had a growth rate of 1.33 x 10^2 gen $h^{-1}$with a doubling time of 74.83 min gen^{-1}. At 20 % and 25 % salinity culture grew with growth rate 1.25 x 10^2 gen h^{-1} and 1.66 x 10^2 gen $h^{-1}$with a doubling time of 79.7 min $gen^{-1}$and 60 min gen^{-1}respectively. At 30 % salinity GUFF-129 had a growth rate of 1.4x 10^2 gen h^{-1} with a doubling time of 70.2 min gen^{-1}.

2.8.3 Effect of temperature on the growth of GUSF-1 and GUFF129

Culture GUSF-1 grew at 20 ºC showed a turbidity of only 0.22 (**Fig. 2.3e**). At 30 ºC, the growth rate was 2.9x10^2 gen $h^{-1}$with a doubling time of 34.48 min gen^{-1}. At 42 ºC, the growth rate was 1.129 x10^2 gen $h^{-1}$with a doubling time 88.56 min gen^{-1}. At 50 ºC and 60 ºC, the growth rate was 7.5 x 10^3 gen $h^{-1}$and 2.056 x10^3 gen $h^{-1}$with a doubling time of 131.86 min gen^{-1} and 486 min gen^{-1} respectively.

In Fe^{2+} containing medium also, GUSF-1 grew at 20 ºC exhibiting a turbidity of 0.22 (**Fig. 2.3f**). At 30 ºC, the growth rate was 2.79x10^2 gen $h^{-1}$with a doubling time of 35.8 min gen^{-1}. At 42 ºC, the growth rate was 2.29 x10^2 gen $h^{-1}$with a doubling time 43.63 min gen^{-1}. At 50 ºC and 60 ºC, the growth rate was 7.5 x 10^3 gen $h^{-1}$and 2.075 x 10^3 gen $h^{-1}$with a doubling time of 131.86 min gen^{-1} and 363.63 min gen^{-1}respectively.

Culture GUFF-129 showed a turbidity of only 0.08 at 20 ºC (**Fig. 2.4e**). At 30 ºC, the growth rate was 3.4x10^2 gen h^{-1} with a doubling time of 28.8 min gen^{-1}. At 42 ºC, the growth rate

was 2.2 x10^2 gen h^{-1} with a doubling time 44.11 min gen^{-1}. At 50 ºC and 60 ºC, the growth rate was 2.5 x 10^2 gen $h^{-1}$and 1.26 x10^2 with a doubling time of 39.93 min gen^{-1} and 79.2 min gen^{-1} respectively.

As observed in **Fig 2.4f** in Fe^{2+} containing medium, GUFF-129 grew at 20 ºC, exhibiting a turbidity of 0.22 with a growth rate of 2.8 x 10^3 gen h^{-1} with a doubling time of 343.3 min gen^{-1}. At 30 ºC, the growth rate was 3.6 x10^2 gen h^{-1} with a doubling time of 27.39 m gen^{-1}. At 42 ºC, the growth rate was 2.26 x10^2 gen $h^{-1}$with a doubling time 44.11 min gen^{-1}. At 50 ºC and 60 ºC, the growth rate was 2.29 x 10^2 gen $h^{-1}$and 1.5 x 10^2 with a doubling time of 43.55 min gen^{-1} and 65.57 min gen^{-1} respectively.

2.8.4 Monitoring of Fe^{2+} / Fe^{3+} inside the growing cells of haloarchaea and culture broth.

As depicted in **Fig. 2.5a** the culture GUSF-1grew with growth rate of 2 x 10^2 gen h^{-1}in NGSM medium, pH6 incubated at 30 ºC with a doubling time of 48 min gen^{-1} while in presence of Fe^{2+} in NGSM medium the culture grew with a growth rate of 1.8 x 10^2 gen h^{-1} having a doubling time of 53.3 min gen^{-1}. At this growth rate, there was a concomitant increase in the $Fe^{2+}$and Fe^{3+} inside the cells by fourth day exhibiting accumulation of 34.6 mg L^{-1} of Fe^{2+} and 15 mg L^{-1} of Fe^{3+} inside the growing cells by ninth day. The Fe^{2+} concentration in culture broth declined from 55 mg L^{-1} to 5 mg L^{-1} by ninth day. Control kept without culture however failed to show such alterations ruling out the possibility of auto conversion.

Similarly, the culture GUFF129 grew with a growth rate of 8.5 x 10^3 gen h^{-1} with a doubling time of 117.6 min gen^{-1}in NGSM medium, pH 6 incubated at 30 ºC while in presence of Fe^{2+}

in NGSM medium with a growth rate of 1.25 x 10^2 gen h^{-1} with a doubling time of 79.7 min gen^{-1} (**Fig. 2.6a**). There was simultaneous increase of Fe^{2+} and Fe^{3+} inside the cells by fifth day and accumulated 31.7 mg L^{-1} of Fe^{2+} and 15.8 mg L^{-1} of Fe^{3+} by tenth day. There was decrease in Fe^{2+} in culture broth from 55 mg L^{-1} to 6 mg L^{-1} by eleventh day. Interestingly, GUSF-1(**Fig. 2.5b**) and GUFF129 (**Fig. 2.6b**) showed similar growth profile in NGSM containing Fe^{3+} having a growth rate of 1.6x 10^2 gen h^{-1} with a doubling time of 59.6 min gen^{-1}. Both the cultures accumulated 30 and 28.3 mg L^{-1} of Fe^{2+} and 10 mg L^{-1} as Fe^{3+} inside the growing cells by tenth day, respectively. There was sharp decrease in Fe^{3+} concentration to 13.8 and 16.5 mg L^{-1} in culture broth by sixth day. The accumulation of metal inside the cells was confirmed by AAS and increase in the dry weight of the cell pellets (**Table 2.1**)

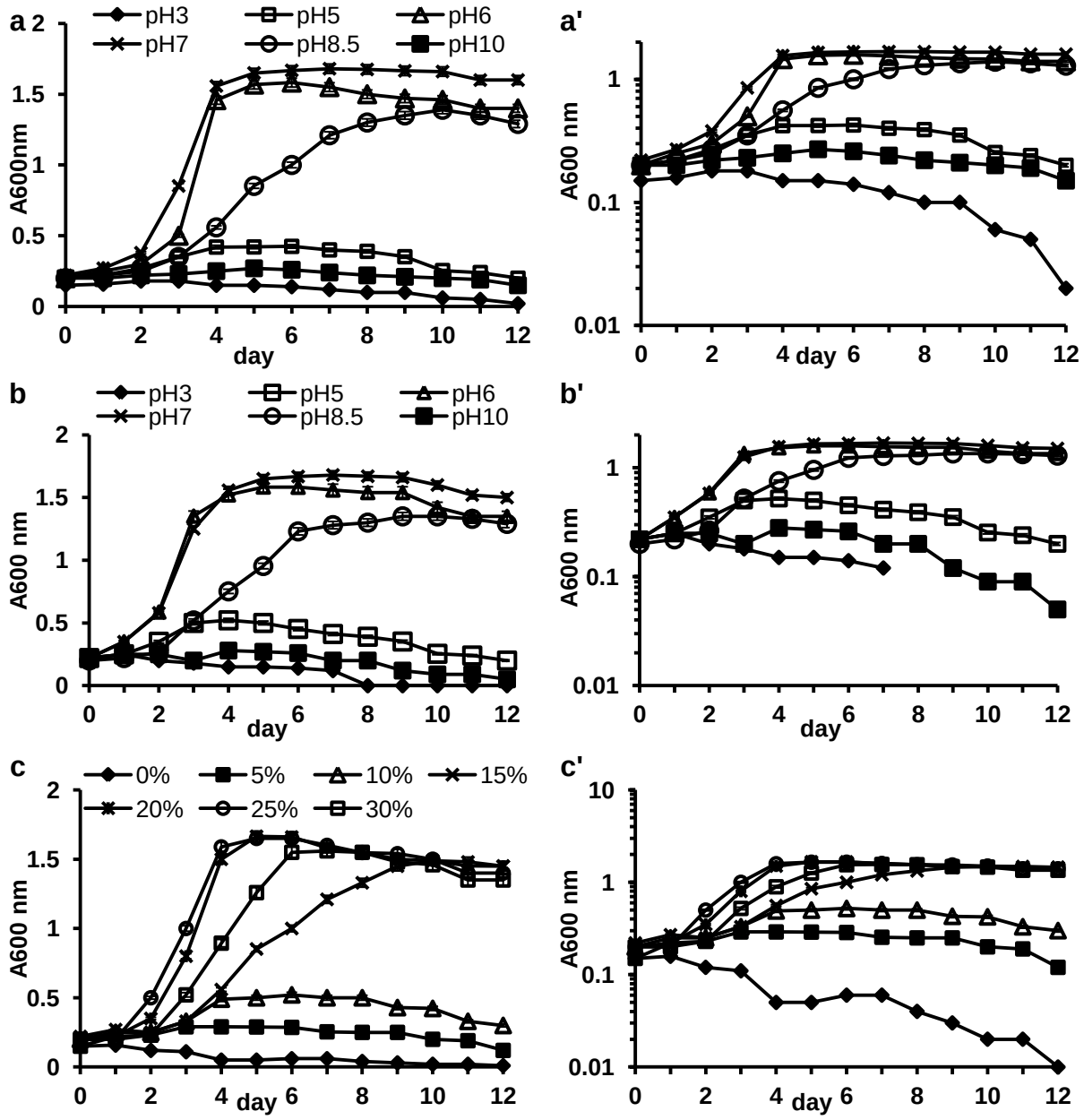

Fig. 2.3 Growth profile of GUSF-1 in mineral salts medium with glucose as carbon source **(a, a')** effect of pH **(b, b')** effect of pH on growth in Fe^{2+} containing medium **(c, c')** effect of salinity; **(')** represents growth profile plotted on log scale

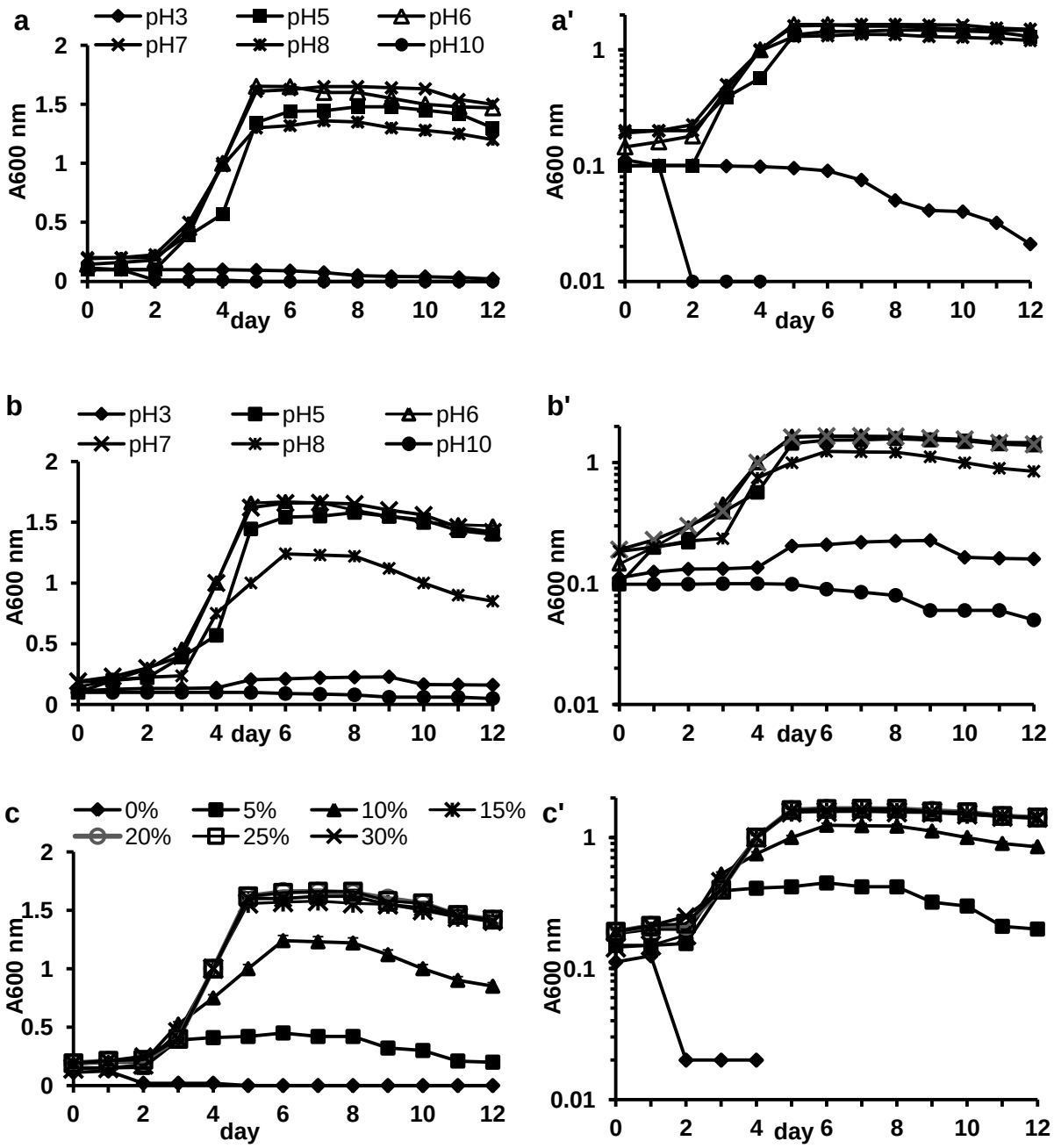

Fig 2.4. Growth profile of GUFF129 in mineral salts medium medium **(a, a')** effect of pH **(b, b')** effect of pH on growth in Fe^{2+} containing medium **(c, c')** effect of different salinity; **(')** represents growth profile plotted on log scale

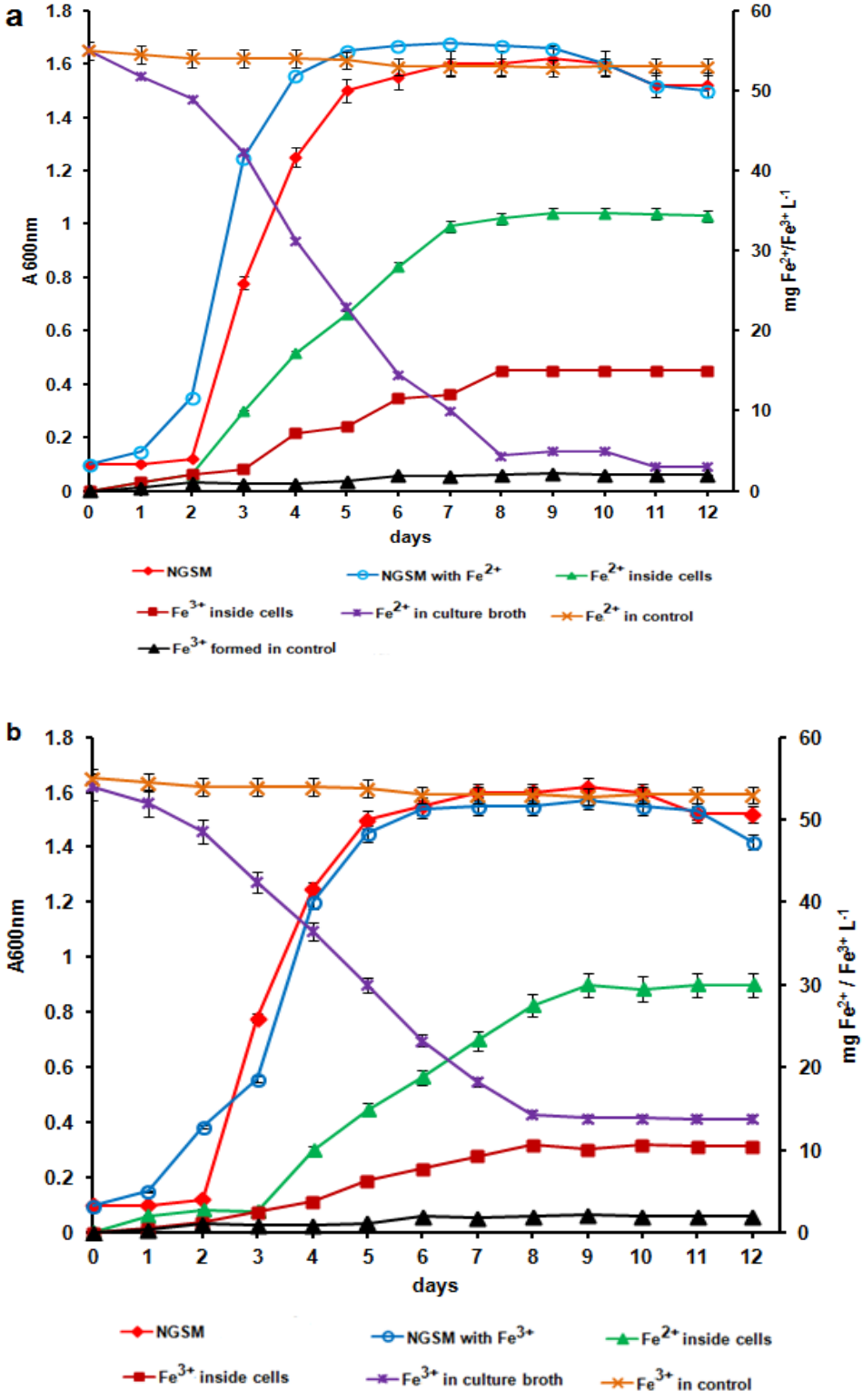

Fig. 2.5 Effect of Fe^{+2}/Fe^{+3} on growth of GUSF -1 in **(a)** Fe^{+2} containing medium **(b)** Fe^{+3} containing NGSM

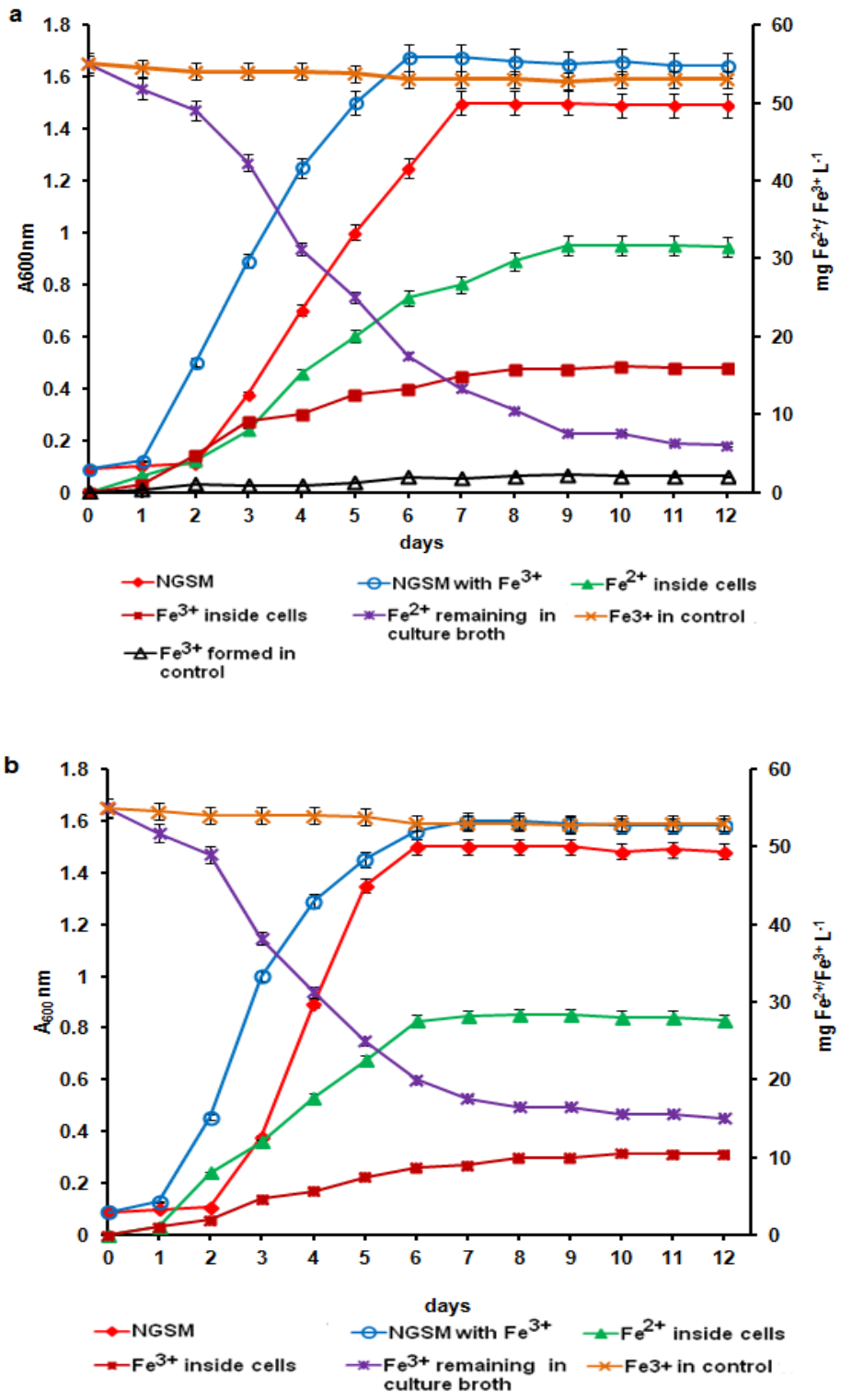

Fig. 2.6 Effect of Fe^{+2}/Fe^{+3} on growth of GUFF129 in **(a)** Fe^{+2} containing medium **(b)** Fe^{+3} containing NGSM

Table 2.1 Dry weight of biomass of culture grown with Fe^{2+}/ Fe^{3+}

Culture	Biomass dry weight (µg ml^{-1})
GUSF-1	64
GUSF-1 with Fe^{2+} / Fe^{3+}	81.8 / 81.6
GUFF129	69.7
GUFF129 with Fe^{2+} / Fe^{3+}	100 / 100.4

2.9 Evaluation of cellular changes during growth on Fe^{2+}

2.9.1 Gram character

The gram stained smears revealed cells of GUSF-1 as gram negative cocci (**Fig. 2.7a**). Interestingly, culture grown with Fe^{2+} disclosed a gram reaction to be positive coccobacilli (**Fig. 2.7b**). GUFF 129 displayed gram negative cocci morphology (**Fig. 2.7c**) with no change in morphology of cells grown with Fe^{2+} (**Fig. 2.7d**) but exhibited a gram positive reaction.

2.9.2 SEM

The SEM revealed the cell morphology of GUSF-1 to be cup shaped when grown without Fe^{2+} (**Fig. 2.8a**). A significant change in cell morphological characteristics were observed in Fe^{2+} grown cells of GUSF-1wherein the cells became elongated and extensively clumped/aggregated in **Fig. 2.8b** . GUFF129 showed a coccoidal morphology when grown in absence of metal in growth medium while the cells exhibited barely any variation in shape when grown in Fe^{2+} containing medium but showed dividing cells. (**Fig. 2.8c, d**).

2.9.3 Cell hydrophobicity

Cultures GUSF-1 and GUFF129 grown in presence of Fe^{2+} showed increase in their cell hydrophobicity as compared to those grown without (**Table 2.2**)

2.9.4 Pigment

The acetone extract of pigment from cell mass of GUSF-1 revealed absorption maxima at 350, 370, 389, 426, 468, 494 and 528 nm (**Fig. 2.9a**) that corresponded to phytofluenes(350 and 370 nm), retinal (389 nm), β- carotene (426 nm), lycopene (468 nm) and bacterioruberin (494 and 528 nm) respectively.

As seen in **Fig. 2.9b** spectral scan of cell extract grown with Fe^{+2} indicated appearance of six peaks of absorption maxima 528 and 494 nm corresponding to bacterioruberin, 468 nm corresponding to lycopene, 388 nm of retinal component. These peaks matched with that of GUSF-1but reduced in their intensities with the peaks observed for pigment of cells grown without Fe^{2+}. An additional peak at 345 nm was also observed for cells grown with Fe^{2+} along with disappearance of peaks at 350 and 370 nm corresponding to phytofluenes. As observed in **Fig. 2.9c** the spectral scan of cell extract of culture grown in Fe^{3+} containing medium indicated the appearance of peaks at 312.5, 349 nm accompanied with 388, 468, 494, 528 nm peaks corresponding to retinal, lycopene and bacterioruberin, respectively.

In case of culture GUFF129 peaks of absorption maxima 321, 370, 388, 470, 495, 528 nm are observed. (**Fig. 2.9d**) Spectral scan of cell extract of those grown with Fe^{+2} indicated the presence of peaks at 370, 388, 470, 496, 529 nm with an additional peak at 353 and 307 nm and disappearance of 321 while that grown in Fe^{3+} indicated the presence of 370, 388, 469.5,

495.5, 529 nm peaks corresponding to phytofluenes, retinal, lycopenes and bacterioruberins, respectively (**Fig. 2.9e, f**).

2.9.5 Proteins

The whole cell protein profiles displayed in **Fig. 2.10**, resolved protein band at 52 kDa, 50 kDa, 40 kDa, 42 kDa, 22 kDa, 17.5 kDa and the upregulation of protein bands at 40 kDa, 42 kDa, 18 kDa and induction of 30 kDa and 20 kDa proteins in GUSF-1 grown in presence of Fe^{2+}.GUFF129 showed presence of proteins bands at 96.8 kDa, 77kDa, 71.2 kDa, 55 kDa, 50 kDa, 35 kDa, 31.2 kDa and 25.8 kDa and induction of protein bands at 70 kDa, 64 kDa and 25.8 kDa.

2.9.6 Lipids

Thin layer chromatograms of lipids extracts of GUSF-1 showed spots corresponding to glycolipids at R_f of 0.3, 0.5 and at R_f of 0.7, 0.8 corresponding to phospholipids (**Fig. 2.11a, b**). The lipids of cells grown in Fe^{2+} had a R_f of 0.44 corresponding to glycolipid with while appearance of phospholipid spots with R_f value of 0.33, 0.88. TLC of archaeol lipids extracted from GUFF129 displayed appearance of glycolipid spots with R_f value of 0.25, 0.5 and phospholipids with R_f value of 0.6, 0.8. The lipids of culture grown in Fe^{2+} containing medium showed a spot of glycolipid with R_f value of 0.34 while phospholipid with R_f value of 0.74 (**Fig. 2.11c, d**) .

2.9.7 Cell stability

GUSF-1and GUFF129 grown in presence of Fe^{2+}were resistant to lysis at decreased salinities of 12 % as compared to that grown in absence of metal. (**Fig. 2.12a,b**)

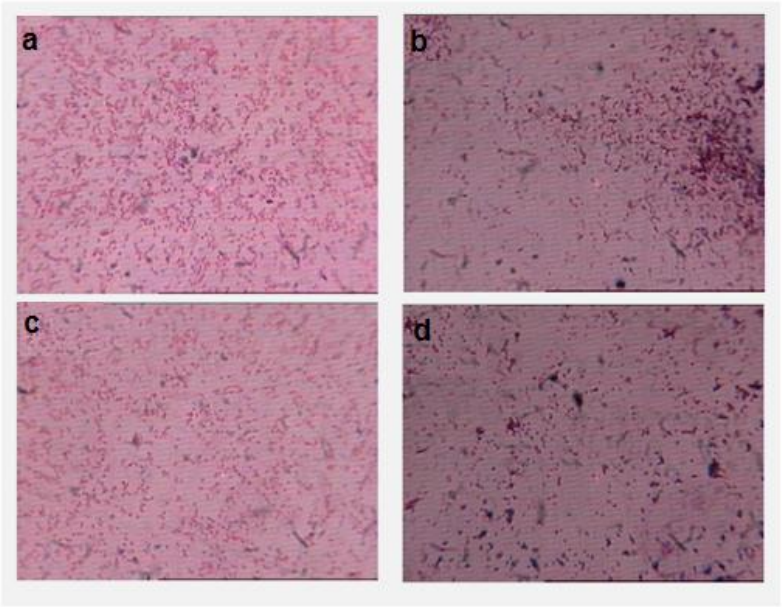

Fig. 2.7 Micrographs of gram stained: **(a)** GUSF-1grown without Fe^{2+} **(b)** with Fe^{2+} **(c)** GUFF129 grown without Fe^{2+} **(d)** with Fe^{2+}

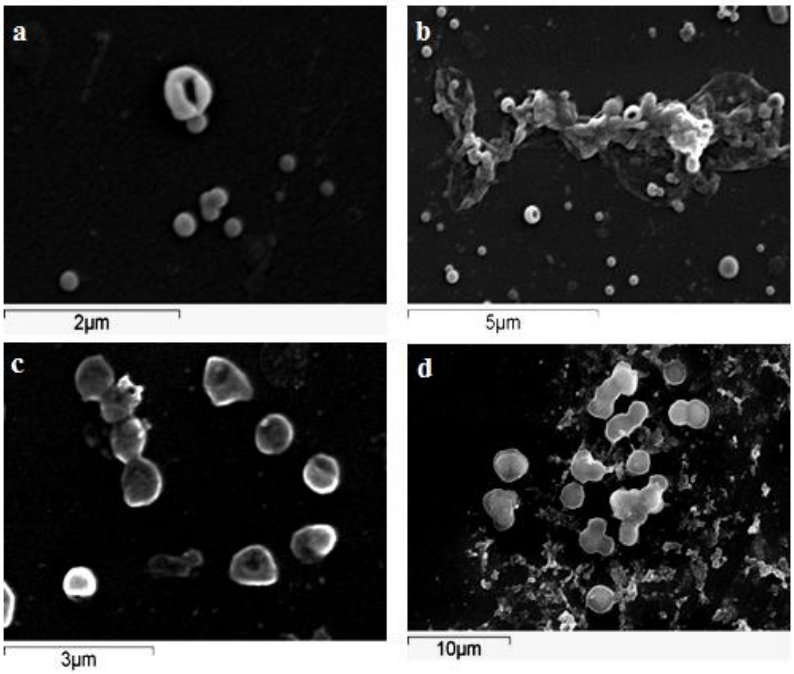

Fig. 2.8 SEM micrographs of **(a)** GUSF-1 grown without Fe^{2+} **(b)** with Fe^{2+} **(c)** GUFF129 grown without Fe^{2+} **(d)** with Fe^{2+}

Table 2.2. Cell hydrophobicity of cultures grown without / with Fe^{2+}

culture	% adherence of cells to hexadecane
GUSF-1	5
GUSF-1 with Fe^{2+}/ Fe^{3+}	65 / 62
GUFF129	8.5
GUFF129 with Fe^{2+}/Fe^{3+}	55

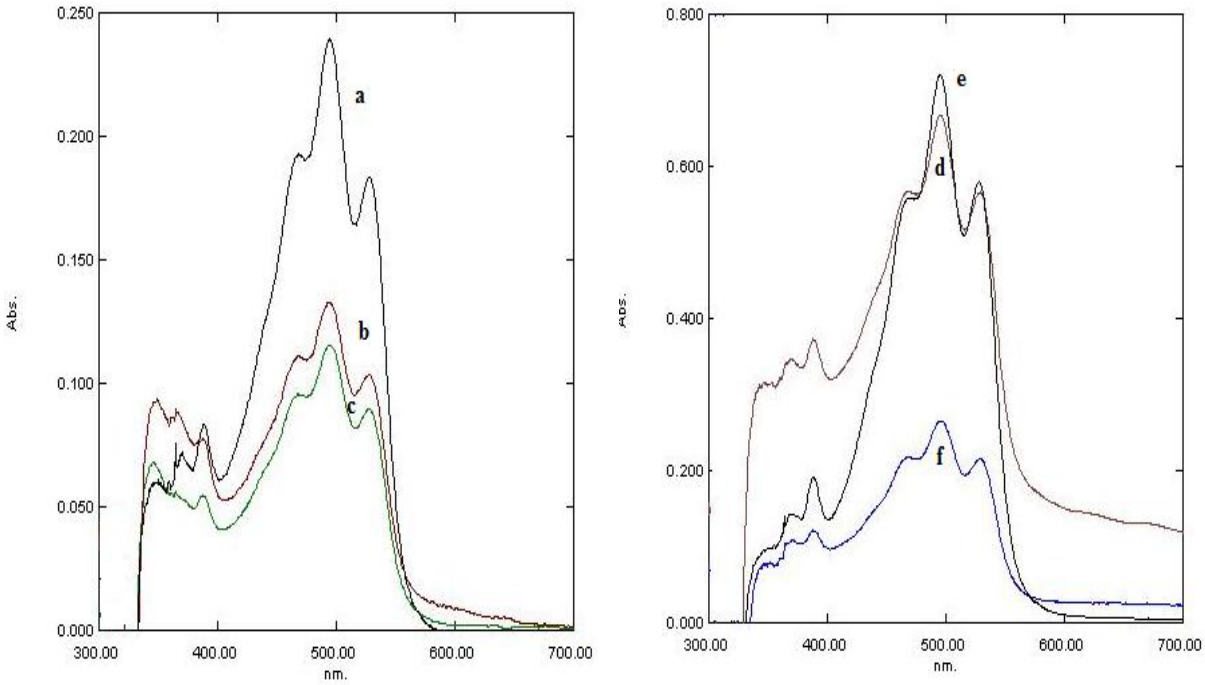

Fig. 2.9 Pigment profile of acetone extracts of GUSF-1 **(a)** grown without metal **(b)** grown in Fe^{2+} containing medium **(c)** Fe^{3+} containing medium and GUFF129 **(d)** grown without metal **(e)** grown in Fe^{2+} containing medium **(f)** Fe^{3+} containing medium.

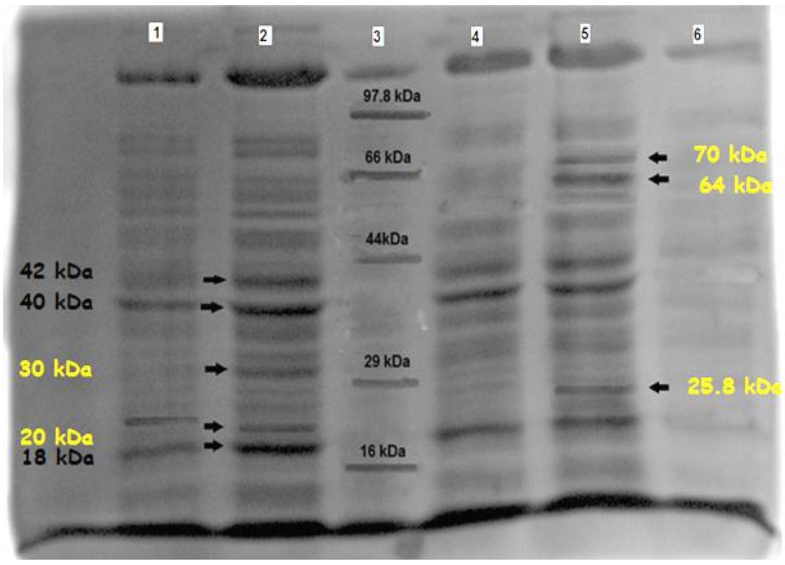

Fig. 2.10. SDS-PAGE profile of whole cells of GUSF-1 and GUFF129 grown with/ without $Fe^{2+:}$ **Lane 1**- GUSF-1; **Lane 2**- GUSF-1 Fe^{2+}; **Lane 3**- Standard Marker; **Lane 4**- GUFF129; **Lane 5**- GUFF129 with Fe^{2+}

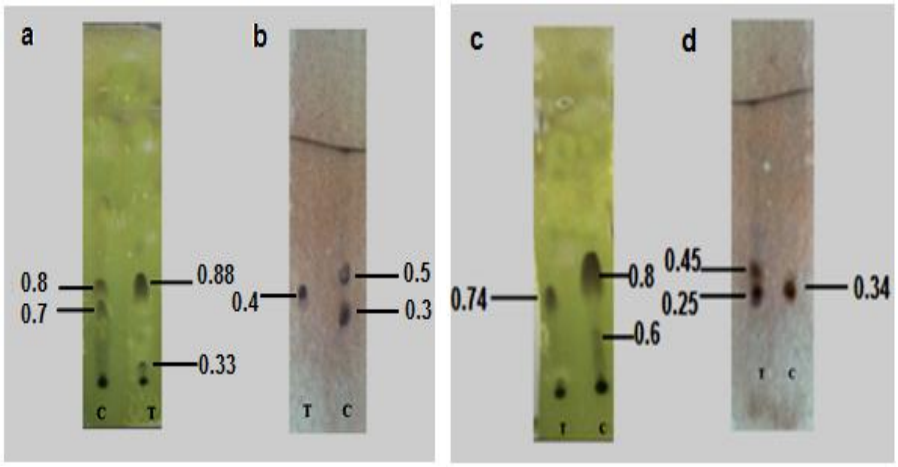

Fig.2.11. Thin layer chromatogram of archaeol lipids of **(a)** GUSF-1 phosholipid (**b)** glycolipid profile **(c)** GUFF129 phospholipid **(d)** glycolipid profile. (T= with Fe^{2+}; C= without Fe^{2+}). The chromatogram was developed once with chloroform: methanol: acetic acid: water (85:22.5:10:4 v/v) and was sprayed for glycolipids and phospholipids, respectively.

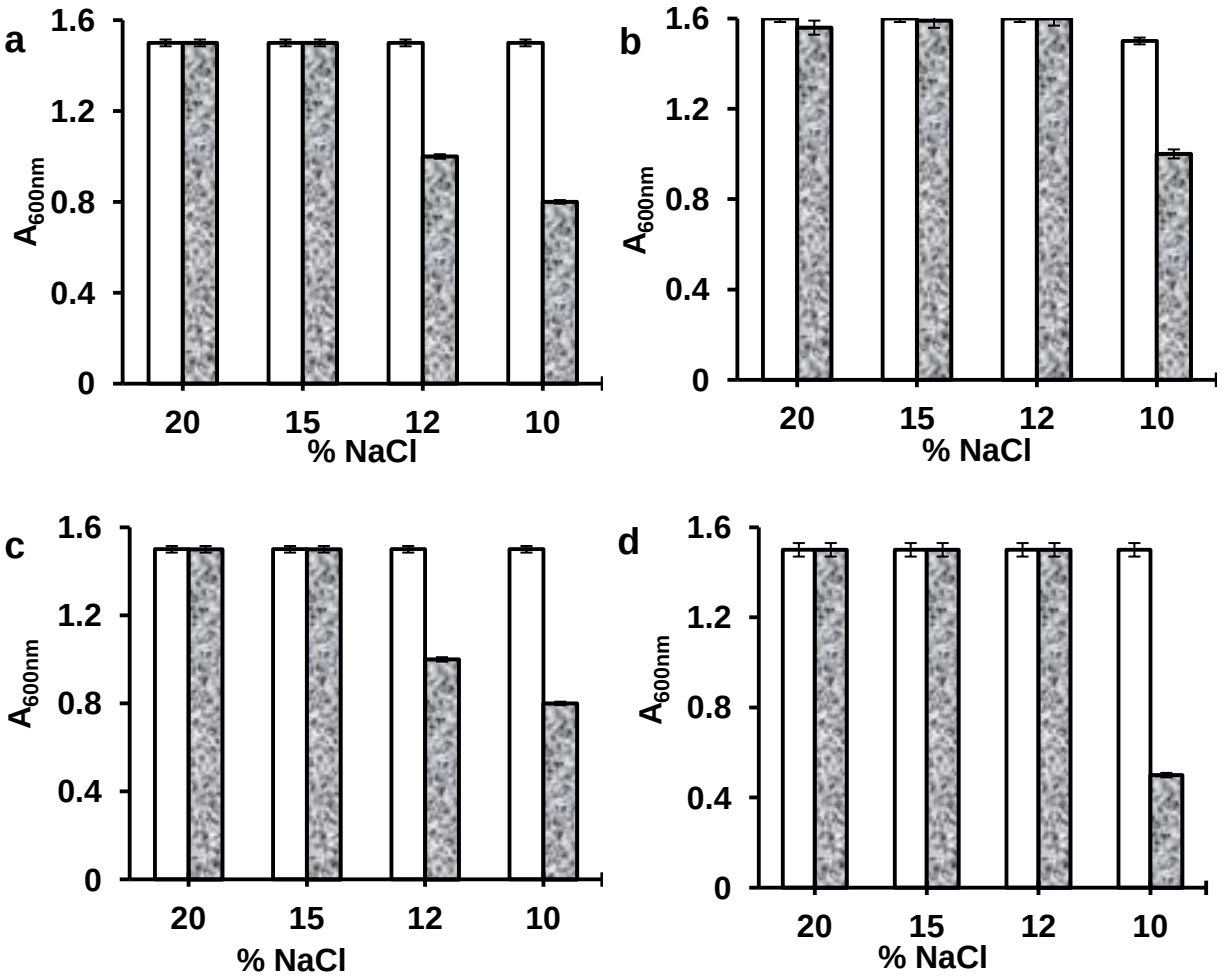

Fig. 2.12 Lysis in water of whole cells of : **(a)** GUSF-1 grown without Fe^{2+} **(b)** GUSF-1 with Fe^{2+} **(c)** GUFF129 grown without Fe^{2+} **(d)** GUFF129 with Fe^{2+} . Lysis of cells was determined after growth of respective cultures in Fe^{2+} containing medium and suspending the recovered cells in different % NaCl solution.

2.10 Detection and quantification of siderophore

2.10.1 Siderophore production in NGSM without Fe^{2+}

Siderophore production by GUSF-1 and GUFF129 was confirmed by color change of CAS reagent from blue to orange in culture supernatant (**Fig. 2.13**). The quantative CAS assay estimation, percentage siderophore units were estimated as the proportion of CAS color shifted. It was calculated to be 71.7 % and 53.3 % siderophore units, respectively.

2.10.2 Siderophore production in NGSM with Fe^{2+}

Culture supernatant of GUSF-1 and GUFF129 grown in Fe^{2+} containing medium showed a decrease in siderophore production which was quantified to be 22.5 % and 25 % respectively.

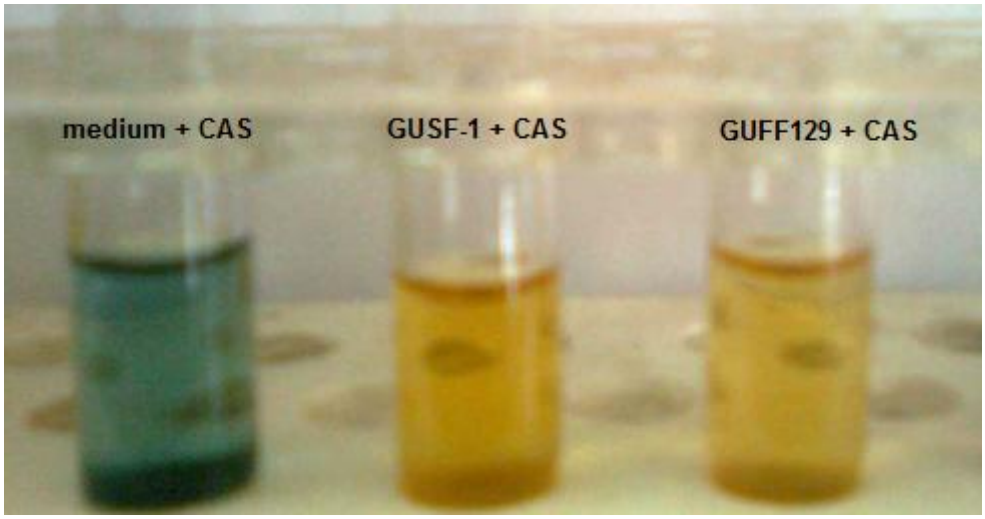

Fig. 2.13 Color change of CAS reagent from blue to yellow orange in qualitative CAS assay.

SECTION B: **Response of haloarchaeal cultures to Mn^{2+}**

2.11 Determination of maximum tolerance concentration of Mn^{2+} for haloarchaeal cultures

2.11.1 NTYE medium

Cultures exhibited high tolerance to Mn^{2+} ions. In nutrient rich medium, all cultures were resistant to 20 mM of Mn^{2+} ions with a growth rate of 72 % (**Fig. 2.14**). 129 > FLF20 = GUSF-1 > BF11 = BF3 = GUFF14 > BF5 > BF15 = GUFF209 > GUFF16 > BF9 = BF2 were resistant to 30 mM of Mn^{2+} ions with a growth of 51, 35, 25, 20, 12 and 10 % respectively. Culture GUFF129 = BF18 = BF11 > GUSF-1 = BF5 = GUFF14 = BF15 were resistant 50 mM of Mn^{2+} ions with growth of 12 % and 10 % while cultures BF11, GUFF14, BF18, BF5, BF15, GUSF-1 and GUFF129 were resistant to 80 mM of Mn^{2+} ions with growth of 5 %.

2.11.2 NGSM medium

In NGSM medium all the cultures were resistant to 20 mM of Mn^{2+} ions with a growth of 70.5 % (**Fig. 2.15**). At 30 mM concentration of Mn^{2+} the growth of GUFF129 = GUFF9 = BF9 > GUFF95 = BF11 = GUSF = GUFF56 = GUFF181 = GUFF168 = FLF20 = BF2 = BF18 > BF2 = BF5 > GUFF209 with growth of 30, 17.6, 10, 5.5 and 5 % respectively. Cultures were resistant to 50 mM of Mn^{2+} ions with GUSF-1 = GUFF129 > BF9 > GUFF9 with growth of 11.7, 5.2 and 5 % respectively.

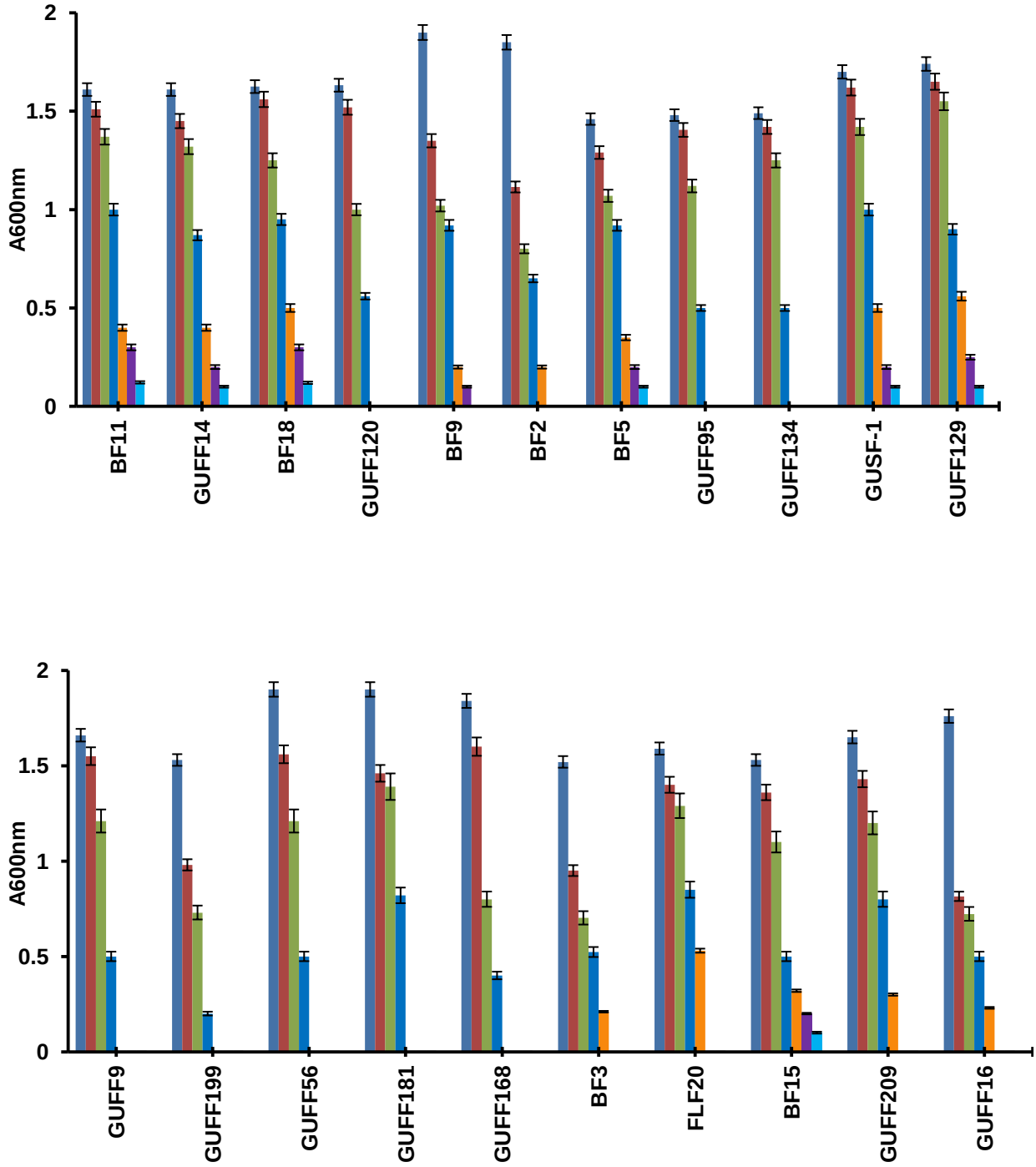

Fig. 2.14 Tolerance of haloarchaeal cultures to different concentrations of Mn^{2+} ions ($MnCl_2.6H_2O$) in NTYE

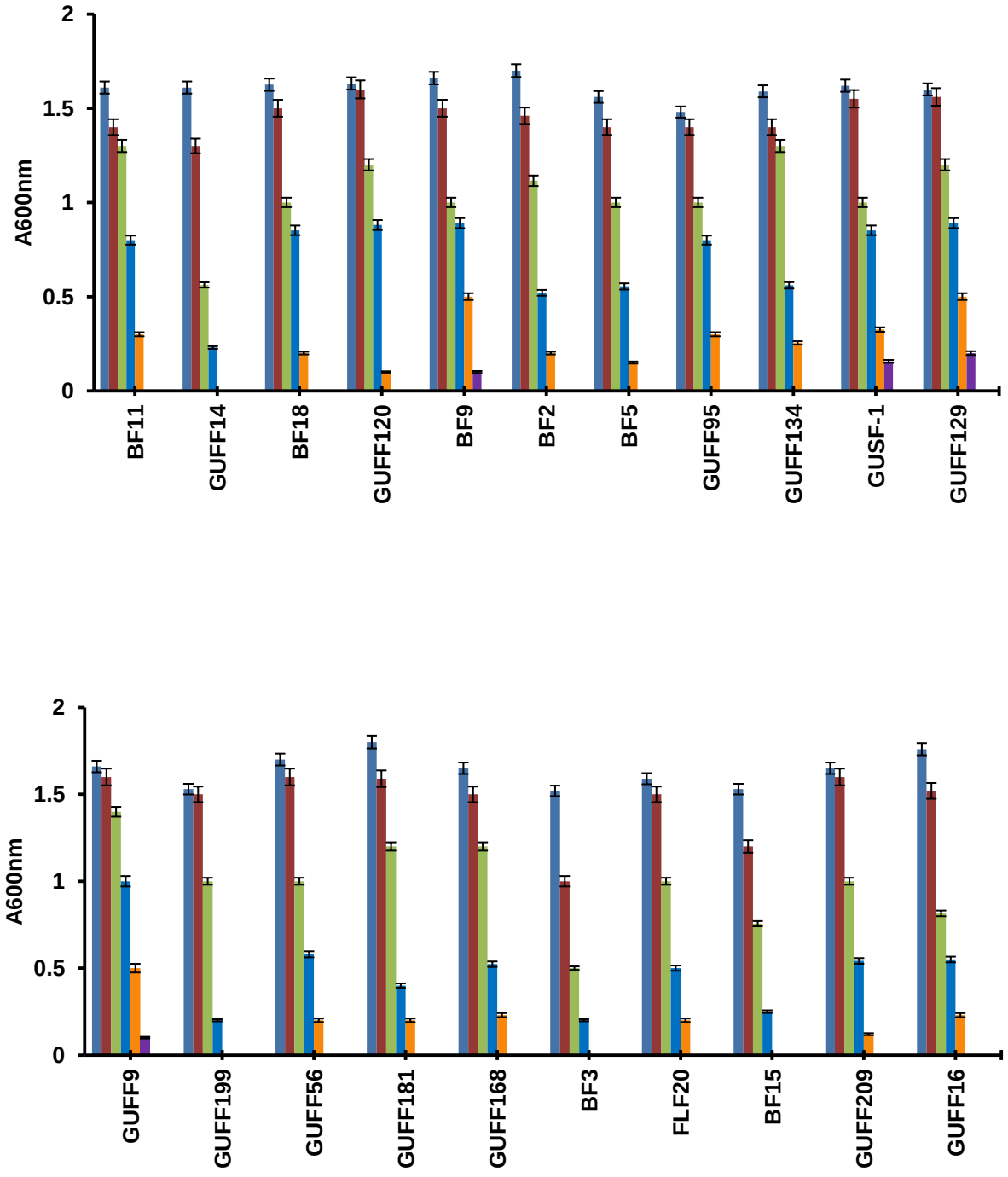

Fig. 2.15 Tolerance of haloarchaeal cultures to different concentrations of Mn^{2+} ions ($MnCl_2.6H_2O$) in NGSM

2.12 Effect of physico-chemical factors on growth of isolates in NGSM with Mn^{2+}

2.12.1 Effect of pH on the growth of GUSF-1 and GUFF129 grown with/without Mn^{2+}

Culture GUSF-1 grew at pH 5.0 with a growth rate of 3.125x $x10^3$ gen h^{-1} with a doubling time of 320 min gen^{-1} (**Fig. 2.16a**). At pH 6.0 and pH 7.0 culture had growth rate of 2.9 x 10^2 gen $h^{-1}$and 1.95$x10^2$ gen $h^{-1}$with doubling time of 33.94 min gen^{-1} and 3.26x 10^4 min gen^{-1}. At pH 8.5, had a growth rate of 7.6$x10^3$ min $gen^{-1}$with doubling time of 130.6 min gen^{-1}. Culture showed no significant growth at pH 3.0 and pH 10.0.

In Mn containing medium, culture GUSF-1 grew at pH 5.0 with a growth rate of 3.75x 10^3 gen h^{-1} with a doubling time of 266.6 min gen^{-1}(**Fig. 2.16b**). At pH 6.0 and pH 7.0 culture had growth rate of 2.1x 10^2 gen $h^{-1}$and 2.03$x10^2$ gen $h^{-1}$with doubling time of 46.6 min gen^{-1} and 49.07 min gen^{-1}. At pH 8.5, had a growth rate of 1.2$x10^2$ min $gen^{-1}$with doubling time of 80.53 min gen^{-1}. Culture showed no significant growth at pH 3.0 and pH 10.0.

As seen in **Fig 2.17a** culture GUFF-129 grew at pH 5.0 with a growth rate of 2 $x10^3$ gen h^{-1} with a doubling time of 480 min gen^{-1}. At pH 6.0 and pH 7.0 culture had growth rate of 1.68 x 10^2 gen h^{-1} and 2.2$x10^2$ gen h^{-1} with doubling time of 59.25 min gen^{-1} and 45.28 min gen^{-1}. At pH 8.5, had a growth rate of 6.25$x10^3$ min gen^{-1} with doubling time of 160 min gen^{-1}. Culture showed no significant growth at pH 3.0 and pH 10.0.

In Mn containing medium, culture GUFF-129 grew at pH 5.0 with a growth rate of 6.25x $x10^3$ gen h^{-1} with a doubling time of 160 min gen^{-1} (**Fig. 2.17b**). At pH 6.0 and pH 7.0 culture had growth rate of 1.79x 10^2 gen h^{-1} and 2.03$x10^2$ gen h^{-1} with doubling time of 55.81 min gen^{-1} and 48 min gen^{-1}. At pH 8.5, had a growth rate of 7.8$x10^3$ min gen^{-1} with doubling time

of 128 min gen^{-1}. Culture showed no significant growth at pH 3.0 and pH 10.0 with low density of 0.2.

2.12.2 Effect of % NaCl on the growth of GUSF-1 and GUFF129 grown with/without Mn^{2+}

Culture GUSF-1 failed to grow at 0 % salinity (**Fig. 2.16c**). At 5 % salinity, culture had a growth rate of 8.3 $x10^4$ gen h^{-1} with a doubling time of 1200 min gen^{-1}. At 10, 15 and 20 %, culture had a growth rate of 2.6 x 10^3, 6.25 x 10^3 and 2.5 x 10^2 gen h^{-1} respectively, with a doubling time of 384, 160 and 40 min gen^{-1}., respectively. At salinity of 25 and 30 % the growth rate was 2.29$x10^2$ and 7.9$x10^3$, with a doubling time of 43.63 and 125.65 min gen^{-1}., respectively.

In Mn^{2+} containing medium, GUSF-1 failed to grow at 0 % salinity **(Fig. 2.16d)**. At 5 % salinity, culture had a growth rate of 1.0 $x10^3$ gen h^{-1} with a doubling time of 960 min gen^{-1}. At 10 %, 15 % and 20 %, culture had a growth rate of 6.9 x 10^3, 1.88 x 10^2 and 2.7 x 10^2 gen h^{-1} respectively, with a doubling time of 144.57, 53.09 and 36.9 min gen^{-1}., respectively. At salinity of 25 and 30 % the growth rate was 1.58$x10^2$ and 9$x10^3$, with a doubling time of 63.15 and 110.85 min gen^{-1}., respectively.

Culture GUFF-129 failed to grow at 0 % salinity (**Fig**. **2.17c**). At 5 % salinity, culture had a growth rate of 1.25 $x10^3$gen h^{-1} with a doubling time of 800 min gen^{-1}. At 10, 15 and 20 %, culture had a growth rate of 1.03x 10^3, 3.54 x 10^3 and 1.06 x 10^2 gen h^{-1} respectively, with a doubling time of 96.7, 282.3 and 9.428 min gen^{-1}., respectively. At salinity of 25 and 30 % the growth rate was 1.7$x10^2$ and 4.6$x10^3$, with a doubling time of 58.53 and 213 min gen^{-1}., respectively.

In Mn containing medium, GUFF-1 failed to grow at 0 % salinity (**Fig. 2.17d**). At 5 % salinity, culture had a growth rate of 1.04 $x10^3$ gen h^{-1} with a doubling time of 960 min gen^{-1}. At 10, 15 and 20 %, culture had a growth rate of 5 x 10^3, 1.1 x 10^2 and 3.25 x 10^2 gen h^{-1} respectively, with a doubling time of 144.57, 53.09 and 30.7 min gen^{-1}., respectively. At salinity of 25 and 30 % the growth rate was $2x10^2$ and $6.6x10^3$, with a doubling time of 50 and 150 min gen^{-1}., respectively.

2.12.3 Effect of temperature on the growth of GUSF-1 and GUFF129 grown with/without Mn^{2+}

As depicted in **Fig. 2.16e** culture GUSF-1 failed to grow at temperature of 20 °C. At 30 °C culture had a growth rate of 1.4 $x10^2$ gen h^{-1} with a doubling time of 71.07 min gen^{-1}. At 42 °C, 50 °C and 60 °C, culture had a growth rate of 1.33 x 10^2, 2.3x 10^3 and 1.5 x 10^3 gen h^{-1} respectively, with a doubling time of 75.07, 434.4 and 648.4 min gen^{-1}., respectively.

In Mn containing medium, GUSF-1 failed to grow at temperature of 20 °C (**Fig. 2.16f**). At 30 °C culture had a growth rate of 2.7 $x10^2$ gen h^{-1} with a doubling time of 35.8 min gen^{-1}. At 42, 50 and 60 °C, culture had a growth rate of 1.14 x 10^2, 8 x 10^3 and 5.5 x 10^3 gen h^{-1} respectively, with a doubling time of 87.27, 125 and 180.9 min gen^{-1}., respectively.

Culture GUFF-129 exhibited low density of only 0.22 at temperature of 20 °C showing a growth rate of 4.17x 10^4 gen h^{-1} with a doubling time of 2400 9 min gen^{-1} (**Fig. 2.17e**). At 30 °C culture had a growth rate of 1.9 $x10^2$ gen h^{-1} with a doubling time of 51.17 min gen^{-1}. At 42, 50 and 60 °C, culture had a growth rate of 2.4 x 10^2, 5.4x 10^3 and 2.06 x 10^3 gen h^{-1} respectively, with a doubling time of 41.6, 183.9 and 486.4 min gen^{-1}, respectively.

In Mn containing medium, GUFF-129 failed to grow at temperature of 20 °C with density of only 0.12 (**Fig. 2.17f**). At 30 °C culture had a growth rate of 2.3 x10^2 gen h^{-1} with a doubling time of 42.3 min gen^{-1}. At 42, 50 and 60 °C, culture had a growth rate of 1.8 x 10^2, 7.5 x 10^3 and 6.8 x 10^3 gen h^{-1} respectively, with a doubling time of 54.5, 131.86 and 146.3 min gen^{-1}., respectively.

2.13 Monitoring of Mn inside the growing cells of haloarchaea and culture broth.

As depicted in **Fig. 2.18a** the culture GUSF-1 grew with growth rate of 1.4x 10^2 gen h^{-1} ^{1}in NGSM medium, pH 7 incubated at 30 ºC with a doubling time of 72 min gen^{-1} while in presence of Mn^{2+} in NGSM medium the culture grew with a growth rate of 3.1 x 10^2 gen h^{-1} having a doubling time of 32 min gen^{-1}. Similarly, the culture GUFF129 grew with a growth rate of 1.07 x 10^2 gen $h^{-1}$with a doubling time of 92.6 min gen^{-1} in NGSM medium, pH 7 incubated at 30 ºC while in presence of Mn^{2+} in NGSM medium with a growth rate of 2.5 x 10^2 gen $h^{-1}$with a doubling time of 40 min gen^{-1} **Fig. 2.18b**; during the early stationary phase in both the cultures there was initiation of accumulation of manganese inside the cells. GUSF-1 accumulated 48.5 mg Mn L^{-1} and GUF129 accumulated 45.5 mg Mn L^{-1}. The quantity of metal inside the cells remained constant at the stationary phase and there was no formation of manganese oxide observed in the culture broth as detected by LBB assay (Lee and Tebo 1994). The accumulation of metal inside the cells was confirmed by increase in the dry weight of the cell pellets. (**Table**. **2.3**).

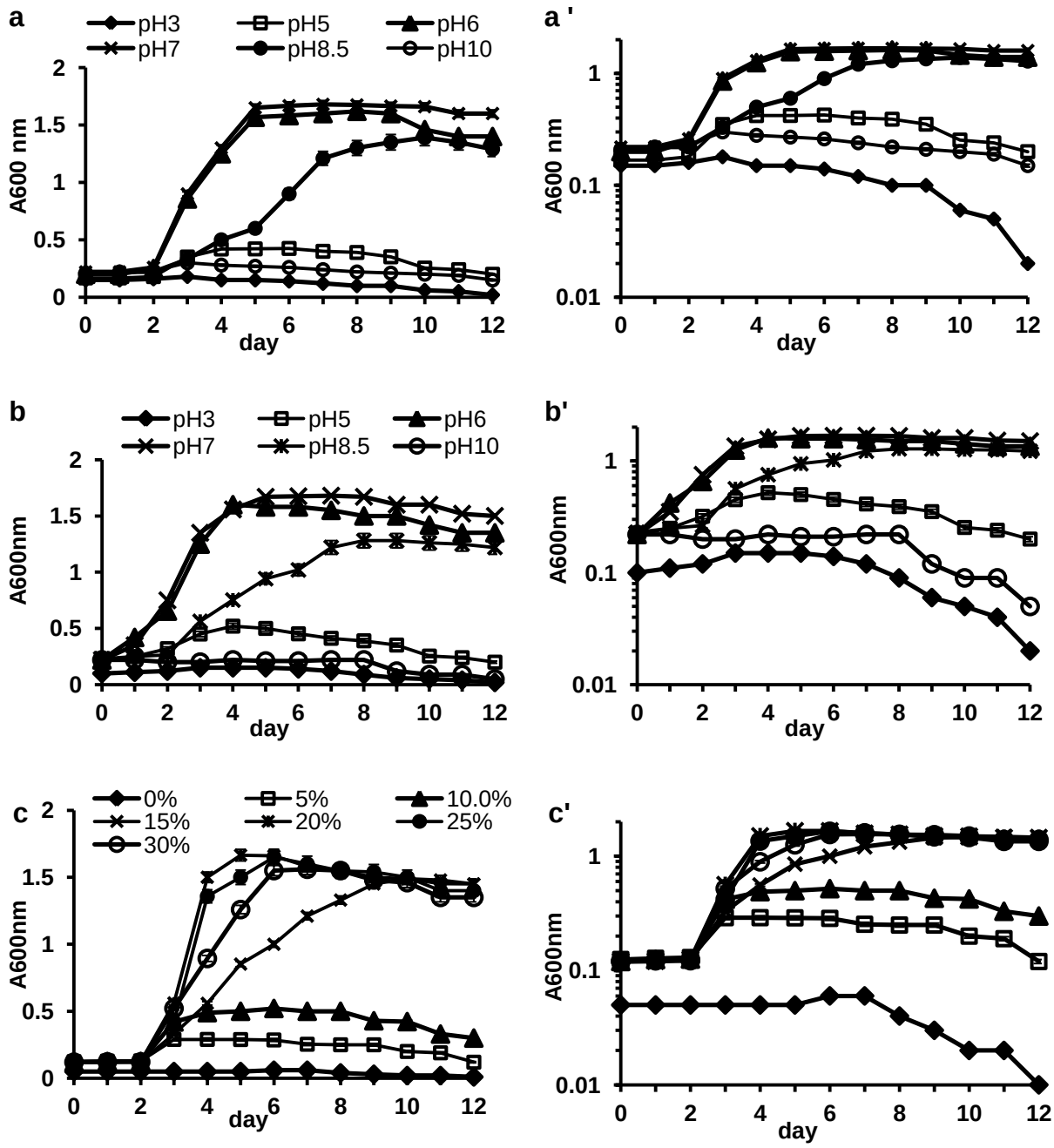

Fig. 2.16 Growth profile of GUSF-1 in mineral salts medium with glucose as carbon source **(a, a')** effect of pH **(b, b')** effect of pH on growth in Mn^{2+} containing medium **(c, c')** effect of different salinity; **(')** represents growth profile plotted on log scale

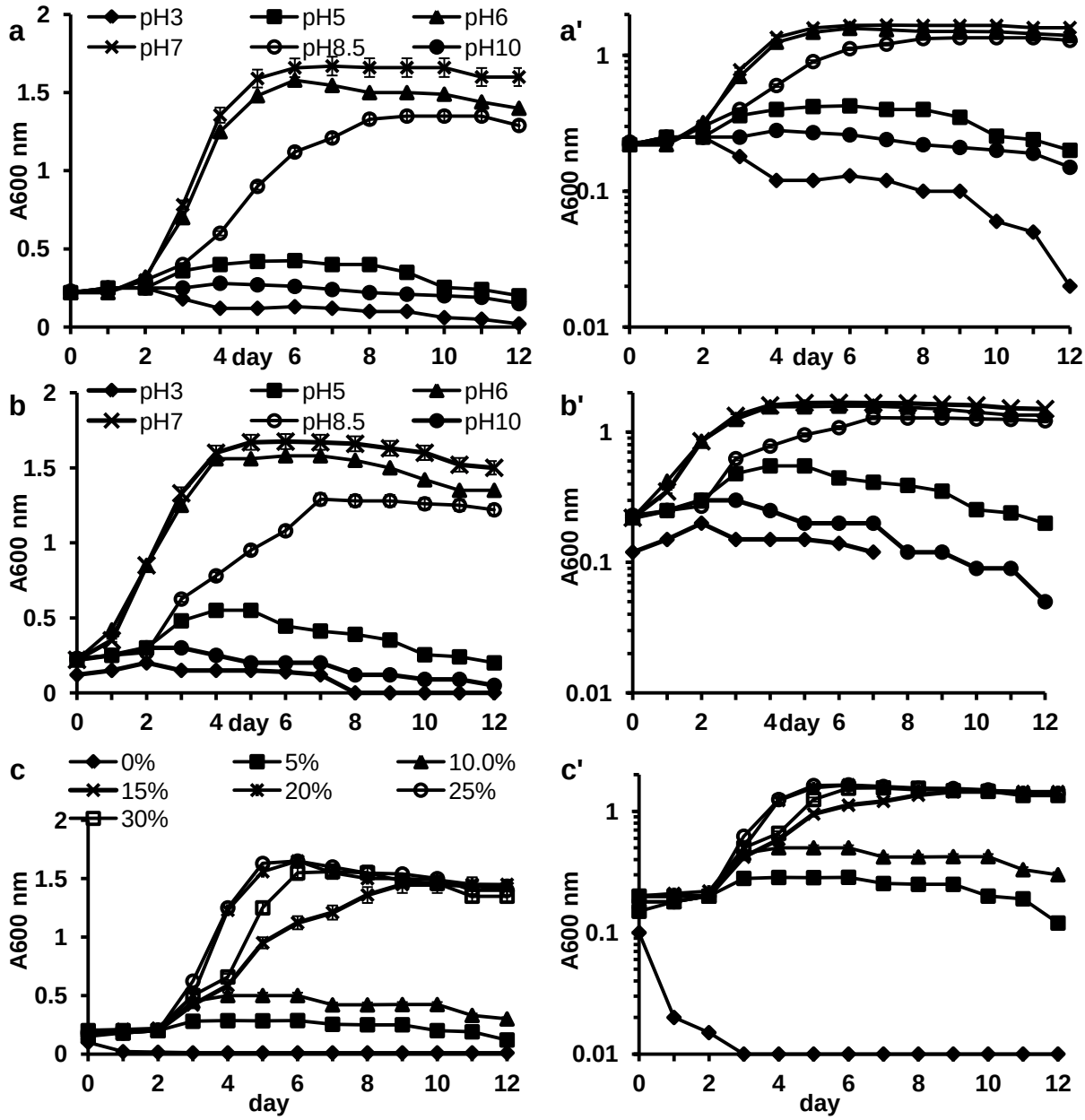

Fig.2.17 Growth profile of GUFF129 in mineral salts medium medium **(a, a')** effect of pH **(b, b')** effect of pH on growth in Mn^{2+} containing medium **(c, c')** effect of different salinity; **(')** represents growth profile plotted on log scale

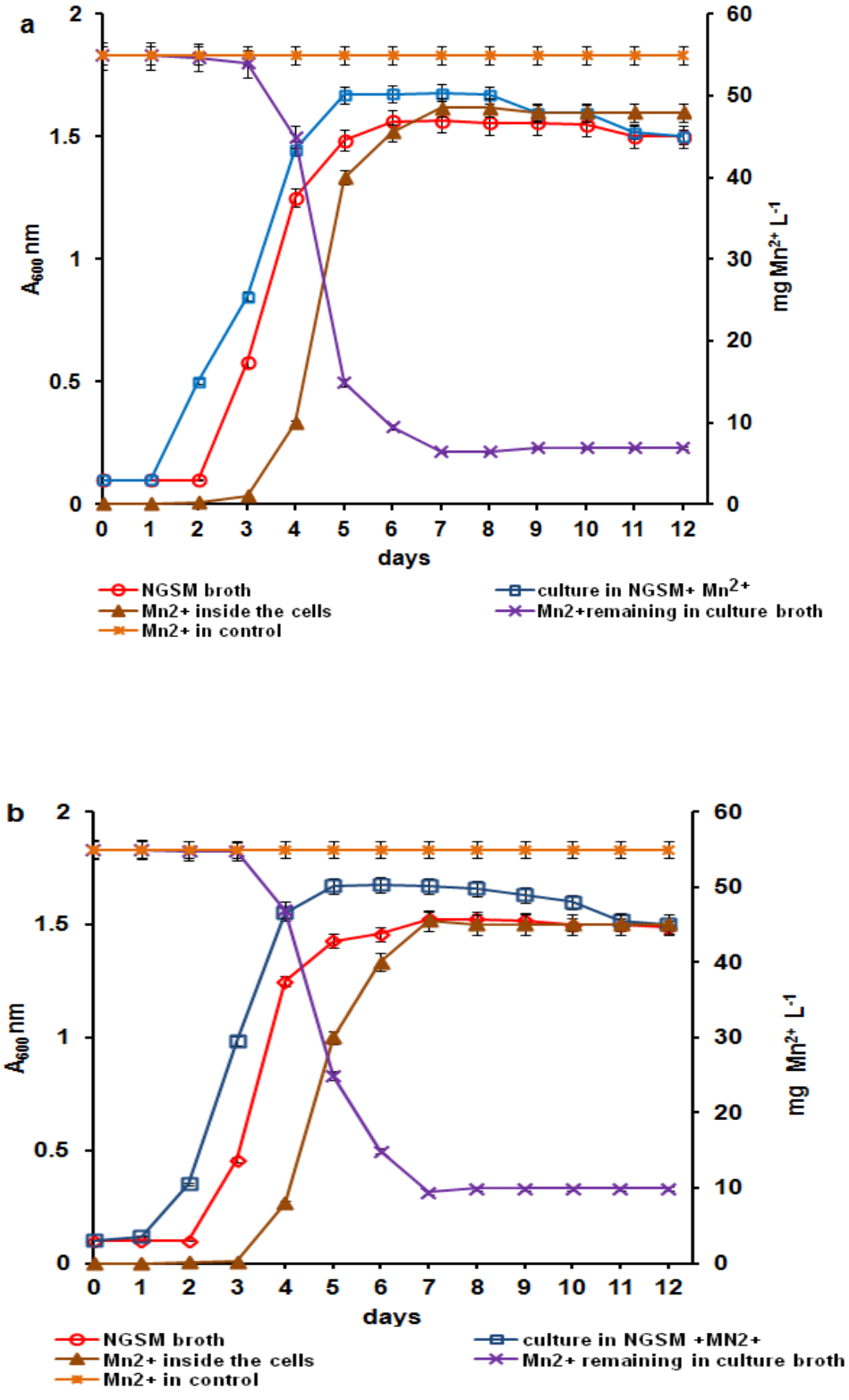

Fig. 2.18. Effect of Mn^{2+} on growth of **(a)** GUSF-1in Mn^{2+} containing medium **(b)** GUFF129 in Mn^{2+} containing NGSM.

Table 2.3 Dry weight of biomass of culture grown with Mn^{2+}

Culture	Biomass dry weight (µg ml^{-1})
GUSF-1	62
GUSF-1 with Mn^{2+}	73
GUFF129	59
GUFF129 with Mn^{2+}	70

2.14 Evaluation of cellular changes during growth with Mn^{2+}

2.14.1 Gram character

The gram stained smears (**Fig. 2.19a**) revealed cells of GUSF-1 as gram negative cocci. Interestingly, culture grown with Mn^{2+} revealed to be positive coccobacilli (**Fig. 2.19b**). GUFF 129 displayed gram negative cocci morphology with a elongation in shape of cells grown with Mn^{2+} exhibiting a gram positive reaction (**Fig. 2.19c, d**).

2.14.2 SEM

The cell morphology of GUSF-1 revealed to be a cup shaped when grown without metal (**Fig. 2.20a**) while the cells grown with manganese were observed to be aggregated and elongated in shape (**Fig. 2.20b**). GUFF129 displayed a coccoidal or disc shaped morphology when grown in absence of metal while the cells exhibited severe aggregates and elongation in shape when grown with Mn^{2+} (**Fig. 2.20c, d**).

2.14.3 Cell hydrophobicity

Cultures GUSF-1and GUFF129 grown in presence of Mn^{2+} showed increase in their cell hydrophobicity as compared to those grown without (**Table 2.4**)

2.14.4 Pigment

The acetone extract of pigment from cell mass of GUSF-1 revealed absorption maxima at 626.5, 528.5, 495, 470, 388, 369.5, 351.5 nm (**Fig. 2.21a**) that corresponded to phytofluenes (351 and 370 nm), retinal (388 nm), lycopene (470 nm), bacterioruberin (495 and 528 nm) and halorhodopsin (626 nm) respectively.

As seen in **Fig. 2.21b** spectral scan of GUSF-1 cell extract grown with Mn^{2+} indicated appearance of peaks at 528.5, 494.5, 468.5, 387, 370.5, 344.5 nm corresponding to bacterioruberin (495 and 528 nm), phytofluene (344 and 370 nm), lycopene (468.5 nm) and retinal (387 nm). It was observed that the halorhodopsin peak at 626 nm was abolished while a phytofluene peak was induced at 344 nm with decrease in intensities of rest of the pigment components.

In case of culture GUFF129 peaks of absorption maxima were observed at 578.5, 522, 495.5, 418, 358 and 303.5 nm (**Fig. 2.21c**) that corresponded to halorhodopsin (578 nm), bacterioruberin (522 and 495.5 nm), β-carotene (418 nm) and phytofluene (358 and 303.5 nm) respectively. In spectral scan of cell extract of those grown with Mn^{+2} indicated the induction of lycopene peak at 470.5 nm, retinal peak at 388.5 nm and phytofluene peak at 373 nm (**Fig. 2.21d**). Interestingly, the bacterioreuberin peaks at 495 and 528.5 nm increased in intensity with a shift in the later.

2.14.5 Whole cell proteins

The whole cell protein profiles displayed in **Fig. 2.22** resolved into protein bands at 75 kDa, 60 kDa, 50 kDa, 35.5 kDa, 18 kDa, and the induction of 48 kDa, 38 kDa, 30.5 kDa, 18 kDa proteins in GUSF-1 grown in presence of Mn^{2+}. GUFF129 showed presence of proteins bands at 96.8 kDa, 66 kDa, 46 kDa, 39 kDa, 38 kDa, 23.5 kDa and the induction of 46 kDa, 29 kDa and 25 kDa proteins in Mn^{2+} grown culture.

2.14.6 Archaeol lipids

Thin layer chromatograms of lipids extracts of GUSF-1 showed spots corresponding to glycolipids at R_f of 0.3 and at R_f of 0.8 corresponding to phospholipids (**Fig. 2.23a, b**). The lipids of cells grown in Mn^{2+} had R_f of 0.38, 0.5 corresponding to glycolipid with while appearance of phospholipid spots with R_f value of 0.6, 0.84. TLC of archaeol lipids extracted from GUFF129 displayed appearance of glycolipid spots with R_f value of 0.34 and phospholipids with R_f value of 0.38, 0.6 and 0.84. The lipids of culture grown in Mn^{2+} containing medium showed a spot of glycolipid with R_f value of 0.25, 0.5 while phospholipid with R_f value of 0.76 and 0.5 (**Fig. 2.23c, d**).

2.14.7 Cell stability

As depicted in **Fig. 2.24,** GUSF-1 and GUFF129 grown in presence of Mn^{2+} were resistant to lysis at decreased salinities of 12 % as compared to that grown in absence of metal.

2.15 Detection of siderophore production in Mn^{2+} growth medium

The culture supernatant of the two cultures grown in Mn^{2+} failed to show any color change in CAS assay indicating no detection of siderophore.

2.15 Role of plasmid DNA in metal tolerance

As seen in **Fig**. **2.25,** the cultures GUSF-1 and GUFF 129 grown with and without Fe^{2+}/ Mn^{2+} in NTYE and NGSM failed to show any visible band corresponding to plasmid DNA.

2.16 Identification of haloarchaeaon GUSF-1 and GUFF 129

2.16.1 Biochemical characterization

Based on biochemical characters listed in Bergey's Manual of systematic bacteriology, in The Prokaryotes: Volume IV (2^{nd} edition) (Tindall 1992) and (Hezayen *et al*. 2001), haloarchaeaon GUSF-1 was tentatively identified as *Haloferax* sp. while GUFF 129 belonged to genus *Natrialba* sp. (**Table 2.5**)

2.16.2 Molecular characterization of GUSF-1

The PCR amplification of genomic DNA resulted in 1 kb PCR product (**Fig. 2.26**). The closest database-relatives of sequence generated were compared to 16S rRNA gene sequences available in the National Centre for Biotechnology Information (NCBI) by BLAST analysis. MEGA version 5.0 was used for Multiple sequence alignment. Phylogenetic tree was constructed using Clustal W by version 1.80 (DNASTAR Inc., USA) by neighbor joining method (**Fig. 2.27**) with bootstrap analysis using 10000 replicates (Tamura et al. 2011). The BLAST analysis of the 16S rRNA gene fragment of culture GUSF-1 showed 97 % similarity to *Haloferax alexandrinus*. The sequence generated was deposited in GenBank with accession number GUF1 **KF796625**.

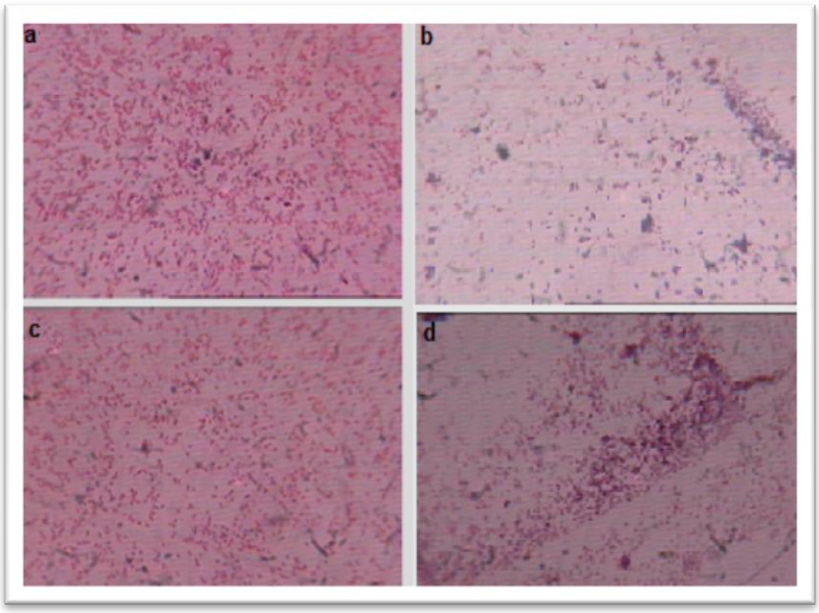

Fig. 2.19. Gram stained micrographs of **(a)** GUSF-1grown without Mn^{2+} **(b)** with Mn^{2+} **(c)** GUFF129 grown without Mn^{2+} **(d)** with Mn^{2+}

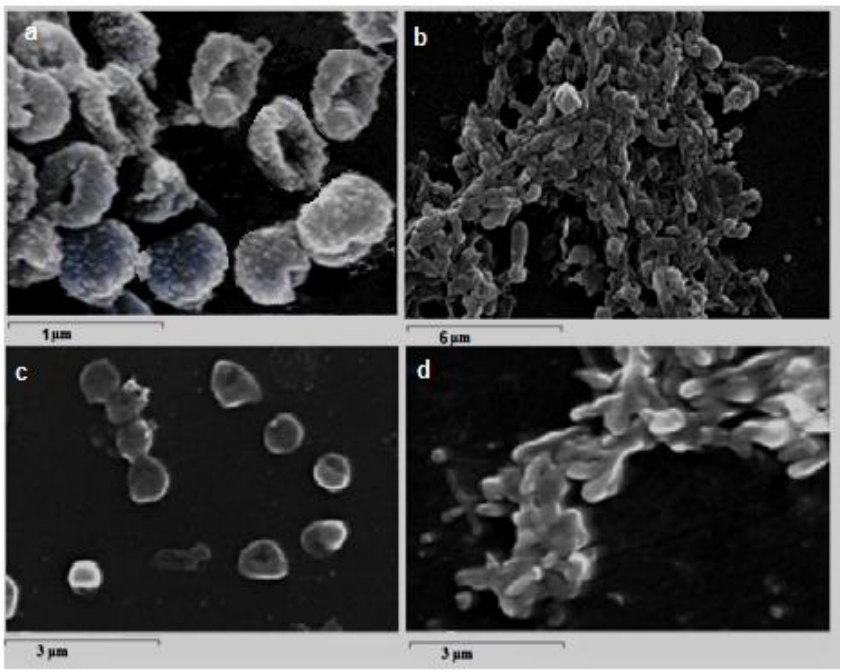

Fig. 2.20. SEM micrographs of **(a)** GUSF-1 grown without Mn^{2+} **(b)** with Mn^{2+} **(c)** GUFF129 grown without Mn^{2+} **(d)** with Mn^{2+}

Table 2.4 Cell hydrophobicity of cultures grown without / with Mn^{2+}

Culture	% adherence of cells to hexadecane
GUSF-1	5
GUSF-1 with Mn^{2+}	55
GUFF129	8
GUFF129 with Mn^{2+}	50

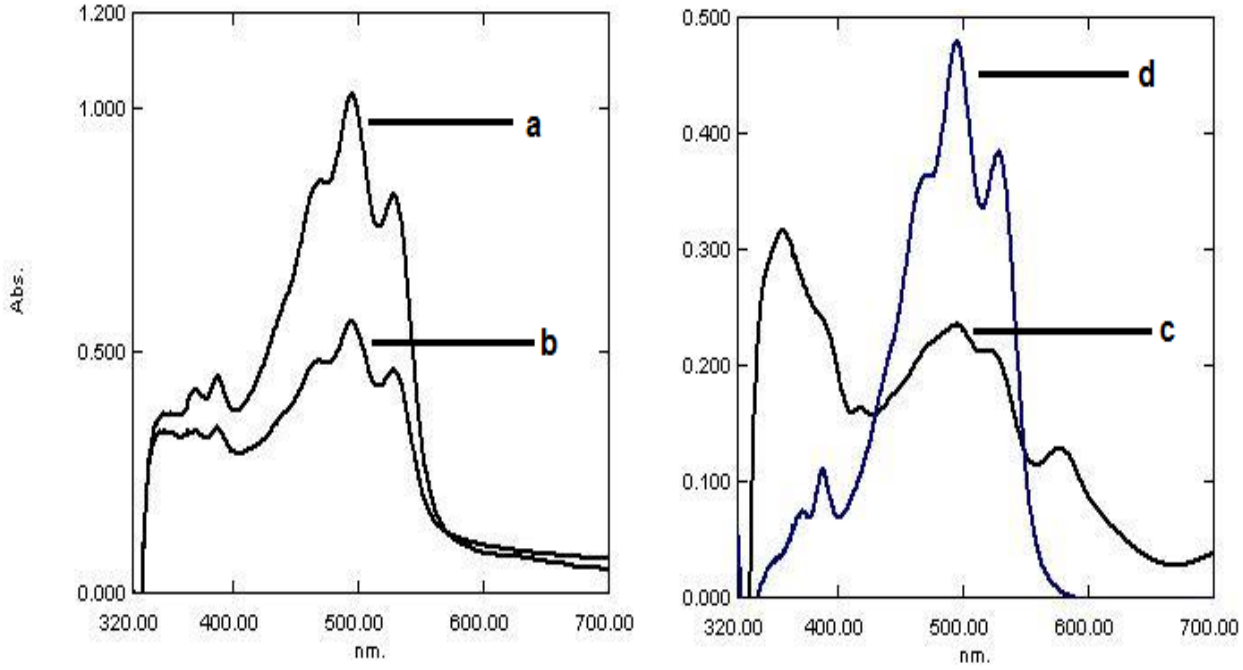

Fig. 2.21 Pigment profile of acetone extracts of GUSF-1 **(a)** grown without metal **(b)** grown in Mn^{2+} containing medium **(c)** GUFF129 grown without metal **(d)** grown in Mn^{2+} containing medium

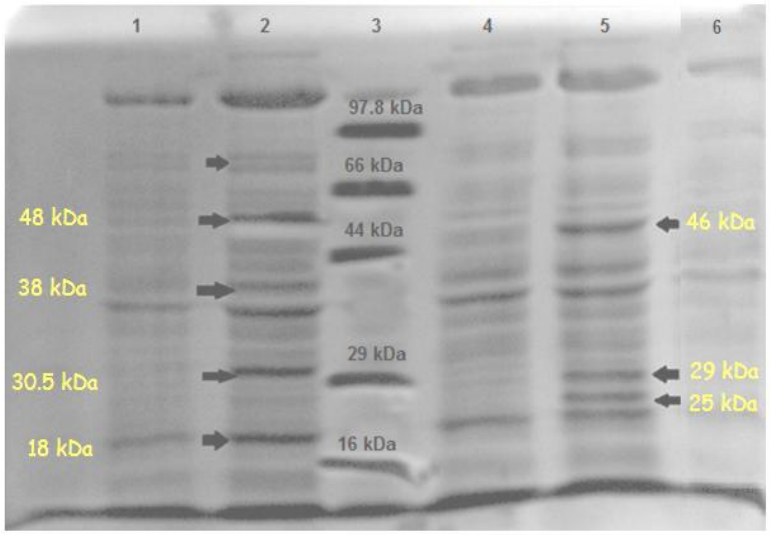

Fig. 2.22 SDS-PAGE profile of GUSF-1 and GUFF129 grown with/ without $Mn^{2+:}$ **Lane 1**- GUSF-1; **Lane 2**- GUSF-1 with Mn^{2+}; **Lane 3**- Standard Marker; **Lane 4**- GUFF129; **Lane 5**- GUFF129 with Mn^{2+}

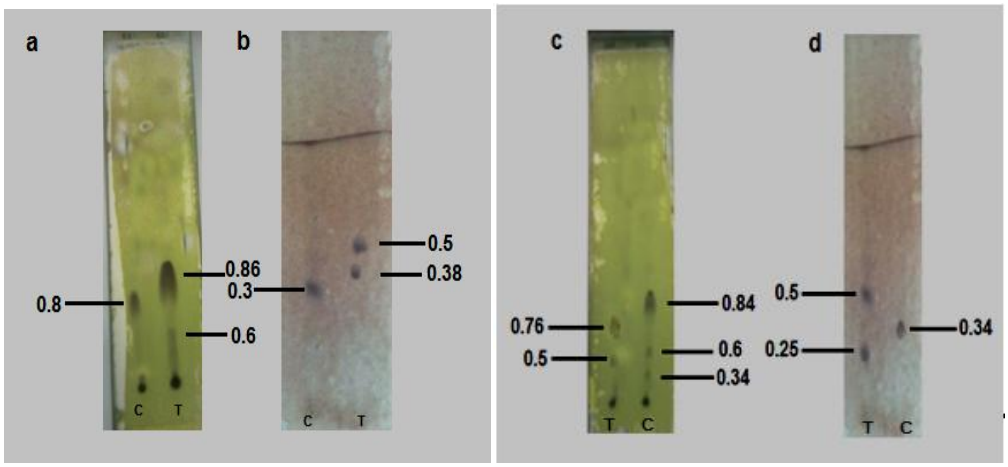

Fig. 2.23 Archaeol lipid profile of **(a)** GUSF-1 phosholipid **(b)** glycolipid profile **(c)** GUFF129 phospholipid **(d)** glycolipid profile. (T= with Mn^{2+}; C= without Mn^{2+}). The silica gel plate was developed once with chloroform: methanol: acetic acid: water (85:22.5:10:4 v/v) and was sprayed for glycolipids and phospholipids, respectively.

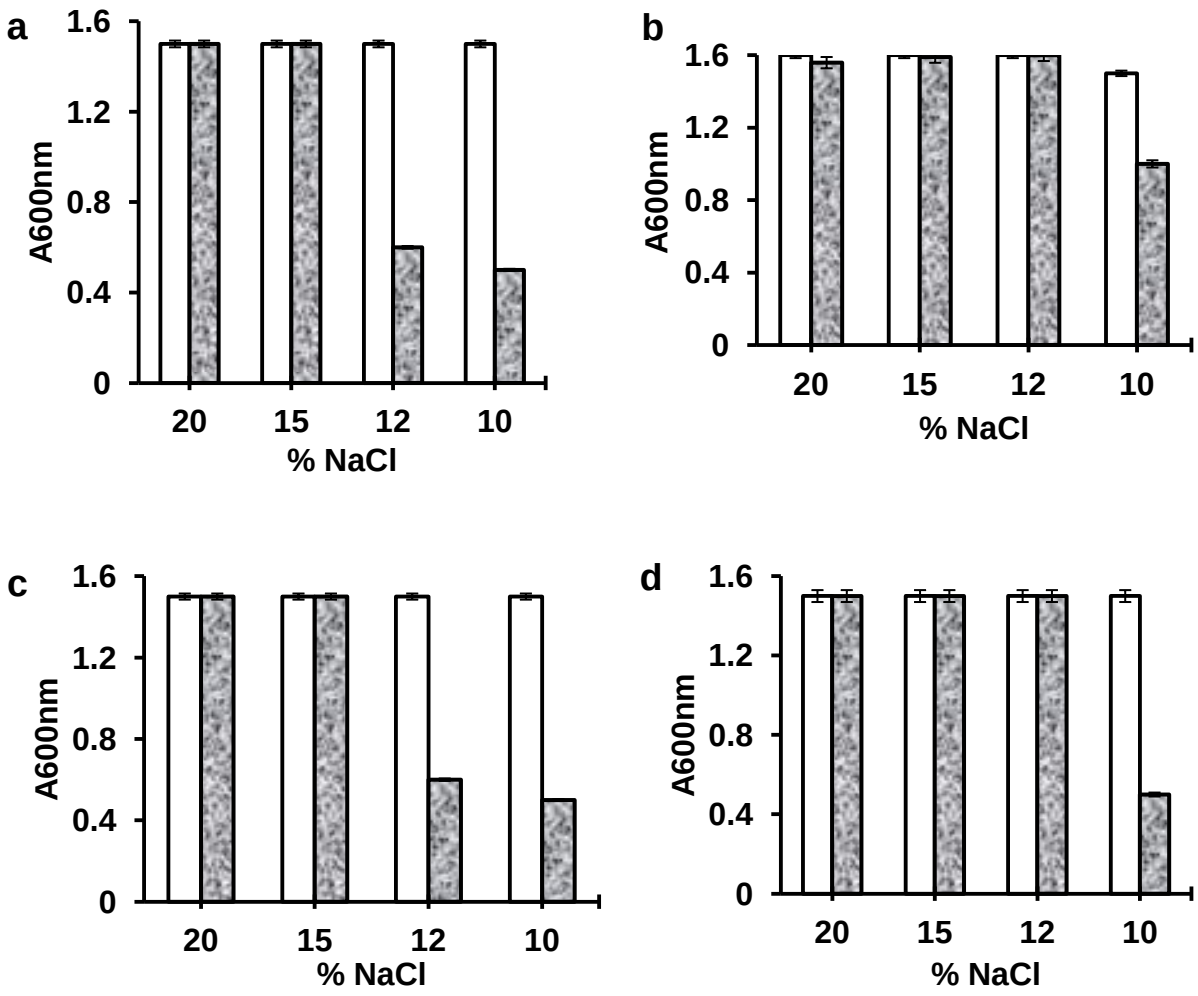

Fig. 2.24 Effect of Mn^{2+} on cell stability of **(a)** GUSF-1; **(b)** GUSF-1 grown with Mn^{2+}; **(c)** GUFF129; **(d)** GUFF129 with Mn^{2+}. Cells of culture grown with/without Mn^{2+} were suspended in different % NaCl solution to determine the effect of Mn^{2+} on cell stability.

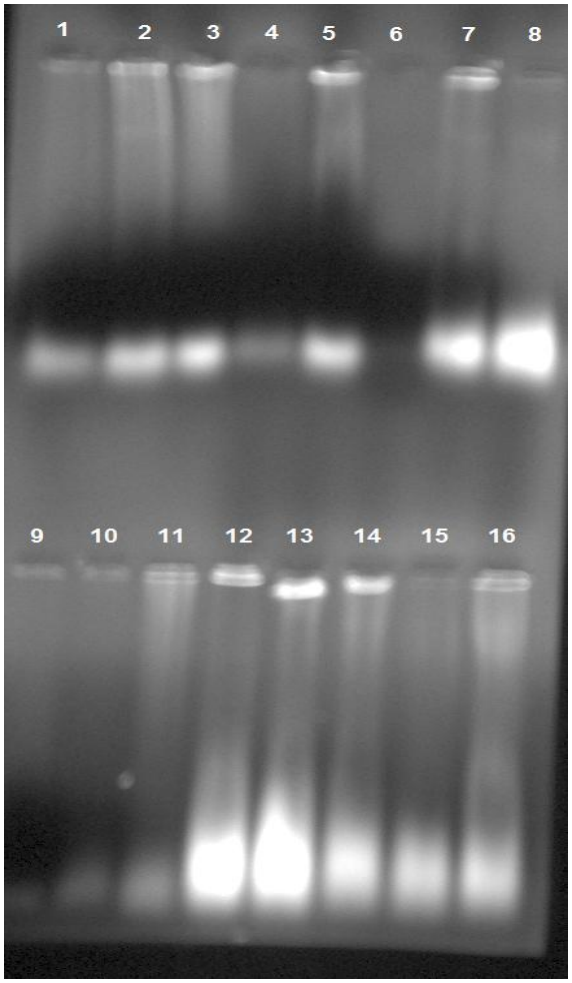

Lane 1: GUSF-1 grown with 1 mM Mn^{2+} in NTYE **Lane 2** : GUSF-1 grown in NTYE, **Lane 3**: GUSF-1 grown with 1 mM Fe^{2+} in NTYE **Lane 5**: GUSF-1 grown with 1 mM Fe^{2+} in NGSM **Lane 7:** GUSF-1 grown with 1mM Mn^{2+} in NGSM **Lane 8:** GUSF-1 grown in NGSM **Lane 10**: GUFF-129 grown with 1 mM Mn^{2+} in NTYE **Lane 11** : GUFF-129 grown in NTYE, **Lane 12**: GUFF-129 grown with 1 mM Fe^{2+} in NTYE **Lane 13**: GUFF-129 grown with 1 mM Fe^{2+} in NGSM **Lane 14:** GUFF-129 grown with 1 mM Mn^{2+} in NGSM **Lane 16:** GUFF-129 grown in NGSM

Fig. **2.25** Agarose gel profile of GUSF-1 and GUFF-129 for detection of plasmid DNA by alkaline lysis method

Table 2.5 Morphological and Biochemical characteristics of haloarchaeon

Biochemical Test	GUFF129	GUSF-1
Gelatinase	+	-
Protease	+	+
Tween 80	+	+
Amylase	+	+
Sorbitol	+	+
Mannitol	+	+
Glucose	+	+
Sucrose	+	+
Fructose	+	+
Galactose	+	+
Lactose	+	+
Ribose	+	+
Arabinose	+	+
Xylose	+	+
Mannose	+	+
Maltose	+	+
Citrate	+	+
Acetate	-	+
Malate	-	-
Pyruvate	+	+
Succinate	-	-
Lactate	-	-
Formate	-	+
Arginine	+	+
PHA	-	+
Gram character	-ve cocci	-ve cocci
SEM	cocci, flat	cup shaped
C_{40} C_{50} Pigment	+	+
Penicillin (700 u ml^{-1}+NTYE)	+	+
Lysis in distilled water	+	+
GDEM	+	+
Tentatively identified as	*Natrialba* sp.	*Haloferax* sp.

Key: (-) negative result; (+) positive result

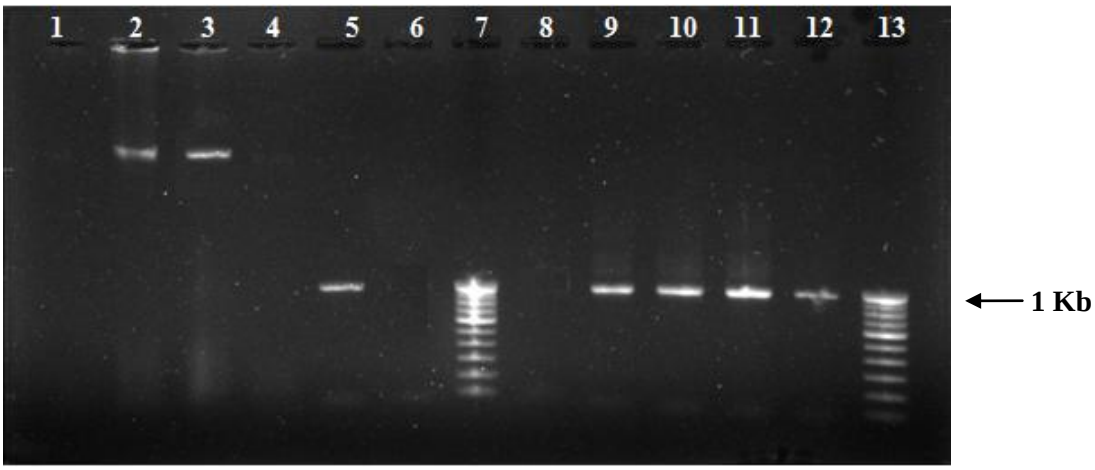

Fig. 2.26 PCR amplification profile of GUSF-1 genomic DNA: **Lane 2** and **3** with genomic DNA of GUSF-1; **Lanes 7** and **13** with 1 Kb Standard DNA ladder; **Lanes 9, 10, 11 and 12** with 1 Kb amplicon using genomic DNA of GUSF-1 as template.

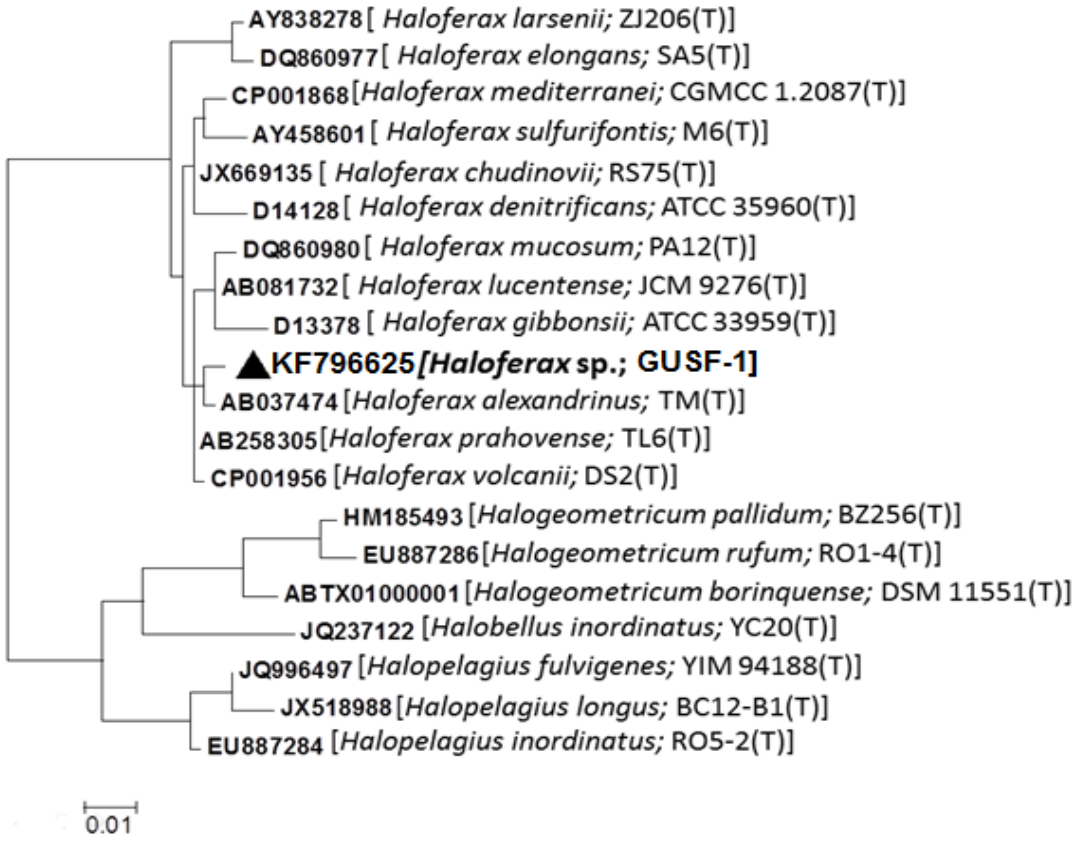

Fig. 2.27 Phylogenetic tree showing the position of GUSF-1 constructed with MEGA 5.0

DISCUSSION

SECTION A: Response of haloarchaeon GUSF-1 and GUFF 129 to Fe^{2+} ions

Metal ions, in general, play a significant role in the physiology of cells. Metal ions Co^{2+}, Cu^{2+}, K^{+}, Mg^{2+}, Ca^{2+}, Fe^{2+}, Mn^{2+}, Cr^{2+}, Na^{+}, Zn^{2+}, serve as essential micronutrients wherein they act as redox centres for cytochrome, iron- sulfur proteins and hence are indispensable in electron transport chain. However, these metal ions at high concentration are toxic to the cells and cause disruption of cell membrane, thereby directly or indirectly compromising DNA and cellular functioning (Nelson 1999). So far, tolerance and resistance exhibited by eubacterial organisms are well documented as plasmid mediated (Neis *et al.* 1998), bioaccumulation, redox immobilization, efflux mechanisms (Gadd 2010). Till date, haloarchaea are reported to exhibit tolerance to metal ions such as Li^{+}, As^{5+}, As^{3+}, Mn^{2+}, Ni^{2+}, Cu^{2+}, $Zn^{2+}/Cd^{2+}/Fe^{2+}/Fe^{3+}$ and Hg^{2+} at concentrations of 200 mM, 60 mM, 3 mM, 50 mM, 5 mM, 2.5 mM and 0.02 mM, respectively (Khandavilli *et al*. 1999; Furtado and Naik 2009, Patil *et al.* 2013). GUSF-1and GUFF129 tolerated 192 mg L^{-1} and 165 mg L^{-1} of Fe^{2+} ions, respectively, in mineral salts medium. Metal toxicity seems to be not directly proportional to its concentration and is often regulated by chemical speciation (Srivastava and Kowshik 2012). With regard to this, parameters such as salinity, pH, temperature, nutrients can singly or collectively influence the response of prokaryotes and eukaryotes to metal as they can alter effective free metal ion concentration in the cell (Babich and Stotzky 1980) or influence the metal state (Nieto *et al.* 1989). For instance, increasing pH from 5 to 9 decreased the toxicity of mercuric chloride, zinc sulfate, lead nitrate, copper sulfate and

nickel sulfate towards growth of *A. flavus*, *P. chrysogenum* while toxicity of cadmium chloride increased with increase in the pH. Increasing concentration of peptone and yeast extract from 0.5 to 1.5 % induced reduction in toxicity of all heavy metal towards growth of fungi (Bagy 1991). Hsu et al 1992 reported that raising the incubation temperature from 25 to 37 ºC increased the susceptibility of *S. cerevisiae* to cadmium and mercury ions. Further, it was interesting to observe that the presence of iron in the medium enhanced the growth of both the cultures which accumulated Fe as Fe^{2+} at a concentration of 64mg L^{-1} compared to Fe^{3+} at 21 mg L^{-1}concentration inside the cells. An earlier study made by Gibbons and Sehgal (1960) states that low concentration of Fe^{2+}, Mn^{2+} , Ni^{2+}, Zn^{2+} enhances the growth of haloarchaea. While studying growth of haloarchaeal cultures in Fe^{2+} medium it should be noted that the medium pH was maintained at 6.0 so that there was no oxidation of Fe abiotically. However, it is reported that the presence of anions such as Cl^{-1}, CO^{2-}_3 and SO^{2-}_4 are known to retard the oxidation rate of Fe^{2+} because they form complexes with Fe^{2+} that are less favorably oxidized as compared to the hydroxide complexes. The exact rate constants associated with each of these complexes have not been established to date (Morgan and Lahav 2007). Additionally, metal ions such as Ag^{2+}, Fe^{2+}, Co^{2+}, Ni^{2+}, and Mn^{2+} either form lipophilic soluble chlorocomplexes or weak chlorocomplexes that dissociate easily and are thus available to microorganisms for uptake (Byrne 2002)

Furthermore, Hubmatcher et al (2007) have proposed in their study of iron uptake by *H. salinarum*, a reductive iron transport system across the cell membrane located at cell surface or existence of a ligand exchange system at cell surface or cell membrane. Such an reductive system is also found in *S. cereviseae* where ferric iron is reduced to ferrous form by one of the Fre- proteins and subsequently taken up as the ferrous species by a low affinity transport

system (Fet4p) or as ferric form by high affinity system composed of a multicopper feroxidase (Fet3p) which reoxidises the ferrous iron and the respective transport protein, the ferric iron permease (Ftr1p) (Kosman 2003; Van ho *et al.* 2002). Dps A which are iron storage/detoxification proteins are known to be expressed in response to excess iron and found in bacteria, eukaryotes as well as Archaea (Andrew *et al.* 2003). The binding of Fe^{2+} to Dps protects cells from oxidative stress by inhibiting the Fe catalysed production of hydroxyl radicals. This is justified by the appearance of metal induced bands especially at 20kDa which is similar to molecular weight of Dps. Additionally, Hubmacher *et al.* (2002) have reported a protein with a apparent molecular mass 50kDa and one upregulated protein 70kDa in iron repleted membranes of *H. salinarum.* DpsA-like proteins of *H. salinarum* possess features of non-haem bacterial ferritins that are expressed to sequester the excess iron, the expression of which is repressed under iron starved condition (Bereswill S 2000). Further, formation of aggregate and severe clumping depicted in GUSF-1in response to Fe^{2+} visible in SEM micrographs, suggest the role of EPS matrix which can trap the metal within, thus, avert the movement of excess metal inside the cell. This result corroborates by a study made by Kawakami *et al*. (2007) which demonstrates the induction of cell aggregate formation of *H. salinarum* by metal ions such as Cr^{2+}, Mn^{2+}, Fe^{2+}, Co^{2+}, Ni^{2+}, Cu^{2+} and Zn^{2+} mediated through binding with EPS wherein these metal ions substitute Ca^{2+} during aggregate formation. This is explained by binding of Ca^{2+} to certain aggregation factors present on the cell surface and induces ionic cross bridging between EPS resulting in aggregation of haloarchaeal cells. The presence of certain receptor proteins especially glycoproteins on the cell surface interact with Ca^{2+} to form cell aggregates.

The cell membrane of organism act as a first point of interaction between the metal and the microbial cell. The alteration or increased content of phospholipids and glycolipids is indicative of responses of culture towards presence of metal in surrounding environment.

According to Popova *et al.* 2007, Cu^{2+} and Cd^{2+} ions lead to increase in the acidic phospholipid content of *Ps. putida* IB28 indicative of their complexation with heavy metal ion (Popova *et al.* 2008). Besides, haloarchaeal cell wall mainly consists of plasma membrane made up of isoprenoid di and tetra ethers and an external S-layer composed of glycoprotein whose carboxyl and hydroxyl groups can also bind metal ions such as U, Ni^{2+}, Cu^{2+} (Pollmann and Matys 2007). In our experiments, Fe^{2+} increases the cell stability preventing lysis at 12 % NaCl environment reflecting the effect of Fe^{2+} on autolytic enzymes. This is contradictory to finding reported by Francois *et al.* (2011) that Fe^{3+} alone fail to stop lysis in *M. jannaschii* cells wherein the combined effect of Fe and Si lead to preservation of cells. Haloarcheal carotenoid pigments such as bacterioruberin and other accessory pigments such as lycopene, retinal components are known to be involved in membrane energetic (Lanyi, 1997; Lanyi Meada 1997) in addition to shielding cells from damage from UV and free radicals (Salto *et al*. 1998). The decrease in intensities of bacterioruberin, lycopene, retinal components, abolishment of phytofluene component of GUSF-1 grown with $Fe^{2+}$and appearance of unidentified components in case of GUFF129 grown in presence of Fe^{2+} indicates shift in physiology or a response mechanism of haloarchaea to subvert the stress exerted by Fe^{2+} ions. As per our understanding reports of metal induced changes in pigmentation of haloarchaea have not been reported earlier. Metal induced alteration or induction of pigment have been reported in eubacterial consortia; incase of *Myxococcus xanthus* copper is found to induce carotenoid synthesis at suboptimal growth conditions

(Moraleda *et al.* 2005). Deiser *et al* (2010) have reported that carotenoid pigmentation increases the resistance of heterotrophic bacteria to environmental stressors such as ultraviolet radiation, temperature.

SECTION B: **Response of haloarchaeon GUSF-1 and GUFF 129 to Mn^{2+} ions**

Manganese is acknowledged as an essential trace element in the cellular physiology of all microorganisms. It is one of the metals involved in the water oxidizing complex of photosynthetic organisms (Ananyev *et al.* 2001) and one of the important metals involved in enzymatic dismutation of superoxide radical anion (Whittaker 2000) .The present study demonstrated the growth response of two haloarchaeal cultures to Mn^{2+} ions in mineral salts growth medium. Both the cultures GUSF-1 and GUFF129 exhibited tolerance to high concentration of Mn^{2+} with a MIC of 50 mM and 20 mM in mineral salts medium. The tolerance to high manganese concentration can be attributed firstly to the origin of the cultures of being isolated from an estuary of Goa - India which is under influence of ferromanganese mining activities hence endowing an innate characteristic of tolerating the former (Alagarsamy 2006). Secondly, the two cultures being an extremely halophilic, they require high concentrations of anions and cations such as sodium, potassium, chlorides making them naturally tolerant to metal ions (Ventosa *et al.* 1998). In contrast, Kaur *et al.* (2006) has reported the inhibitory concentration of Mn^{2+} to be 2 mM in *Halobacterium* NRC-1 which seems to be a consequence of growth inhibition and not the killing effect of the metal. As discussed in section A (Chapter 2) the influence of physico-chemical parameters such as salinity, pH, temperature, was evident from the response of haloarchaeons to manganese as it can alter effective free metal ion concentration in the cell (Babich and

Stotzky 1980). Interestingly, the existence of manganese in the medium enhanced the growth of GUSF-1 and GUFF129 which accumulated 48.5 mg L^{-1} and 45.5 mg L^{-1} of the metal inside the cells that corroborated with a early study of Gibbons and Sehgal (1960) as discussed in Section A where low concentration of Mn^{2+} is known to enhance the growth of haloarchaea. Additionally, it was also noticed that during the log phase of both the haloarchaea there was less accumulation of manganese as compared to that when culture entered the stationary phase and continued to do so till the late stationary phase. This is supported by the fact that rapidly growing cells tend to contain less Mn^{2+} then slowly growing or stationary cells. However, the transcriptional regulation relative to this is unclear (Kehres and Maguire 2003). GUSF-1 and GUFF129 showed an absence of manganese oxidation in presence of glucose as a carbon source which is contradictory to that reported for fungi and bacteria (Torre and Gomez 1994; Fernandes *et al.* 2005). The undetectable oxidation of manganese could possibly due to increase in uptake of Mn^{2+} for cellular functions or by manganese requiring enzymes for scavenging of free radicals if formed thus not being oxidized by the organism. Besides, induction of proteins bands in Mn grown whole cells elucidates the role of proteins in manganese tolerance. Kaur *et al.* (2006) proposed in their study with *Halobacterium* NRC-1 that around 91 % of early response genes deviates from normal transcripts level on exposure to transition metal ions which are reverted to prepertubation levels once the damaged protein or transcript is replaced by new proteins for managing metal stress. These included transcriptional regulator genes, transporter genes for phosphate, metals and peptides, ribosomal protein genes and protein export genes. This also can be related to the expression of phospholipid being enhanced when exposed to manganese in our study. Haloarcheal carotenoid pigments such as bacterioruberin and other accessory

pigments such as lycopene, retinal components are known to be involved in membrane energetics (Lanyi, 1997; Lanyi Meada 1997) in addition to shielding cells from damage from UV and free radicals (Salto *et al.* 1998). The decrease in the intensities of bacterioruberin, phytofluenes, retinal, lycopene in GUSF-1 and the induction or deletion of pigment components in GUFF129 reflects a protective response mechanism of the cultures toward manganese. This is also substantiated by the fact that the bacterioruberin in the lipid membranes of the haloarchaeal cell greatly increase the rigidity and decrease the water permeability (Lazrak *et al.* 1988). This is evident from the cell stability of GUSF-1 and GUFF129 exposed to manganese being stable at salinity of 12 % due to the circuitous protection provided by the pigment components. Furthermore, the alteration in cell morphology to elongated forms and severe aggregation of cells could be a strategy to withstand metal rich environment. This result corroborates to that of *Acidiphilium symbioticum* H8 which exhibited alteration of coccobacilli to coccoidal, lenticular shape with constrictions in the presence of cadmium and to round cells induced by copper (Chakravarthy and Banerjee, 2008). The absence of siderophore detection can be attributed to presence of manganese which can substitute for Fe^{2+} in control of siderophore synthesis making the medium iron repleted (Sayyed and Chincholkar 2010). Further, although haloarchaea are known to possess plasmids (Garcia *et al.* 1996), in our study no plasmid responsible for metal tolerance were detected in the GUSF-1 and GUFF129. Hence, we conclude that the metal tolerance ability of the two haloarchaeon was confined to its genomic DNA. The biochemical characterization of GUSF-1 and GUFF129 revealed that the two haloarchaeon belonged to genus *Haloferax* sp. and *Natrialba* sp. respectively which confirmed their haloarchaeal identity also proved by the 16S rRNA analysis of GUSF-1.

Chapter 3

Uptake studies of Fe^{2+} and Mn^{2+} ions by Haloferax sp. GUSF-1

Intact cells of microorganisms live or dead and their components are highly efficient sorbent of both soluble and particulate forms of cations and anions (Aksu and Kutsal 2011). Various microbial species have been shown to be relatively efficient in uptake of metal ions from polluted effluents (Geethi *et al*. 2014). High concentration of salt in wastewater treatment systems poses a major problem for conventional biological treatments. Halophilic and extremely halophilic microbes are suitable candidates for cleaning up the same, since anions and cations are needed for their growth (Ventosa 2004). In fact, immobilsation / sequestration of metal ions by cell surface components are studied for eubacterial and eukaryotic organisms (Gadd 2010). Attempts were made at elucidation of such processes if any, studied using the resting cells of haloarchaea forms the content of this chapter. The relevant similar methodologies are clubbed together while the results are presented under two sections Section A:- Uptake of Fe^{2+} by *Haloferax* sp. GUSF-1and Section B:- Uptake of Mn^{2+} by *Haloferax* sp. GUSF-1. Finally, this chapter ends with a common discussion.

METHODOLOGY

3.1. Preparation of resting cells of haloarchaea

5 liter benchtop fermentor (B Braun) containing 3 l NTYE medium, pH 7.0 was inoculated with seed culture of *Haloferax* sp. GUSF-1for mass production of cellular mass. The stirrer rpm was maintained at 300 with an incubation temperature of 30^{o}C. The cells having A_{600nm}= 1.5 were harvested from culture broth on 5th d by centrifuging at 12000 rpm, 4 °C, washed and resuspended in 15 % NaCl and stored at 10 °C in refrigerator and used within four days of preparation for uptake studies of Fe^{2+}/ Mn^{2+} ions.

3.2 Formulation of batch assay for uptake of Fe^{2+}/ Mn^{2+}

Glassware used, were soaked overnight in 10 % nitric acid (HNO_3) and rinsed twice with milliQ water (H_2O). Fresh 1 M stock solution of Fe^{2+} as $FeSO_4.7H_2O$ / $MnSO_4.7H_2O$ (Merck Ltd. India) was prepared using deoxygenated water prepared by bubbling oxygen free N_2 in deionized high purity water (18 MΩ- cm) for 24 h in standard volumetric flask and appropriately diluted to obtain the desired concentration as per the requirement. For use in experiments, portions were appropriately diluted to obtain the desired concentration for an experiment. For uptake of Fe^{2+}/ Mn^{2+}, 100 ml of 2 mM $FeSO_4.7H_2O$ / $MnSO4.7H_2O$ was mixed with 1 g of resting cells (or dry biomass), shaken at 150 rpm**,** at 30 ºC. After 5 h, the reaction mixture was centrifuged at 12000 rev min^{-1}; the cell free supernatant thus obtained was digested with nitric acid (HNO_3) and sulfuric acid (H_2SO_4) (2:1 v/v) and was estimated for Fe / Mn by atomic absorption spectrophotometer (AAS). Standard of Fe / Mn solution of known concentration for AAS was prepared in 0.1 N nitric acid in the range of 0-15 ppm to obtain a standard graph. Each experiment was conducted in triplicates and plotted with standard error bars. Abiotic Fe^{2+} oxidation was also avoided by using freshly prepared $FeSO_4.7H_2O$ solution at acidic pH.

3.3 Optimization of uptake of Fe^{2+} / Mn^{2+} by *Haloferax* sp. GUSF-1

3.3.1 Contact time

Resting cells were added to a flask containing Fe^{2+} / Mn^{2+} (110 mg L^{-1}/ 109.54 mg L^{-1}, respectively) prepared in 15 % NaCl solution was incubated at different time interval 0 , 1 , 2 , 3 , 4 and 5 h respectively on rotary shaker at 150 rpm and 30 ºC (room temperature). The respective metal ion was estimated as detailed in sub section **3.2**

3.3.2 pH

Resting cells were added to a flask containing Fe^{2+} / Mn^{2+} prepared in 15 % NaCl solution with pH adjusted to pH 2, 4, 6, 8 (in case of Fe^{2+}) and pH 3.0, 5.0, 6.0, 6.8, 7.0, 8.0, 10 (incase of Mn^{2+}) using 0.1 N HCl and 0.1 N NaOH, incubated at 150 rpm for respective optimum contact time. The respective metal ion was estimated as detailed in sub section **3.2**

3.3.3 % NaCl

Resting cells were added to a flask containing Fe^{2+}/ Mn^{2+} prepared in 5, 10, 15, 20, and 25 % NaCl solution incubated at 150 rpm for 5 h. The respective metal ion was estimated as detailed in sub section **3.2.**

3.3.4 Fe^{2+}/ Mn^{2+} concentration

Wet biomass were added to a flask containing 25, 50, 100, 150 and 200 mg of Fe^{2+}/ Mn^{2+} per liter of 15 % NaCl adjusted to respective optimum pH and at optimum contact time for each of the metal. The metal in the filtrate was estimated as mentioned in sub section **3.2**

3.3.5 Biomass concentration

Uptake of Fe^{2+}/ Mn^{2+} was studied by incubating separately 0.2, 0.4, 0.6, 0.8, 1, 1.2 g wet weight of resting cells, respectively, in 100 mL of Fe^{2+}/ Mn^{2+} prepared in 15 % NaCl solution, at 150 rpm, 30 ºC. Metal was estimated as detailed in sub section **3.2**

3.3.6 Temperature

Resting cells were added to flask containing Fe^{2+}/ Mn^{2+} in 15 % NaCl solution and incubated at temperature of 20, 30,40, 50ºC, respectively, on incubator shaker at 150 rpm. Metal filtrate was estimated as described in sub section **3.2**

3.4 Evaluation of efficiency of uptake

Fe^{2+} / Mn^{2+} ions uptake by resting cells was calculated from

$$Q = (Ci - Cf) \times V/M \quad (1)$$

where Q is Fe^{2+}/ Mn^{2+} uptake (mg g^{-1} dry weight), V is the volume of Fe^{2+}/ Mn^{2+} sorbate (L), Ci and Cf are the initial and the final concentrations of Fe^{2+}/ Mn^{2+} (mg L^{-1}) respectively, and M is the weight of resting cells (g).

The efficiency of resting cells in terms of % removal of Fe^{2+}/ Mn^{2+} ions was calculated as

$$R = 100 \times [(Ci - Cf)/Ci]. \quad (2)$$

3.5 Nature of uptake isotherm

3.5.1 Homogeneity of resting cells for Fe^{2+}/ Mn^{2+} ions was evaluated using Langmuir equation (Langmuir, 1918)

$$q_e = Q_{max} (b\ C_e / 1+bC_e) \quad (3)$$

where, C_e (mg L^{-1}) corresponds to the Fe^{2+}/ Mn^{2+} ion concentration in the uptake assay at equilibrium while q_e (mg g^{-1}) was obtained from the concentration of Fe^{2+}/ Mn^{2+} ions uptake per unit weight of resting cells at equilibrium. The Langmuir constants, Q_{max} and b, related to

maximum uptake capacity of Haloarchaeal resting cells and bonding energy of uptake, respectively, were obtained by plotting $1/q_e$ versus $1/C_e$. Q_{max} and b were calculated from the intercept and slope of the plot.

3.5.2 Heterogeneity of resting cells was determined by Freundlich equation (Fruendlich, 1906)

$$\text{Log } Q_e = (1/n) \text{ Log } C_e + \text{Log } K_F \quad (4)$$

where Q_e is the amount of Fe^{2+}/ Mn^{2+} ion uptake at equilibrium mg g^{-1} and C_e is the amount of Fe^{2+}/ Mn^{2+} ions in solution at equilibrium (ppm), were obtained by plotting log Q_e versus log C_e.; The values of Freundlich parameters i.e. n and K_F (L g^{-1}) were computed from the slope and intercept of straight portion of the plot.

3.6 Evaluation of kinetics of uptake

The mechanism of uptake of Fe^{2+}/ Mn^{2+} by resting cells was evaluated using

(i) the pseudo-first order rate equation expressed as

$$\text{Log } (q_e - q_t) = \text{Log } q_e - k_1 t/2.303 \quad (5)$$

where q_e and q_t are the amounts of Fe^{2+}/ Mn^{2+} ions (mg g^{-1}) absorbed at equilibrium and at time t, respectively, and k_1 is the first-order rate constant (min^{-1}). k_1 was obtained from the slope of the plot of log (q_e - q_t) versus t.

(ii) The pseudo-second-order kinetic model has the linear form of

$$t/q_t = 1/k_2 \, q^2_e + t/q_e \quad (6)$$

where q_e is the maximum uptake capacity (mg g^{-1}) and k_2 is the equilibrium rate constant (g mg^{-1} min^{-1}). k_2 and q_e were calculated from the plot of t/q_t versus t (Ho *et al*., 2001).

3. 7 Recycling of resting cells

The resting cell mass was separated from the reaction mixture after respective optimum time of uptake by centrifugation at 12000 rpm for 10 min. The resting cell biomass was washed twice by suspending in 15 % saline and dried overnight at 80 ºC and reused for a subsequent uptake cycles.

3.8 Evaluation of Fe^{2+}/ Mn^{2+} loaded haloarchaeal resting cells

3.8.1 SEM-EDX analysis of resting cells

Samples of resting cells and those loaded with Fe^{2+}/ Mn^{2+} were separately dried at 80 ºC, till constant weight, powdered and coated on gold stubs and each was scanned using scanning electron microscope coupled with energy dispersive X-ray analyzer SEM-EDX (JEOL JSM 5800LV).

3.8.2 FTIR analysis of resting cell biomass

Samples of dry resting cells and those loaded with Fe^{2+}/ Mn^{2+} were ground separately with KBr (1:10, w/w), each was then exposed to IR as a KBr tablet in a IR spectrophotometer (Prestige-21 FTIR Shimadzu) for IR profile.

3.9 Evaluation of mechanism of uptake in resting cells

3.9.1 Preparation of heat killed cells

One gram wet weight resting cells of *Haloferax* sp. GUSF-1 was autoclaved for 15 min and allowed to cool at 30 ^{o}C. The dead cells obtained were then suspended in 15 % saline containing 2 mM of $FeSO_4.7H_2O$ / $MnSO_4.7H_2O$ solution and incubated at 30 ^{o}C in rotary incubator shaker at 150 rpm. Cells were separated by centrifugation at 12000 rpm from the metal solution and Fe^{2+}/ Mn^{2+} ions remaining in solution were quantified as described in sub section **3.2**.

3.9.2 Effect of metabolic inhibitors on the Fe^{2+}/ Mn^{2+} uptake

To study the effect of metabolic inhibitors on the metal uptake, the whole cells on subsequent washing with 15 % saline were resuspended in same, containing 10 mM 2,4-dinitrophenol (2,4-DNP) ,1 mM sodium azide and 400 µM DCCD for 60 min respectively prior to exposure to respective metal solution. Cells were separated by centrifugation at 12000 rpm from the metal solution and metal uptake was quantified as described in sub section **3.2**.

3.9.3 Localization of Fe^{2+}/ Mn^{2+} in cells

Resting cells exposed to Fe^{2+}/ Mn^{2+} ions were separated by centrifugation at 12000 rpm for 15 min and the cell pellet obtained was sonicated for 3 min at a duty cycle of 0.5 seconds until complete disruption occurred. The sonicated cell suspension was then centrifuged at 12000 rpm for 10 min at 4 °C to remove whole cells if any and cell debri. The supernatant was decanted and recentrifuged at 19000 rpm for 1 h at 4 °C. The sedimented cell envelope and supernatant were collected separately and analyzed for Fe^{2+}/ Mn^{2+} content in respective fractions as described in 3.2.

RESULTS

SECTION A

3.10 Uptake of Fe^{2+} by *Haloferax* sp. GUSF-1

3.10.1 Preparation of resting cells for uptake studies

Haloferax sp. GUSF-1 grew optimally with a lag of one day producing an orange red pigment. Growth of the culture at an absorbance of 1.7 A_{600nm} yielded 2.36 mg ml^{-1} dry weight of cells.

3.10.2 Optimization of uptake of Fe^{2+} ions

3.10.2.1 Contact time

As seen in **Fig. 3.1a** the resting cells of *Haloferax* sp. GUSF-1 showed a uptake of 32.4 mg of Fe^{2+} g^{-1} of biomass in 1h followed by maximum uptake of 41 mg in 2 h, following which the uptake remains constant indicated by 41 mg of uptake at 3 , 4 and 5 h, respectively per gram of resting cells.

3.10.2.2 Temperature

The effect of temperature on uptake of Fe^{2+} was evident with 14.8 mg at 20 ºC, 40.6 mg at 30 ºC with a decrease in uptake at 40 ºC and 50 ºC showing 35.9 mg and 33.8 mg, respectively of Fe^{2+} per g of resting cells (**Fig. 3.1b**)

3.10.2.3 pH

As illustrated in **Fig. 3.1c**, influence of pH on uptake of Fe^{2+} was observed. At acidic pH 2.0 and 4.0 the biomass of resting cells took up 30 mg and 33 mg Fe^{2+} per g of biomass. At pH 6.0 an optimum uptake was observed of 41 mg while at pH 8.0 it decreased to 20 mg of Fe^{2+} per g of wet biomass.

3.10.2.4 Fe^{2+} concentrations

At different initial concentration of Fe^{2+} an increase in uptake with increase in Fe^{2+} concentration was observed (**Fig**. **3.1d**). At 25, 50, 100, 150 and 200 mg $L^{-1}$the uptake was 10.2, 20.87, 41, 62.74, and 83.2 mg of Fe^{2+} per gram of wet biomass.

3.10.2.5 Weight of the resting cells

Interestingly, the uptake of Fe^{2+} also increased with increase in the wet biomass evident with 27.8 mg, 32 mg, 35 mg, 39 mg and 40 mg of Fe^{2+} being taken up with biomass concentration of 0.2, 0.4, 0.6, 0.8 and 1 g (**Fig. 3.1e**).

3.10.2.6 % NaCl

At salinity of 0 % and 5 %, the uptake of Fe^{2+} was 5 mg and 10 mg of Fe^{2+} per g of wet biomass (**Fig. 3.1f**) while at 10 % and 15 % the uptake of Fe^{2+} was 35 mg and 40 mg, respectively. At 20 % NaCl the uptake decreased to 30 mg of Fe^{2+} per gram of wet biomass.

3.11 Evaluation of efficiency of uptake

The results of optimization were incorporated to formulate an uptake assay consisting of 100 mg L^{-1} of Fe^{2+} and 1 g wet weight of biomass, suspended in 15 % NaCl solution, pH 6.0

mixed at 150 rpm and 30 ºC for 120 min (**Fig. 3.2**). The specific amount of Fe^{2+} adsorbed (Q) at optimum condition was 40 mg g^{-1} wet weight of resting cell biomass with a removal efficiency of 99 %.

3.12 Nature of Fe^{2+} uptake isotherm

Maximum amount of Fe^{2+} taken up (Qmax) by resting cells of *Haloferax* sp. GUSF-1 was 67.11 mg g^{-1} wet weight, with a bonding energy of uptake (b) of 0.0169 (L mg^{-1}) and had a homogeneity corresponding to Langmuir isotherm (**Fig**. **3.3a**).

Further, the heterogeneity of uptake fitted well with Fruendlich isotherm having magnitude of uptake capacity (K_F intercept) of 1.17 mg g^{-1} and uptake constant (n) 1 (**Fig**. **3.3b**)

3.13 Kinetics of uptake of Fe^{2+}

The values of average determination coefficients (R^2) derived from **Fig**. **3.4a,b** in **Table 3.1** indicated that the uptake process followed pseudo-second order kinetics since an increase in equilibrium concentration (q_e) resulted in corresponding linear decrease in equilibrium rate constant (k_2), with an increase of initial Fe^{2+}concentration.

3.14 Reuse of resting cells

The resting cells of haloarchaeon were 99 % efficient up to two recycle (**Fig. 3.5**). However, its uptake capacity declined progressively by 48, 24.75 and 24 % in the third, fourth and the fifth cycle, respectively.

3.15 Evaluation of Fe^{2+}loaded resting biomass

3.15.1 SEM-EDX analysis of resting cells

An SEM profile of resting cells of haloarchaeon, showed a crystalline surface that appeared to be bright and shiny (**Fig**. **3.6a, b**). The EDX spectra after uptake revealed peaks due to Fe^{2+} at 2.2, 6.2 and 6.4 keV along with a shift in the phosphorous peak from 2.2 to 2.8 keV.

3.16 Mechanism of uptake of Fe^{2+}

3.16.1 Uptake of Fe^{2+} by heat killed cells and effect of metabolic inhibitors on uptake efficiency

The heat killed cells showed uptake of 23.2 mg of Fe^{2+}per g of resting cells (**Fig. 3.7**). The metabolic inhibitors affected the uptake of Fe^{2+} adversely. Treatment of cells with 2, 4 dinitrophenol reduced the uptake of iron by 36 % with 23.07 mg of Fe^{2+} per g of resting cells. In case of sodium azide the uptake was reduced to 48 % with 26.8 mg and DCCD reduced the uptake 48 % with 26.9 mg of Fe^{2+} per g of resting cells.

3.16.2 Localisation of accumulated Fe^{2+}

It was observed in **Fig. 3.8** that Fe^{2+} is taken up by different layers of cells. It was revealed that 75 % of Fe^{2+} is localized on the cell envelope whereas only 25 % is taken up by the cell into the cytoplasm

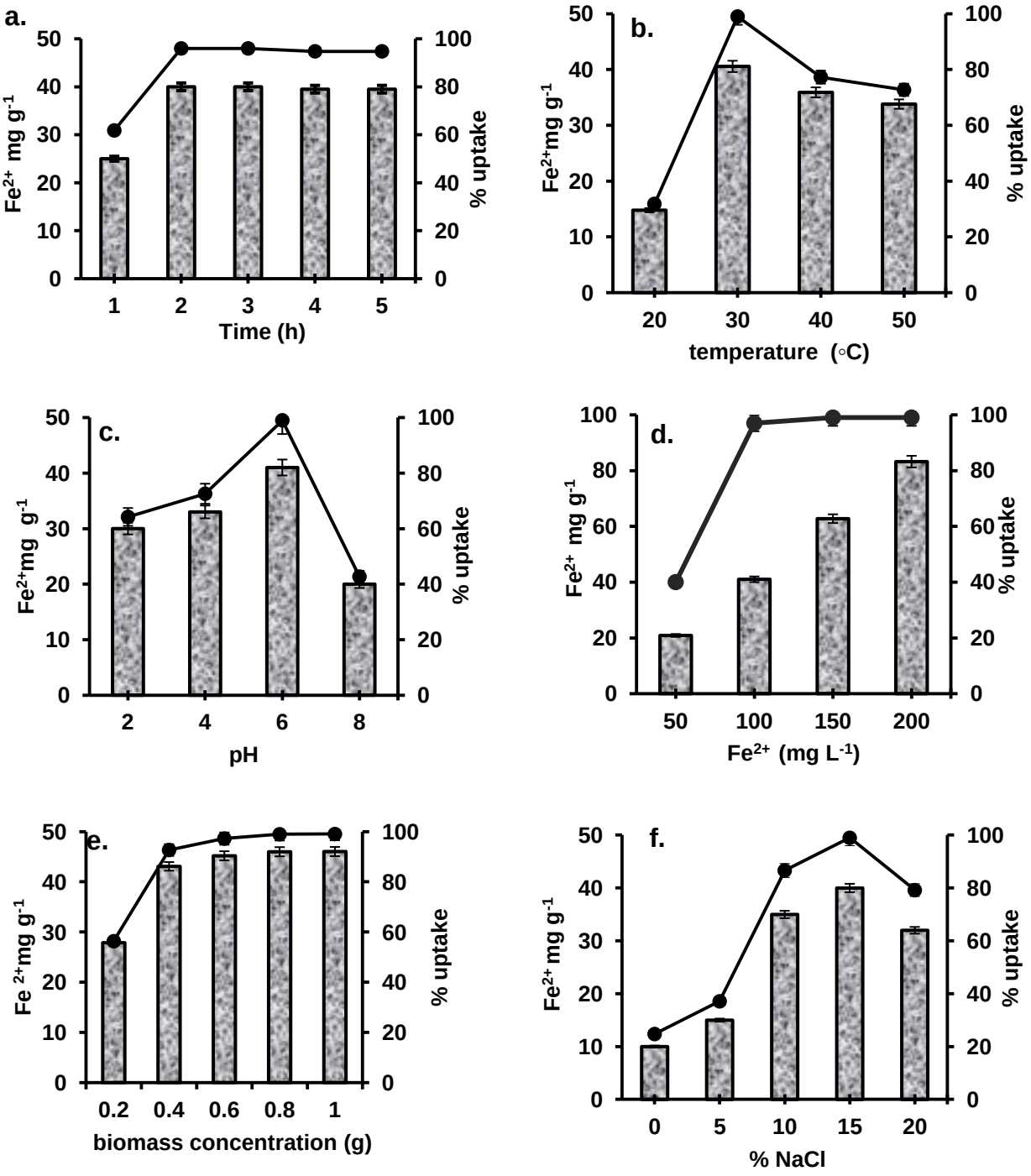

Fig. 3.1 Optimization of parameters for optimum uptake of Fe^{2+} ions by *Haloferax* sp. GUSF-1

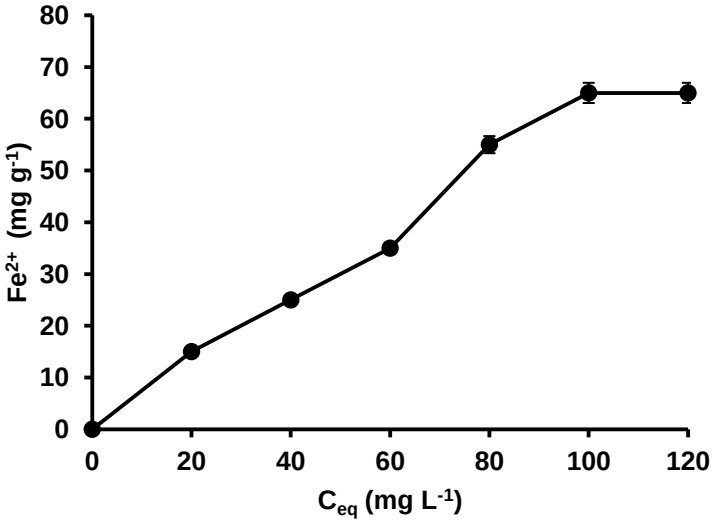

Fig. 3.2 Non-linear uptake isotherm of Fe^{2+} ions by haloarchaeon *Haloferax* sp. GUSF-1 at optimum uptake conditions

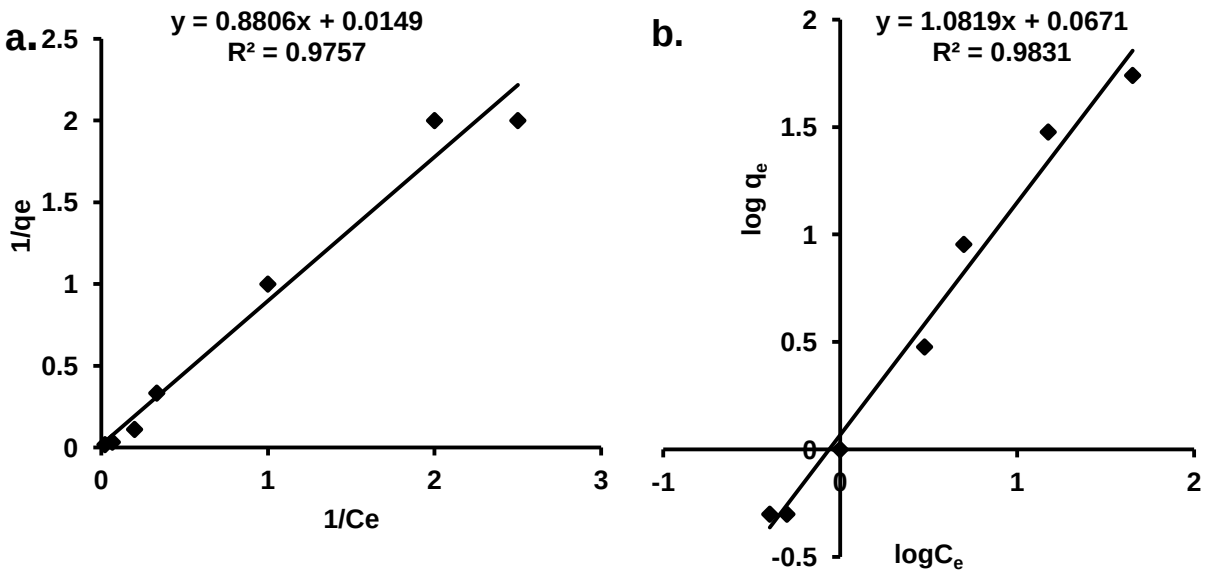

Fig. 3.3 Isotherm modeling of uptake of Fe^{2+} ions by Haloarchaeon *Haloferax* sp. GUSF-1 **(a)** Langmuir model **(b)** Fruendlich model.

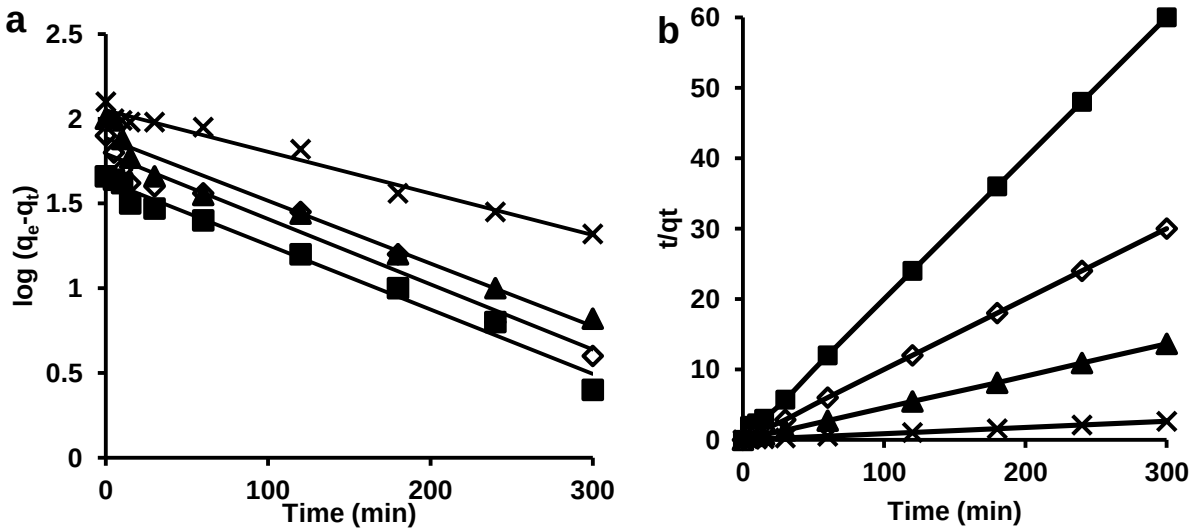

Fig. **3.4** Kinetics of uptake of Fe^{2+} ions by haloarchaeon *Haloferax* sp. GUSF-1 **(a)** Pseudo-first order **(b)** Pseudo second order.

Table 3.1. Comparison of pseudo- first order and pseudo-second order kinetic model for uptake of Fe^{2+} ions.

Fe^{2+} concentration (mg L^{-1})	**Pseudo first order**			**Pseudo second order**		
	q_e (mg g^{-1})	k_1 (min^{-1})	R^2	q_e (mg g^{-1})	k_2 (g mg^{-1} min^{-1})	R^2
50	24.09	0.245	0.60	2.67	0.474	0.99
100	51.8	0.215	0.73	5.27	0.27	0.98
150	69.55	0.261	0.58	8.31	0.135	0.99
200	89.9	0.274	0.59	11.36	0.091	0.98

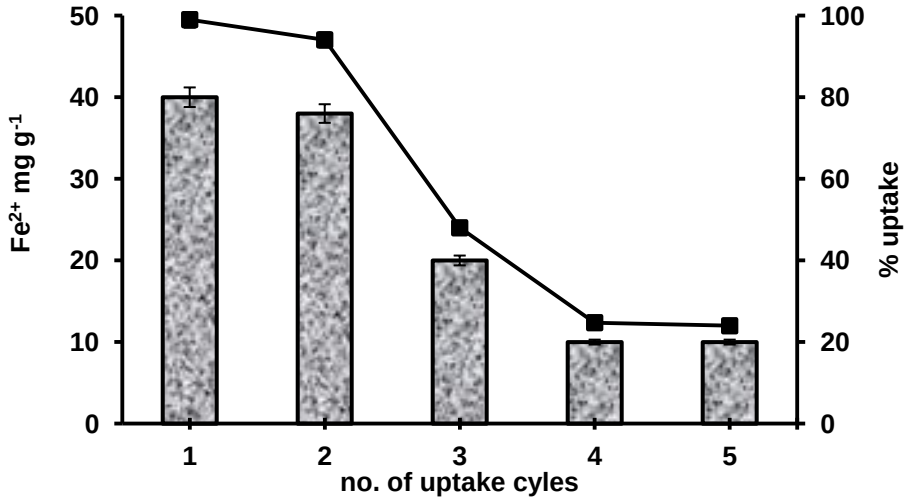

Fig. 3.5. Number of cycles resting cell biomass of haloarchaeon *Haloferax* sp. GUSF-1 used for Fe^{2+} uptake

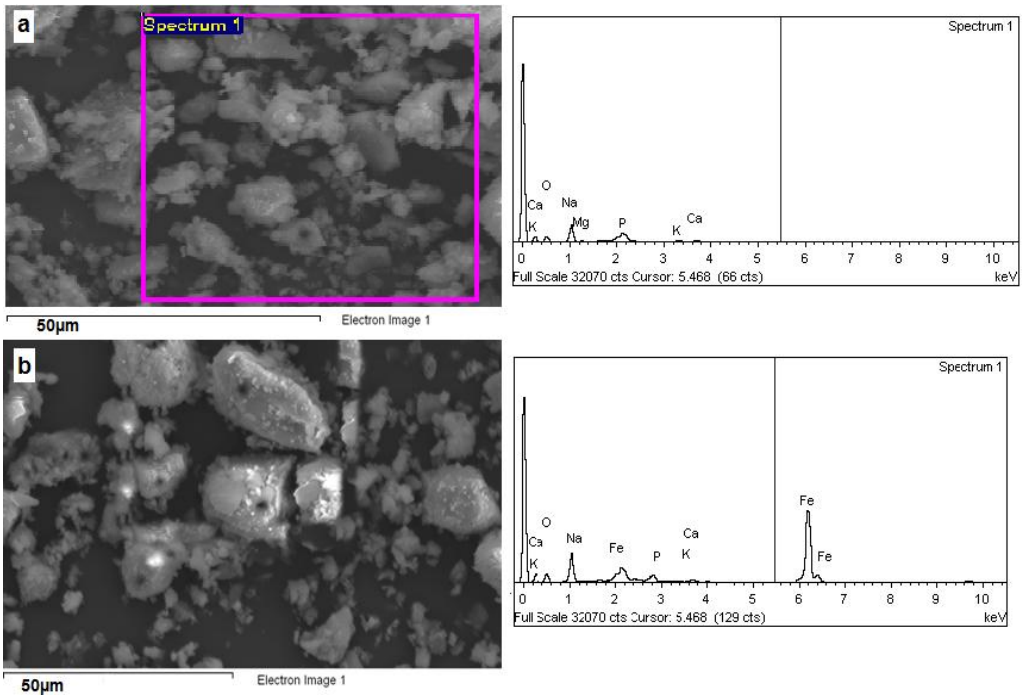

Fig. **3.6** SEM –EDX profile of *Haloferax* sp. GUSF-1 **(a)** before Fe^{2+} uptake **(b)** after Fe^{2+} uptake

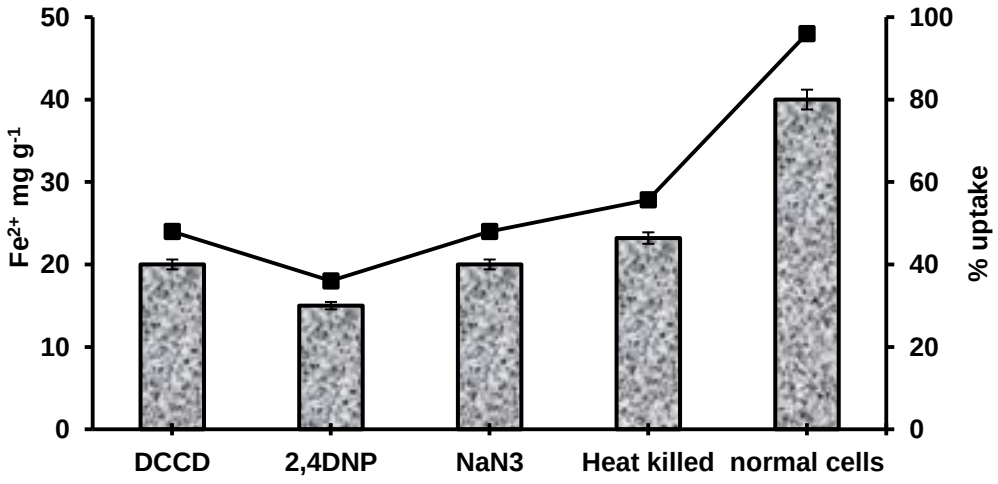

Fig. **3.7.** Effect of metabolic inhibitors and heat killed cells on uptake of Fe^{2+} by haloarchaeon *Haloferax* sp. GUSF-1

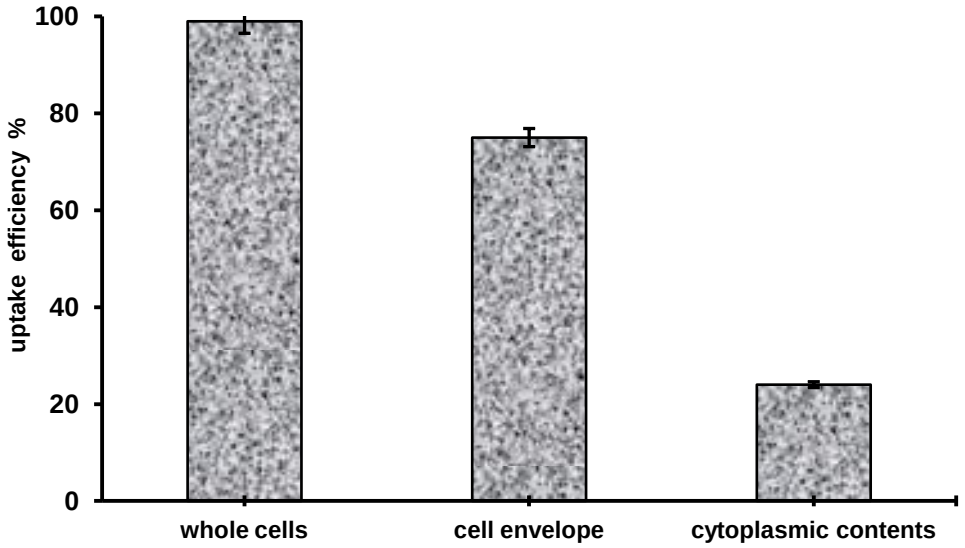

Fig. 3.8 Localisation of Fe^{2+} in cell components of haloarchaeon *Haloferax* sp. GUSF-1 after uptake.

SECTION B

3.17 Uptake of Mn^{2+} by *Haloferax* sp. GUSF-1

3.17.1 Optimization of Mn^{2+} uptake

3.17.1.1 Time

Fig. 3.9 depicts the progress of Mn^{2+} uptake over time. Resting cells of *Haloferax* sp. GUSF-1 took up 45.5 mg of Mn^{2+} in a time period of 45 min per g of resting cells.

3.17.1.2 Temperature

The uptake of Mn^{2+} ions was observed to be affected by increasing temperature of incubation in **Fig. 3.10**. At lower temperature of 20 ^{o}C the uptake was 14.5 mg of Mn^{2+} while at temperature of 30 ^{o}C the uptake of Mn^{2+} was 45 mg per g of cells in 45 min. At a higher temperature of 40 ^{o}C and 50 ^{o}C the uptake reduced to 42 mg and 28 mg of Mn^{2+} per g of cells in same time.

3.17.1.3 pH

As depicted in **Fig. 3.11** the uptake of Mn^{2+} ions increased with increasing pH up to pH 6.0, with 15.5 mg at pH 2.0 , 31 mg at pH 4.0 and 46.5 mg of Mn^{2+} at pH 6.0 per g of resting cells in 45 min. Although Mn^{2+} can form hydroxide at higher pH, resting cells took up 32.5 mg of Mn^{2+} per g of resting cells at pH 8.0 in same time.

3.17.1.4 Mn^{2+} concentration

With increasing initial concentration of Mn^{2+}, the uptake of Mn^{2+} per g of resting cells increased in 45 min from 14.5 mg to 116 mg per g of resting cells as seen in **Fig**. **3.12.**

3.17.1.5 Weight of the resting cells

Increasing the weight of resting cells from 0.25 g to 1.25 g increased the uptake of Mn^{2+} from 14.5 mg to a maximum of 46 mg per g of cells in 45 min (**Fig. 3.13**).

3.17.1.6 % NaCl

As evident in **Fig**. **3.14**, uptake progressed in absence as well as in presence of NaCl. At 0 % salinity the cells displayed an uptake of 15.5 mg of Mn^{2+} per g of resting cells in 45 min. At salinity of 5, 10 and 15 % the uptake increased from 35 mg, 42 mg to maximum of 45.5 mg, respectively, per g of resting cells in 45 min. However, at 20 and 25 % salinity the uptake decreased to 32 mg and 26 mg of Mn^{2+} per g of cells.

3.17.2 Efficiency of uptake of Mn^{2+} ions

Based on the results of optimization a uptake assay was formulated consisting of 100 mg L^{-1} of Mn^{2+} and 1 g resting cell biomass, suspended in 15 % NaCl solution, pH 6.0 mixed at 150 rpm and 30 ºC for 45 min. The specific amount of Mn^{2+}adsorbed (Q) at optimum condition was 45.5 mg g^{-1} weight of resting cells (**Fig. 3.15**)

3.17.3 Modelling of uptake using isotherms

The linear Langmuir isotherm showed homogenous uptake with Q max value of 88.5 mg g^{-1} and bonding energy (b) of 0.013 (**Fig**. **3.16a**). The Fruendlich isotherm (**Fig. 3.16b**) exhibited a better fit with an uptake capacity (K_F intercept) of 1.35 mg g^{-1} and binding constant (1/n) of 0.97.

3.17.4 Uptake kinetics of Mn^{2+}

At various initial concentrations of Mn^{2+}, the values of average determination coefficients (R^2) (**Table 3.2**) were higher than that of pseudo first order kinetic model (**Fig 3.17a, b**) indicating increase in metal uptake with increase in time exhibiting saturation kinetics.

3.17.5 Recycling of resting cells for uptake

The resting cells of haloarchaeon were 99 % efficient up to two recycle (**Fig. 3.18**). However, its uptake capacity declined progressively by 48, 24.75 and 24 % in the third, fourth and the fifth cycle, respectively.

3.18 Evaluation of Mn^{2+} loaded resting cells

3.18.1 SEM EDX analysis

The SEM micrograph (**Fig. 3.19a,b**)revealed a crystalline surface with deposition of Mn revealed by EDX spectrum showing Mn peaks at 0.5, 2.2, 5.8 keV and minor peak at 6.2 keV, respectively.

3.19 Mechanism of uptake of Mn^{2+}

3.19.1 Uptake of Mn^{2+} by heat killed cells and effect of metabolic inhibitors on uptake efficiency.

As illustrated in **Fig.3.20**, the uptake by dead cells was 10 mg of Mn^{2+} while the metabolic inhibitors sodium azide, DCCD, 2,4 –DNP reduced the uptake to 12, 22.5 and 20 mg of Mn^{2+} per g of resting cells in 45 min.

3.19.2 Localisation of Mn^{2+} during uptake

As seen **Fig.3.21 t**he cell envelope of *Haloferax* sp. GUSF-1 took up 30 mg of Mn^{2+} while the cell cytoplasm showed a uptake of 16 mg of Mn^{2+} per g of resting cells in 45 min.

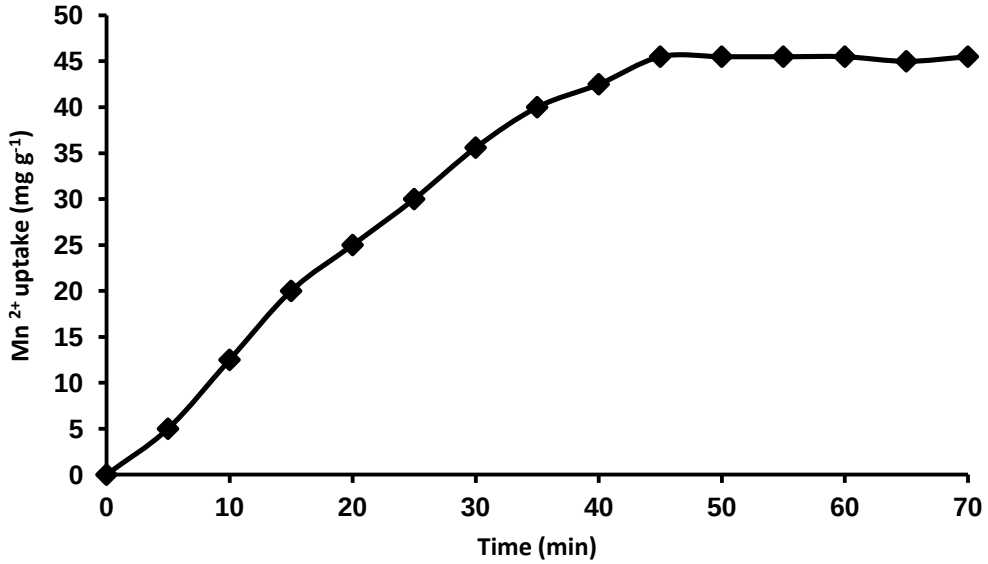

Fig. 3.9. Time course of Mn^{2+} uptake by *Haloferax* sp. GUSF-1

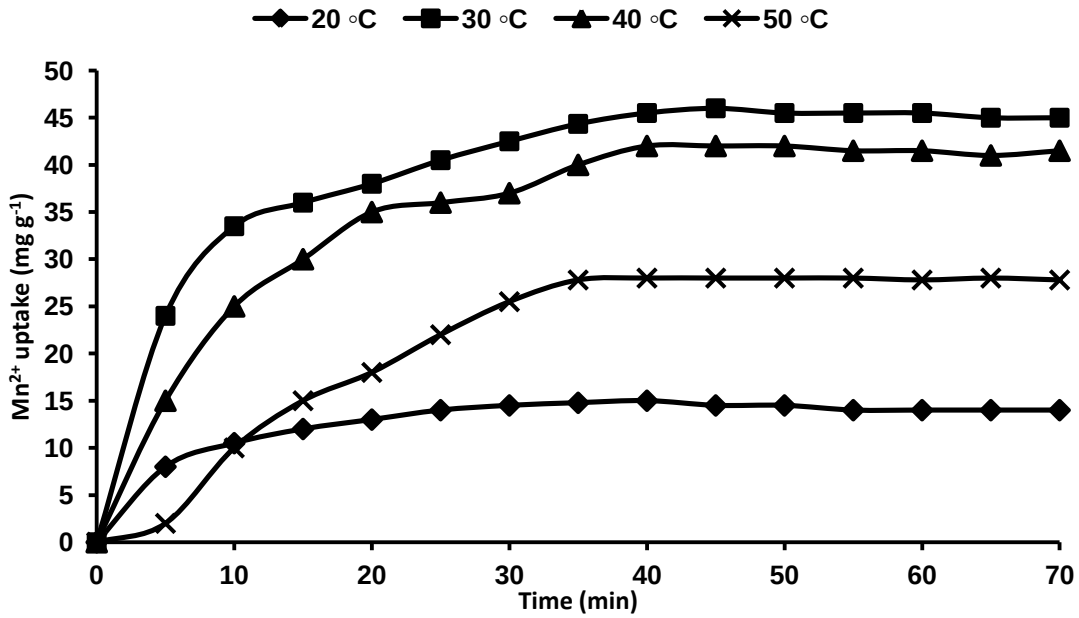

Fig. 3.10 Effect of temperature on uptake of Mn^{2+} by *Haloferax* sp. GUSF-1

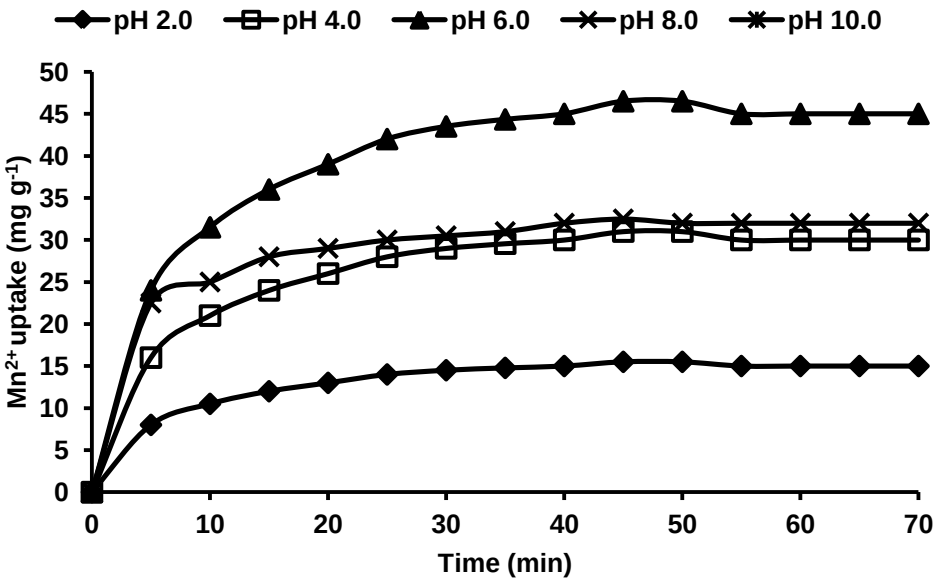

Fig. 3.11 Effect of pH on Mn^{2+} uptake by *Haloferax* sp. GUSF-1

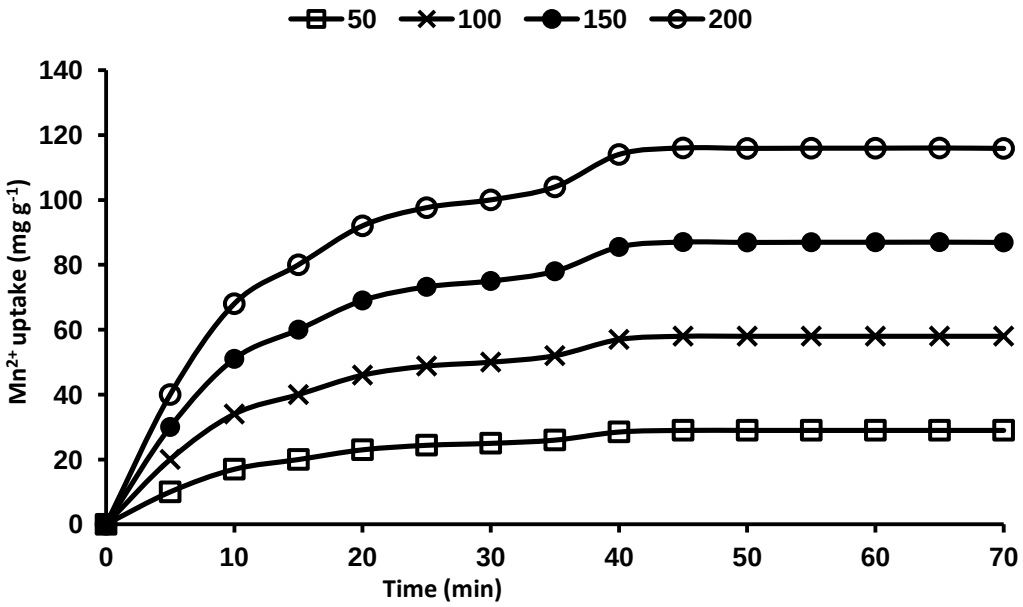

Fig. 3.12 Effect of Mn^{2+} concentration on uptake

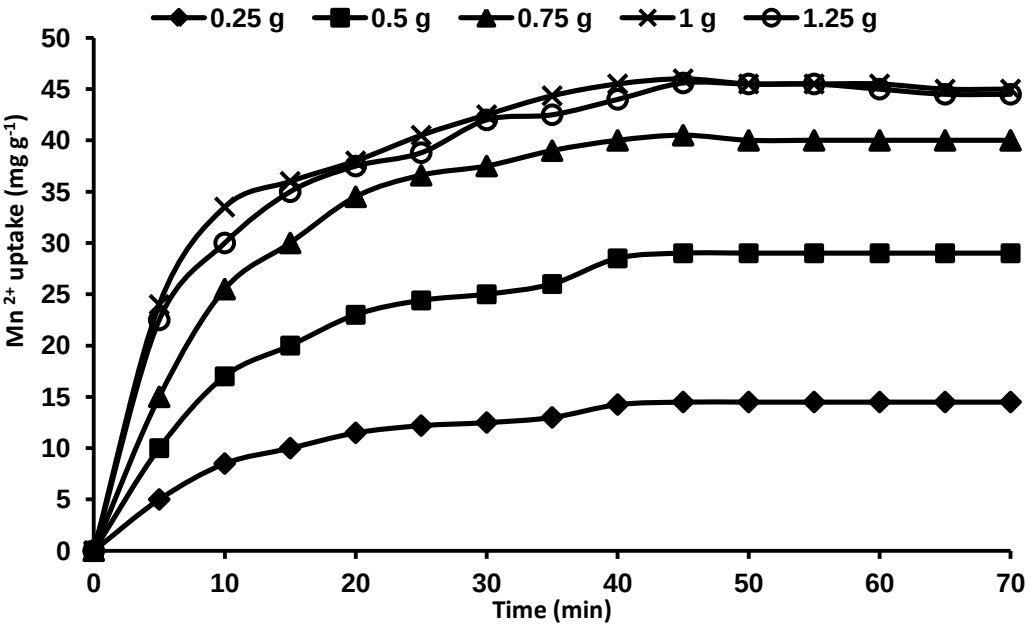

Fig. 3.13 Effect of weight of resting cells of *Haloferax* sp. GUSF-1 on Mn^{2+} uptake

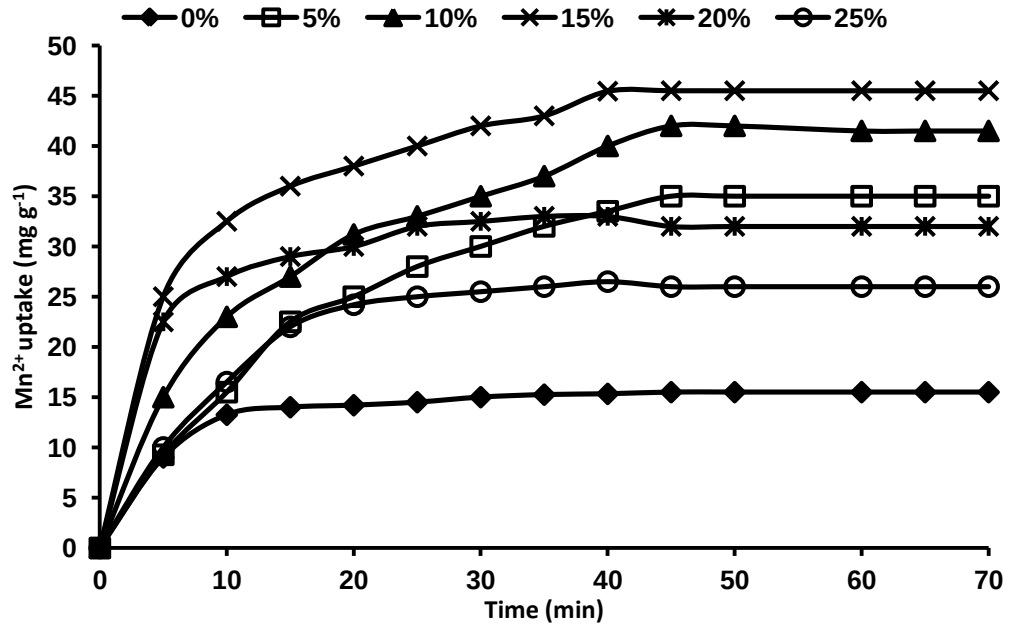

Fig. 3.14 Effect of % NaCl on uptake of Mn^{2+} by *Haloferax* sp. GUSF-1

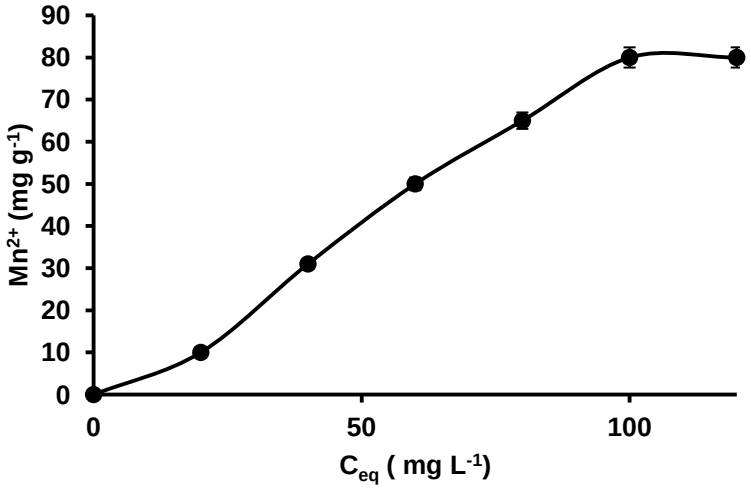

Fig. 3.15 Non-linear uptake isotherm of Mn^{2+} ions by haloarchaeon *Haloferax* sp. GUSF-1

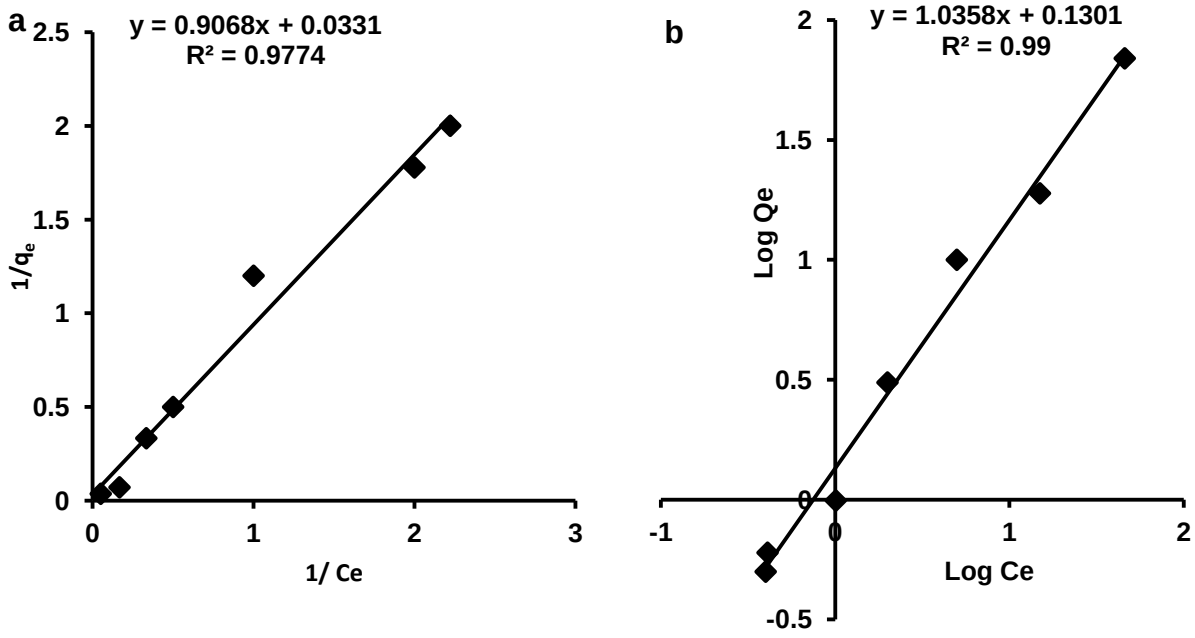

Fig. 3.16 Isotherm modeling of uptake of Mn^{2+} ions by haloarchaeon *Haloferax* sp. GUSF-1 **(a)** Langmuir isotherm **(b)** Freundlich isotherm.

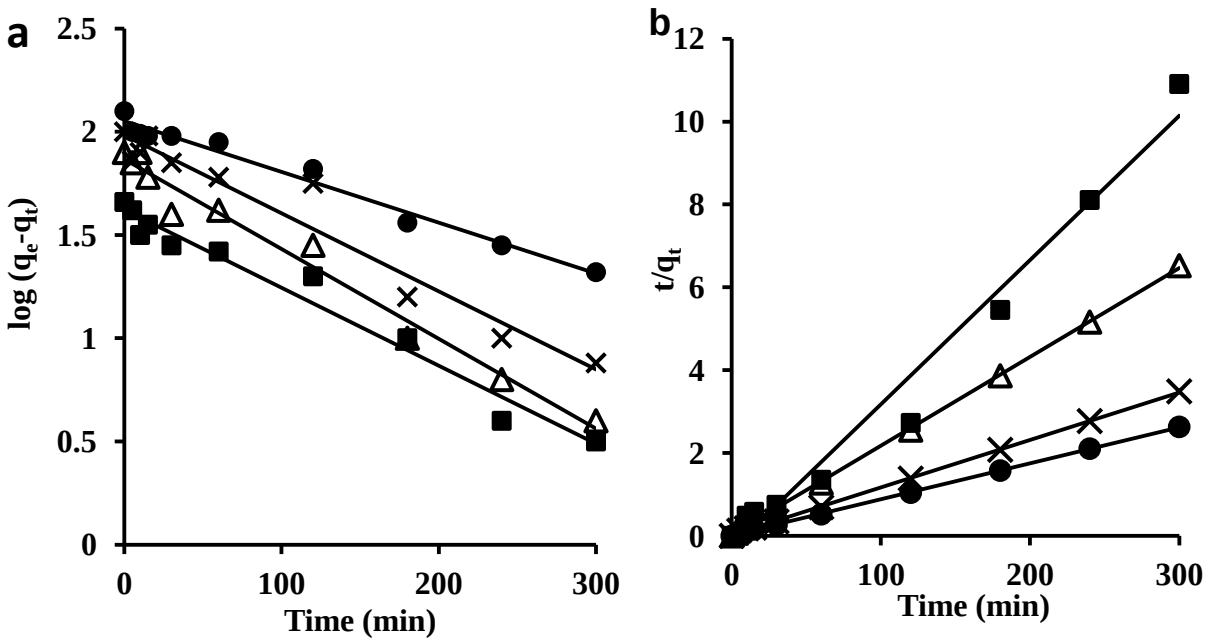

Fig. 3.17 Kinetics of Mn^{2+} uptake by resting cells of *Haloferax* sp. GUSF-1 **(a)** Pseudo first order **(b)** Pseudo second order ■ 50mg L^{-1} △ 100mg L^{-1} × 150mg L^{-1} ● 200mg L^{-1}

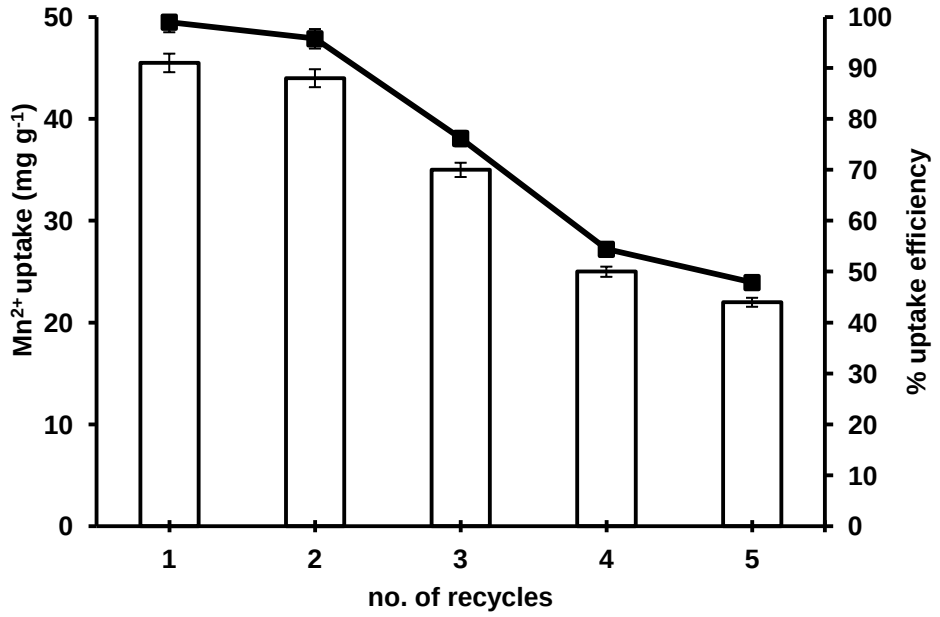

Fig.3.18 Recycling of resting cells of *Haloferax* sp. GUSF-1 for Mn^{2+} uptake

Table 3.2 Kinetic parameters for uptake of Mn^{2+} by haloarchaeon *Haloferax* sp. GUSF-1

Initial Mn^{2+} conc (mg L^{-1})	**Pseudo- first order**			**Pseudo- second order**		
	K_1 (min^{-1})	**q_e (mg g^{-1})**	**R^2**	**q_e (mg g^{-1})**	**K_2 (g mg^{-1} min^{-1})**	**R^2**
50	0.937	2.655	0.96	2.725	0.297	0.99
100	0.836	4.58	0.94	9.435	1.022	0.989
150	0.721	7.7	0.95	13.69	0.495	0.99
200	0.718	12.4	0.90	7.299	0.722	0.996

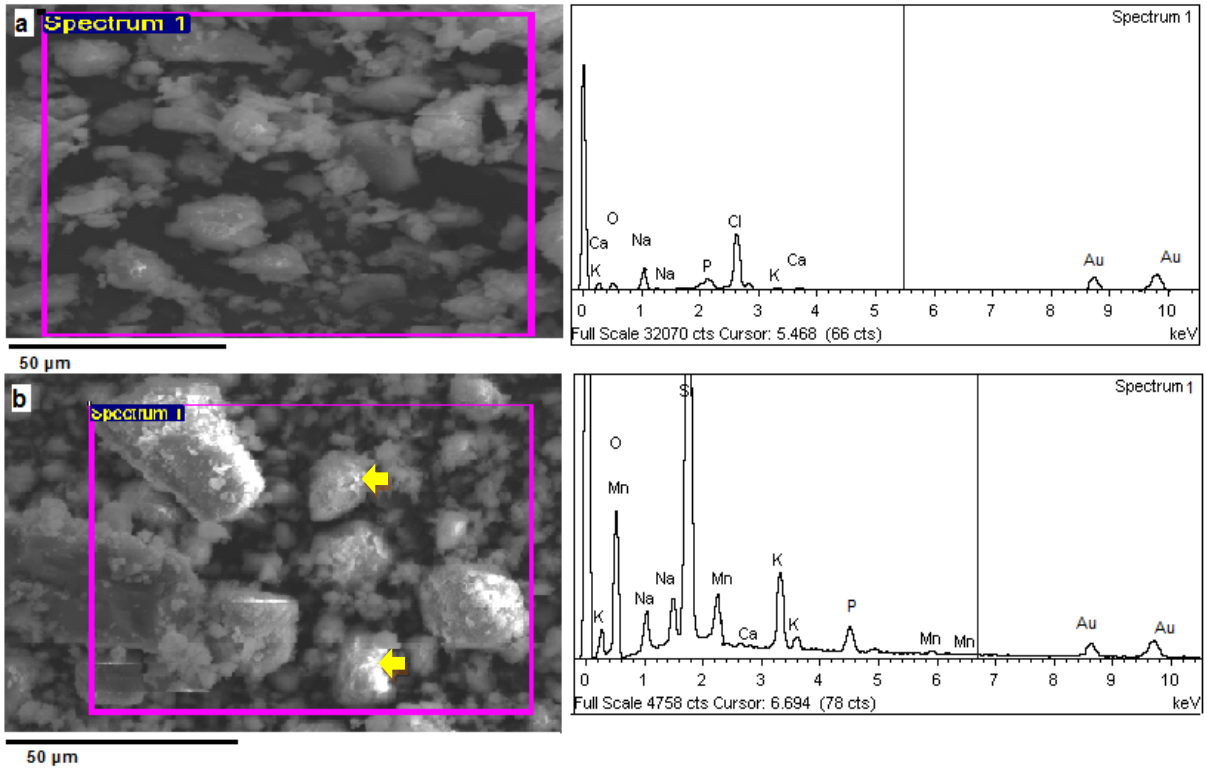

Fig. 3.19 SEM EDX profile of resting cells of *Haloferax* sp. GUSF-1 (a) before Mn^{2+} uptake (b) after Mn^{2+} uptake

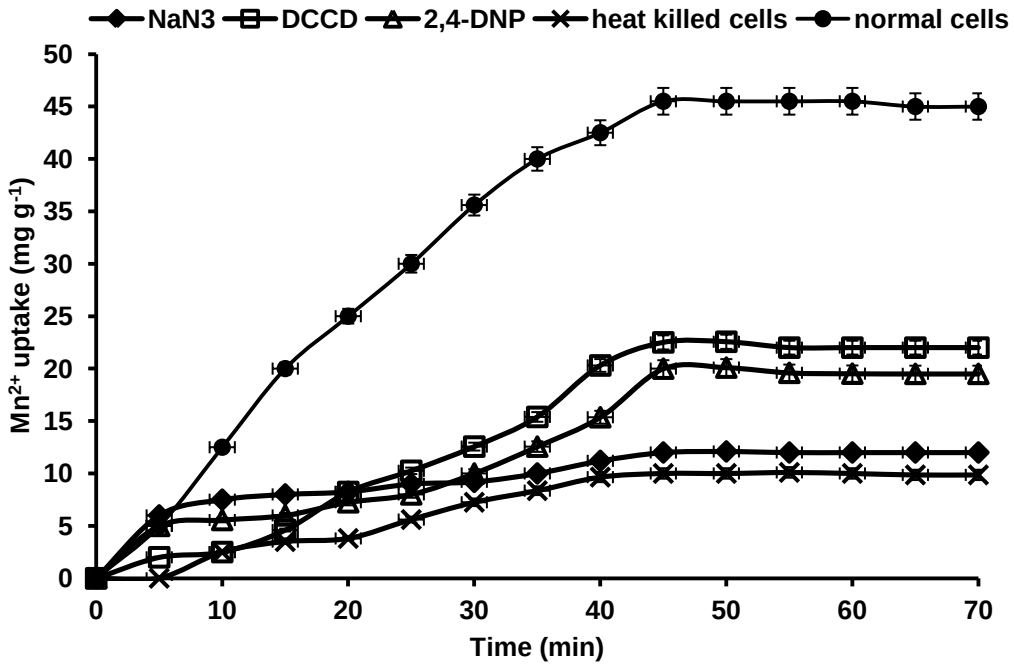

Fig. 3.20 Effect of metabolic inhibitors and heat killed cells on uptake of Mn^{2+}

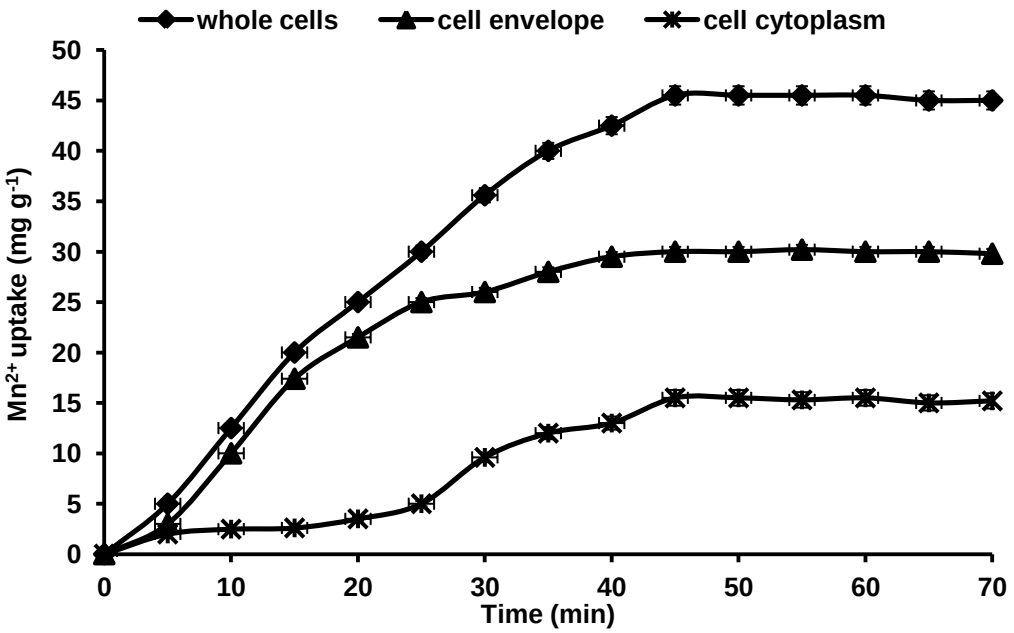

Fig.3.21 Localization of Mn^{2+} in cell components of *Haloferax* sp. GUSF-1

DISCUSSIONS

The uptake mechanism of $Fe^{2+}$and Mn^{2+} ions by live cells of *Haloferax* sp. GUSF-1 was studied. Uptake of any metal involves the contact of metal ion with the cell surface of the microorganism in study. The fact that the cells used were live resting cells, the mode of uptake is an active process that involves two distinct phases. Firstly, there is an initial rapid step which is metabolism and temperature independent and is proclaimed to entail cation binding to the cell surface while the second phase is slower metabolism dependant which is considered to transport metal ions inside the cells (Sintuprapa *et al.* 2000). This was also evident from the initial uptake of 42 mg Mn^{2+} per g of cells in 40 min followed by a slower uptake of 45.5 mg Mn^{2+} per g of cells in 45 min while for Fe^{2+} it was 32 mg in first 60 min followed by a uptake of 40 mg Fe^{2+} per g of cells in 120 min. The metabolism dependence of the uptake is substantiated by the reduced uptake of Fe^{2+} and Mn^{2+} ions to 50 % and 40 % respectively, when exposed to respiratory chain inhibitor sodium azide. The temperature independent and metabolism dependent uptake is also exhibited by uptake of 40 mg Fe^{2+} and 45.5 mg Mn^{2+} per g of cells at 30 ^{o}C. Further, temperature of the uptake medium is known to be important for energy dependant mechanisms and energy independent mechanisms are less likely to be affected by temperature (Zouboulis *et al.* 2004). This was demonstrated by the 10 fold decrease in metal uptake at 50 ^{o}C. The reduction of Fe^{2+} and Mn^{2+}ion uptake by 2,4 DNP an uncoupler and DCCD, a ATP synthetase inhibitor to 48 % - 36 % and 25 % - 30 % ,respectively, supports the energy dependence of uptake wherein the proton motive force required to drive the Fe^{2+} and Mn^{2+}ions across the plasma membrane into the cell cytoplasm is inhibited. Energy in the form of ATP is required to transport metal ions across the cell membrane in to the cell cytoplasm evident with 35 % of Mn^{2+} ion in the cytoplasm and 65 %

in cell envelope and 24 % and 74.5 % in case of Fe^{2+}. This was also established from crystalline cell surface and visible Mn and Fe peaks in the EDX spectrum. The actively respiring cell machinery is required for active uptake proved by 20 % and 50 % decrease of uptake of Mn^{2+} and Fe^{2+} ions, respectively, by heat killed cells that is much less then with the chemical treatments, most likely due to the alteration occurring on the binding sites and subsequent destruction and denaturation of components of cell surface as previously reported by Malekzadeh *et al.* 2007 and Ghorbanzadeh *et al*. 2009. Furthermore, the uptake of Mn^{2+} and Fe^{2+}ions by resting cells increased with the increase in pH to maximum of 99 % at pH 6.0 followed by a decrease of 35 % at pH 8.0. The pH influences both the metal chemistry in solution and the protonation/ deprotonation of the metal (Peacock and Sherman 2004). The speciation profile of manganese as well as iron indicates the formation of manganese hydroxide above pH 8.0 while iron forms iron hydroxide above pH 6.0; hence affecting the availability of Mn^{2+} and Fe^{2+} ions for uptake (Takeno 2005). The increase in Mn^{2+} and Fe^{2+}ions uptake with the increase in pH can be explained on the basis of a decrease in competition between the protons and Fe^{2+} / Mn^{2+} cations for the same functional groups/ binding sites and by decrease in the positive surface charge that results in a lower electrostatic repulsive force between the surface and metal ions ions before ion exchange (Li *et al.* 2008).

Ionic strength is proportional to the salt concentration of solution directly. Ionic strength besides pH is also one of the important factors that influence the equilibrium uptake (Ghazvini and Mashkani 2009). The optimum salinity for Fe^{2+}/ Mn^{2+} uptake was 15 %, above which the uptake of iron and manganese ions decreased progressively by 10 folds. This behavior is attributed to the rigidity provided to cell surface by salt showing a inhibitory

on the permeability of cell membrane for Fe^{2+}/ Mn^{2+} ions and relative competition between Na^{+} and metal ions on the active centres of *Haloferax* sp. GUSF-1 (Maurya *et al.* 2006).The initial concentration provides a driving force to overcome all mass transfer resistances of the metal ion in the aqueous and the solid phase that leads to higher probability of collision between the metal and the active site of the cell. The surface of the cell being the first point of contact with the metal ion, the surface uptake sites become exhausted at some point of time attaining a equilibrium at which no more metal is taken up from solution. The equilibrium uptake increased with increasing concentration of metal ions at the range of experimental concentration. The resistance of the metal uptake decreased as the mass transfer driving force increased leading to greater initial rate of uptake than for higher initial metal concentration (Ghazvini and Mashkani 2009). Moreover, the increase in uptake with increasing biomass is justified by availability of more binding sites for interaction to take place explained in adsorption process. Additionally, the smaller ionic radius of $Fe^{2+}$and Mn^{2+} of 0.76 Å and 0.67 Å increases its affinity for binding sites. The uptake of Fe^{2+} and Mn^{2+} ions showed a better fit with Freundlich model having R^2= 0.98 and 0.99, respectively, then Langmuir model. The higher determination coefficient indicated the Fe^{2+}/ Mn^{2+} uptake process to be pseudo second order that was supported by increase in equilibrium concentration and corresponding linear decrease in equilibrium rate constant at increasing initial Fe^{2+}/ Mn^{2+} concentration.

Chapter 4

Biomineralisation studies of

Fe^{3+} and Mn^{2+} ions by

Haloferax sp. GUSF-1

Microbial respiration is often times linked with mineralization of organic matter and the dissimilatory reduction of metals (Zhang *et al*., 2009; Vandieken *et al*., 2013). Because of this microbes play a significant role in the formation of minerals (Gadd and Raven, 2010). Biominerals deposited by microbes may be nanosized crystals or colloidal forms having catalytic and other properties which are relevant to the development of novel biomaterials for technological and antimicrobial purposes (Gadd, 2010). Hence, to elucidate the ability of haloarchaeon *Haloferax* sp. GUSF-1 to biomineralise Fe^{3+} /Mn^{2+} forms the basis of this chapter. The methodologies for respective metal ion mineralization are divided into two sections, namely Section A**:** Biomineralisation of Fe^{3+} to nanosized γFe_2O_3 by *Haloferax* sp.GUSF-1 followed by results and discussion on same and Section B: Biogenic formation of rhodochrosite by haloarchaeon *Haloferax* sp. GUSF-1 accompanied by its results and discussion detailed separately.

SECTION A

4.1 Biomineralisation of Fe^{3+} to nanosized γFe_2O_3 by *Haloferax* sp. GUSF-1

METHODOLOGY

4.1.1 Growth medium and conditions used for growth of *Haloferax* sp.GUSF-1 in presence of Fe^{3+}.

Culture *Haloferax* sp. GUSF-1 was inoculated 5% v/v in 500 ml flasks containing 200 ml of mineral salts medium (NSM) adjusted to pH 6.2 with 1N KOH, 30 ºC. 0.2 % sodium acetate

was used as sole source of carbon; 2 mM of $FeCl_3.6H_2O$ as source of Fe^{3+} was added. The growth of the culture was monitored by taking an absorbance at 600nm using UV–Vis spectrophotometer (UV2401 Shimadzu- Japan). All the glassware used, were soaked overnight in 10 % nitric acid (HNO_3) and rinsed twice with milli Q water.

4.1.2 Monitoring of reduction of Fe^{3+} during growth

For detection of Fe in culture broth, aliquot was taken in an eppendorf tube and spun at 12000 rpm for 10 min at 4 ºC followed by separation of supernatant and the pellet. Metal inside the cells was released by exposing the cell pellet to distilled water for 20-30 min. These contents were centrifuged again at 12000 rpm for 10 min at 4 ºC and monitored colorimetrically by 1, 10- phenanthroline assay for iron. (Mendham *et al.* 2009). The phenanthroline method was slightly modified by adding 1,10- phenanthroline reagent directly to the test sample solution and measuring the peak maxima at 510 nm for Fe^{2+} content while for Fe^{3+} content hydroxylamine was added followed by phenanthroline reagent to the test sample solution. Appropriate controls were also maintained with Fe^{3+} and without culture. Quantification results were confirmed by atomic absorption spectrophotometer (AAS).

4.1.3 Quantification of iron by atomic absorption spectrophotometer

The iron in the cell pellet and the supernatant was quantified by aseptically withdrawing 1 ml aliquot of the culture broth followed by removal of oxides with 0.2 mM ascorbate and centrifuging at 10,000 *g* for 10 min. The cell pellet and the supernatant were separately digested using nitric acid (HNO_3) and sulfuric acid (H_2SO_4) (2:1 v/v). The clear digest was estimated for iron by atomic absorption spectrophotometer (AA-6300, Shimadzu). Standard

of iron solution of known concentration for AAS was prepared in 1 M nitric acid, in the range of 0-10 ppm to obtain a standard graph.

4.1.4 Estimation of iron reductase assay

Iron reductase activity was measured by the modified method of Dailey (Huyer and Page 1989). The method involves use of ferrous iron chelator, ferrozine [3-(2- pyridyl)-5, 6-bis(4-phenylsulfonic acid)-1,2,4-triazine]. Ferrozine reacts with ferrous iron to form a purple colored chelator, with absorption maxima at 562 nm. The assay mixture in the final volume of 2 ml contained 50 µl of NADH, 100 µl of ferrozine, 50 µl of 5 mM ferric citrate, and 200 µl of culture supernatant added to 2 mM phosphate buffer (pH 7.2). Assay mixture was incubated at room temperature for 10 - 20 min at static conditions. Spectral measurement was carried out on a uv-visible spectrophotometer (Shimadzu 2401 Japan) operated at a resolution of 1 nm at 562 nm. In the control experiment for assay, all of the reagents were added as is while culture supernatant obtained by growing culture in the absence of iron salt was added with the rest of components. To confirm the presence of iron reductase in the formation of brown mineral, reaction was carried out in the presence of 100 µM of Zn^{2+} ions, an inhibitor of iron reductase (Crow *et al.* 2009).

4.1.5 Recovery of biomineral

The growth medium was centrifuged at 10,000 rpm for 15 min. The pelleted crystalline brown mineral was re-suspended in deionised water. The mineral pellet was washed with distilled water thrice to ensure the removal of culture broth impurities and haloarchaeal cells. The brown pellet was then emptied on a clean and dry petridish followed by drying in an oven at 80 $^{\circ}$C till constant weight of 100 mg.

4.1.6 Mineralogical characterization

4.1.6.1 X- ray Diffraction analysis

The dried mineral recovered was crushed in an agate mortar and pestle. The fine powder was then placed on a special slide with an indentation to hold the powder. Using another glass slide, the excess powder was wiped off and the sample was pressed flat. The slide holding the sample was then placed in the sample holder of the X-ray machine and scanned from 10- 70^{o} measured at 0.02^{o} 2θ intervals with 40 s counting time per step by Rigaku Miniflex powder diffract meter equipped with a Ultima IV solid- state detector at a voltage of 40 kV and current of 20 mA with Cu-Kα radiation, λ = 1.5418 Å. The data obtained from XRD machine was plotted and FWHM (Full Width Half Maxima) was calculated using Origin 8.0 software.

The crystal size was calculated by applying the Scherer's formula given as

$D = k\lambda/\beta\cos\theta$

where D is the mean grain size, k is a constant, λ is the X-ray wavelength for Cu-Kα radiation, β is the FWHM of the diffraction peak in radians and θ is the diffraction angle.

4.1.6.2 Scanning Electron Microscopy and Electron Diffraction X -ray analysis

To determine the chemical composition of mineral, the fine powder was coated on to the copper stubs as thin layer. These stubs were then sputter coated with gold using high vacuum evaporator. The position of the stage was set in such a way that the stub was approximately 50 mm from the bottom of the sputter head. After sputtering the specimen with a 10-15 nm film of gold, the stub was placed in the sample chamber of the scanning electron equipped with EDX (JEOL JSM-5800LV) and observed.

4.1.6.3 Transmission Electron Microscopy and Selected Area Electron Diffraction

TEM micrographs of mineral was obtained by drop coating of brown homogenous solution obtained by sonicating the mineral powder in 200 µl of milli Q water for 5-10 min onto 2 mm carbon coated copper grids of 200-300 mesh followed by air drying. The grid was then placed in the sample chamber of the TEM (Philips CM200 Supertwin STEM) equipped with SAED, operated with the voltage of 200 kV and imaged.

4.1.6.4 Atomic Force Microscopy

For AFM analysis, the sample slide was prepared by drop coating of brown homogenous solution obtained by sonicating the mineral powder in 200 µl of acetone for 5 min onto freshly cleaved mica followed by air drying for 15 min. Sample was immediately transferred into the AFM microscope and imaged by AFM (NTEGRA PRIMA system NTMDT) operating in a semi-contact mode. Micro-fabricated cantilever tip (NSG-01) with a resonance frequency of 124 kHz was used.

4.1.6.5 Fourier Transform Infra- Red analysis

Dried, finely ground powder was encapsulated with KBr (1:10, w/w) as discs and exposed to IR (Prestige-21 FTIR- Shimadzu) to determine the functional groups.

4.2 RESULTS

4.2.1 Growth and reduction of Fe^{3+} by *Haloferax* sp.GUSF-1 in mineral salts medium

As depicted in **Fig. 4.1,** *Haloferax* sp.GUSF-1 grew with lag of 2 d, a log phase of 5 d in mineral salts medium with sodium acetate as sole source of carbon and a growth rate of 1.3 x 10^2 gen $h^{-1}$and doubling time of 76.8 min gen^{-1}, reached a maximum absorbance of 1.25 at 600nm. The culture attained a stationary phase on the 8^{th} d.

Further, in Fe^{3+} ($FeCl_3.6H_2O$) incorporated mineral salts medium, grew with a shortened lag of only 1 d but an extended log phase of 2 d at a fold increase in growth rate of 9.7 x 10^3 gen $h^{-1}$and a doubling time of 103 min gen^{-1}, attained a maximum absorbance of 1.5 which was followed by a stationary phase as during growth in acetate alone. During this time, the concentration of $Fe^{2+}$and Fe^{3+} inside the cells increased to 30 mg L^{-1} and 10 mg L^{-1} respectively, by fourth day and to 50 mg L^{-1} of Fe^{2+} and 30.6 mg L^{-1} of Fe^{3+} by ninth day, respectively with concomitant decrease in added Fe^{3+} to 3.6 mg L^{-1} . Interestingly, the accumulation of iron as Fe^{3+} and Fe^{2+} inside the cells is also accompanied by deposition of a brown colored amorphous substance (**Fig. 4.2**) and formation of Fe^{2+} in the culture broth, detectable to a concentration of 27 mg L^{-1} by ninth day.

4.2.2 Iron reductase assay

The Fe^{3+} reductase activity was demonstrated in culture supernatant as a strong purple colored ferrozine - ferrous iron complex with absorbance maxima at A_{562} nm (**Fig. 4.3**). Ferric reductase activity was induced only in presence of Fe^{3+}. Culture growing with Fe^{3+} when spiked with Zn^{2+} ions failed to show the ferric reductase activity and the accumulation of the brown material.

4.2.3 Mineralogical characterization

4.2.3.1 Recovery of biogenic mineral

The brown colored mineral was separated from the growth medium by centrifugation at 10,000 rpm for 15 min and re-suspended in deoxygenated water prepared by bubbling oxygen free N_2 in deionized high purity water (18 MΩ- cm) for 24 h . The mineral pellet was washed twice with deoxygenated water to ensure the removal of culture broth impurities. The washed pellet was emptied on a clean glass plate and dried in an oven at 80 $^{\circ}$C (**Fig. 4.4**).

4.2.3.2 X- ray Diffraction analysis

Fig. **4.5** depicts the X-ray diffractogram of the brown material having d spacings for the respective *hkl* planes as 2.96 (220), 2.514 (311), 2.086 (410), 1.6 (511), 1.45 (440) that matched with Bragg's pattern and corroborated with records of JCPDS card no. 25-1402 characteristic for γFe_2O_3 (maghemite). The nanocrystallites mean size analysis performed using Scherer's formula indicated the average size of mineral formed in the biogenic reduction process to be 23 nm.

4.2.3.3 SEM-EDX analysis

The SEM profile of the mineral powder displayed cubic and irregularly shaped minute particles (**Fig. 4.6a**). The EDX spectra showed peaks due to Fe at 0.6, 6.4 , 6.6 keV and weak peak at 7 keV, respectively. Peaks due to phosphorus, carbon and oxygen were visible at 2.2, 1.6 keV and at 0.2 keV and 0.6 keV, respectively (**Fig**. **4.6b**).

4.2.3.4 TEM-SAED

Fig. 4.7a displays the TEM micrographs revealing the clusters of electron dense nano-sized particles roughly in the range of 12-23 nm. The SAED analysis (**Fig. 4.7b**) showed a concentric pattern of light scattering with well defined diffraction spots that were consistent

with the polycrystalline nature of biosynthesized maghemite crystal structure and corroborated with the records for maghemite crystal structure given in JCPDS chart no. 25-1402.

4.2.3.4 AFM

The AFM image (**Fig. 4.8**) revealed a smooth topography of aggregate of particles with average size of 4.73 µm.

4.2.3.5 FTIR

FTIR spectrum (**Fig. 4.9a**) revealed a broad band at 3400 -3330 cm^{-1} that corresponded to stretching and bending vibrations of water molecule. A peak at 1450 cm^{-1} was observed indicating the formation of iron oxyhydroxide as an intermediate that can be assigned to γ-FeOOH stretching bond vibrations (Bharde et al. 2008). Two broad peaks were observed at 555 cm^{-1} and 463 cm^{-1} **(Fig. 4.9b**) that corresponded to Fe – O bond tetrahedral and octahedral stretching vibration mode, respectively, of γFe_2O_3 (Kim et al. 2010)

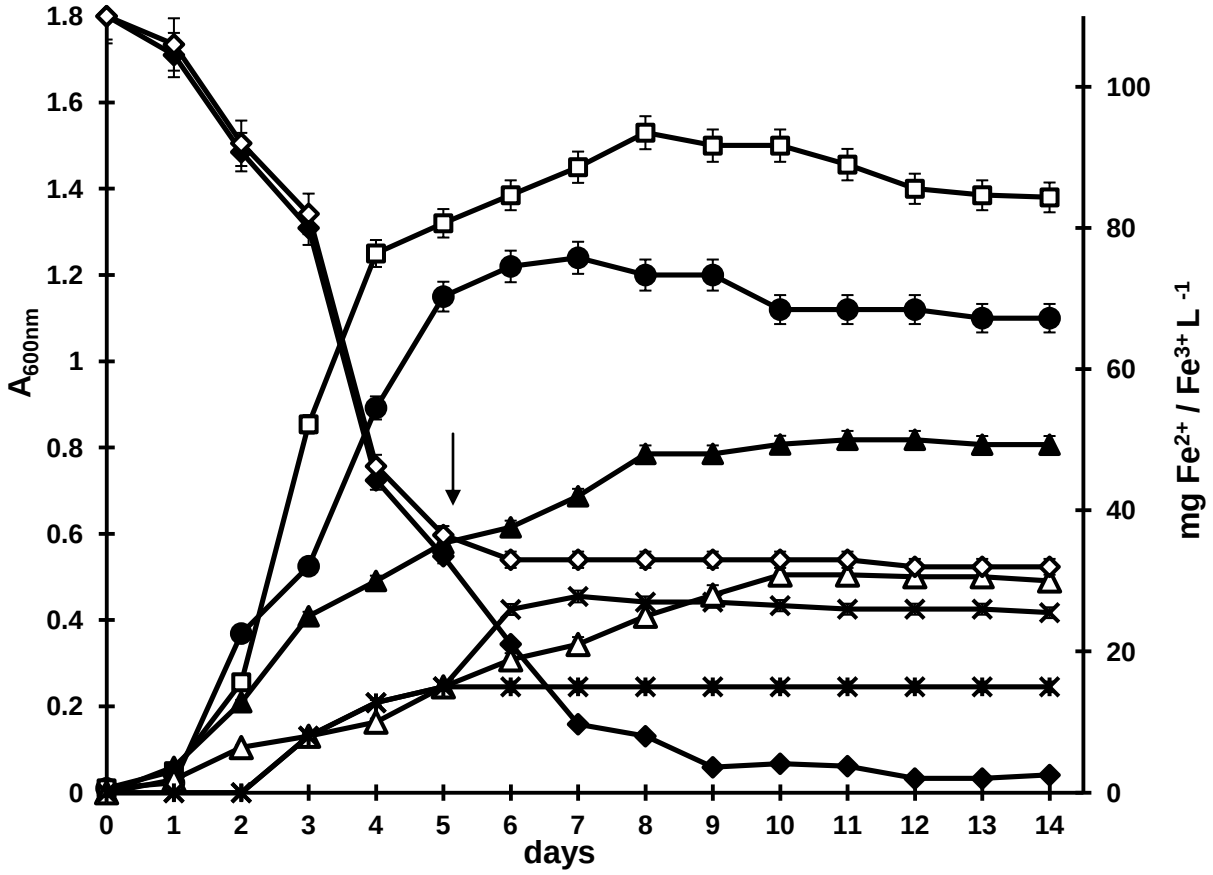

Fig. 4.1 *Haloferax* sp.GUSF-1 growing in mineral salts medium with sodium acetate as sole source of carbon. ( ) culture in NASM; ( ) culture in NASM containing Fe^{3+} ($FeCl_3.6H_2O$); ( ) Fe^{2+} inside the cells; ( ) Fe^{2+} formed in the culture broth; ( ) Fe^{3+} remaining in culture broth; ( ) Fe^{3+} inside the cells; ( ) Fe^{3+} in culture broth spiked with Zn^{2+} indicated with arrow; ( ) Fe^{2+} formation arrested by Zn^{2+} ions.

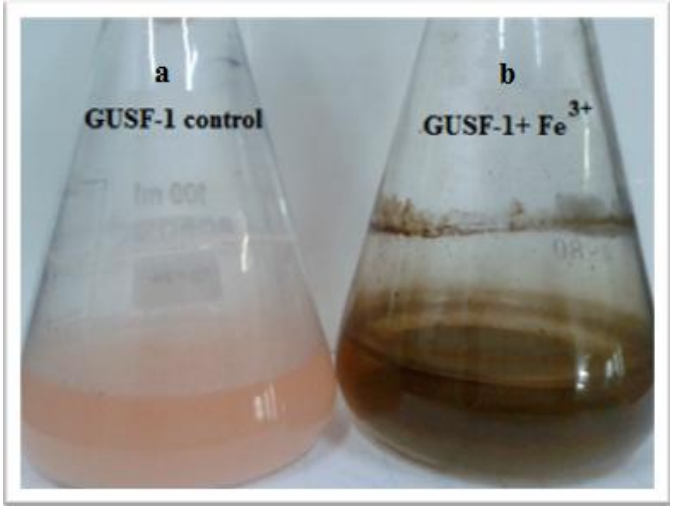

Fig. 4.2 Flasks showing *Haloferax* sp. GUSF-1 in **(a)** NASM **(b)** NASM with Fe^{3+}

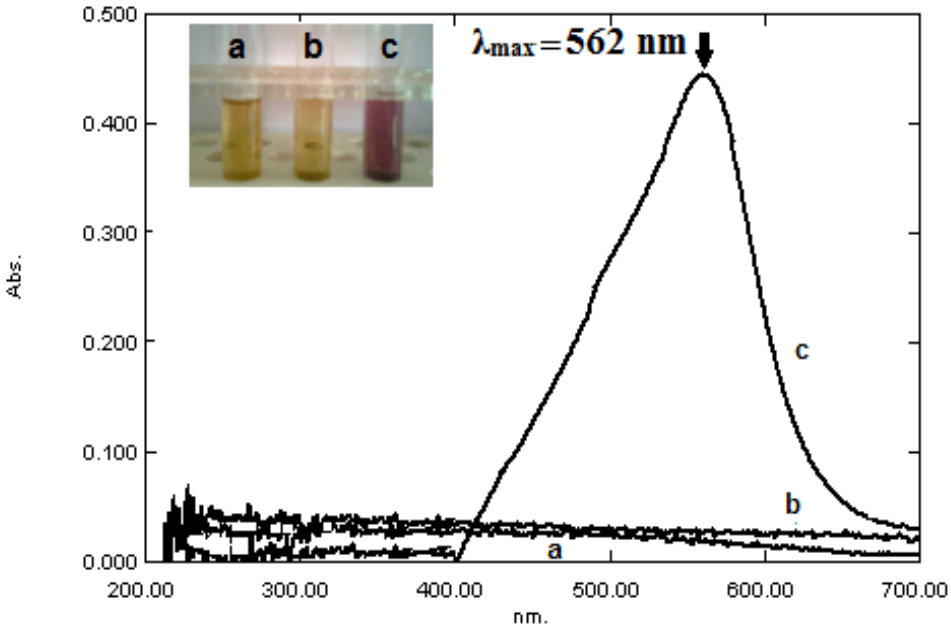

Fig. 4.3 (a) Iron reductase activity of *Haloferax* sp.GUSF-1 growing in mineral salts medium with sodium acetate and $FeCl_3.6H_2O$ with maximum absorbance; **(b)** control with absence of reductase activity; **Inset (a)** negative activity in control with Fe^{3+} only **(b)** negative activity with Zn^{2+} ions **(c)** positive ferric reductase activity.

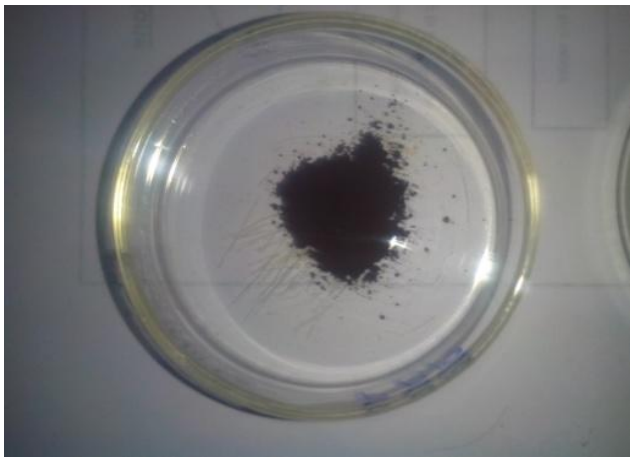

Fig. 4.4 Recovered biomineral produced by *Haloferax* sp. GUSF-1

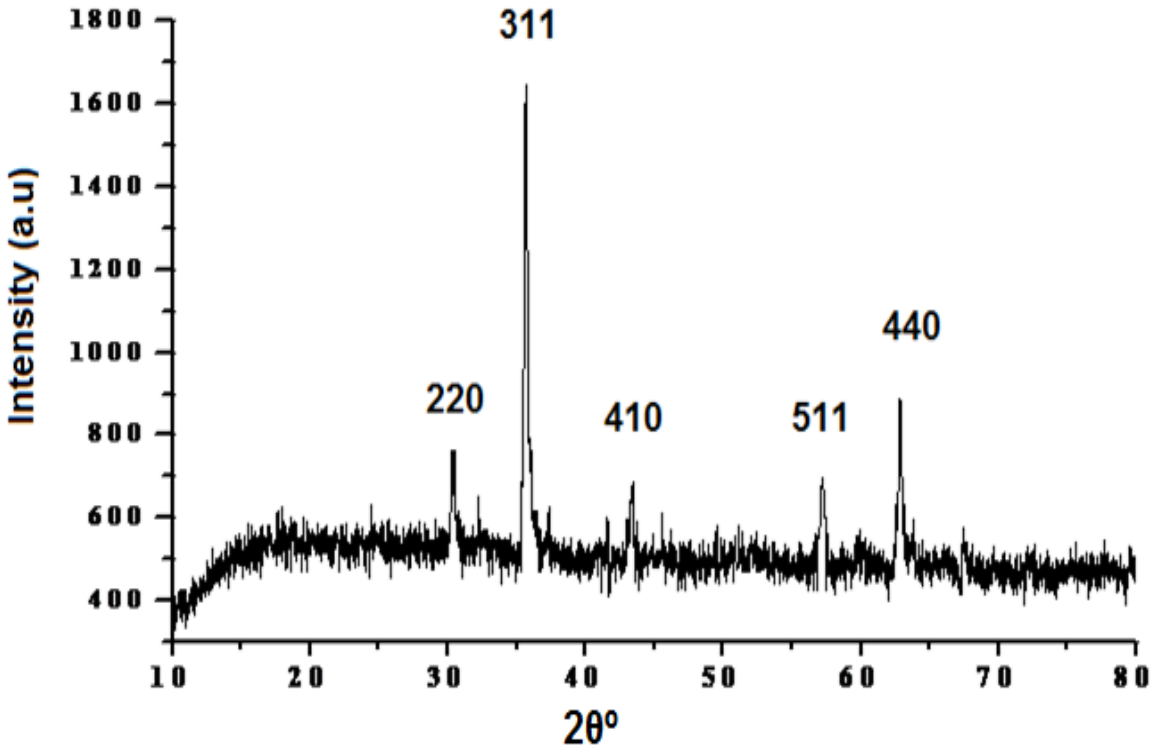

Fig. 4.5 X-ray diffractogram of purified biomineral produced by *Haloferax* sp.GUSF-1 in the mineral salts medium containing Fe^{3+} (JCPDS pattern 25-1402).

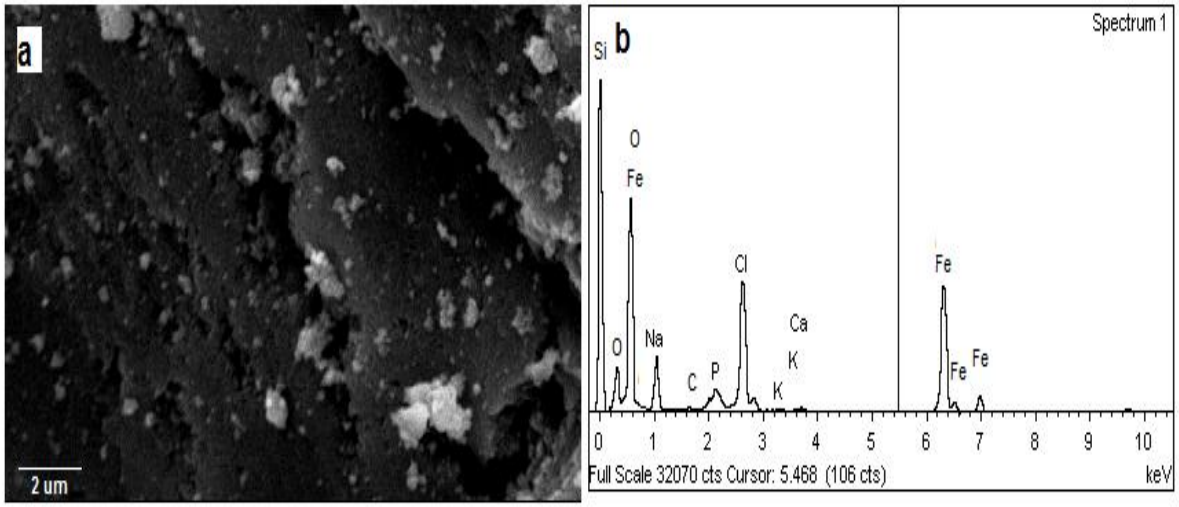

Fig. 4.6 (a) Scanning electron micrograph and (b) energy dispersive X-ray profile of purified biomineral produced by *Haloferax* sp. GUSF-1.

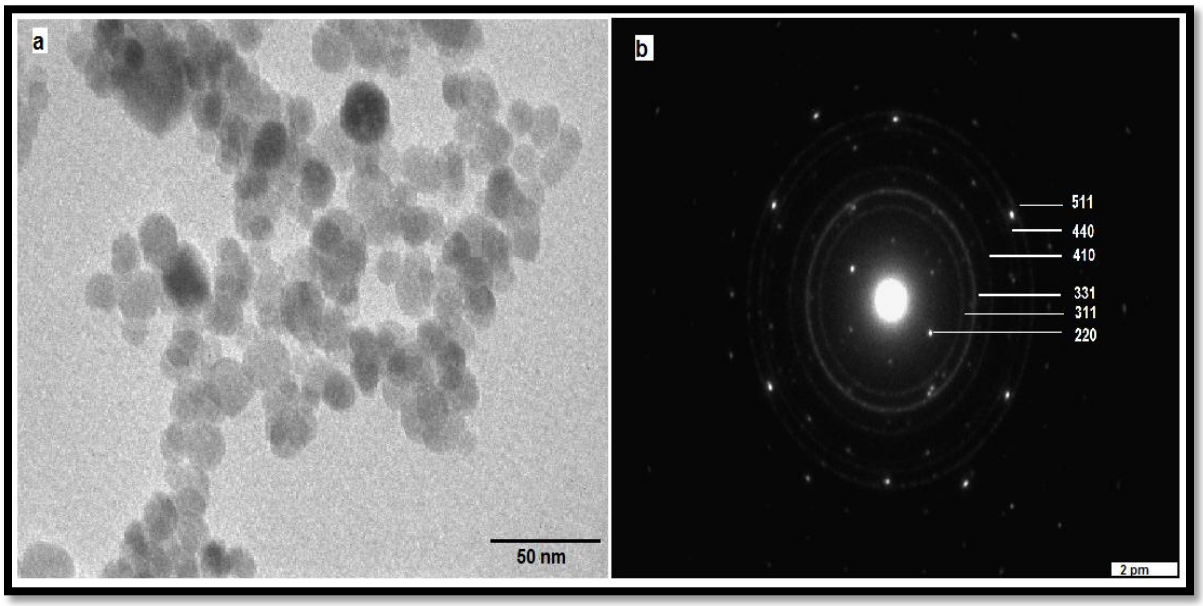

Fig. 4.7 (a) TEM micrograph with **(b)** SAED of nanosized γFe_2O_3.

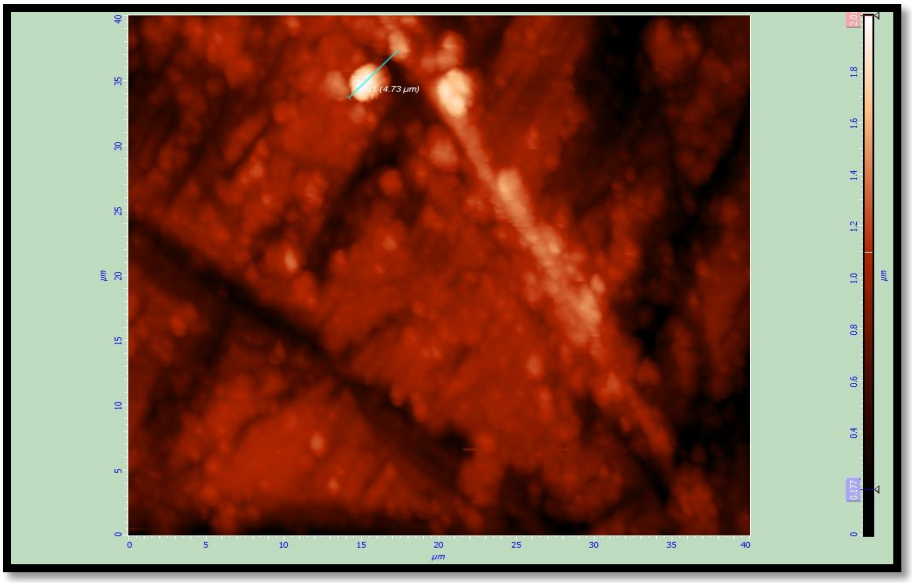

Fig. 4.8 AFM micrograph of nano sized γFe_2O_3 showing surface topography of aggregate of particles. Marked area = 4.73 µm

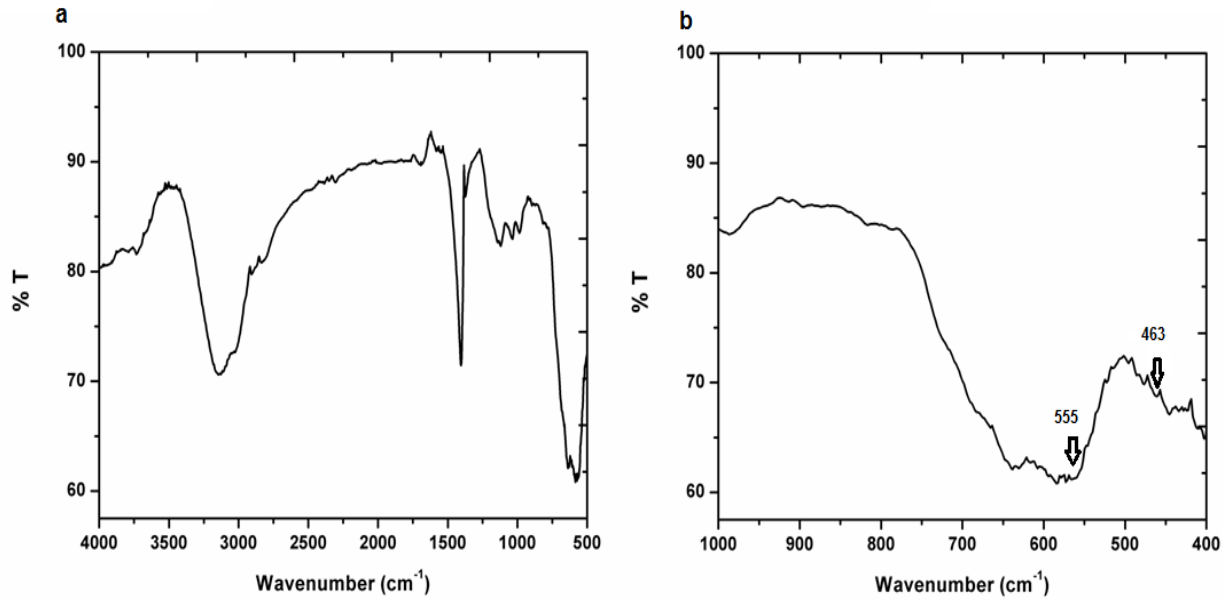

Fig. 4.9 (a) FTIR spectrum of γFe_2O_3 **(b)** FTIR spectrum of γFe_2O_3 showing Fe-O stretching and bending vibrations.

4.3 DISCUSSION

Microorganisms are known to act as a vital component of natural biogeochemical cycles for metals through metal speciation, mineral mobilization, mineral transformations, and decomposition through bioweathering and sediment formation. (Gadd 2010).

In this study, we have reported the potential of haloarchaeon *Haloferax* sp.GUSF-1to reduce Fe^{3+} to nanosized maghemite (γFe_2O_3) during its growth in acetate as sole source of carbon. A simultaneous increase in $Fe^{2+}$and Fe^{3+} inside the growing cells indicating the accumulation of Fe^{2+} and Fe^{3+} inside the cells, thus, showed that Fe^{3+} reduction is coupled to the oxidation of organic compound such as acetate. This result is similar to that of *Geobacter metallireducens* known as the first acetate oxidizing Fe^{3+} reducer (Lovley *et al.* 1993; Lovley *et al*. 2004) and that conserves energy to support growth as demonstrated by an additional increase in the absorbance measures in presence of Fe^{3+} than in medium with acetate alone. *Shewanella putrefaciens* is another bacteria that is also reported to conserve energy to support growth by coupling the oxidation of organic compound such as lactate to the reduction of Fe^{3+} (Lovley *et al*. 2004). The increase in absorbance reflecting more cell growth than in the medium with acetate alone suggests that energy is conserved from Fe^{3+} reduction. The accumulation of iron as Fe^{3+} and Fe^{2+} inside the cells accompanied by deposition of a brown colored amorphous substance and formation of Fe^{2+} in the culture broth indicated the role of ferric reductase substantiated by development of purple colored ferrozine - ferrous iron complex in the culture supernatant of *Haloferax* sp.GUSF-1 grown with Fe^{3+} while no color complex was formed when grown without Fe^{3+}. Spiking the growth medium with Zn^{2+} ions the inhibitor of ferric reductase confirmed the role of reductase in the the reduction of Fe^{3+} and formation of brown material in the culture broth. X-ray

diffractogram revealed the brown material to be γFe_2O_3 chemically known as maghemite. To our understanding, *Haloferax* sp. GUSF-1 reduced Fe^{3+} to Fe^{2+} and then to γFe_2O_3 which was determined to be of nano sized as calculated by Scherer's formula. The crystalline nature and presence of Fe – O peaks was evident from SEM-EDX images confirmed by Fe-O bond vibrations in the FTIR profile which also showed a low intensity oxyhydroxide peak at 1450 cm^{-1} acting as an intermediate. This result also corroborated with that reported by Bharde *et al*. (2008) stating the role of oxyhydroxide as an intermediate in the formation of maghemite by *Actinobacter* sp. Further, TEM analysis confirmed the nano size of the material accompanied by SAED showing well defined diffraction spots that were consistent with the polycrystalline nature of biosynthesized maghemite crystal structure. The formation of nanosized maghemite by haloarchaeal culture *Haloferax* sp.GUSF-1 at room temperature during its growth on acetate in mineral salts medium, in presence of 20 % NaCl contributes to environmentally affable and energy conserving nature of the haloarchaeal culture. Further, production of nanosized maghemite is of significance as methods of chemical synthesis of iron oxides such as sol-gel, forced hydrolysis, sonochemical and electrochemical are energy intensive, employ chemicals and organic solvents thereby, impeding biomedical applications. Maghemite, is exploited for magnetic recording, magnetic storage devices, ferrofluids, and contrast enhancers in MRI and in other biomedical applications (Matsunaga *et al*. 2004; Silva *et al*. 2013).

Thus, we infer that the haloarchaeon *Haloferax* sp.GUSF-1 is significant in iron cycling in estuarine environment. The biogenic process of formation of maghemite has exploitability for green synthesis of nanosized γFe_2O_3 .

SECTION B

4.4 Biogenic formation of rhodochrosite by haloarchaeon *Haloferax* sp. GUSF-1

METHODOLOGY

4.4.1 Growth experiments

5 % (v/v) of freshly grown 4 d old *Haloferax* sp. GUSF-1 was inoculated in sterile 500 mL flasks containing 200 mL of mineral salts medium (NSM) supplemented with sodium acetate 0.2 % as sole source of carbon, adjusted to pH 7.0 with 1 N KOH, on an orbital shaker (150 rpm), in the presence of 1 mM of Mn^{2+} as $MnCl_2.6H_2O$ for 14 days. The growth of the culture was monitored by taking an absorbance A_{600} nm by UV–Vis spectrophotometer (UV2401 Shimadzu- Japan).

4.4.2 Estimation of Manganese oxide

The Mn-oxide concentration in the culture broth was determined calorimetrically with Leukoberbelin blue (LBB) assay (Lee & Tebo, 1994). At regular intervals, samples of 0.1 mL were aseptically removed and added to 1 mL of 0.04 % Leukoberbelin blue in 45 mM acetic acid, and the absorbance was read at A_{620} nm. Any cells present in the samples were removed by centrifugation at 10000 rpm, 4 ºC for 10 min before measurement of the absorbance. The oxidation of Leukoberbelin blue proceeded with the development of a blue color. Standard curves with $KMnO_4$ showed that the absorbance was linear up to A_{620} = 1.5 where 40 µM $KMnO_4$ corresponded to 100 µM MnO_2 equivalents. The effect of Mn oxides on the absorbance of Mn^{2+} grown culture was determined by remeasuring the absorbance A_{600} nm, of cultures after removal of the oxides with 200 µM ascorbate.

4.4.3 Detection of manganese content by AAS

Manganese content in the cells was determined by removing aseptically 1 mL of culture broth followed by addition of 200 µM ascorbate and centrifuging at 10000 rpm for 10 min. The cell pellet was then digested with nitric acid (HNO_3) and sulfuric acid (H_2SO_4) (2:1 v/v) and was estimated for Mn by atomic absorption spectrophotometer (AA-6300 SHIMADZU). Standard of manganese solution of known concentration for AAS was prepared in 0.1 N nitric acid in the range of 0-15 mg L^{-1} to obtain the standard graph.

4.4.4 Mineralogical characterization of biogenically formed mineral

4.4.4.1 Recovery of biogenic mineral

Pinkish brown colored mineral was separated from the growth medium by centrifugation at 10,000 rpm for 15 min and re-suspended in deionised water. The mineral pellet was washed twice with distilled water to ensure the removal of culture broth impurities or residual Mn^{2+}. The washed pellet was emptied on a clean glass plate and dried in an oven at 80 $^{\circ}$C.

4.4.4.2 X- ray Diffraction profiling

XRD analysis of biogenic mineral was done as described in section **4.1.6.1.**

4.4.4.3 Scanning Electron Microscopy with Energy Dispersive X-ray analysis

To determine the chemical composition of mineral, SEM EDX analysis were carried out of dried and finely powdered material as detailed in section **4.1.6.2.**

4.4.4.4 Transmission Electron Microscopy

The morphology of biogenic mineral was evaluated using Philips CM200 transmission electron microscope **(**TEM) operating at 200 kV. Samples were prepared by steps detailed in section **4.1.6.3.**

4.4.4.5 Fourier Transform Infra- Red analysis

FTIR analysis was carried out to determine the functional groups of biogenic mineral as described in section **4.1.6.5.**

4.5 RESULTS

4.5.1 Growth response and Mn^{2+} oxidation-reduction by haloarchaeon *Haloferax* sp. GUSF-1

The haloarchaeon *Haloferax* sp. GUSF-1 grew with lag of 2 d in mineral salts medium with sodium acetate as sole source of carbon and reached a maximum absorbance of 1.05 at A_{600} nm after 5 d (**Fig. 4.10a**). The culture attained a stationary phase on the 8^{th} d. In medium incorporated with Mn^{2+} ion as $MnCl_2.6H_2O$ shortened the lag phase of growth of culture by 1 d and extended the log phase by 2 d, with absorbance reaching a maximum of 1.4 at A_{600} nm. With the onset of the stationary phase on 9^{th} d, the culture flasks showed increasing deposit of a light brown colored material (**Fig. 4.11**), not seen in un-inoculated flasks incubated under identical conditions. Simultaneously, analysis of culture broth with LBB (**Plate 4.1**) showed presence of MnO_2 corresponding to a total of 485.5 µM of MnO_2 equivalents. However, the formation of light brown colored deposit interfered with the monitoring of absorbance A_{600} nm and hence its correlation to growth of *Haloferax* sp.GUSF-1. Addition of 200 µM of ascorbate resulted in disappearance of light brown deposit, permitting the monitoring of actual absorbance due to growth of the culture. Further, addition of 2 mM sodium azide arrested the growth of *Haloferax* sp. GUSF-1 and the accumulation of the light

brown deposit. Also, when the growing culture broth was spiked with sodium azide separately on the 9th d, the conversion of MnO_2 formed to pinkish brown material was arrested.

Manganese was also detected inside the growing cells on 4th d, and the same increased to 745.6 µM mL $^{-1}$ by the 9th d and declined thereafter to 500 µM mL $^{-1}$ by the 16th d with no further change (**Fig. 4.10b**). The pinkish brown material recovered from the culture supernatants on the 16th d, totaled to 5 mg L^{-1} dry weight.

4.5.2 Mineralogical characterization of biogenic material

4.5.2.1 X- ray Diffraction analysis

The XRD pattern of this pinkish brown deposit (**Fig. 4.12**) matched with Bragg's pattern and corroborated with the records of JCPDS card no. 7-268, featuring the distinct characteristic of $MnCO_3$, the mineral rhodochrosite, with d spacing for the respective *hkl* planes as 3.66 (012), 2.84 (104), 1.770 (018), 1.763 (116). The average grain size of mineral formed by *Haloferax* sp. GUSF- 1 was 25 nm, determined using Scherer's formula.

4.5.2.2 SEM- EDX analysis

SEM profiles of the pinkish brown material, showed a crystalline surface with cubic shape (**Fig. 4.13a**). The EDX spectra displayed a peak due to Mn at 0.5, 3.3 keV and weak peaks at 5.9 keV and 6.5 keV, respectively, along with a phosphorous peak at 4.5 keV. The carbon peaks were evident at 1.2, 1.6 keV and a weak peak at 2.4 keV. Peaks due to oxygen were visible at 0.2 keV (**Fig. 4.13b**).

4.5.2.3 TEM analysis

The TEM micrographs of pinkish brown material revealed the presence of small electron dense particles of 18-25 nm in size (**Fig. 4.14**).

4.5.2.4 FTIR

IR spectrum of pinkish brown material revealed a broad band at 3400 cm^{-1} and other band at 1641 cm^{-1} that was due to the stretching vibrations of hydroxyl group of water molecule (**Fig. 4.15**). The characteristic peaks at 1462 cm^{-1} and 860 cm^{-1} were assigned to carbonyl stretching and bending vibrations of carbonate groups (Refat and Al-Qehtani 2011). The weak peaks at 750-500 cm^{-1}corresponded to Mn-O stretching vibrations (Parikh and Chorover 2005).

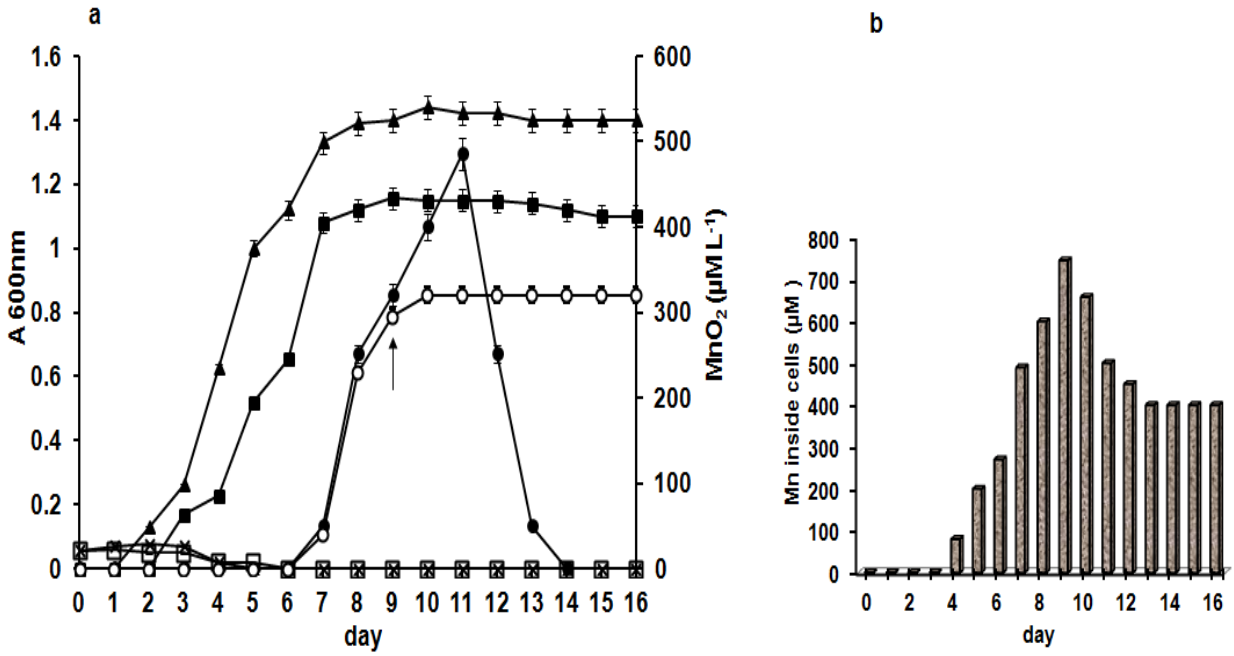

Fig. 4.10 (a) Growth curve of *Haloferax* sp. GUSF-1 in: NASM ( ), Mn^{2+} containing NASM ( ), Sodium azide added to NASM ( ), Mn^{2+} + sodium azide in NASM ( ) and MnO_2 formed in NASM ( ), MnO_2 accumulated due to spiking with sodium azide on 9th d ( )(arrow indicates day of spiking); **(b)** Mn^{2+} accumulated inside the cells of *Haloferax* sp. GUSF-1.

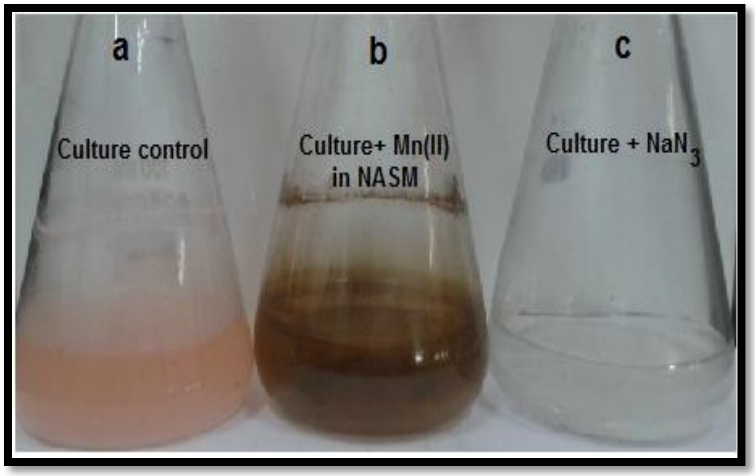

Fig. 4.11 Flasks showing (left to right) culture *Haloferax* sp. GUSF-1 grown in **(a)** absence of Mn^{2+} **(b)** Mn^{4+} reduction **(c)** inhibition by sodium azide in NASM.

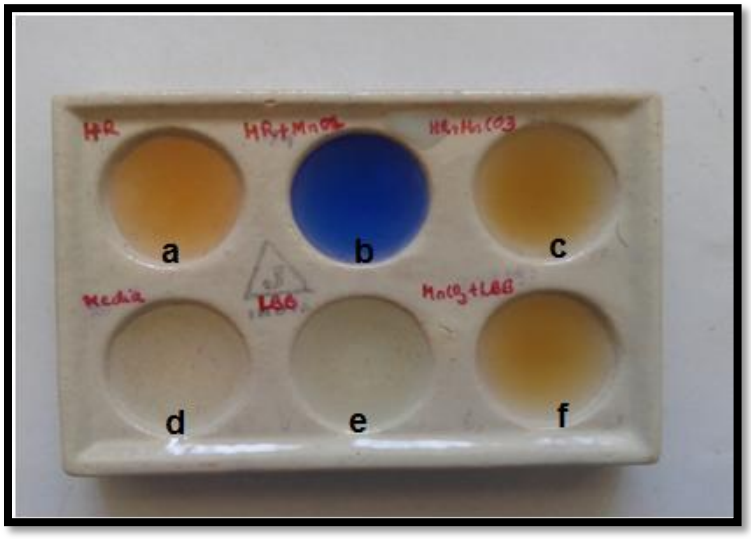

Plate 4.1. Leukoberbelin Blue test showing manganese oxide**: (a)** *Haloferax* sp.GUSF-1 culture broth without Mn2+ (negative test) **(b)** positive manganese oxide test detected in culture broth grown with Mn^{2+} **(c)** negative test shown after reduction of manganese oxide **(d)** uninoculated medium control **(e)** LBB reagent control **(f)** manganese carbonate with LBB control.

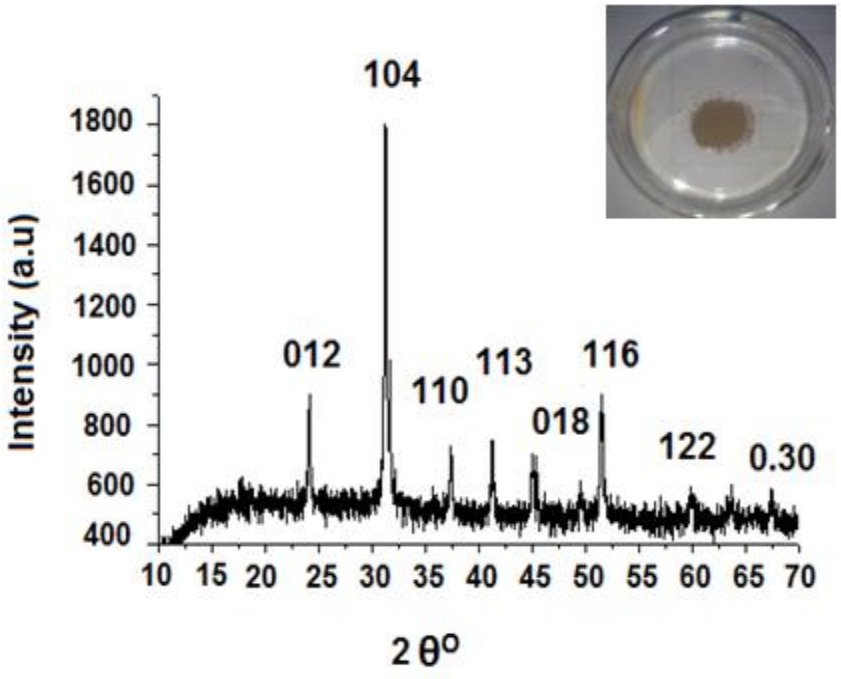

Fig. 4.12. X-ray diffractogram of the pinkish brown deposit $MnCO_3$ (rhodochrosite) formed by *Haloferax* sp. GUSF-1 recovered by centrifuging of culture broth, drying the pinkish brown pellet at 80 ^{o}C and crushing it to a fine powder (inset) .

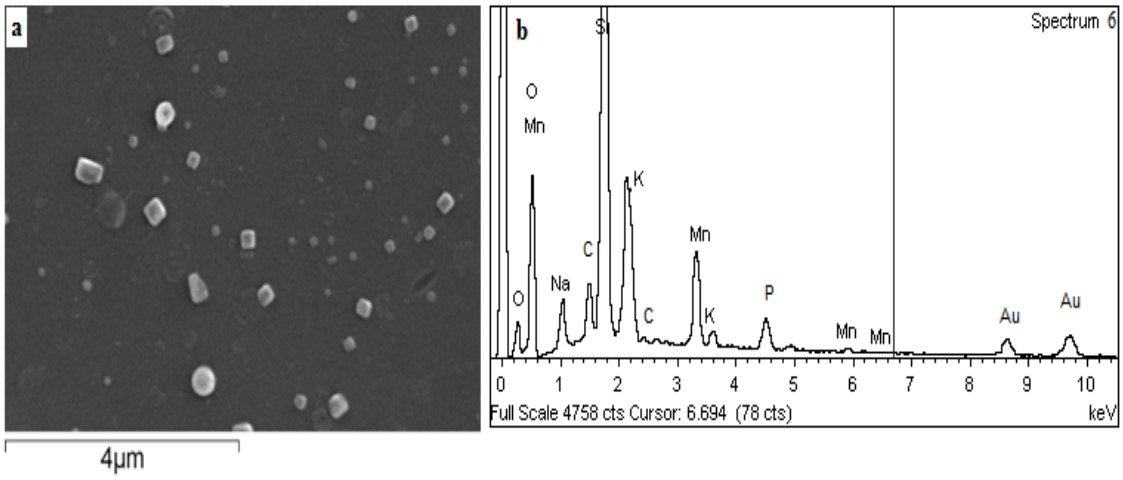

Fig. 4.13. Scanning electron micrograph (a) and Energy- dispersive X-ray profile (b) of the pinkish brown material $MnCO_3$ (rhodochrosite) formed by *Haloferax* sp. GUSF-1.

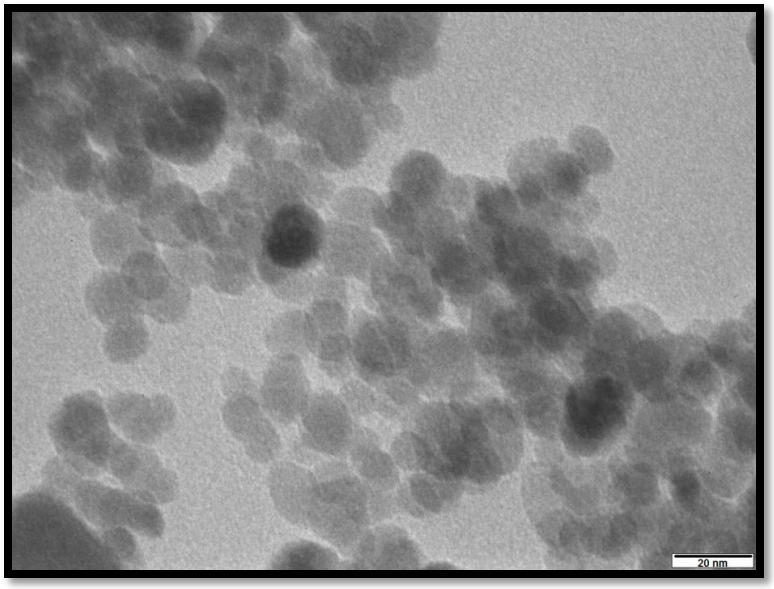

Fig. 4.14. Transmission electron micrographs of biogenic $MnCO_3$ (rhodochrosite) formed by *Haloferax* sp.GUSF-1.

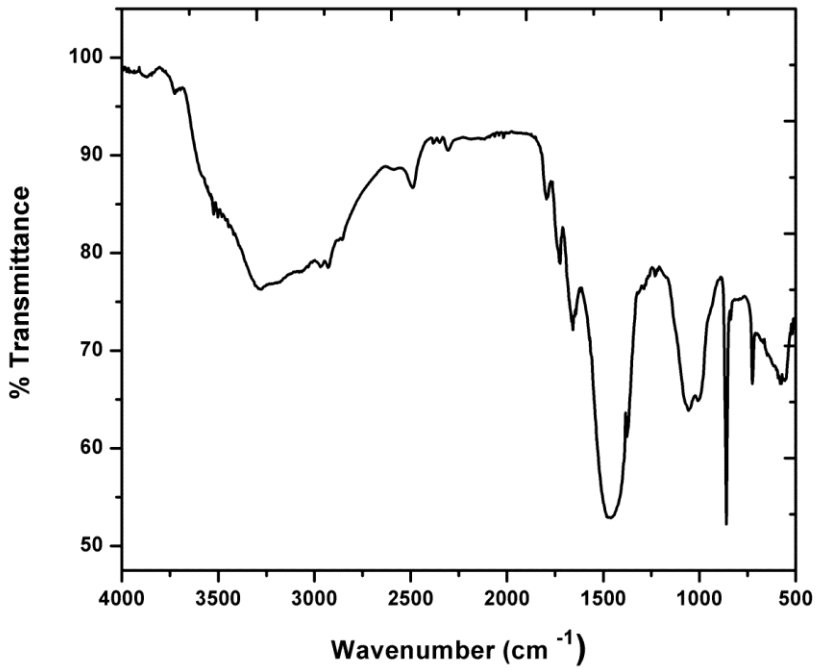

Fig. 4.15 FTIR spectrum of biogenic $MnCO_3$

DISCUSSION

Our study demonstrates the formation of mineral "rhodochrosite" by haloarchaeaon *Haloferax* sp. GUSF-1 of the domain Archaea. Mechanistically, the culture during its growth on acetate converts $MnCl_2$ [Mn^{2+}] $\longrightarrow$ MnO_2 [Mn^{4+}] $\longrightarrow$ $MnCO_3$ [Mn^{2+}]. The process is biogenic involving manganese oxidase followed by a reduction to $Mn^{2+}$and simultaneous incorporation of acetate results in formation of rhodochrosite. Eubacterial thermophile, *Thermoanaerobacter ethanolicus* is known for Mn^{4+} reducing ability during growth under anaerobic conditions utilizing lactate as electron donor (Roh *et al*., 2002). Similarly, *Shewanella oneidensis* MR-1 is also reported to reduce MnO_2 using either H_2 or lactate as an electron donor leading to the formation of $MnCO_3$ (Lee *et al*., 2011). Among archaea, only *Pyrobaculum islandicum*, a hyperthermophile is reported to reduce Mn^{4+} to Mn^{2+}at temperature of 100 ºC under anaerobic condition using hydrogen as electron donor with the formation of manganese carbonates (Kashefi & Lovley, 2000). The haloarchaeal culture used in this study, *Haloferax* sp.GUSF-1 is a habitant of estuarine saltpan of Goa-India, growing optimally at ambient temperature/ 30 ºC in an aerobic environment, reduces manganese leading to the formation of mineral rhodochrosite ($MnCO_3$). This ability of haloarchaeal culture to produce $MnCO_3$ thus proves to be a cost effective over that of eubacteria and hyperthermophilic archaea growing at high temperatures and anaerobic conditions. The potential of *Haloferax* sp.GUSF-1 to oxidize Mn^{2+} to MnO_2 and reduce it further to $MnCO_3$ appears to be coupled with the growth as reflected by the growth studies and indicated by oxidation of manganese followed by reduction of the oxide, only in the presence of the organism. This is supported by the failure of the culture to show a visible growth as well as reduction of manganese oxide in the presence of metabolic inhibitor sodium azide.

Furthermore, the mineral formation was perceptible only in the presence of sodium acetate which possibly served as an electron donor. The reduction of Mn^{4+} coupled with oxidation of acetate by *Haloferax* sp. GUSF-1 is comparable to that of *Geobacter metallireducens* wherein the acetate is stipulated to act as an electron donor (Lovley *et al*., 2004). The reduction of manganese oxide to $MnCO_3$ only in the presence of acetate and not in the presence of glucose (unpublished data), as sole carbon source, suggests its role in the cycling of Mn. The growth of culture in Mn^{2+} containing medium reached cell densities (A_{600} = 1.4) as compared to control without metal ion (A_{600}= 1.05) suggesting that Mn^{2+} or manganese oxide enhances the overall growth yield of haloarchaeal culture. This is in agreement with the hypothesis proposed by Francis and Tebo (2002), suggesting that manganese oxide enhances the cell growth by protecting it against various harmful agents such as UV- light, viral attack, scavenging of trace metals required for growth. Further, the onset of manganese oxide formation in the stationary phase of *Haloferax* sp. GUSF-1 is evident from the accumulation of the dark brown precipitate settling at the bottom of the flask. This result corroborates with previous studies in a eubacteria *P. putida* strain MnB1 (Toner B *et al.*, 2005) and encourages us to suggest that the process to be induced by starvation of nutrients. Furthermore, the observed gradual decrease in the manganese oxide is indicative of, the onset of reduction process wherein the dark brown precipitate commences to turn pale or pinkish brown. Bacterial manganese oxidation mechanisms are enzymatic or non- enzymatic (Tebo *et al*., 2005; Dick *et al.*, 2009). In our study, the enzymatic liability in manganese oxidation was substantiated by inhibition of growth of *Haloferax* sp. GUSF-1 with sodium azide and the consequent absence of manganese oxidation reduction processes. From the results it is clear that the reduction process by this haloarchaea has led to the formation of Mn^{2+}

containing mineral $MnCO_3$, which is confirmed by X- diffraction studies. The crystalline peaks of $MnCO_3$ resemble to mineral rhodochrosite as compared with relative intensity and positioning of peaks to the data reported by Roh *et al*., (2002). The particle size of the rhodochrosite ($MnCO_3$) in the range of 18-25 nm opens its prospects in nanostudies, particularly as chemical synthesis of nano $MnCO_3$ requires a cumbersome, sophisticated process functional at high temperatures (Yuan *et al.,* 2013). Thus our culture is significant in producing $MnCO_3$ a compound already recognized for its application as an additive to ameliorate manganese deficient soils and increase sustainability of crops thereof (Ozbahce & Zengin, 2010; Scaeteanu *et al*., 2013). *Haloferax* sp. GUSF-1 is previously reported for biosynthesis of silver nanoparticles (Patil *et al*., 2013).

In conclusion, *Haloferax* sp. GUSF-1 is the first haloarchaea forming biogenic mineral rhodochrosite, the other archaea being hyperthermophilic. The formation of nanosized rhodochrosite opens its prospects as a microbial cell factory for large scale production of this mineral in the world of microbial nanotechnology.

Chapter 5

Formulation of Haloarchaeal Adsorbent for adsorption of Fe^{2+} and Mn^{2+} ions for its use in remediation of Fe^{2+} and Mn^{2+} from saline waters

Release of inorganic and organic wastes into the marine environment either in soluble or insoluble forms, leads to serious water pollution issues. Since, metals are non biodegradable and have the ability to accumulate in living organisms (Abdel *et al*. 2013), new emerging and attractive technologies are developed that are directed towards removal of metal ions from water bodies using adsorbents made up of biomasses of bacteria, yeast, fungi and algae, respectively (Wang and Chen 2009). Of late, these biosorbent have a limitation of being inefficient in saline environment due to salting out of their proteins at concentrations of 35 g L^{-1} (Oren 2008) and studies on using haloarchaea as an adsorbent are scarce (Prakash *et al*. 2012a,b). Hence, attempt to formulate a haloarchaeal adsorbent efficient enough to remediate saline waters contaminated with Fe^{2+} and Mn^{2+} ions forms the basis of this chapter. The methodology related to adsorbent preparation, optimization and characterization is clubbed together for Fe^{2+} and Mn^{2+} ions while the results for respective metal ion adsorption is divided into two sections; Section A: Adsorption of $Fe^{2+}$by dried cells of haloarchaeon *Haloferax* sp. GUSF-1 and Section B: Adsorption of Mn^{2+} ions by dried cells of *Haloferax* sp. GUSF-1. Finally, the chapter ends with a common discussion.

METHODOLOGY

5.1. Preparation of adsorbent of haloarchaea

For preparation of dry adsorbent, biomass was harvested from mass culture grown in NTYE as detailed in Chapter 3 section 3.1. The biomass was dried at 80 ºC and used for adsorption of Fe^{2+}/ Mn^{2+} ions.

5.2 Formulation of adsorption assay

Glassware used, were soaked overnight in 10 % nitric acid (HNO_3) and rinsed twice with milliQ water(H_2O). A stock solution of 1 M $FeSO_4.7H_20$ /$MnSO_4.7H_20$ (Merck Ltd. India) was prepared in milliQ water as described in section 3.2. For use in experiments, portions were appropriately diluted to obtain the desired concentration for an experiment. For adsorption of Fe^{2+}/ Mn^{2+}, 100 ml of 2 mM $FeSO_4.7H_20$/ MnSO4.7H20 was mixed with 1 g of dry biomass, shaken at 150 rpm**,** at 30 ºC. After 5 h, the reaction mixture was centrifuged at 12000 rpm; the cell free supernatant thus obtained was digested with nitric acid (HNO_3) and sulfuric acid (H_2SO_4) (2:1 v/v) and was estimated for Fe/Mn by atomic absorption spectrophotometer (AAS). Standard of Fe/Mn solution of known concentration for AAS was prepared as detailed in section 3.2. Each experiment was conducted in triplicates and plotted with standard error bars.

5.3 Optimization of adsorption of Fe^{2+}/Mn^{2+} by Haloarchaeon

5.3.1 Contact time

Dried biomass was added to a flask containing Fe^{2+}/ Mn^{2+} (110 mg L^{-1}/ 109.54 mg L^{-1}, respectively) prepared in 15 % NaCl solution was incubated at different time interval 0 , 1 , 2 , 3 , 4 and 5 h, respectively on rotary shaker at 150 rpm and 30 ºC (room temperature). The respective metal ion was estimated as detailed in sub section **3.2**

5.3.2 pH

Dried biomass was added to a flask containing Fe^{2+}/ Mn^{2+} prepared in 15 % NaCl solution with pH adjusted to pH 2, 4, 6, 8 (in case of Fe^{2+}) and pH 3.0, 5.0, 6.0, 6.8, 7.0, 8.0,10

(incase of Mn^{2+}) using 0.1 N HCl and 0.1 N NaOH, incubated at 150 rpm for respective optimum contact time. The respective metal ion was estimated as detailed in sub section **3.2**.

5.3.3 % NaCl

Dried biomass was added to a flask containing Fe^{2+}/ Mn^{2+} prepared in 5, 10, 15, 20, and 25 % NaCl solution incubated at 150 rpm for 5 h. The respective metal ion was estimated as detailed in sub section **3.2**.

5.3.4 Fe^{2+}/ Mn^{2+} concentration

Dried biomass was added to a flask containing 25, 50, 100, 150 and 200 mg of Fe^{2+}/ Mn^{2+} per liter of 15% NaCl adjusted to respective optimum pH and at optimum contact time for each of the metal. The metal in the filtrate was estimated as mentioned in sub section **3.2**.

5.3.5 Biomass concentration

Adsorption of Fe^{2+}/ Mn^{2+} was studied by incubating separately 0.2, 0.4, 0.6, 0.8, 1, 1.2 g dry weight of adsorbent, respectively, in 100 mL of Fe^{2+}/ Mn^{2+} prepared in 15 % NaCl solution, at 150 rpm, 30 ºC. Metal was estimated as detailed in sub section **3.2**

5.3.6 Temperature

Dried biomass was added to flask containing Fe^{2+}/ Mn^{2+} in 15 % NaCl solution and incubated at temperature of 20, 30, 40 and 50 ºC, respectively, on incubator shaker at 150 rpm. Metal filtrate estimated as described in sub section **3.2**

5.4 Evaluation of efficiency of adsorption

Fe^{2+}/ Mn^{2+} ions adsorbed by the adsorbent was calculated from

$$Q = (Ci - Cf) \times V/M \quad (1)$$

where Q is Fe^{2+}/ Mn^{2+} adsorbed (mg g^{-1} dry weight), V is the volume of Fe^{2+}/ Mn^{2+} sorbate (L), Ci and Cf are the initial and the final concentrations of Fe^{2+}/ Mn^{2+} (mg L^{-1}) respectively, and M is the dry weight of the adsorbent (g).

The efficiency of adsorbent in terms of % removal of Fe^{2+}/ Mn^{2+} ions was calculated as

$$R = 100 \times [(Ci - Cf)/Ci]. \quad (2)$$

5.5 Nature of adsorption isotherm

5.5.1 Homogeneity of adsorbent for Fe^{2+}/ Mn^{2+} ions was evaluated using Langmuir equation (Langmuir, 1918)

$$q_e = Q_{max} (b\ C_e / 1+bC_e) \quad (3)$$

where, C_e (mg L^{-1}) corresponds to the Fe^{2+}/ Mn^{2+} ion concentration in the adsorption assay at equilibrium while q_e (mg g^{-1}) was obtained from the concentration of Fe^{2+}/ Mn^{2+} ions adsorbed per unit weight of adsorbent at equilibrium. The Langmuir constants, Q_{max} and b, related to maximum adsorption capacity of Haloarchaeal adsorbent and bonding energy of adsorption, respectively, were obtained by plotting $1/q_e$ versus $1/C_e$. Q_{max} and b were calculated from the intercept and slope of the plot.

5.5.2 Heterogeneity of adsorption of adsorbent was determined by Freundlich equation (Fruendlich, 1906)

$$\text{Log } Q_e = (1/n) \text{ Log } C_e + \text{Log } K_F \quad (4)$$

where Q_e is the amount of Fe^{2+}/ Mn^{2+} ion adsorbed at equilibrium mg g^{-1} and C_e is the amount of Fe^{2+}/ Mn^{2+} ions in solution at equilibrium (ppm), were obtained by plotting log Q_e versus log C_e.; The values of Freundlich parameters i.e. n and K_F (L g^{-1}) were computed from the slope and intercept of straight portion of the plot.

5.6 Evaluation of kinetics of adsorption

The mechanism of adsorption of Fe^{2+}/ Mn^{2+} by adsorbent was evaluated using (i) the pseudo-first order rate equation expressed as

$$\text{Log } (q_e - q_t) = \text{Log } q_e - k_1 t/2.303 \qquad (5)$$

where q_e and q_t are the amounts of Fe^{2+}/ Mn^{2+} ions (mg g^{-1}) adsorbed at equilibrium and at time t, respectively, and k_1 is the first-order rate constant (min^{-1}). k_1 was obtained from the slope of the plot of log (q_e - q_t) versus t.

(ii) The pseudo-second-order kinetic model has the linear form of

$$t/q_t = 1/k_2\, q^2_e + t/q_e \qquad (6)$$

where q_e is the maximum adsorption capacity (mg g^{-1}) and k_2 is the equilibrium rate constant (g mg^{-1} min^{-1}). k_2 and q_e were calculated from the plot of t/q_t versus t (Ho et al., 2001).

5.7 Desorption and recycling of adsorbent

The adsorbent was separated from the reaction mixture after respective optimum time of adsorption by centrifugation at 12000 rpm for 10 min. The adsorbent was washed twice by suspending in 15% saline and dried overnight at 80 ºC and reused for a subsequent adsorption run.

5.8 Evaluation of Fe^{2+}/ Mn^{2+} loaded haloarchaeal adsorbent

5.8.1 SEM-EDX analysis of adsorbent

Samples of dry adsorbent and those loaded with Fe^{2+}/ Mn^{2+} were separately dried at 80 ºC, till constant weight, powdered and coated on gold stubs and each was scanned using scanning electron microscope coupled with energy dispersive X-ray analyzer SEM-EDX (JEOL JSM 5800LV).

5.8.2 FTIR analysis of adsorbent

Samples of dry adsorbent and those loaded with Fe^{2+}/ Mn^{2+} were ground separately with KBr (1:10, w/w), each was then exposed to IR as a KBr tablet in a IR spectrophotometer (Prestige-21 FTIR Shimadzu) for IR profile.

RESULTS

SECTION A: Adsorption of Fe^{2+} by dried cells of haloarchaeon *Haloferax* sp. GUSF-1

5.9. Adsorbent of haloarchaeon *Haloferax* sp. GUSF-1 was prepared by drying at 80 ºC till constant weight, cells grown in TYE containing 20 % NaCl, pH 6.8, at 30 ºC.

5.10 Optimization of adsorption of Fe^{2+} by haloarchaeaon *Haloferax* sp. GUSF-1

5.10.1 Contact time

Dried biomass of *Haloferax* sp. GUSF-1 adsorbed 32.45 mg of Fe^{2+} and 33 mg of Fe^{2+} per g of dry biomass in time period of 1 h and 2 h, respectively (**Fig. 5.1a**), while adsorbed maximum of 47 mg of Fe^{2+} per g of dry biomass in contact time of 3 h. In time period of 4 and 5 h, it adsorbed 44.94 mg and 43.9 mg of Fe^{2+} per g of dry biomass, respectively.

5.10.2 pH

Dried biomass of *Haloferax* sp. GUSF-1 adsorbed 15 mg of Fe^{2+} and 33 mg of Fe^{2+} per g of dry biomass at pH of 2.0 and 4.0 respectively (**Fig. 5.1b**), while adsorbed maximum of 47 mg of Fe^{2+} per g of dry biomass at pH 6.0 and at pH 8.0 adsorbed 15 mg of Fe^{2+} per g of dry biomass, respectively.

5.10.3 Temperature

At temperature of 20 ºC, the adsorbent of *Haloferax* sp. GUSF-1 adsorbed 15.84 mg of Fe^{2+} and a maximum adsorption of 46.8 mg of Fe^{2+} at 30 ºC per g of dry adsorbent while at 40 ºC and 50 ºC, it adsorbed 36.5 mg and 35 mg of Fe^{2+} per g of dry adsorbent, respectively(**Fig. 5.1c**).

5.10.4 Fe^{2+} concentration

At initial Fe^{2+} concentration of 50 and 100 mg L^{-1}, the dried adsorbent of *Haloferax* sp. GUSF-1 adsorbed, 22 mg and 47 mg Fe^{2+} per g of dry biomass while at 150 and 200 mg L^{-1}, the adsorbent adsorbed 86.7 and 110 mg Fe^{2+} per g of dry biomass, respectively (**Fig. 5.1d**).

5.10.5 % NaCl

At % NaCl of 5 % and 10% , the dried adsorbent adsorbed 25.35 mg and 40.14 mg of Fe^{2+} per g of dry biomass respectively(**Fig. 5.1e**), while at 15 % showed maximum adsorption of 47.1 mg Fe^{2+} per g of dry biomass and at 20 % showed adsorption of 25.9 mg Fe^{2+} per g of dry biomass.

5.10.6 Dry weight of biomass

0.2 g and 0.4 g of dry adsorbent of *Haloferax* sp. GUSF-1 adsorbed 27.88 mg and 41.36 mg Fe^{2+} per g of dry biomass respectively (**Fig. 5.1f**). 0.6 and 0.8 g of dry adsorbent adsorbed 44.15 mg and 46 mg Fe^{2+} per g of dry adsorbent while 1 g and 1.2 g of dry adsorbent showed maximum adsorption of 47 mg Fe^{2+} per g of dry adsorbent respectively.

5.11 Evaluation of efficiency of adsorption

Fig. **5.2** displays the non-linearized adsorption isotherm of Fe^{2+}onto the adsorbent of *Haloferax* sp. GUSF-1. The results of optimization were therefore incorporated to formulate an adsorption assay consisting of 100 mg L^{-1} of Fe^{2+} and 1 g dry weight of biomass, suspended in 15 % NaCl solution, pH 6.0 mixed at 150 rpm and 30 ºC for 3 h. The specific amount of Fe^{2+}adsorbed (Q) at optimum condition was 46.5 mg g^{-1} dry weight of adsorbent with a removal efficiency of 99.5 %.

5.12 Nature of adsorption isotherm

Maximum amount of Fe^{2+}adsorbed (Qmax) by adsorbent of *Haloferax* sp. GUSF-1 was 74.07 mg g^{-1} dry weight, with a bonding energy of adsorption (b) of 0.017 (L mg^{-1}) and had a homogeneity corresponding to Langmuir isotherm (**Fig**. **5.3a**).

Further, the heterogeneity of adsorption fitted well with Fruendlich isotherm having magnitude of adsorptive capacity (K_F intercept) of 1.38 mg g^{-1} and adsorption constant (n) 0.96 (**Fig. 5.3b**)

5.13 Kinetics of adsorption of Fe^{2+}

The values of average determination coefficients (R^2) derived from **Fig**. **5.4a, b** in **Table 5.1** indicated that the haloarchaeal adsorption followed pseudo-second order kinetics since an increase in equilibrium concentration (q_e) resulted in corresponding linear decrease in equilibrium rate constant (k_2), with an increase of initial Fe^{2+}concentration.

5.14 Desorption and recycling of adsorbent

The haloarchaeal adsorbent was 99.5 % efficient up to three recycles and retained 92 % removal efficiency for Fe^{2+}at fourth adsorption –desorption cycle (**Fig. 5.5**). However, the

efficiency declined progressively by 81.8 %, 54.5 % and 27.3 % in the fifth, sixth and the seventh adsorption-desorption cycle, respectively.

5.15 Evaluation of Fe^{2+}loaded haloarchaeal adsorbent

5.15.1 SEM-EDX analysis of adsorbent

SEM profiles of the dried cells of haloarchaeon adsorbent showed minute surface depressions, while the cell surface post adsorption appeared crystalline with metallic shine (**Fig. 5.6a, b**). The EDX spectra of adsorbent, carried out at pre and post adsorption showed a peak due to Fe^{2+}at 2.2 keV and weak peak at 6.4 keV along with a shift in phosphorous peak from 2.8 keV to 2.2 keV.

5.15.2 FTIR analysis of adsorbent

The FTIR spectra of adsorbent, Fe^{2+} loaded adsorbent and Fe^{2+} unloaded adsorbent, confirmed the participation of functional groups present on surface of adsorbent (**Fig**. **5.7a,b,c**). The adsorbent, displayed absorption peaks at 3500-3200 cm^{-1} corresponding to the stretching of the N-H bond of amino groups and indicated bonded hydroxyl group. A change in peak position in the spectrum of the Fe^{2+} loaded adsorbent indicated the binding of iron with amino and hydroxyl groups. The absorption peaks at 2900–3000 cm^{-1} were ascribed to the asymmetric stretching of γC–H bond of the –CH2 groups combined with that of the CH3 groups. Interestingly, the 1544 cm^{-1} peak increased with the presence of Fe^{2+}, suggesting an interaction of $Fe^{2+}$with carboxyl groups. This was supported by presence of peaks in the range of 1300–1067 cm^{-1}, attributed to the carboxyl and phosphate groups. Further, carboxy group were also present in the spectrum of unloaded adsorbent representing the γC=O of amide I and γNH/γC= O combination of the amide II bond at 1650 and 1544 cm^{-1}, respectively.

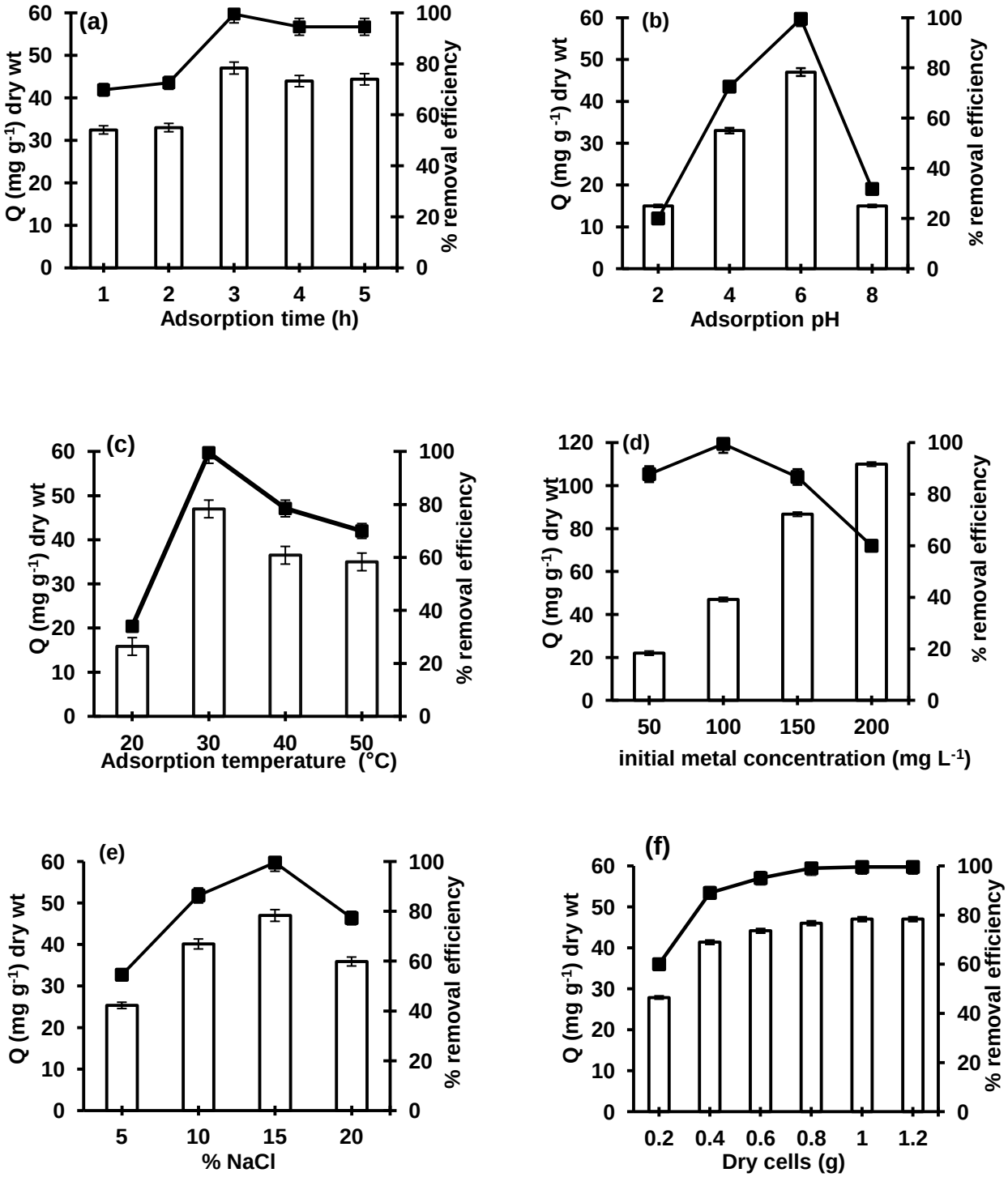

Fig. 5.1. Effect of physicochemical parameters on adsorption (column) and % removal efficiency (line) of Fe^{2+} ions by adsorbent of *Haloferax* sp. GUSF-1: **(a)** time **(b)** pH **(c)** temperature **(d)** initial metal concentration **(e)** % NaCl **(f)** weight of dried cells.

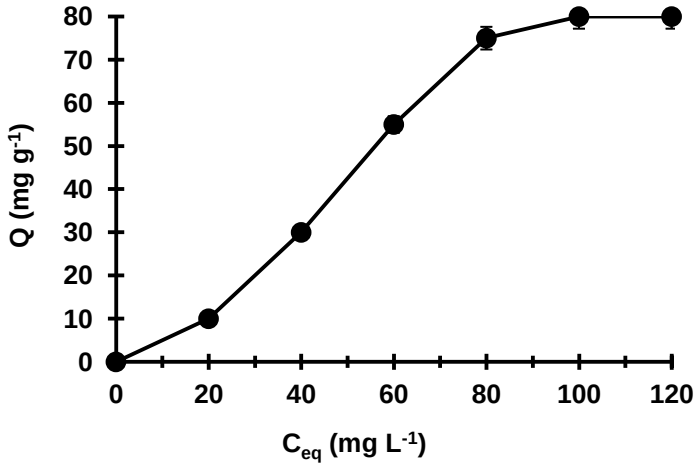

Fig. 5.2 Adsorption isotherm of Fe $^{2+}$ ions for adsorption by haloarchaeon *Haloferax* sp. GUSF-1.

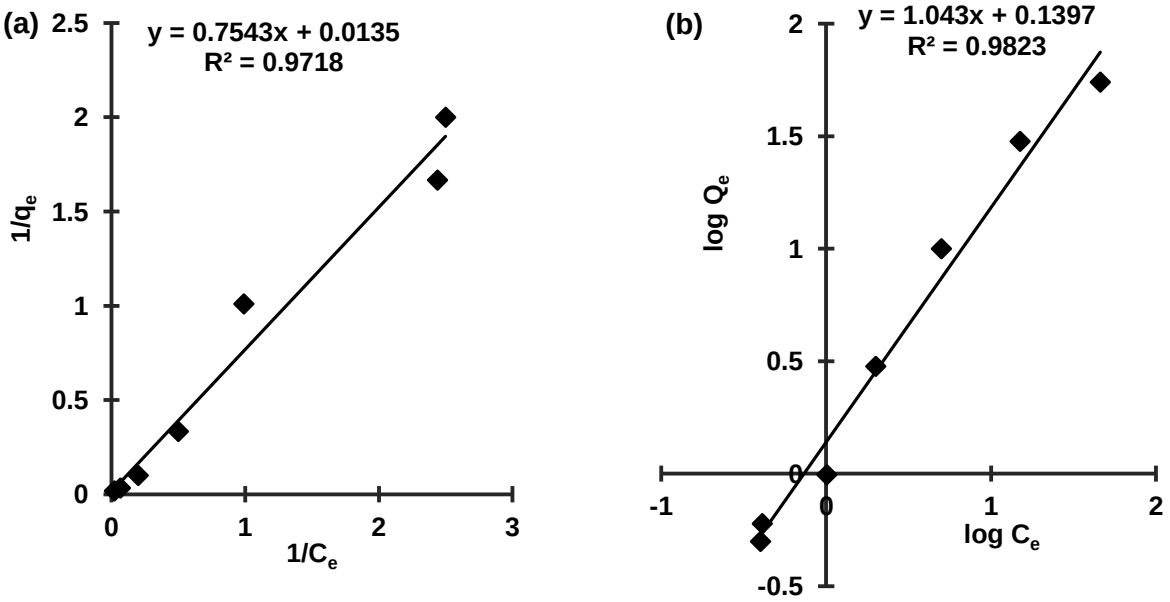

Fig. 5.3 Linear adsorption isotherm of Fe^{2+} ions onto adsorbent of *Haloferax* sp. GUSF-1 **(a)** Langmuir isotherm **(b)** Fruendlich isotherm.

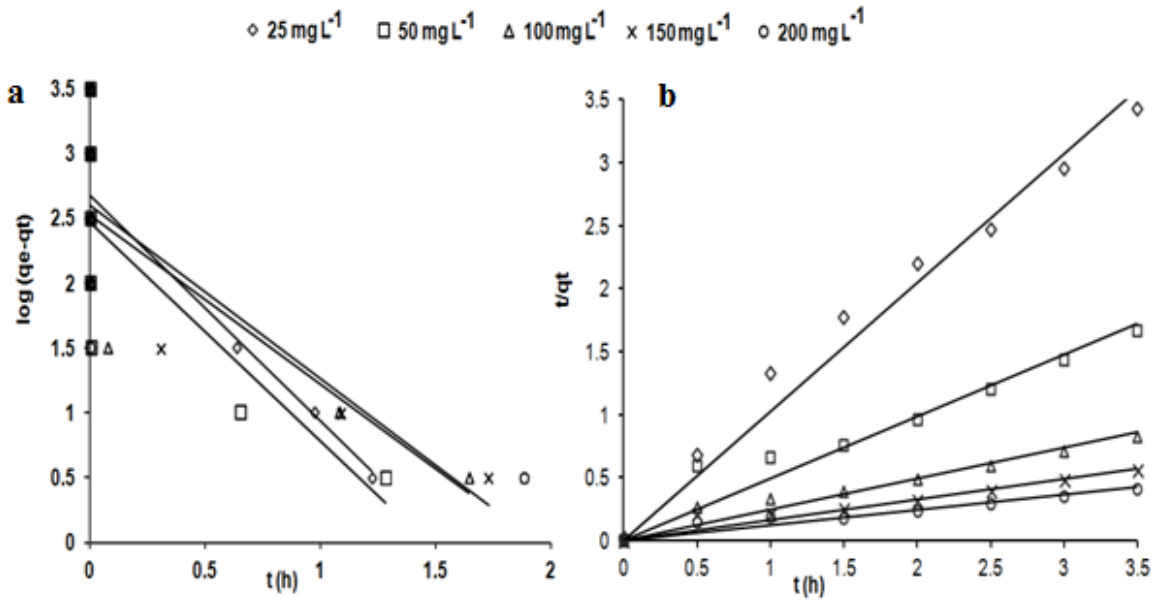

Fig. 5.4 Kinetic model for Fe^{2+} adsorption by adsorbent of *Haloferax* sp. GUSF-1 at different initial concentrations of Fe^{2+} **(a)** Pseudo- first order plot **(b)** Pseudo- second order plot.

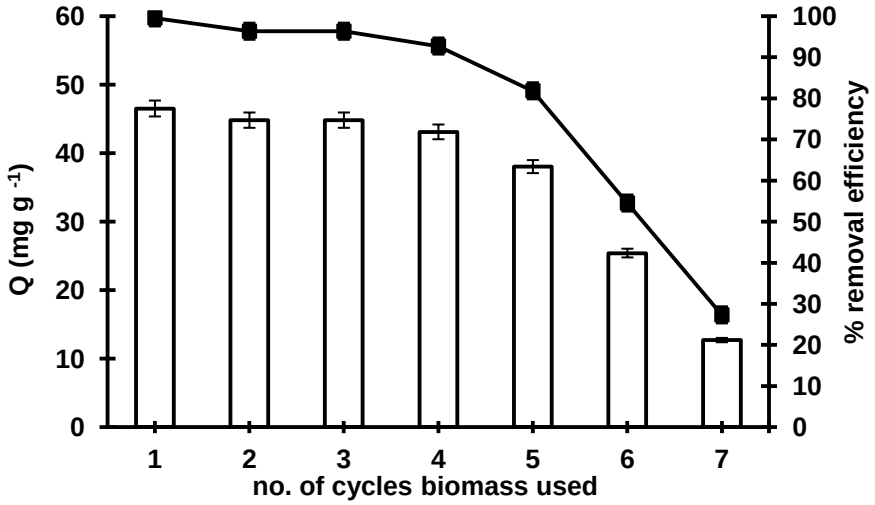

Fig. 5.5 Recycling of adsorbent of *Haloferax* sp. GUSF-1 for adsorption (column) and % removal efficiency (line) of Fe^{2+}

Table 5.1 Kinetic parameters for adsorption of Fe^{2+} by *Haloferax* sp. GUSF-1 at various initial Fe^{2+} concentrations.

Fe^{2+} concentration ($mg\ L^{-1}$)	Pseudo first order			Pseudo second order		
	q_e ($mg\ g^{-1}$)	k_1 (min^{-1})	R^2	q_e ($mg\ g^{-1}$)	k_2 ($g\ mg^{-1}\ min^{-1}$)	R^2
25	19.22	1.024	0.78	1.145	2.023	0.99
50	10.32	0.847	0.62	3.44	0.225	0.97
100	26.60	1.179	0.67	5.25	0.263	0.99
150	35	1.263	0.73	8.149	0.122	0.98
200	10.09	0.437	0.32	10	0.098	0.988

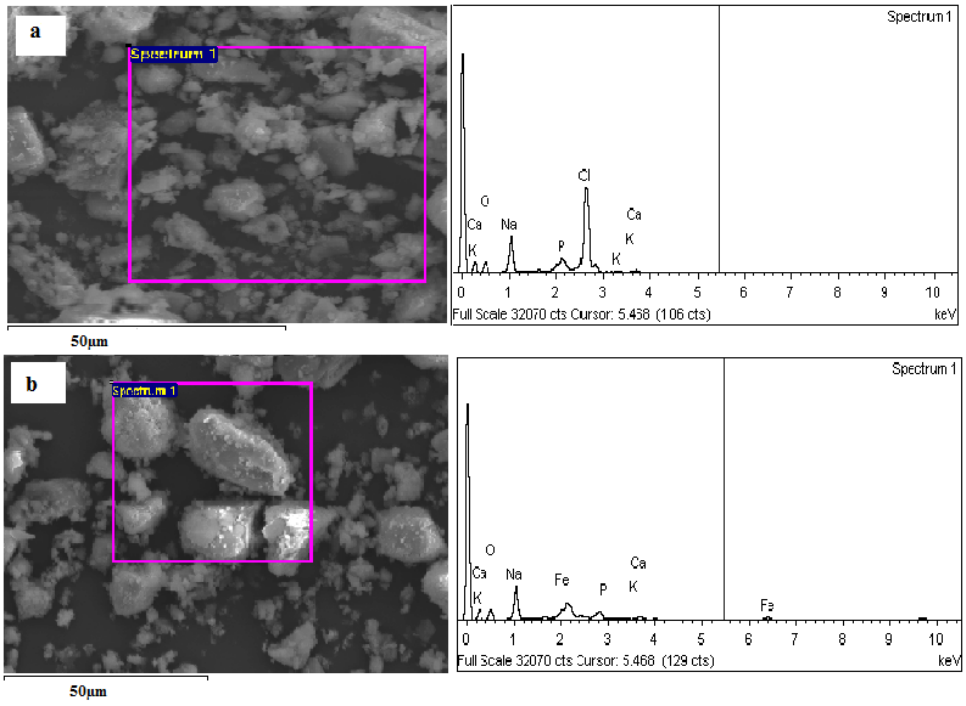

Fig. 5.6 Scanning electron micrographs and EDX spectra of adsorbent of *Haloferax* sp. GUSF-1: **(a)** before exposure to Fe^{2+} **(b)** after exposure to Fe^{2+}

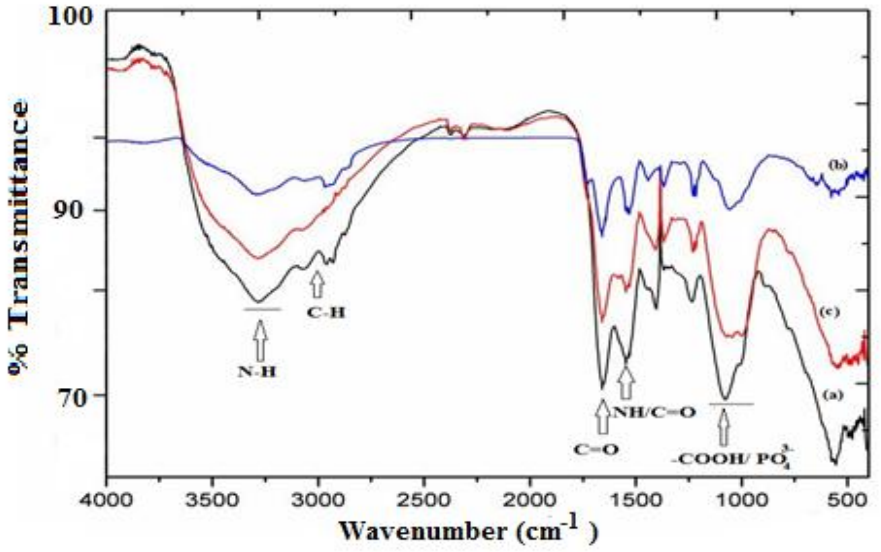

Fig. 5.7 FTIR spectra of: **(a)** adsorbent of *Haloferax* sp. GUSF-1 **(b)** Fe^{2+} loaded adsorbent **(c)** Fe^{2+} unloaded adsorbent post recovery.

RESULTS

SECTION B: Adsorption of Mn^{2+} by dried cells of haloarchaeon *Haloferax* sp. GUSF-1

5.16 Adsorbent of haloarchaeon *Haloferax* sp. GUSF-1 was prepared by drying at 80 ºC, cells grown in TYE containing 20 % NaCl, pH 6.8, at 30 ºC.

5.17. Optimization of adsorption of Mn^{2+} by *Haloferax* sp. GUSF-1

5.17.1 Contact time

Dried biomass of *Haloferax* sp. GUSF-1 adsorbed 12.27 mg of Mn^{2+} and 18.52 mg of Mn^{2+} per g of dry biomass in time period of 5 and 10 min, respectively (**Fig. 5.8**). At 15 and 30 min, 32.77 mg and 44.77 mg Mn^{2+} per g of dry biomass. A maximum adsorption was observed at 60 min with 46 mg of Mn^{2+} g^{-1} per g of dry biomass after which it remained constant to 46 mg of Mn^{2+} at 120 min to 300 min, respectively.

5.17.2 % NaCl

As depicted in **Fig. 5.9** adsorption occurred in the presence as well as in the absence of NaCl. At 0% salinity, a maximum of 15.5 mg Mn^{2+} per g of adsorbent was taken up in 60 min. At 5, 10, and 15% concentrations of NaCl, 35, 42, and 47 mg Mn^{2+} were adsorbed, respectively, in 60 min per g of adsorbent, whereas at 20 % and 25 % salinity, 34 and 27.8 mg Mn^{2+} per g of adsorbent were taken up, respectively, in 60 min.

5.17.3 pH

As illustrated in **Fig. 5.10**, an influence of initial pH on adsorption of Mn^{2+} was observed. At acidic pH 2.0 and 4.0, maximum adsorption of Mn^{2+} was 15.8 mg and 28.3 mg per g of

adsorbent while at pH 6.0, 47 mg Mn^{2+} was taken up per g of adsorbent, respectively, in 60 min. Despite a precipitation of Mn^{2+} at pH 8.0, the amount of Mn^{2+} adsorbed was 14.2 mg in 60 min per g adsorbent.

5.17.4 Temperature

Adsorption of Mn^{2+} onto the haloarchaeon adsorbent *Haloferax* sp. GUSF-1 was significantly influenced by temperature. As depicted in **Fig. 5.11**, maximum adsorption was seen at 30ºC with 47 mg Mn^{2+} taken up in 60 min per g adsorbent as compared to 13 mg, 46 mg, 25.6 mg and 10.3 mg Mn^{2+} adsorbed, at 20, 40 and 50ºC, respectively.

5.17.5 Mn^{2+} concentration

The amount of Mn^{2+} taken up in 60 min per g of adsorbent changed with a change of initial Mn^{2+} concentration (**Fig. 5.12**). At initial concentration of 25, 50, 100, 150 and 200 mg L^{-1} of Mn^{2+}, the amount of Mn^{2+} adsorbed was 10, 22, 47, 70.5 and 94 mg L^{-1} , respectively, in 60 min per g of adsorbent.

5.17.6 Dry weight of biomass

Increasing the amount of adsorbent from 0.2 g to 1.2 g dry weight increased the adsorption from 5 mg to 47 mg Mn^{2+} per g of adsorbent in 60 min, evident from **Fig. 5.13**.

5.18 Evaluation of efficiency of adsorption

The results of optimization were therefore incorporated to formulate an adsorption assay consisting of 100 mg L^{-1} of Mn^{2+} and 1 g dry weight of biomass, suspended in 15 % NaCl solution, pH 6.0 mixed at 150 rpm and 30 ºC for 60 min (**Fig. 5.14**). The specific amount of

Mn^{2+}adsorbed (Q) at optimum condition was 47 mg g^{-1} dry weight of haloarchaeon adsorbent with a removal efficiency of 99.5 %.

5.19 Nature of adsorption isotherm

Maximum amount of Mn^{2+}adsorbed (Qmax) by adsorbent of *Haloferax* sp. GUSF-1 was 62.5 mg g^{-1} dry weight, with a bonding energy of adsorption (b) of 0.018 (L mg^{-1}) and had a homogeneity corresponding to Langmuir isotherm (**Fig**. **5.15a**).

Further, the heterogeneity of adsorption fitted well with Fruendlich isotherm having magnitude of adsorptive capacity (K_F intercept) of 1 mg g^{-1} and adsorption constant (n) 1.1 (**Fig**. **5.15b**)

5.20 Kinetics of adsorption of Mn^{2+}

The values of average determination coefficients (R^2) derived from **Fig**. **5.16a, b** in **Table 5.2** indicated that the haloarchaeal adsorption followed pseudo-second order kinetics since an increase in equilibrium concentration (q_e) resulted in corresponding linear decrease in equilibrium rate constant (k_2), with an increase of initial Mn^{2+}concentration.

5.21 Desorption and recycling of adsorbent

The haloarchaeal adsorbent was 99.5 % efficient up to fourth recycle (**Fig. 5.17**). However, its ability to adsorb declined progressively by 73.7, 44.2 and 21.06 % in the fifth, sixth and the seventh cycle, respectively.

5.22 Evaluation of Mn^{2+}loaded haloarchaeal adsorbent

5.22.1 SEM-EDX analysis of adsorbent

An SEM profile of adsorbent consisting of the dried cells of haloarchaeon, showed minute surface depressions which after adsorption of Mn^{2+}appeared bright and crystalline (**Fig. 5.18a, b**). The EDX spectra before and after adsorption revealed a peak due to Mn^{2+} at 0.2 keV, 2.2 keV and a weak peak at 5.8 keV along with a shift in the phosphorous peak from 2.2 keV to 1.6 keV.

5.22.2 FTIR analysis of adsorbent

The FTIR spectra of adsorbent and metal loaded adsorbent taken in the range of 500-4000 cm^{-1}, confirmed the participation of functional groups present on the surface of the adsorbent (**Fig. 5.19a, b**). The adsorbent displayed absorption peaks at 3500-3200 cm^{-1} corresponding to the stretching of the N-H bond of amino groups and indicative of bonded hydroxyl group. The absorption peaks at 2900-3000 cm^{-1} were ascribed to the asymmetric stretching of the γC-H bond of the –CH2 groups combined with that of the CH3 groups. A decrease in intensity of the peak for amino and hydroxyl groups in the spectrum of the Mn^{2+} loaded adsorbent indicated the binding of Mn^{2+} to the adsorbent. Interestingly, the 1540 cm^{-1} peak decreased with the presence of Mn^{2+} suggesting an interaction of Mn^{2+} with carboxyl groups. Occurrence of the peaks in the range 1250–1067 cm^{-1} were attributable to the presence of carboxyl and phosphate groups and corresponded to P-O-C linkage of organo phosphorous groups. The metal loaded adsorbent showed peaks at 1650 cm^{-1} for γC=O and at 1544 cm^{-}1 for γNH/γC= O which correspond to an amide-I and amide-II bond, respectively, indicating the presence of carboxyl groups.

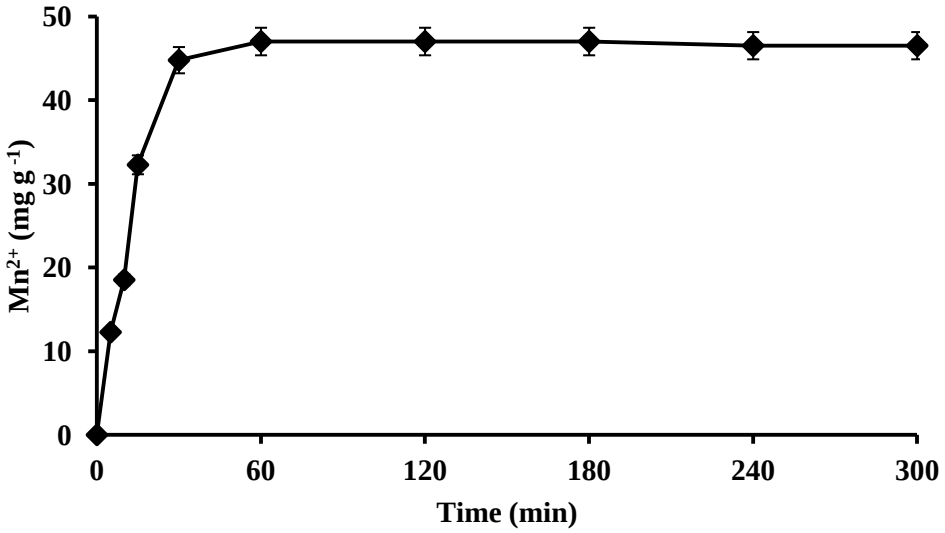

Fig. 5.8 Time course of manganese adsorption by haloarchaeon *Haloferax* sp. GUSF-1

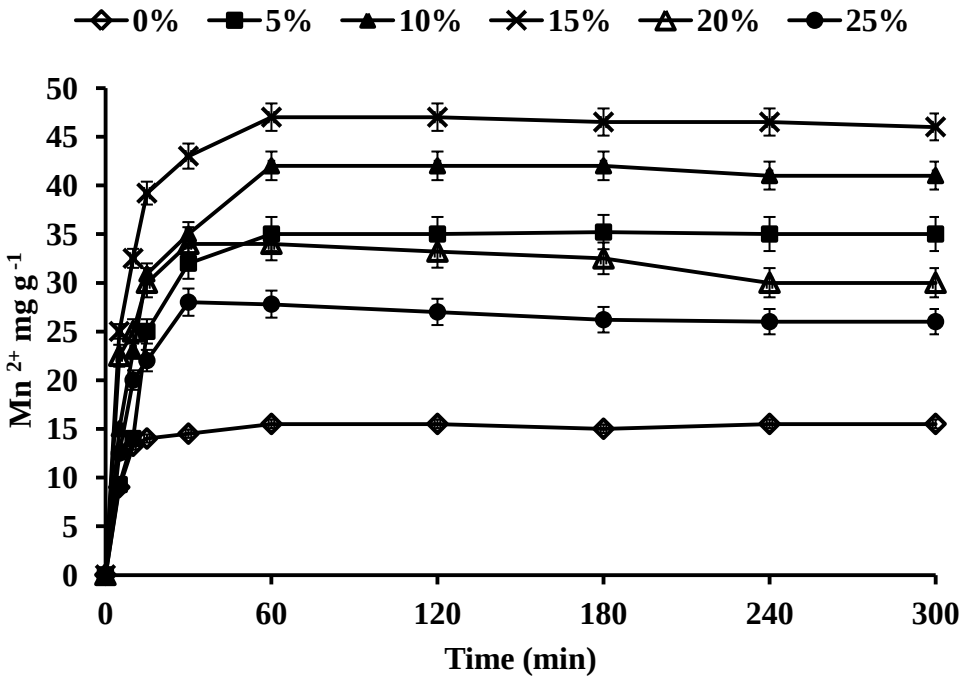

Fig. 5.9 Effect of salinity on adsorption of manganese by haloarchaeon *Haloferax* sp. GUSF-1

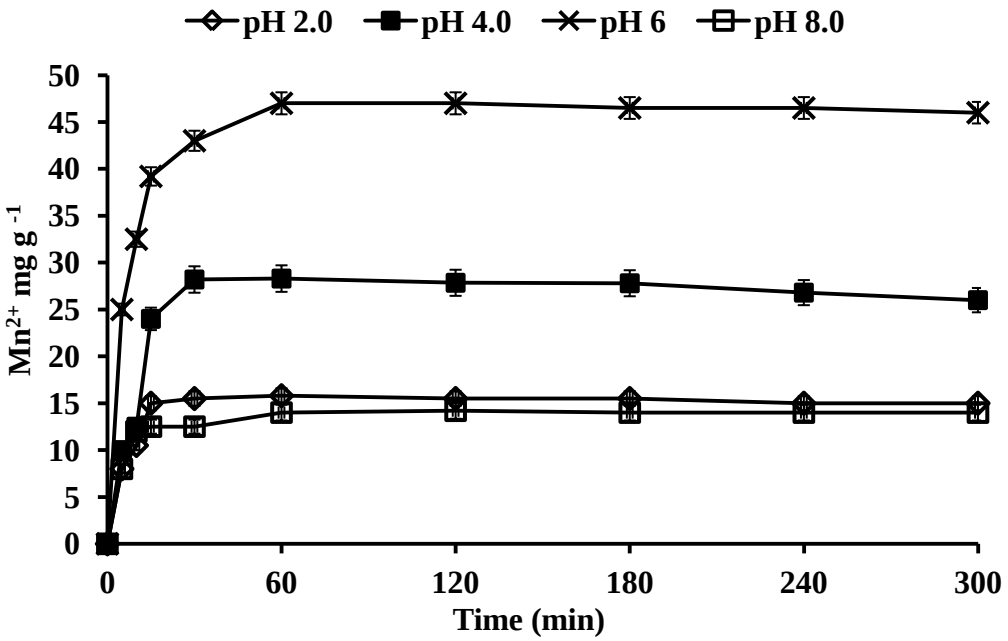

Fig. 5.10 Effect of pH on adsorption of manganese quantified after different durations of adsorption cycle.

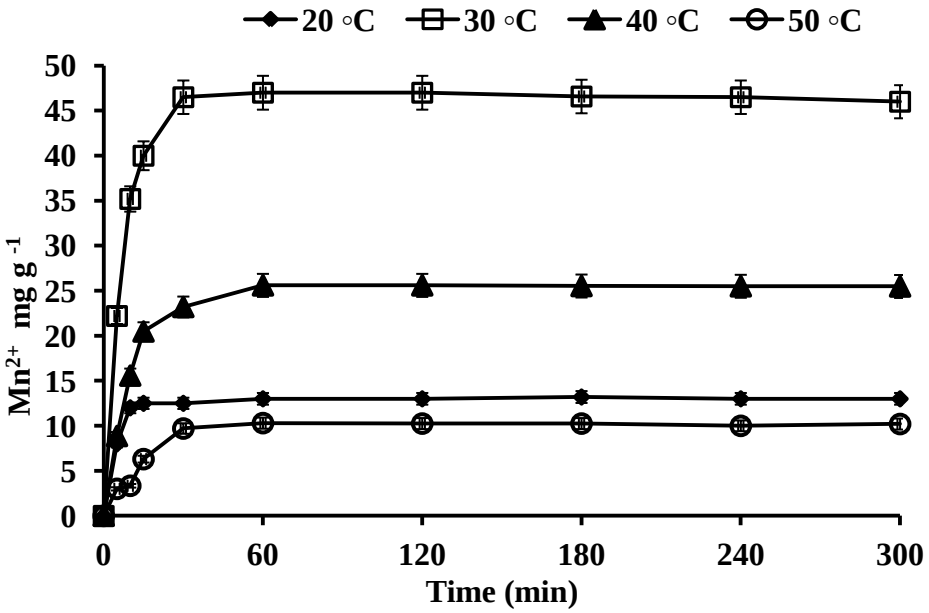

Fig. 5.11 Effect of temperature on adsorption of manganese

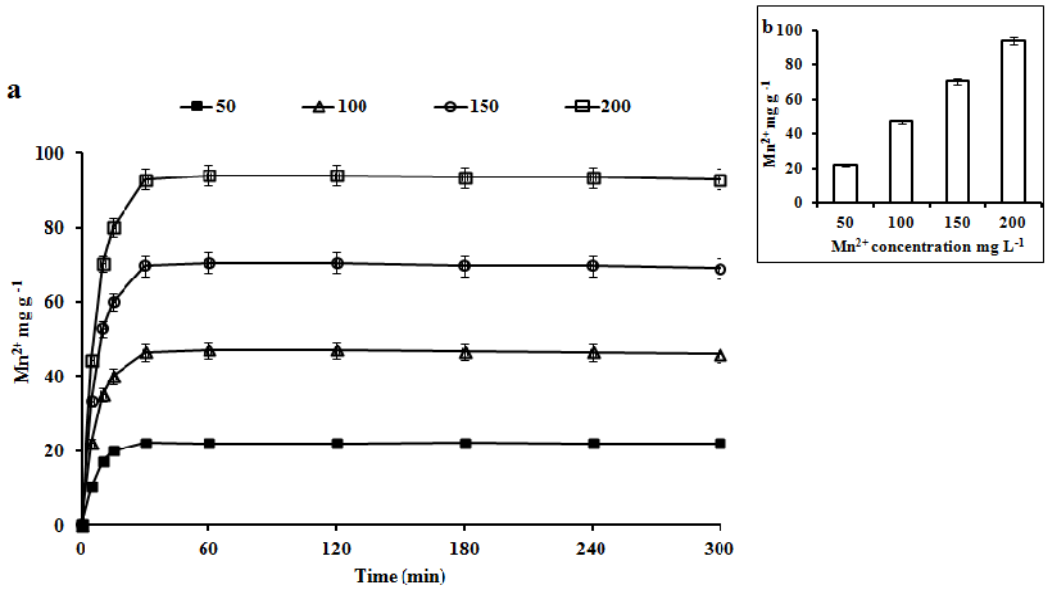

Fig. 5.12 Adsorption of manganese at **(a)** different initial Mn^{2+} concentration **(b)** (inset) on maximum Mn^{2+} adsorption at 60 min

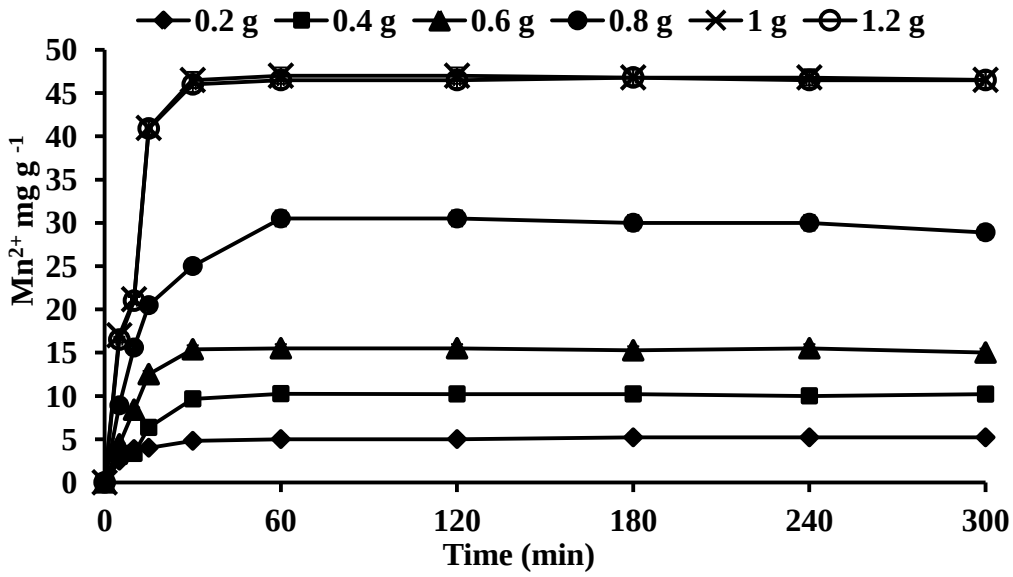

Fig. **5.13** Effect of biomass concentration on adsorption of manganese

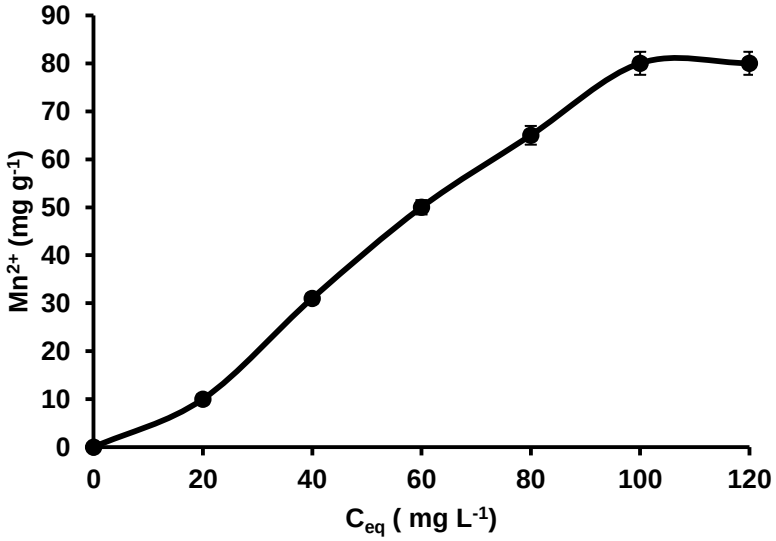

Fig. 5.14 Adsorption isotherm of Mn^{2+} ions by haloarchaeon *Haloferax* sp. GUSF-1

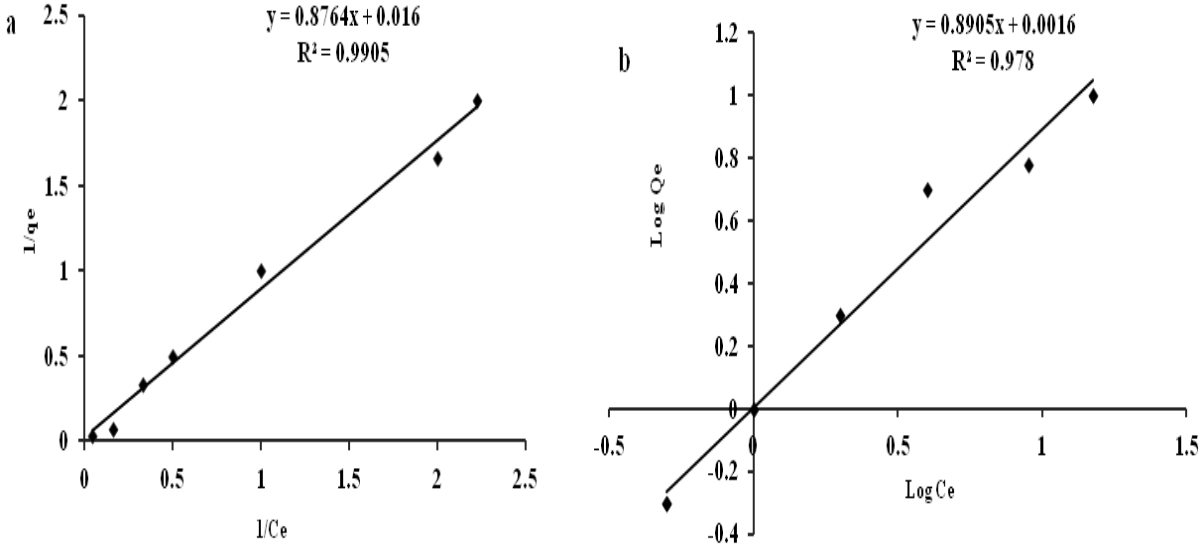

Fig. 5.15 Adsorption isotherm models of Mn^{2+} ions onto haloarchaeon **(a)** Langmuir isotherm model **(b)** Fruendlich isotherm model.

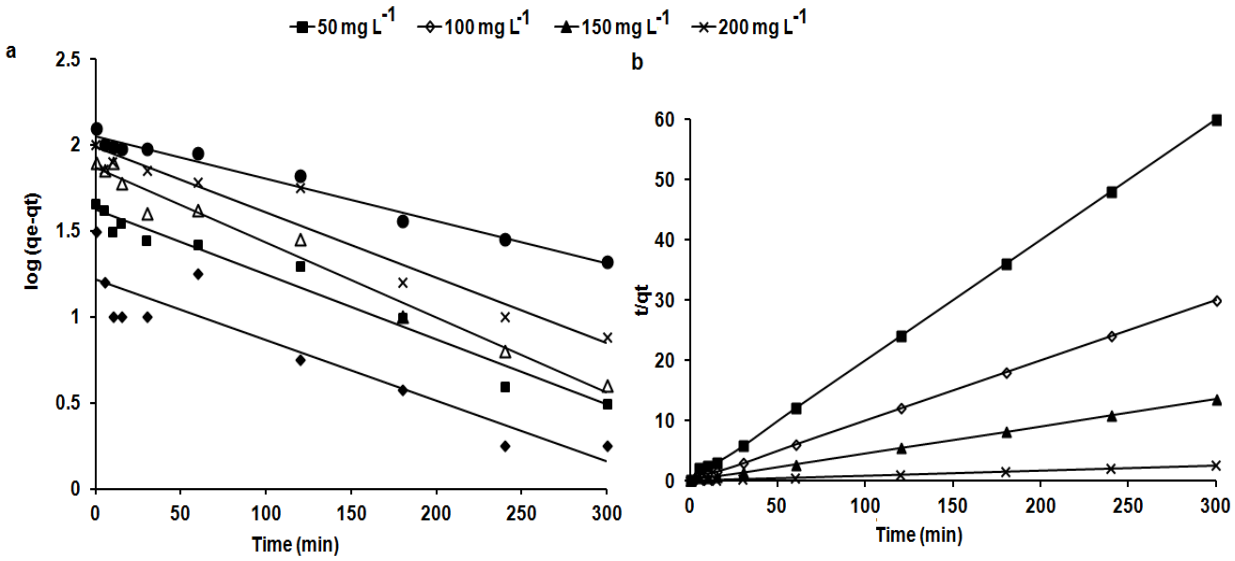

Fig. 5.16 Kinetics for Mn^{2+} adsorption by haloarchaeon at different initial Mn^{2+} concentrations **(a)** Pseudo- first order plot **(b)** Pseudo- second order plot

Table 5.2 Kinetic parameters for adsorption of Mn^{2+} by haloarchaeon *Haloferax* sp. GUSF-1

Mn^{2+} concentration (mg L^{-1})	**Pseudo first order**			**Pseudo second order**		
	q_e (mg g^{-1})	**k_1 (min^{-1})**	**R^2**	**q_e (mg g^{-1})**	**k_2 (g mg^{-1} min^{-1})**	**R^2**
25	0.0057	16.45	0.95	10.05	0.0997	0.99
50	0.0087	41.94	0.96	22.22	0.0258	0.99
100	0.0101	73.7	0.95	46.73	0.0140	0.989
150	0.0087	96	0.94	86.95	0.00495	0.99
200	0.0057	112	0.95	114.94	0.00461	0.996

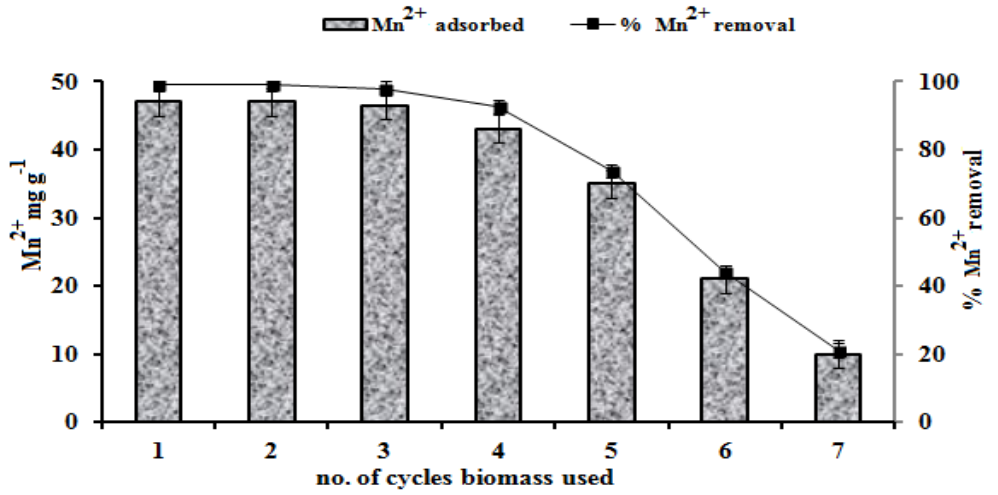

Fig. **5.17** Mn^{2+} adsorbed by haloarchaeon *Haloferax* sp. GUSF-1 in repeated cycles

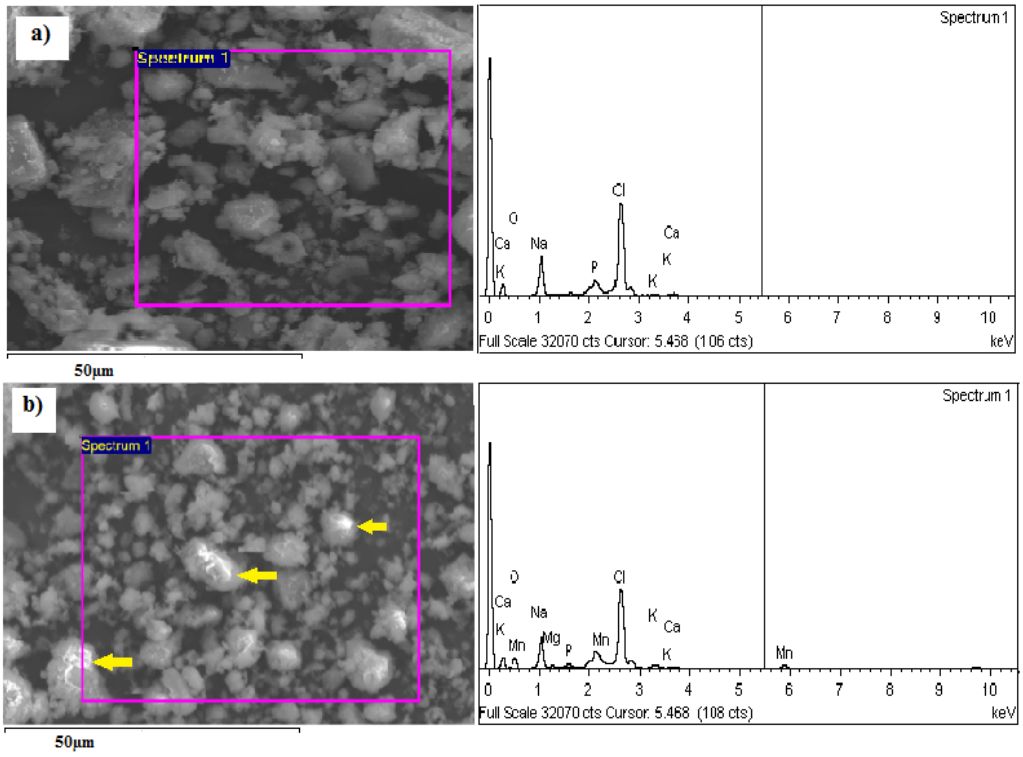

Fig. 5.18. Scanning electron micrographs and EDX spectra of dried adsorbent of haloarchaeon *Haloferax* sp. GUSF-1: **(a)** before exposure to Mn^{2+} **(b)** after exposure to Mn^{2+} (arrows indicate metallic sheen).

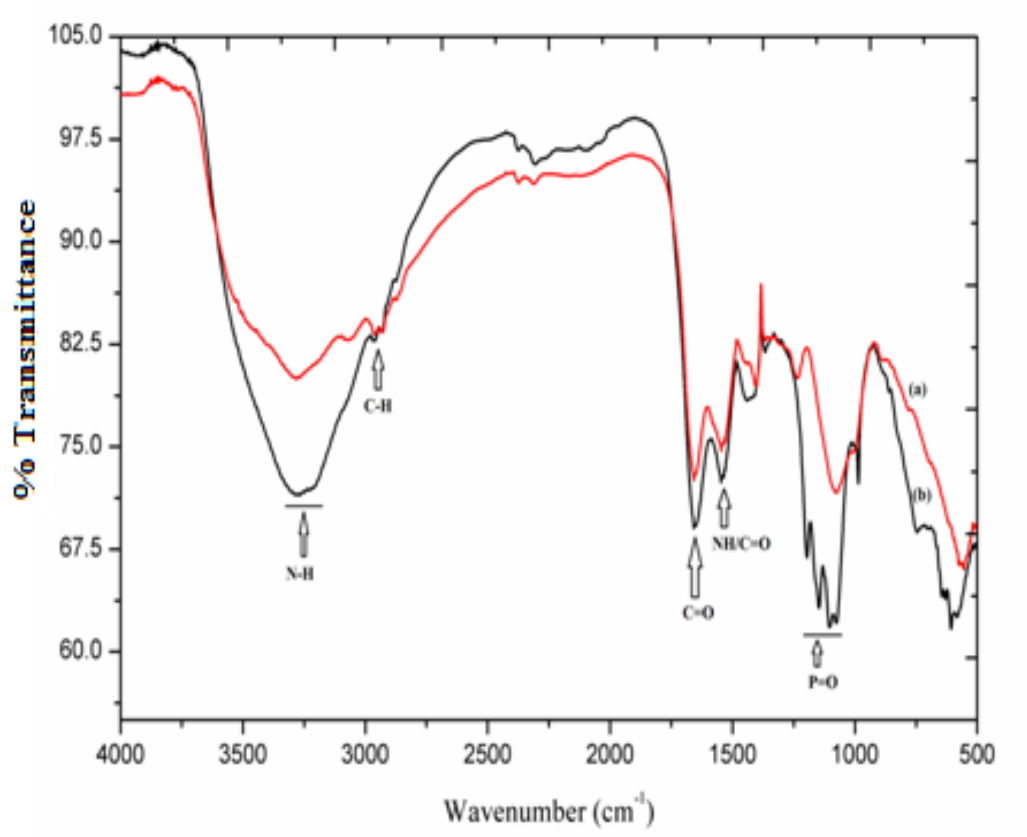

Fig. 5.19 FTIR spectra of dried biomass of haloarchaeon *Haloferax* sp. GUSF-1 **(a)** adsorbent before Mn^{2+}adsorption **(b)** Mn^{2+} loaded adsorbent

DISCUSSIONS

Both living and non living microbial biomass are able to passively bind metal ions. Contact of living biomass with the metal results in sequestration followed by accumulation of passively bound ions, across the cell surface into cytosol (Gupta *et al*., 2000), a phenomenon not seen with the dead biomass. We prepared an adsorbent of haloarchaeon by drying at 80 ºC, stationary phase whole cells of *Haloferax* sp. GUSF-1. These cells were metabolically inactive but had original surface integrity. Further, we ensured that there was no abiotic Fe^{2+} oxidation by preparing sorbate solution of $FeSO_4.7H_20$ at acidic pH, just prior to the adsorption experiments using deoxygenated water as detailed.

The adsorption of Fe^{2+} by *Haloferax* sp. GUSF-1 adsorbent was rapid, exhibited saturation in 3 h while adsorption of Mn^{2+} by metabolically inactive dried biomass is a contact time dependent surface adsorption phenomenon, reaching equilibrium in 60 min with a 99 % efficiency Mn^{2+} adsorption by the biomass. Such adsorption is expected to involve a stoichiometric interaction between the metal and the reactive chemical groups in the eukarya and eubacterial cell wall which consist of a variety of polysaccharides and proteins (Beveridge and Murray, 1980).

Haloferax sp. GUSF-1 with its cup-shaped morphology and resemblance to the genera *Haloferax* with S-layers, forming 15 % of total cell envelope proteins. The S-layers of type culture *Haloferax volcanni* contain mannosyl- (β 1-4) - galactosyl phosphodolichol, with sulfated and/or phosphorylated dihexosyl phosphodolichol and dolichol phosphate bearing a tetrasaccharide comprising of mannose, galactose and rhamnose. The acidic amino acids and surface glucans of these layers contribute, to the net negative charge. (Sara and Sleytr, 2000).

Although, a maximum adsorption efficiency of 99.5 % of Fe^{2+} and Mn^{2+} is achieved at 30 ºC, the adsorption is reduced to 78 % with 10 ºC and 70 % with 20 ºC increase in adsorption temperature in case of Fe^{2+} while for Mn^{2+} adsorption reduced to 50 % and 20 % with the respective rise in temperature. This phenomenon can be explained as due to the distortion of some attachment/adsorption sites on the surface of adsorbents as reported for *Citrobacter* strain MCM B181 by Puranik and Paknikar (1999).

The adsorption process in microorganisms is influenced by pH. In our experiments, iron and manganese adsorption increased gradually with an increase in initial pH from 2.0 to 6.0.

The rise in removal percentage of Fe^{2+}/ Mn^{2+} ions at slightly elevated pH can be argued to be because of the decrease in H^+ ion concentration which in turn results in decreased competition between H^+ ion and metal ion for the same binding site. The increase in adsorption capacity with increase in pH from pH 2 to pH 6, corroborates with data reported for eubacteria and eukarya; and is attributed to correspond to dissociation of functional groups or their de-protonation, resulting in increase in the negative charge density of the functional groups which in turn promote the efficient binding of positively charged metal ions to the carboxyl or phosphate groups of the cell wall (Volesky, 2007). We infer, that in afore described adsorption system employing, *Haloferax* sp. GUSF-1, having S-layer protein in its outermost surface, it is the carboxyl, amino, hydroxyl and phosphate groups which contributed to the negative charge density and affected an increased adsorption with increase in pH from pH 2 - pH 6, with approximately 15 % increase for every one unit rise in pH.

The initial concentration of metal ion provides a favorable driving force to overcome all mass transfer resistance of Fe^{2+}/Mn^{2+} ion between the aqueous and solid phases, which enhances the adsorption process. The effect of initial metal ion concentration on adsorption is related

to the number of available active sites on the surface of the adsorbent (Joo *et al.* 2010). This is evident from the linear increase in adsorption of the adsorbent from 5 mg to 62.8 mg of Mn^{2+} per g of adsorbent within 5 min at an initial concentration of 25 mg L^{-1} to 200 mg L^{-1} while in case of Fe^{2+} linear increase was from 10 mg to 86.7 mg. This indicates a high affinity of the haloarchaeal adsorbent for Fe^{2+} and Mn^{2+}, and extensive interaction of the metal ions with the haloarchaeal adsorbent, similar to that reported with dry biomass of eukaryotic *A. niger* and *S. cerevisiae* for biosorption of chromium by Goyal *et al.* (2003). The decline in Fe^{2+}/ Mn^{2+} removal efficiency in adsorption system having 20 % salinity can be explained as an effect of multiple factors, singly or cumulatively. i) Due to electrostatic interaction, wherein metal ions and haloarchaeal adsorbent present in aqueous adsorption assay systems get surrounded by an electrical double layer and thus their interaction with one another is influenced by concentration of background electrolyte as is evident in our observation of decrease in adsorption with increase in ionic strength. ii) Due to complexation of metal ions with chloride ions of the electrolyte (NaCl). iii) Enhancement of stability of S-layers of haloarchaeon by NaCl (Donmez and Aksu, 2002; Li and Xu, 2008).

The adsorption of Fe^{2+} ions as well as Mn^{2+} ions is seen to be increased by an increase in the biomass concentration, which can be attributed to an increase in the active metal binding sites on adsorbent.

The adsorption isotherms reveal the specific relationship between the concentration of the adsorbate and its degree of accumulation onto the biomass surface at a constant initial metal ion concentration and a constant temperature of 30 ºC. The Q_{max} of *Haloferax* sp. GUSF-1 is nearly double to that reported for Fe^{2+}ion adsorption by the cyanobacteria *Synechocystis* sp. E35 of domain eubacteria (Sevgi *et al.*, 2009). The adsorption is also several measures stable

as the bonding energy value is half to that seen for *Synechocystis* sp. E35. Further, the smaller b values obtained imply strong binding of Fe^{2+} ions to the adsorbent. We attribute the values of Q_{max} obtained to the involvement of S-layers which also true for Mn^{2+} binding. The equilibrium data fitted well with Langmuir and Fruendlich indicating near equal determination coefficient R^2 for homogeneous as well as heterogeneous adsorption of Fe^{2+}. The equilibrium data fitted slightly well with Langmuir isotherm model then Fruendlich isotherm for adsorption of Mn^{2+} as seen from determination coefficient R^2 values. In particular, a value of n, when approaching 1 or greater than 1, indicates that the adsorbate was effectively adsorbed under all examined experimental conditions. Hence, the overall adsorption of Fe^{2+} and Mn^{2+} on the adsorbent involves ion exchange, surface complexation and electrostatic attraction**.** Comparisons of the correlation coefficients obtained at various initial concentrations of Fe^{2+} and Mn^{2+} for the pseudo- first order kinetic model with that obtained for pseudo-second order kinetic model showed that the average correlation coefficient R^2 values of pseudo-second order kinetic model were higher than that of pseudo-first order kinetic model. This indicates that the kinetics of Fe^{2+} and Mn^{2+} adsorption by haloarchaeon adsorbent is better described by pseudo-second order kinetic model. Interestingly, it was observed that with an increase in the initial respective metal ion concentration, qe increased and k_2 decreased linearly.

The ability of regenerated adsorbent of *Haloferax* sp. GUSF-1 to adsorb fresh Fe^{2+} and Mn^{2+} to the same degree, even after three adsorption-desorption cycles, makes the process costs effective, ensures metal recovery and reuse of the adsorbent.

Surface depression in SEM micrographs of adsorbent are attributed to the S-layers of the adsorbent glisten on loading of Fe^{2+}/ Mn^{2+} metal. Further, the FTIR analysis confirmed

involvement of the functional groups of the surface glucans and the amino acids of S-layers in the adsorption.

CONCLUSIONS

1) From the present research study, we have screened 21 haloarchaeal isolates that were moderately to highly tolerant/ resistant to moderate and high concentrations of Fe^{2+} and Mn^{2+}, respectively.

2) Two highly resistant haloarchaeon *Natrialba* sp. GUFF129 and *Haloferax* sp. GUSF-1 were selected for interaction studies with metal ions from which it was concluded that the haloarchaea inhabiting the estuarine econiches of Goa, India which receive a continuous flux of Fe/Mn resist/ tolerate these two metal ions by alteration of their cell surface properties viz. alteration in shape and size, increase in cell adherence, changes in cell membrane characteristics exhibited by alteration in pigment profile, lipids and whole cell proteins with induction and over expression of some proteins. Thus, making the two haloarchaea potential biological indicators of Fe and Mn pollution in saline waters.

3) Uptake studies revealed the involvement of membrane transporters of intact live haloarchaeal cell of *Haloferax* sp. GUSF-1 in uptake of Fe^{2+} and Mn^{2+}.

4) Design and development of haloarchaeal adsorbent that can efficiently adsorb Fe^{2+} and Mn^{2+}, from saline system where other eubacteria and eukaryotes fail ; thus, the use of haloarchaeon *Haloferax* sp. GUSF-1 in bioremediation of highly saline waste waters.

5) Haloarchaeon *Haloferax* sp. GUSF-1 has a potential to be exploited for the production of nano sized particles of maghemite and rhodochrosite, respectively, which are of nano biotechnological significance.

SUMMARY

Haloarchaeal cultures previously isolated from saltpans of Goa, India were studied for their interaction with metals Fe^{2+} and Mn^{2+} ions. In all 21 cultures were screened for their metal tolerance ability in nutrient rich medium (NTYE) and mineral salts medium (NGSM). All the cultures were resistant to 3 mM of Fe^{2+} and 20 mM of Mn^{2+} ions in NTYE medium while in NGSM medium all were resistant to resistant to 2 mM of Fe^{2+} ions and 20 mM of Mn^{2+} ions, respectively. Cultures GUSF-1 and GUFF 129 were resistant to 3.5 mM and 3 mM of Fe^{2+} ions in NTYE and NGSM medium respectively, and resistant to 20mM and 50 mM of Mn^{2+} ions in NTYE and NGSM medium respectively. Cultures GUSF-1 and GUFF 129 due to their high tolerance to both the metal ions were characterized as *Haloferax* sp. and *Natrialba* sp. respectively, by biochemical tests and 16S rRNA gene sequence analysis of GUSF-1 revealed 96 % similarity with *Haloferax* sp. and was used in the study of interaction.

The growth profile of the two cultures in metal containing medium was influenced by salinity, incubation temperature and pH of the growth medium. The cells of *Haloferax* sp. GUSF-1 accumulated 34.6 mg $L^{-1}$of Fe^{2+} and 30 mg $L^{-1}$of Fe^{3+} while *Natrialba* sp. GUFF129 accumulated 31.7 mg $L^{-1}$of Fe^{2+} and 28.3 mg $L^{-1}$of Fe^{3+}during growth in 55 mg L^{-1} of Fe^{2+} ($FeSO_4.7H_2O$). The acetone extracts of *Haloferax* sp. GUSF-1 showed abolishment of phytofluene component while appearance of unknown components at 353nm and 307nm in case of acetone extracts of *Natrialba* sp. GUFF129 grown in Fe^{2+}. The cup shaped morphology of *Haloferax* sp. GUSF-1cells changed to elongated form with visible aggregation, while *Natrialba* sp. GUFF129 exhibited dividing cells evident in SEM profiles. Induction of protein bands at 20kDa corresponding to molecular weight of Dps protein was demonstrated in whole cell protein profiles. Interestingly, the cells increased in their

hydrophobicity and were resistant to lysis at decreased salinities of 12%. Thin layer chromatograms revealed the role of glycolipids and phospholipids in metal interaction.

Study pertaining to growth and accumulation of Mn^{2+} by the cells of *Haloferax* sp. GUSF-1showed accumulation of 48.93 mg L^{-1} while *Natrialba* sp. GUFF129 displayed accumulation 45 mg $L^{-1}$of Mn^{2+} during growth in 54.93 mg L^{-1} of Mn^{2+}. The acetone extracts of *Haloferax* sp. GUSF-1showed abolishment of halorhodopsin component while appearance of phytofluene components at 344 nm while induction of phytofluene, retinal and lycopene in case of acetone extracts of *Natrialba* sp. GUFF129 grown in Mn^{2+}. The cup shaped morphology of *Haloferax* sp. GUSF-1 and *Natrialba* sp. GUFF129 cells changed to elongated form with visible aggregation evident in SEM profiles. The response to manganese was further exhibited by induction of protein bands at 46 kDa, 29 kDa and 25 kDa by GUFF129 and at 48 kDa, 38 kDa, 30.5 kDa, 18 kDa by *Haloferax* sp. GUSF-1, increased hydrophobicity and resistance to lysis at decreased salinities of 12%. Thin layer chromatograms revealed the effect of glycolipids and phospholipids on metal interaction.

The resting cells of *Haloferax* sp. GUSF-1exhibited uptake of 67.11 mg Fe^{2+} g^{-1} as demonstrated by Langmuir model and having bonding energy of 0.069 L mg^{-1}while showed a better fit with Freundlich model with K_F of 1.17mg $g^{-1}$and uptake intensity n of 1, respectively. The optimum uptake was observed at pH of 6.0 at 30ºC with biomass of 1g at metal concentration of 100mg L^{-1} in 2h.The uptake was reduced to 38.8 % in heat killed cells and was demonstrated to be a energy dependant process as demonstrated by reduction of uptake by metabolic inhibitors sodium azide, DCCD and 2,4 DNP. This was also proved by 80 % uptake by cell envelope and 20 % in cell cytoplasm evident from SEM-EDX analysis showing crystalline surface with Fe peaks.

The optimum uptake of 45.5 mg of Mn^{2+} g^{-1} was observed at pH of 6.0 at 30ºC per g of biomass at metal concentration of 100mg L^{-1} in 45 min. The resting cells of *Haloferax* sp. GUSF-1 exhibited a Qmax of 88.5 mg Mn^{2+} g^{-1} as demonstrated by Langmuir model and having bonding energy of 0.013 L mg^{-1} while showed a better heterogenous uptake with Freundlich model exhibiting a K_F of 1.35 mg $g^{-1}$and uptake intensity n of 0.97, respectively. The uptake of Mn^{2+} was revealed to be an energy dependant process proved by reduction of uptake by metabolic inhibitors sodium azide, DCCD and 2, 4 DNP. This was also established by 65 % uptake by cell envelope and 35 % in cell cytoplasm evident from SEM-EDX analysis showing crystalline surface with Mn peaks.

Dried cells of *Haloferax* sp. GUSF-1adsorbed 99.5 % Fe^{2+} at pH 6.0, 30 ºC in 3 h at an efficiency of 81.8 %, upto four adsorption-desorption cycles. Adsorption involved the carboxyl, amino, hydroxyl and phosphate groups of S-layers, showed saturation, followed a pseudo-second order kinetics, corroborated with homogeneity of Langmuir and fitted well with heterogeneity of Fruendlich models with R^2 of 0.97, Q_{max} of 74.07 mg g^{-1} and binding energy of 0.017 L mg^{-1}; K_F of 1.38 mg g^{-1} with the n value of 0.96, respectively. Adsorption of Fe^{2+} ions was also evident from SEM-EDX analysis displaying a shiny surface with prominent metal peaks.

Dried cells of *Haloferax* sp. GUSF-1 adsorbed 99 % Mn^{2+} in 60 min at pH 6.8 and 30 ºC on contact with 109.54 mg Mn^{2+} per liter in saline solution. Adsorbed Mn^{2+} was demonstrated on the cell surface by SEM-EDX analysis. Mn^{2+} adsorbed to functional groups of the adsorbent revealed the role of carboxyl, amino, hydroxyl and phosphate groups, respectively. The adsorption process of Mn^{2+} showed saturation and followed pseudo second order kinetics and was consistent with the homogeneity of the Langmuir model (R^2 of 0.99),

exhibited a Q_{max} of 62.5 mg g^{-1} and a binding energy of 0.018 L mg^{-1}. The Mn^{2+}adsorption was also consistent with the heterogeneity of the Freundlich model by exhibiting a K_f of 1.0 mg g^{-1} with an n value of 1.1. Adsorption efficiency of 99 % was retained even after a third adsorption-desorption cycle.

Alternatively, *Haloferax* sp. GUSF-1 when growing with Fe^{3+} in mineral salts medium with acetate as sole source of carbon showed interesting results. The culture grew in NASM with a growth rate of 9.7 x 10^3 gen h^{-1} than when the culture grew without $Fe^{3+}$with a growth rate of 1.3 x 10^2 gen h^{-1}. The growth was accompanied by a concomitant increase in $Fe^{2+}$and Fe^{3+} inside the cells, exhibiting a accumulation of 50 mg L^{-1} of Fe^{2+} and 30.6 mg L^{-1} of Fe^{3+} inside the growing cells. Interestingly, accumulation of a brown colored mineral was observed in the culture broth with ferric reductase having a role in the formation of same detected by a maximum absorption peak at 560 nm. The mineral formed in its XRD, SEM-EDX and TEM exhibited *d* values of 2.96, 2.514, 2.086, 1.6 and 1.45, displayed cubic and irregularly shaped minute particles with peaks for Fe at 0.6 keV, 6.4 keV, and 6.6 keV also evident in FTIR and revealing a particle size of 12-23 nm. Furthermore, the SAED analysis showed a concentric pattern of light scattering with well defined diffraction spots consistent with maghemite (γFe_2O_3) crystal structure.

Interaction of culture *Haloferax* sp. GUSF-1 with Mn^{2+} in mineral salts medium having sodium acetate as a sole source of carbon exhibited a cell density of 72 % more than when the culture grew without manganese by 6^{th} d. Growth was observed to be accompanied with initial oxidation of Mn^{2+} with the deposition of 485.5 µM MnO_2 equivalents extracellularly and accumulation of 495.8 µM mL^{-1} Mn^{2+}inside the cells. In the late stationary phase of growth, MnO_2 was reduced to and resulted in the accumulation of an extracellular pale /

pinkish brown colored, amorphous material which in its XRD, TEM and SEM-EDX exhibited *d* values of 3.66, 2.84, 1.770, 1.763, electron dense regions with crystalline cubic shape corresponding to features for mineral rhodochrosite ($MnCO_3$) with carbonyl group stretching and bending vibrations seen in FTIR.

Outcome of research

- **Research findings**

1. First record of design and development of haloarchaeal adsorption assay that could sorb Fe^{2+} in 3 h and Mn^{2+} in 60 min.
2. Elucidation of the Fe^{2+} and Mn^{2+} uptake systems in Haloarchaea
3. First record of use of *Haloferax* sp.GUSF-1 as a source for the formation of nano sized particles of

   a) γFe_2O_3 (maghemite)

   b) $MnCO_3$ (rhodochrosite)
4. Deposition of 16S rDNA sequence in GenBank
5. Research papers

BIBLIOGRAPHY

Abdel-Aty, A.M., Anmar, N.S., Ghafar, A., Ali, R.K. 2013. Biosorption of cadmium and lead from aqueous solutionby fresh water alga *Anabaena sphaerica* biomass. J Adv Res 4(4):367-374.

Abdul-Tehrani, H., Hudson, A.J., Chang, Y.S., Timms, A.R., Hawkins, C., Williams, J.M., Harrison, P.M., Guest, J.R., Andrews, S.C. 1999. Ferritin mutants of Escherichia coli are iron deficient and growth impaired, and fur mutants are iron deficient. J Bacteriol 181: 1415-1428.

Agarwal., S. G., Bhuptawat., K., H., Chaudhar., S. 2006. Biosorption of aqueous chromium (VI) by *Tamarindus indica* seeds. Bioresour Technol 97:949–956.

Aharon, O**.** 2008**.** Microbial life at high salt concentrations: phylogenetic and metabolic diversity**.** Saline Systems 4: 2**.**

Ahluwalia, S.S., Goyal, D. 2007. Microbial and plant derived biomass for removal of heavy metals from wastewater. Bioresour Technol. 98:2243–57.

Aisen, P., Enns, C., Wessling-Resnick, M. 2001. Chemistry and biology of eukaryotic iron metabolism. Int J Biochem Cell Biol 33:940-959.

Aksu, Z., Kutsal, T. 2011. A comparative study for biosorption characteristics of heavy metals ions with *C. vulgaris*. Environ. Technol 11: 979-987.

Alagarsamy, R. 2006. Distribution and seasonal variation of trace metals in surface sediments of the Mandovi estuary, west coast of India. Estuar Coast Shelf S 67:333–339.

Albers, S.V., Szabó, Z., Driessen,A. J. M. 2006. Protein secretion in the Archaea: multiple paths towards a unique cell surface. Nat Rev Microbiol 4:537-547.

Al-Gheethi, A.A.S, Norli, I., Lalung, J., Azlan, A.M., Nur F., Z., A., Kadir, M.O.A. 2014. Biosorption of heavy metals and cephalexin from secondary effluents by tolerant bacteria. Clean Technologies and Environmental Policy 16(1): 137-148.

Aller, R.C. 1994. The sedimentary Mn cycle in long island sound: its role as intermediate oxidant and the influence of bioturbation, O2, and C org flux on diagenetic reaction balances. J Mar Res 52(2): 259–295.

Al-Saraj, M., Abdel-Latif, M.S., El-Nahal, I., Baraka, R. 1999. Bioaccumulation of some hazardous metals by sol–gel entrapped microorganisms. J Non-Cryst Solids. 248:137–40.

Ananyev, G.M., Zaltsman, L., Vasko, C. and Dismukes, G.C. 2001. The inorganic biochemistry of photosynthetic oxygen evolution/water oxidation. Biochim Biophys Acta 1503: 52-68.

Andrews SC, Robinson AK, Rodriguez-Quinones F. 2003. Bacterial iron homeostasis. FEMS Microbiol Rev 27:215–237.

Anton, A., Große, C., Reißmann, J., Pribyl, T., Nies, D. H. 1999. CzcD is a heavy metal ion transporter involved in regulation of heavy metal resistance in Ralstonia sp. strain CH34. J Bacteriol 181(22) 6876–6881.

Aschner, M., Erikson, K.M., Dorman, D.C. 2005. Manganese dosimetry: species differences and implications for neurotoxicity. Crit Rev Toxicol 35 : 1-32.

Aschner, M., Guilarte, T.R., Schneider, J.S., Zheng, W. 2007. Manganese: recent advances in understanding its transport and neurotoxicity. Toxicol Appl Pharmacol 221 : 131-47.

Asker, D., Awad, T., Ohta, Y. 2002. Lipids of *Haloferax alexandrinus* strain TM(T): an extremely halophilic canthaxanthin-producing archaeon. J Biosci Bioeng 93(1):37-43.

ASTDR. 2000. Toxicological profile for manganese. Atlanta Georgia: US Department of Health and Human Services, agency for toxic substances and disease registry: 1-466.

Avila, D.S., Puntel, R.L., Aschner M. 2013. Manganese in Health and Disease. Metal ions in Life Sciences. In: Interrelations between Essential Metal Ions and Human Diseases. Sigel, A., Sigel, H., Sigel, R.K.O. (Eds.) 13 Springer Netherlands.

Babich, H. Stotzky, G. 1980. Environmental factors that influence the toxicity of heavy metal and gaseous pollutants to microorganisms. Crit Rev Microbiol 8: 99–145.

Baden, S.P., Ericksson, S.P. 2006. Role, routes and effect of manganese in crustaceans. Oceanography and Marine Biology: An Annual Review 44:61-83.

Bag, H., Turker, A.R., Lale, M. 1999. Determination of trace metals in geological samples by atomic absorption spectrophotometry after preconcentration by Aspergillus niger immobilized on sepiolite. Anal Sci 15:1251–1256.

Bagy, M.M., el- Sharouny, H.M., el-Shanawany, A.A. 1991. Effect of pH and organic matter on the toxicity of heavy metals to growth of some fungi. Folia Microbiol (Praha) 36(4): 367-74.

Bahafid, W., Joutey, N.T., Hanane, S., Mohamed, I., Ghachtouli, El. N. 2013. Chromium adsorption by three yeast strains isolated from sediments in Morocco. 30(5) 422-429.

Baker, A.R., Croot, P.L.2010. Atmospheric and marine controls on aerosol iron solubility in seawater. Mar Chem 120: 4–13.

Baliga, N. S., Bonneau, R., Facciotti, M. T. *et al.* 2004. Genome sequence of *Haloarcula marismortui*: a halophilic archaeon from the dead sea. Gen Res 14(11): 2221– 2234.

Balska, A.K., Lipiak, M. 2013. Critical Role of a ferritin-like protein in the control of *Listeria monocytogenes* cell envelope structure and stability under β-lactam pressure. PlosOne doi: 10.1371/journal.pone.0077808.

Banfield, J.F., Zhang, H. 2001. Nanoparticles in the environment. Rev Mineral Geochem 44: 1-58.

Bang, S.W., Clark, D.S., Keasling, J.D. 2000. Engineering hydrogen sulfide production and cadmium removal by expression of the thiosulfate reductase gene (phsABC) from *Salmonella enterica* Serovar Typhimurium in *Escherichia coli*. Appl Environ Microbiol 66(9): 3939–3944.

Barceloux D.G. 1999. Manganese. J Toxicol Clin Toxicol. 37 : 293-307.

Barkay, T., Miller, S.M., Summer, A.O. 2003. Bacterial mercury resistance from atoms to ecosystems. FEMS Microbiol Rev 27: 355-384.

Bäuerlein, E. 2003. Biomineralization of unicellular organisms: An unusual membrane biochemistry for the production of inorganic nano- and microstructures. Angew Chem Int 42: 614-641.

Baumgartnera, J., Morin, G., Menguy, N., Gonzalez, T.P., Widdrat, M., Cosmidis, J., Faivre, D. 2013. Magnetotactic bacteria form magnetite from a phosphate-rich ferric hydroxide via nanometric ferric (oxyhydr)oxide intermediates. doi/10.1073/pnas.1307119110.

Bazylinski ,D.A., Frankel, R.B. 2003. Biologically controlled mineralization in prokaryotes. Rev Mineral Geochem 54:217-247.

Bazylinski, D. A. 1996. Controlled biomineralization of magnetic minerals by *Magnetotactic* bacteria. Chemical Geology 132: 191–198.

Bazylinski, D. A., Frankel, R. B. 2003. Biologically controlled mineralization in prokaryotes. In Dove, P. M., De Yoreo, J. J., and Weiner, S. (eds.), Rosso, J. J. (series ed.), Biomineralization. Reviews in Mineralogy and Geochemistry. Washington DC, USA: Mineralogical Society of America and Geochemical Society 54, pp. 217–247.

Bazylinski, D.A., Frankel, R.B. 2000. Biologically controlled mineralization of magnetic iron minerals by magnetotactic bacteria. In ed. Lovley, D.R., Environmental Microbe-Mineral Interactions. Washington DC: ASM Press, pp. 109-144.

Bazylinski, D.A., Frankel, R.B. 2004. Magnetosome formation in prokaryotes. Nat ReV Microbiol 2:217–230.

Bazylinski, D.A., Schubbe, S. 2007. Controlled biomineralization by and applications of magnetotactic bacteria. Adv Appl Microbiol 62: 21–62.

Beal, E.J., House, C.H., Orphan, V.J. 2009. Manganese- and iron dependent marine methane oxidation. Science 325: 184–187.

Beard, B.L., Johnson, C.M. 2004. Fe isotope variations in the modern and ancient earth and other planetary bodies. Rev Mineral Geochem 55: 319-357.

Becker, M., Asch, F. 2005. Iron toxicity in rice- condition and management concepts. Journal of Plant Nutrition and Soil Science 168: 558-573.

Beech, I. B., Cheung, C. W. S. 1995. Interactions of exopolymers produced by sulphate-reducing bacteria with metal ions. Int Biodeterior Biodegrad 35: 59-72.

Bennett, W., Teasdale, P. R., Welsh, D. T., Panther, J., Stewart, R. R., Price, H. L. & Jolley, D. F. 2012. Inorganic arsenic and iron(II) distributions in sediment porewaters investigated by a combined DGT - colourimetric DET technique. Environmental Chemistry, 9 (1):31-40.

Bentley, R.,Thomas, G.C. 2002. Microbial methylation of metalloids: arsenic, antimony, and bismuth. Microbiol Mol Biol 66(2): 250–271.

Berelson W, McManus J, Coale K, Johnson K, Burdige D, Kilgore T, Colodner D, Chavez F, Kudela R, Boucher J. 2003**.** A time series of benthic flux measurements from Monterey Bay, CA. Cont Shelf Res; 23:457–481.

Bereswill, S., Greiner, S., VanVliet A. H. M. 2000. Regulation of ferritin-mediated cytoplasmic iron storage by the ferric uptake regulator homolog (Fur) of *Helicobacter pylori*. Journal of Bacteriology 182(21): 5948–5953.

Bever, L.E., Theil, E.C. 2011. Maxi- and Mini-Ferritins: minerals and protein nanocages. Prog Mol Subcell Biol 52: 29–47.

Beveridge, T. J. 1986. The immobilisation of soluble metals by bacterial walls. Biotechnol Bioeng Symp 16:127-139.

Beveridge, T.J., Forsberg, C.W., Doyle, R.J. 1990. Major sites of metal binding in *Bacillus licheniformis* walls. Bacteriol 150(3):1438-1448.

Beveridge, T.J., Murray, R.G.E. 1980. Sites of metal deposition in the cell wall of *Bacillus subtilis*. Journal of Bacteriology 141: 876-887.

Bharde, A. A., Paraikh, R. Y., Baidakova, M., Jouen, S., Hannoyer, B., Enoki, T., Prasad, B. L. V., Shouche, Y. S., Ogale, S., Sastry, M. 2008. Bacteria-mediated precursor-dependent biosynthesis of superparamagnetic iron oxide and iron sulfide nanoparticles. Langmuir 24:5787–5794.

Bharde, A., Rautaray, D., Bansal, V., Ahmad, A., Sarkar, I., Yusuf, S., M., Sanyal, M., Sastry, M. 2006. Extracellular biosynthesis of magnetite using fungi. Small 2(1): 135-141.

Bharde, A., Wani, A., Shouche, Y., Joy, P.A., Prasad, B.L.V., Sastry, M. 2005. Bacterial aerobic synthesis of nanocrystalline magnetite. J Am Chem Soc 127:9326-9327.

Bhaskar, P.V. and Bhosle, N.B. 2006. Bacterial extracellular polymeric substances (EPS) a carrier of heavy metals in the marine food-chain. Environment International. 32: 192-198.

Bini, E. 2010. Archaeal transformation of metals in the environment. FEMS Microbiol Ecol. 73(1) 1–16.

Birnboim, H.C., Doly, J. 1979. A rapid alkaline extraction procedure for screening recombinant plasmid DNA. Nucleic Acids Res. 7: 1513-1523.

Blindauer, C.A., Harrison, M.D., Robinson, A.K., Parkinson, J.A., Bowness, P.W., Sadler, P.J.,Robinson, N.J. 2002. Multiple bacteria encode metallothioneins and SmtA- like fingers. Mol Microbiol 45: 1421-1432.

Bolhuis, H., Palm, P., Wende, A.*et al.* 2006. The genome of the square archaeon *Haloquadratum walsbyi*: life at the limits of water activity. BMC Genomics 7: 169.

Bonatti, E., Nayudu, Y.R. 1965. The origin of manganese nodules on the ocean floor. Am J Sci, 263, 17-39. ISSN 1945-452X.

Braganca, J. 2003. Uptake of arsenic and cadmium by halophilic archaeabacteria. Ph.D Thesis, Goa University, Goa. India.

Braganca, J. Furtado, I. 2001. Removal of cadmium from saline water using haloarchaeal cell bioprocess. Proceedings of 1st European Bioremediation Conference, Greece.

Braganca, J.M., Furtado, I. 2009 Isolation and characterization of Haloarchaea from low salinity coastal sediments and waters of Goa – India. Curr Sci 96(9): 1182 – 1184.

Braissant, 0., Decho, A.W., Dupraz, C., Glunk, C., Przekop, K.M. and Visscher, P.T. 2007. Exopolymeric substances of sulfate-reducing bacteria: Interactions with calcium at alkaline pH and implication for formation of carbonate minerals. Geobiology.5: 401-411.

Bramhachari, P.V., Kavi Kishor, P.B., Ramadevi, R., Kumar, R., Rao, B.R., Dubey, S.K. 2007. Isolation and characterization of mucous exopolysaccharide produced by *Vibrio furnissii* VB0S3. J. Microbiol. Biotechnol. 17: 44-51.

Braun, V., Hantke, K. and Ko« ster, W. 1998. Bacterial iron transport, mechanisms, genetics, and regulation. In: Metal Ions in Biological Systems (Sigel, A. and Sigel, H., Eds.), 35:pp. 67-145.Marcel Dekker, New York.

Braun, V.1998. Regulation of iron uptake minimizes iron mediated oxidative stress. J Bioscience. 23(4): 483-489.

Brewer, G. 2009. Risks of copper and iron toxicity during aging in humans. Chemical Research in Toxicology 2: 319–326.

Brouwers, G. J., de Vrind, J. P. M., Corstjens, P. L., Cornelis, P., Baysse, C. de Vrind-de Jong, E. W. 1999. cumA, a gene encoding a multicopper oxidase, is involved in Mn(II) oxidation in *Pseudomonas putida* GB-1. Appl Environ Microbiol 65: 1762–1768.

Brouwers, G. J., Vijgenboom, E., Corstjens, P. L. A. M., De Vrind, J. P. M., De Vrind-De Jong, E. W. 2000. Bacterial Mn^{2+} oxidizing systems and multicopper oxidases: an overview of mechanisms and functions. Geomicrobiol J 17: 1–24.

Bruland, K.W., Rue, E.L. In: Turner, D.R, Hunter, K.A, Eds. The Biogeochemistry of iron in seawater. Chichester, West Sussex: John Wiley & Sons, 2001:255–289.

Bustard, M., McHale, A.P. 1998. Biosorption of heavy metals by distillery-derived biomass. Bioprocess Engineering.19:351–3.

Byrne, R.H. 2002. Inorganic speciation of dissolved elements in seawater: the influence of pH on concentration ratios. Geochemical Transactions 3: 11–16.

Cervantes, C. J., Campos-Garcia, S., Devars, F., Gutierrez-Corona, H., Loza-Tavera, Torres-Guzman, J. C., Moreno-Sanchez, R. 2001. Interactions of chromium with microorganisms and plants. FEMS Microbiol Rev. 25**:**335-347.

Chakravarty, R., Banerjee, P.C. 2008. Morphological changes in an acidophilic bacterium induced by heavy metals. Extremophiles 12 (2):279-84.

Chan, C.S., Fakra, S.C., Emerson, D., Fleming, E.J., Edwards, K.J. 2011. Lithotrophic iron-oxidizing bacteria produce organic stalks to control mineral growth: implications for biosignature formation. The ISME Journal 1–11.

Chang, J.S., Law, R., Chang, C.C. 1997. Biosorption of lead, copper and cadmium by biomass of *Pseudomonas aeruginosa* PU21. Water Research.31:1651–8.

Chapman, P. M., Wang, F. 2001. Assessing sediment contamination in estuaries. Environ Toxicol Chem 20(1): 3–22.

Châtellier, X., Fortin, D., West, M. M., Leppard, G. G., Ferris, F. G. 2001. Effect of the presence of bacterial surfaces during the synthesis of Fe oxides by oxidation of ferrous ions. Euro J Mineral 13(4):705–714.

Chavadar, M. S., Bajekal, S. S. 2008. South seeking magnetic bacteria from Lonar Lake. In Taal 2007: The 12th World Lake Conference. M. Sengupta and R. Dalwani (Eds.). pp. 444–447.

Chen, X.C., Wang, Y.P., Lin, Q., Shi, J.Y., Wu, W.X., Chen, Y.X. 2005. Biosorption of copper (II) and zinc (II) from aqueous solution by Pseudomonas putida CZ1. Colloids and Surfaces B: Biointerface 46: 101–107.

Chime, T.O. 2013. Optimization of process variables for the biodephosphorization of iron ore using *Leptospirillum Ferrooxidans*. International Journal of Multidisciplinary Sciences and Engineering (4)2:57-64.

CICAD (2004) Manganese and its compounds: environmental aspects. Concise international chemical assessment document 63. WHO, Geneva, Switzerland, Available from http://www.who.int/ipcs/publications/cicad/cicad63_rev_1.pdf.

Claus, H., Akca, E., Debaerdemaeker, T., Evrard, C., Declercq, J.P., Konig, H. 2002. Primary structure of selected archaeal mesophilic and extremely thermophilic outer surface layer proteins. Systematic and Applied Microbiology 25: 3-12.

Colomina, M.T., Domingo, J.L., Llobet, J.M., Corbella, J. 1996. Effect of day of exposure on the developmental toxicity of manganese in mice. Veter Hum Toxicol 38(1): 7–9.

Conklin, D.S, McMaster, J.A., Culbertson, M.R., Kung, C. 1992. COT1, a gene involved in cobalt accumulation in *Saccharomyces cerevisiae.* Mol Cell Biol 12(9):3678-88.

Coombs, J.M. and Barkay, T. 2005. New findings on evolution of metal homeostasis genes: Evidence from comparative genome analysis of bacteria and archaea. Appl. Environ. Microbiol. 71: 7083-7091.

Crichton R.2009. Iron metabolism, from molecular mechanisms to clinical consequences, 3rd edn. Wiley Interscience, Chichester, West Sussex.

Crow, A., Lawson, T.L., Lewin, A., Moore, G.R., Le Brun, N.E. 2009. Structural basis for iron mineralization by bacterioferritin. J Am Chem Soc 131: 6808-6813.

Crowley, J.A., Traynor, D.A., Weatherburn, D.C. 2000. Enzymes and proteins containing manganese: an overview. Metal ions in biological systems 37: 209-278.

Cullen, W. R., Bentley, R. 2005.The toxicity of trimethylarsine: an urban myth. J Environ Monitor 7 (1): 11–15.

Culotta, V.C., Yang M., Hall, M.D. 2005. Manganese transport and trafficking: lessons learned from S. cerevisiae. Euk Cell 4(7)1159.

Daoud, J., Karamanev, D. 2006. Formation of jarosite during Fe^{2+} oxidation by *Acidithiobacillus ferrooxidans*. Minerals Engineering, 19(9): 960–967.

DasSarma, S., Berquist, B.R., Coker, J.A., DasSarma, P., Muller, J.A. 2006. Post-genomics of the model haloarchaeon *Halobacterium* sp. NRC-1. Aquatic Biosystems 2:3.

DasSarma, S., Capes, M., DasSarma, P. 2009. Haloarchaeal megaplasmids. In: Microbial Megaplasmids, E. Schwartz, Ed., pp. 3–30, Springer-Verlag, Berlin, Germany.

Das, S.K., Guha, A.K. 2009. Biosorption of hexavalent chromium by *Termitomyces clypeatus* biomass: Kinetics and transmission electron microscopic study. J Hazard Mater doi:10.1016/j.jhazmat.2009.01.037.

Daughney, C. D., Châtellier, X., Chan, A., Kenward, P., Fortin, D., Suttle, C. A., Fowl, D. 2004. Adsorption and precipitation of iron from seawater by a marine bacteriophage (PWH3a-P1). Mar Chem 91: 101–115.

Dave, B.P., Anshuman, K., Hajela, P. 2006. Siderophores of halophilic archaea and their chemical characterization. Indian J Exp Biol 44(4): 340–344.

Davis, T.A., Volesky, B.,Mucci, A.2003. A review of the biochemistry of heavy metal biosorption by brown algae. Water Res 37:4311-4330.

Davison, W., DeVitre, R. 1992. Iron particles in freshwater. In: Buffle, J and Leeuwen van, H.P. (eds.) Environmental particles Vol.1, Environmental analytical and physical chemistry series, I ed:315-355.

de Baar HJW, de Jong JTM. 2001. In: Turner DR, Hunter KA, eds. The Biogeochemistry of Iron in Seawater. Chichester, West Sussex: John Wiley & Sons: 123–253.

de la Torre, M.A., Gomez, A.G. 1994. Manganese and iron oxidation by fungi isolated from building stone. Microb Ecol. 27(2):177-88.

De Schamphelaire, L., Rabaey, K., Boon, N., Verstraete, W., Boeckx, P. 2007. Minireview: The potential of enhanced manganese redox cycling for sediment oxidation. Geomicrobiol J, 24, (7-8): 547–558.

De, J., Ramaiah, N., Vardanyan, L. 2008. Detoxification of toxic heavy metals by marine bacteria highly resistant to mercury. Mar Biotechnol 10:471-477.

Decho, A.W. 1990. Microbial exopolymer secretion in ocean environment, their roles in food webs and marine processes. In: Barnes, M (ed). Ocean Mar Biol Annu Rev 28: 73-153.

Deng, S.B., Ting, Y.P. 2005. Characterization of PEI-modified biomass and biosorption of Cu(II), Pb (II) and Ni,(II). Water Res. 39:2167–77.

Desai, C., Jain, K.,Madamwar, D. 2008. Hexavalent chromate reductase activity in cytosolic fractions of *Pseudomonas* sp. G1DM21 isolated from Cr (VI) contaminated industrial landfill. Process Biochem. 4:713-721.

Dessai, D.V.G., Nayak, G.N. Distribution and speciation of selected metals in surface sediments, from the tropical Zuari estuary, central west coast of India. Environ Monit Assess 158:117–137.

Dias, M.A., Lacerda, I.C.A., Pimentel, P.F., de Castro, H.F., Rosa, C.A. 2002. Removal of heavy metals by an *Aspergillus terreus* strain immobilized in a polyurethane matrix. Lett Appl Microbiol. 34:46–50.

Dick, G.J., Anantharaman, K., Sheik, C.S. 2013. The microbiology of deep-sea hydrothermal vent plumes: ecological and biogeographic linkages to seafloor and water column habitats. Fronteirs in Microbiology 4:124

Dick, G.J., Clement, B.G., Webb, S.M., Fodrie, J.F., Bargar, R.J., Tebo, B.M. 2009. Enzymatic microbial Mn(II) oxidation and Mn biooxide production in the Guaymas Basin deep-sea hydrothermal plume . Geochim Cosmochim Acta 73:6517-6530.

Dieser, M., Greenwood, M., Foreman, C. M. 2010. Carotenoid Pigmentation in Antarctic Heterotrophic Bacteria as a Strategy to withstand Environmental Stresses. Arctic, Antarctic, and Alpine Research 42(4): 396–405.

Ding, J.N., Gao, J., Wu, X., Zhang, C.G., Qiu, G.Z. 2007. Jarosite-type precipitates mediated by YN22, *Sulfobacillus thermosulfidooxidans*, an their influences on strain. Transactions of Nonferrous Metals. Society of China, 17(5): 1038–1044.

Donald, R., Southam, G. 1999. Low temperature anaerobic bacterial diagensis of ferrous monosulfide to pyrite. Geochim Cosmochim Act. 63(13/14): 2019–2023.

Donmez., G., Aksu., Z. 2002. Removal of chromium(VI) from saline wastewaters by *Dunaliella* species. Process Biochem 38:751–762.

Dubinin, A.V., Korsakova, M.N.R. 2011. Geochemistry of rare earth elements in bottom sediments of the Brazil Basin, Atlantic Ocean. Lithology and Mineral Resources 46(1):1-16.

Dupraz, C., Reid, R. P., Braissant, O., Decho, A. W., Norman, R.S., Visscher, P.T. 2009. Processes of carbonate precipitation in modern microbial mats. Earth Sci Rev 96, 141–162.

Dussault, H.P.1995. An improved technique for staining red halophilic bacteria. J Gen Microbiol 70:484-485.

ECDG. 2002. European Commission DG ENV. E3 Project ENV. E.3/ETU/0058. Heavy metals in waste. Final report.

Edris, G., Alhamed, Y., Alzahrani, A. 2014. Biosorption of cadmium and lead from aqueous solutions by *Chlorella vulgaris* biomass: equilibrium and kinetic study. Arabian J Sci Eng 39(1) 87-93.

Egal, M., Casiot, C., Morin, G., Parmentier, M., Bruneel, O., Lebrun, S., Elbaz-Poulichet, F. 2009. Kinetic control on the formation of tooeleite, schwertmannite and jarosite by *Acidithiobacillus ferrooxidans* stains in an As(III)-rich acid mine water. Chemical Geology. 265(3–4): 432–441.

Ehrlich, H.L., Newman, D.K. 2009. Geomicrobiology. 5th edn. Boca Raton, FL: CRC Press/Taylor & Francis.

Eisler, R. 2006.Mercury hazards to living organisms. CRC Press Boca Raton.

El-Morsy, E.M., El-Dein, M.M.N. El-Didamoney, S.M.M. 2013. *Mucor racemosus* as a biosorbent of metal ions from polluted water in Northern Delta of Egypt. Mycosphere. 4(6) 1118-1131.

Elrod, V.A., Berelson,W.M., Coale, K.H., Johnson, K.S. 2004. The flux of iron from continental shelf sediments: A missing source for global budgets. Geophysical Research Letters, 31: L12307.

Emmerich, M., Bhansali A., Behrens, L.T., Schroder, C., Kappler, A. Behrens, S. 2012. Abundance, distribution and activity of Fe(II) oxidizing and Fe(III) reducing microorganisms in hypersaline sediments of Lake Kasin, Southern Russia. Appl Environ Microbiol 78**:**4386-4399.

Emsley, J. 2011. John Emsley Nature's Building Blocks: An A-Z Guide to the Elements, Oxford University Press, 2nd Edition.

Erikson, K.M., Aschner, M. 2003. Manganese neurotoxicity and glutamate-GABA interaction. Neurochem Int 43 : 475-80.

Fagan, M. J., Saier Jr., M. H. 1994. P-type ATPases of eukaryotes and bacteria: sequence analyses and construction of phylogenetic trees. J Mol Evol. 38(1): 57– 99.

Faivre, D., Schüler, D. 2008. Magnetotactic bacteria and magnetosoms. Chem Rev 108:4875–4898.

Falb, M., Pfeiffer, F., Palm P. et al. 2005. Living with two extremes: conclusions from the genome sequence of *Natronomonas pharaonis*. Gen Res 15(10) 1336–1343.

Faraldo-G´omez, J.D., Sansom, M. S. P. 2003. Acquisition of siderophores in gram-negative bacteria. Nat Rev Mol Cell Biolog 4: 105–116.

Farina, M., Esquivel, D.M.S., Lins de Barros, H.G.P. 1990. Magnetic iron-sulphur crystals from magnetotactic microorganism. Nature 343: 256–258.

Feng, X.H., Zhu, M., Ginder-Vogel, M., Ni, C., Parikh, S. J., Sparks, D.L. 2010. Formation of nano-crystalline todorokite from biogenic Mn oxides. Geochim Cosmochim Act 74:3232–3245.

Fenton, H.J.H. 1894. Oxidation of tartaric acid in presence of iron. J Chem Soc Trans 65(65):899-911.

Fernandes, S.O., Krishnan, K.P., Khedekar, V.D., LokaBharathi, P.A. 2005. Manganese oxidation by bacterial isolates from the Indian ridge system. Biometals 18(5):483-92.

Finley, J.W., Penland, J.G., Pettit, R.E., Davis, C.D. 2003. Dietary manganese intake and type of lipid do not affect clinical or neuropsychological measures in healthy young women. J Nutr 133 : 2849-56.

Flora, S.J.S., Mittal, M., Mehta., A. 2008. Heavy metal induced oxidative stress & its possible reversal by chelation therapy. Indian J Med Res. 128 :501-523.

Florence, T.M, Stauber, J.L., Ahsanullah, M. 1994. Toxicity of nickel ores to marine organisms. Sci Total Environ 148: 139-155.

Fortin, D., Beveridge, T.J. 2000. Mechanistic routes to biomineral surface development. In Bäuerlein, E. (ed.), Biomineralization: From Biology to Biotechnology and Medical Application. Weinheim: Wiley-VCH GmbH, pp. 7–24.

Fortin, D., Davis, B., Beveridge, T.J. 1996. Role of *Thiobacillus* and sulfate-reducing bacteria in iron biocycling in oxic and acidic mine tailings. FEMS Microbiol Ecol 21(1) :11–24.

Francis, C.A, Co, E.M., Tebo, B.M. 2001. Enzymatic manganese (II) oxidation by a marine alpha Proteobacterium. Appl Environ Microbiol 67: 4024-4029.

Francis, C.A., Tebo, B.M. 2002. Enzymatic manganese (II) oxidation by metabolically dormant spores of diverse Bacillus species. Appl Environ Microbiol 68:874–880.

Francois, O., Jean, R.D., Frances, W., Daneil, P., Patrick, B. 2011. Metal cation binding by the hyperthermophilic microorganism, archaea Methanocaldococcus jannaschii and its effect on silicification. Palaeontology. 54(5): 953–964.

Freundlich, H. 1906. Adsorption in solutions. Journal of Physical Chemistry 57: 385–470.

Fuller, S.J., McMillan, D.G., Renz, M.B., Schmidt, M., Burke, I.T., Stewart, D.I. 2014. Extracellular electron transport-mediated Fe(III) reduction by a community of alkaliphilic bacteria that use flavins as electron shuttles. Appl Environ Microbiol 80(1):128-37.

Furness, R.W., Rainbow, P.S. 1990. Heavy metals in the marine environment. CRC Press, Boca Raton, FL.

Furtado, I., Naik, S. 2009. Tolerance and sorption of diverse metal ions by haloarchaea. Proceedings of International Symposium on Advanced Inorganic Biological Chemistry (SABIC 2009), Tata Institute of Fundamental Research Centre, Mumbai- India, pp. 113-114.

Gadd, G. 2009. Biosorption: critical review of scientific rationale, environmental importance and significance for pollution treatment J Chem Technol Biotechnol 84: 13–28.

Gadd, G.M, White, C. 1993. Microbial treatment of metal pollution- a working biotechnology.Trends in biotechnology11:353-359.

Gadd, G.M. 1993. Interactions of fungi with toxic metals. Phytol 124: 25–60.

Gadd, G.M. 2010. Metals, minerals and microbes: geomicrobiology and bioremediation. Microbiology 156: 609-643.

Gadd, G.M., Raven, J.A. 2010. Geomicrobiology of eukaryotic microorganisms. Geomicrobiol J 27(6):491-519.

Gadd, G.M., White, C. 1992. Removal of thorium from simulated acid process streams by fungal biomass — potential for thorium desorption and reuse of biomass and desorbent. J Chem Technol Biotechnol. 55:39–44.

Gaikwad, R.W, Gupta, D.V. 2008. Review on removal of heavy metals from acid mine drainage. Applied Ecology and Environmental Research 6(3):81-88.

Garcia, P. L., Amils, R., Anton, J. 1996. Sizing chromosomes and megaplasmids in haloarchaea. Microbiol 142:1423-1428.

Gavrilescu, M. 2004. Removal of heavy metals from the environment by biosorption. Engineering in Life Science 4: 219-232.

Gazem, A.H.M., Nazareth, S. 2012. Isotherm and kinetic models and cell surface analysis for determination of the mechanism of metal sorption by *Aspergillus versicolor*. World J Microbiol Biotechnol 28(7): 2521-30.

Gerber, G.B., L´eonard, A., Hantson, P. 2002. Carcinogenicity, mutagenicity and teratogenicity of manganese compounds. Cr Rev Oncol Hem 42: 25-34.

Ghazvini, P.T.M., Mashkani, S.G. 2009. Effect of salinity on vanadate biosorption by Halomonas sp. GT-83: Preliminary investigation on biosorption by micro-PIXE technique. Bioresour Technol 100: 2361–2368.

Ghorbanzadeh Mashkani, S., Tajer Mohammad Ghazvini, P., Agha Aligo, D., 2009. Uptake of Re (VII) from aqueous solutions by *Bacillus* sp. GT-83–23. Bioresour Technol 100: 603–608.

Gledhill, M., Buck, K.N. 2012. The organic complexation of iron in the marine environment: a review. Frontiers in Microbiology. Microbiological Chemisty 3(69): 1-17.

Gong, P., Ogra, O. Y., Koizumi, S. 2000. Inhibitory effects of heavy metals on transcription factor Sp1. Ind Health 38**:**224-227.

Goyal, N., Jain, S.C., Banerjee, UC. 2003. Comparative studies on the microbial adsorption of heavy metals. Adv Environ Res 7: 311–319.

Grass, G., Große, C., Nies, D. H. 2000. Regulation of the *cnr* Cobalt and Nickel Resistance Determinant from *Ralstonia* sp. Strain CH3. Bacteriol 82(5): 1390–1398.

Guha, H., Jayachandran, K., Maurrasse, F. 2001. Kinetics of chromium (VI) reduction by a type strain Shewanella alga under different growth conditions. Environmental Pollution 115(2): 209-218.

Gupta A, Zhuo J, Zha J, Reddy S, Olp J, Pai A. 2010. Effect of different intravenous iron preparations on lymphocyte intracellular reactive oxygen species generation and subpopulation survival. BMC Nephrol 11:16.

Gupta, H., Kao, S., Dai, M. 2012. The role of mega dams in reducing sediment fluxes: A case study of large Asian rivers. J Hydrol 464-465: 447-458.

Gupta, R., Ahuja, P., Khan, S., Saxena, R.K., Mohapatra, H. 2000. Microbial biosorbents: meeting challenges of heavy metal pollution in aqueous solutions. Curr Sci 78:967–73.

Haber, F., Weiss, J. 1932. Uber die katalyse des hydroperoxydes. Naturwissenschaften 20(15):948-950.

Hallberg, K.B., Johnson, D.B. 2005. Biological manganese removal from acid mine drainage in constructed wetlands and prototype bioreactors. Sci Total Environ 338:115–124.

Hallberg, R., Ferris, F. G. 2004. Biomineralization by *Gallionella.* Geomicrobiol J 21: 325–330.

Haney, C.J., Grass, G., Franke, S., Rensing, C. 2005. New developments in the understanding of the cation diffusion facilitator family. J Indus Microbiol Biotechnol 32(6): 215–226.

Hansel, C.M., Santelli, C.M., Zeiner, C.A.,Webb, S.M. 2012. Mn (II) oxidation by an ascomycete fungus is linked to superoxide production during sexual reproduction. Proc Natl Acad Sci USA109: 12621-12625.

Harrison, P.M., Arosio, P. 1996. The ferritins: molecular properties, iron storage function and cellular regulation. Biochimica et Biophysica Acta. 1275(3):161–203.

Hartman, A.L., Norais, C., Badger J.H. et al. 2010. The complete genome sequence of *Haloferax volcanii* DS2, a model archaeon. PloS One 5(3)9605.

Harwood-Sears, V., Gordo, A.S. 1990. Copper-induced production of copper- binding supernatant proteins by the marine bacterium *Vibrio alginolyticus*. Appl Environ Microbiol 56: 1327-1332.

Hasan, H.A., Abdullah, S.R.S., Kofli, N.T., Kamaruddin, S.K. 2010. Biosorption of manganese in drinking water by isolated bacteria. Journal of Applied Sciences 10: 2653-2657.

Hazen, R.M., Papineau, D., Bleeker, W., Downs R.T., Ferry J.M., Mccoy T.J., Sverjensky, D.A.,Yang, H. 2008. Mineral evolution. American Mineralogist 93:1693–1720.

Hedrich, S., Schlomann, M., Johnson, D.B. 2011. The iron-oxidizing proteobacteria. Microbiology. 157, 1551–1564.

Hezayen, F. F., Rehm, B. H. A., Tindall, Steinbuchel, B. J. A. 2001. International Journal of Systematic and Evolutionary Microbiology 51: 1133–1142.

Ho, V. A., Ward, D.M., Kaplan, J. 2002. Transition metal transport in yeast. Annu Rev Microbiol 56:237–261.

Ho, Y.S. 2006. Review of second-order models for adsorption systems. J Hazard Mater 136:681–9.

Ho, Y.S., Chiang, C.C., Hsu, Y.C. 2001. Sorption kinetics for dye removal from aqueous solution using activated clay. Journal of Separation Science and Technology 36: 2473-2488.

Hosseinkhani, B., Emtiazi, G. 2011. Synthesis and characterization of a novel extracellular biogenic manganese oxide (bixbyite-like Mn_2O_3) nanoparticle by isolated *Acinetobacter* sp. Curr Microbiol 63:300–305.

Howard, D.H. 1999. Aquisition, transport and storage of iron by pathogenic fungi. Clin Microbiol Rev 12:394–404.

Howe, P., Malcolm, H., Dobson, S. 2004. Manganese and its Compounds: Environmental Aspects. World Health Organization, Geneva: 63.

Hronec, O., Vilcek, J., Toma , J., Adamiin, P., Huttmanova , E. 2010. Environmental components quality problem areas in Slovakia. Mendelova univerzita, Brno, 227-235.

Hsu, T., Lee, L.W, Chang, T.H.1992. Influence of temperature and nutrient strength on the susceptibility of Saccharomyces cerevisiae to heavy metals. Bulletin of Environmental Contamination and Toxicology 49(3):444-448.

Hubmacher, D., Matzanke, B., Anemuller, F.S. 2007. Iron uptake in the Euryarchaeon *Halobacterium salinarum*. Biometals 20: 539-547.

Hubmacher, D., Matzanke, B.F., Anemuller, S. 2002. Investigations of iron uptake in *Halobacterium salinarum*. Biochem Soc Trans 30:710–712.

Hunt, C.D. 1983. Variability in the benthic Mn flux in coastal marine ecosystems resulting from temperature and primary production. Limnol Ocean 28(5): 913–923.

Huyer, M., Page, W.J. 1989. Ferric reductase activity in *Azotobacter vinelandii* and its inhibition by Zn^{2+}. J Bacteriol 171(7): 4031-4037.

Ikeda, S., Yamaguchi, Y., Sera, Y., Ohshiro, H., Uchino, S., Yamashita, Y. et al. 2000. Manganese deposition in the globus pallidus in patients with biliary atresia. Transplantation. 69 : 2339-43.

Imke, S., Johnson, E., de Vries , S. 2003. Microbial ferric iron reductases. FEMs Microbiol Rev 27:427-447.

Imlay, J.A., Chin, S.M., Linn, S. 1988. Toxic DNA damage by hydrogen peroxide through the Fenton reaction in vivo and in vitro. Science 240:640-642.

IOM. 2001. Institute of Medicine. Dietary reference intakes: Vitamin A, vitamin K, arsenic, boron, chromium, copper, iodine, iron, manganese, molybdenum, nickel, silicon, vanadium, and zinc. Washington DC: National Academy Press.

Ito, A., Xu, L. 2013. Response of acid mobilization of iron-containing mineral dust to improvement of air quality projected in the future. Atmos Chem Phys Discuss 13: 28173–28223.

Iyer, A., Mody, K., Jha, B. 2004. Accumulation of hexavalent chromium by an exopolysaccharide producing marine *Enterobacter cloaceae.* Mar Poll Bullet 49: 974-977.

Jensen, L. T., Ajua-Alemanji, M., Culotta,V.C. 2003. The *Saccharomyces cerevisiae* high affinity phosphate transporter encoded by PHO84 also functions in manganese homeostasis. J Biol Chem 278:42036–42040.

Jerez, C. A. 2009. Metal extraction and biomining. In Encyclopedia of Microbiology, 3rd edn, pp. 407–420. Edited by M. Schaechter. Amsterdam: Elsevier.

Jickells, T.D., Spokes, L.J. 2001. Atmospheric iron inputs to the oceans. In: The Biogeochemistry of Iron in Seawater, Turner, D. R., Hunter, K. (Eds) SCOR/IUPAC Series, J. Wiley, 85–121.

Johnson, D.B., Kanao, T., Hedrich, S. 2012. Redox transformations of iron at extremely low pH:fundamental and applied aspects. Fronteirs Microbiol 3: 2-13.

Johnson, K.L., Younger, P.L. 2005. Rapid manganese removal from mine waters using an aerated packed-bed bioreactor. J Environ Qual 34: 987–993.

Joo, J.H., Hassan, S.H.A., Oh, S.E. 2010. Comparative study of biosorption of Zn^{2+} by Pseudomonas aeruginosa and Bacillus cereus. Int Biodeterior Biodegrad 64:734-741.

Jörg, S. 2006. From genomes to function: haloarchaea as model organisms. Microbiology 152 (3):585-590.

Jun. D., Xiaolon, M. Jingjie, L. 2013. Removal of aromatic hydrocarbons from aquifers by oxidation coupled with dissimilatory bacterial reduction of iron. Chem Technol Fuel Oil 49(1): 70-80.

Kabata-Pendias, A., Pendias, H. 2001. Trace elements in soils and plants. 3rd edition, CRC Press, USA: 331.

Kachur, A.V., Koch, C.J., Biaglow, J.E. 1998. Mechanism of copper-catalyzed oxidation of glutathione. Free Radic Res 28**:**259-269.

Kappler, A., Straub, K.L. 2005. Geomicrobiological cycling of iron. Reviews in mineralogy and geochemistry. 59:85-108.

Kapoor, A., Viraraghavan, T. 1995. Fungal biosorption — an alternative treatment option for heavy metal bearing wastewaters: a review. Bioresour Technol.53:195–206.

Kashefi, K., Moskowitz, B.M. Lovley, D.R. 2008a. Characterization of extracellular minerals produced during dissimilatory Fe (III) and U (VI) reduction at 100 degrees C by *Pyrobaculum islandicum*. Geobiol 6: 147–154.

Kashefi, K., Shelobolina, E.S, Elliott, W.C., Lovley, D.R. 2008b. Growth of thermophilic and hyperthermophilic Fe(III)- reducing microorganisms on a ferruginous smectite as the sole electron acceptor. Appl Environ Microb 74: 251–258.

Kashefi, K., Tor, J.M., Nevin, K.P., Lovley, D.R. 2001. Reductive precipitation of gold by dissimilatory Fe(III)-reducing bacteria and archaea. Appl Environ Microbiol 67: 3275–3279.

Kaur, A., Pan, M., Meislin, M., Facciotti, M.T., El-Gewely, R., Baliga, N.S. 2006. A systems view of haloarchaeal strategies to withstand stress from transition metals. Genome Res 16(7): 841–854.

Kavitha, B., Jothimani, P., Ponmani, S., Sangeetha, R. 2013. Phytoremediation of Heavy Metals- A Review. International Journal of Research Studies in Biosciences. 1(2): 17-23.

Kawakami, Y., Hayashi, N., Ema, M., Nakayama, M. 2007. Effects of divalent cations on *Halobacterium salinarum* cell aggregation Journal of Bioscience and Bioengineering 104(1): 42–46.

Kawakami, Y., Hayashi, N., Ema, M., Nakayama, M. 2007. Effects of divalent cations on *Halobacterium salinarum* cell aggregation. J Bios Bioeng 104(1): 42–46.

Kehres, D., Maguire, M.E. 2003. Emerging themes in manganese transport, biochemistry and pathogenesis in bacteria. FEMS Microbiol Rev 23:263-290.

Kehres, D.G., Janakiraman, A., Slauch, J.M. and Maguire, M.E. 2002. SitABCD is the alkaline Mn^{2+} transporter of *Salmonella enterica* serovar Typhimurium. Bacteriology 184:3159-3166.

Kell, D.B. 2009. Iron behaving badly: inappropriate iron chelation as a major contributor to the aetiology of vascular and other progressive inflammatory and degenerative diseases. BMC Medical Genomics 2:2.

Kennedy, C.B., Scott, S.D., Ferris, F.G. 2004. Hydrothermal phase stabilization of 2-line ferrihydrite by bacteria. Chemical Geology 212:269–277.

Khandavilli, S., Sequeira, F,. Furtado, I. 1999. Metal tolerance of extremely halophilic bacteria isolated from estuaries of Goa, India. Ecol Environ Conserv 5: 149 —152.

Kieber, R. J., Williams, K., Willey, J. D., Skrabal, S., Avery, G. B., Jr. 2001. Iron speciation in coastal rainwater: concentration and deposition to seawater. Mar Chem 73: 83–95.

Kim, T., Nunnery, G.A., Jacob, K., Schwartz, J., Liu, X., Tannenbaum, R. 2010. Synthesis, characterization, and alignment of magnetic carbon nanotubes tethered with maghemite nanoparticles. J Phys Chem C 114 (15) 6944–6951.

Kinkle, B.K., Sadowsky, M.J., Johnstone, K., Koskinen, W.C. 1994. Tellurium and selenium resistance in Rhizobia and its potential use for direct isolation of Rhizobium meliloti from soil. Applied and Environmental Microbiology 60:1674-1677.

Klein, J.S., Lewinson, O. 2011. Bacterial ATP-driven transporters of transition metals: physiological roles, mechanisms of action, and roles in bacterial virulence. Metallomics 3(11): 1098–1108.

Koretsky, C.M., Haas, J.R., Miller, D., Ndenga, N.T. 2006. Seasonal variations in pore water and sediment geochemistry of littoral lake sediments (Asylum Lake, MI, USA). Geochemical Transactions. 7:11.

Kosman, D.J. 2003. Molecular mechanisms of iron uptake in fungi. Mol Microbiol 47:1185–1197.

Kosman, D.J. 2003. Molecular mechanisms of iron uptake in fungi. Mol Microbiol 47:1185–1197.

Kozubal, M.A., Macur, R.E.,Jay, Z.J., Beam, J.P., Malfatti, S.A et al. 2012. Microbial ironcycling in acidic geothermal springs of Yellowstone National Park: integrating molecular surveys, geochemical processes, and isolation of novel Fe-active microorganisms. Fronteirs in Microbiology 3: 1-16.

Kukkadapu, R.K., Zachara, J.M., Fredrickson, J.K., Kennedy, D.W. 2004. Biotransformation of two-line silica-ferrihydrite by dissimilatory Fe(III)-reducing bacterium: formation of carbonate green rust in the presence of phosphate. Geochim Cosmochim Acta 68(13): 2799–2814.

Kumar, A., Sarin, M.M. 2010. Aerosol iron solubility in a semi-arid region: temporal trend and impact of anthropogenic sources. Tellus. 62B:125–132.

Kumar, C.S.R., Joseph, M.M., Kumar,T.R.G., Renjith, K.R., Manju, M.N., Chandramohanakumar, N. 2010. Spatial variability and contamination of heavy metals in the inter-tidal systems of a tropical environment. International J of Environ Res 4(4): 691–700.

Kuroda, M., Dey, S., Sanders O.I., Rosen B.P. 1997. Alternate energy coupling of ArsB, the membrane subunit of the ars anion-translocating ATPase. J Biol Chem 272: 326-331.

Kuyucak, N., Volesky, B. 1990. Biosorption of heavy metal.CRC, Boca Raton,FL.

Laemmli, U.K. 1970. Cleavage of structural proteins during assembly of head of the bacteriophage T4. Nature 227:680-685.

Langmuir, I. 1918. The adsorption of gases on plane surfaces of glass, mica and platinum, J Am Chem Soc: 1361–403.

Lanyi, J.K , Maeda, A. 1997. Structural basis of information transfer and energy transduction in rhodopsins. Photochem Photobiol 66:733-734.

Lanyi, J.K. 1997. Mechanism of ion transport across membranes: bacteriorhodopsin as a prototypefor proton pumps. J Biol Chem 272:31209-31212.

Lazrak, T., Wolff, G., Albrecht, A.-M., Nakatani, Y., Ourisson, G., Kates, M. 1988. Bacterioruberins reinforce reconstituted Halobacterium lipid membranes. Biochim Biophys Acta 939: 160-162.

Lee, J.H., Kennedy, D.W., Dohnalkova, A., Moore, D.A., Nachimuthu, P., Reed, S.B., Fredrickson, J.K. 2011. Manganese sulfide formation via concomitant microbial manganese oxide and thiosulfate reduction. Environ Microbiol 13(12):3275–3288.

Lee, Y., Tebo, B.M. 1994. Cobalt oxidation by the marine manganese (II)-oxidizing Bacillus sp. strain SG-1. Appl Environ Microbiol 60: 2949–2957.

Lemire, J.A., Harrison, J.J., Turner, R.J. 2013. Antimicrobial activity of metals: mechanisms, molecular targets and applications. Nature Reviews Microbiology 11:371–384.

Leone, S., Castro, C.D., Pariilli, M., Baldi, F., Lanzeta, R. 2007. Structure of the iron-binding exopolysaccharide produced anaerobically by the gram-negative bacterium *Klebsiella oxytoca* bas-10. Eur J Org Chem 31:5183–5189.

Li, S., Xu, R. 2008. Electrical double layers' interaction between oppositely charged particles as related to surface charge density and ionic strength. Colloids and Surfaces A: Physicochemical and Engineering Aspects 326:157-161.

Li, Z.J., Yuan, H.L., Hu, X.D. 2008. Cadmium-resistance in growing *Rhodotorula* sp. Y11. Bioresour. Technol. 99: 1339–1344.

Lim, M.K., Lee, C.K., Ju, Y.S., Cho, Y.S., Lee, M.S., Yoo, B., Moon, H.B. 2001. Serum ferritin as a serological marker of activity in systemic lupus erythematosus. Rheumatol Int 20:89-93.

Lin, C.C., Lai, Y.T. 2006. Adsorption and recovery of lead (II) from aqueous solutions by immobilized Pseudomonas aeruginosa PU21 beads. J Hazard Mater 137:99-105.

Lin, C.Y., Abdullah, M.H., Musta, B., Praveena, S.M., Aris, A.Z.2011. Stability behavior and thermodynamic states of iron and manganese in sandy soil aquifer, Manukan Island, Malaysia. Natural Resour Res 20(1):45-55.

Lin, X., Gao, A., Chen, H. 2008. Isolation and phylogenetic analysis of cultivable manganese bacteria in sediments from the Arctic Ocean. Acta Ecologica Sinica 28(12): 6364-6370.

Litchfield, C.D., Gillevet, P.M. 2002. Microbial diversity and complexity in hypersaline environments: a preliminary assessment. J Ind Microbiol Biotechnol 28(1): 48-55.

Liu, H.L., Chen, B.Y., Lan, Y.W., Cheng, Y.C. 2004. Biosorption of Zn(II) and Cu(II) by the indigenous *Thiobacillus thiooxidans*. Chem Eng J. 97:195–201.

Liu, S.V., Zhou, J., Zhang, C., Cole, D.R., Gajdarziska-Josifovska, P., Phelps, T.J. 1997. Thermophilic Fe(III)-reducing bacteria from the deep subsurface: the evolutionary implications. Science 277:1106–1109.

Liu, T., Nakashima, S., Hirose, K., Uemura, Y., Shibasaka, M., Katsuhara, M., Kasamo, K. 2003. A metallothionein and CPx-ATPase handle heavy-metal tolerance in the filamentous cyanobacteria *Oscillatoria brevis*. FEBS Letters 542: 159-163.

Liu, Z., Yang, S., Bai, Y., Xiu, J., Yanh, H. et al. 2011. Alteration of cell membrane of sulfate reducing bacteria in the presence of Mn (II) and Cd (II). Minerals Eng 24(8): 839-844.

Lobo, V., Patil, A., Phatak, A., Chandra N. 2010. Free radicals, antioxidants and functional foods: Impact on human health. Pharmacogn Rev 4(8)118-126.

Lovley, D. R., Holmes, D. E., Nevin, K.P. 2004. Dissimilatory Fe(III) and Mn(IV) reduction. Adv Microb Physiol 49**:** 219-286.

Lovley, D.R. 2000. Environmental Microbe-Mineral Interactions ed. Lovley, D.R. Washington, DC: ASM Press.

Lovley, D.R., Giovannoni, S.J., White, D.C., Champine, J.E., Phillips, E.J.P. 1993. *Geobacter metallireducens* gen. nov. sp. nov., a microorganism capable of coupling the complete oxidation of organic compounds to the reduction of iron and other metals. Arch Microbiol 159:336-344.

Lovley, D.R., Holmes, D.E. Nevin, K.P. 2004. Dissimilatory Fe(III) and Mn(IV) reduction. Adv Microb Physiol 49:219-286.

Lowenstam, H.A., Weiner, S. 1989. On Biomineralization. Oxford University Press, New York.

Lu, W. B., Shi, J. J., Wang, C. H., Chang, J. S. 2006. Biosorption of lead, copper and cadmium by an indigenous isolate *Enterobacter* sp. J1 possessing high heavy-metal resistance. J Hazard Mater. 134: 80–86.

Madern, D., Ebel, C., Zaccai, G. 2000. Halophilic adaptation of enzymes. Extremophiles4 :91-98.

Maezato, Y., Blum, P. 2012. Survival of the fittest: Overcoming oxidative stress at the extremes of acid, heat and metal. Life 2:229-242.

Majer, B.J., Tscherko, D., Paschke, A., Wennrich, R., Kundi, M., Kandeler, E., Knasmüller, S. 2002. Effects of heavy metal contamination of soils on micronucleus induction in Tradescantia and on microbial enzyme activities: a comparative investigation. 515(1-2): 111-124.

Majestic, B.J., Schauer, J.J., Shafer, M. 2007. Development of a manganese speciation method for atmospheric aerosols in biologically and environmentally relevant fluids. Aerosol Sci Tech 41: 925-933.

Malekzadeh, F., Ghorbanzadeh Mashkani, S., Ghafourian, H., Soudi, M.R., 2007. Biosorption of tungstate by a *Bacillus* sp. isolated from Anzali lagoon. World J Microbiol Biotechnol 23: 905–910.

Malki, L., Yanku, M., Borovok, I., Cohen, G., Mevarech, Aharonowitz, M.Y. 2009. Identification and characterization of gshA, a gene encoding the glutamate-cysteine ligase in the halophilic archaeon *Haloferax volcanii*. J Bacteriol 191(16): 5196–5204.

Mameri, N., Boudries, N., Addour, L., Belhocine, D., Lounici, H., Grib, H. 1999. Batch zinc biosorption by a bacterial nonliving *Streptomyces rimosus* biomass. Water Res 33:1347–54.

Mane,P.C, Bhosle, A.B., Vishwakarma, C.V., Tupkar, L.G.2010. Effect of pretreatment of algal biomass on bioadsorption of manganese. I J Eng Sci Technol 2(12):7550-7554.

Margesin, R., Schinner, F. 2001. Potential of halotolerant and halophilic microorganisms for biotechnology. Extremophiles 5: 75-83.

Maring, H., Savoie, D.L., Izaguirre, M.A., Custals, L., Reid, J.S. 2003. Mineral dust aerosol size distribution change during atmospheric transport. J Geophys Res 108: 1984-2012.

Markich, J., Brown, P. L., Batley, G. E., Apte, S. C., Stauber, J. L. 2001. Incorporating metal speciation and bioavailability into water quality guidelines for protecting aquatic ecosystems. Australian Journal of Ecotoxicology 7(2): 109–122.

Marriott, B. P., White, A., Hadden, L., Davies J.C., Wallingford, J.C. 2011. World Health Organization (WHO) infant and young child feeding indicators: associations with growth measures in 14 low-income countries. Maternal and Child Nutrition. doi: 10.1111/j.1740-8709.2011.00380.x.

Matsunaga, T., Okamura, Y.,Tanaka, T. 2004. Biotechnological application of nano-scale engineered bacterial magnetic particles. J Mater Chem 14: 2099– 2105.

Maurya, N.S., Mittal, A.K., Cornel, P., Rothe, E., 2006. Biosorption of dyes using dead macro fungi: effect of dye structure, ionic strength and pH. Bioresour Technol 97: 512–521.

Mendham, J., Denney, R.C., Barnes J.D., Thomas, M., Sivasankar, B. 2009. Vogel's textbook of quantitative chemical analysis. Pearson Education, India.

Miot, J., Benzerara, K., Morin, G., Kappler, A., Bernard, S., Obst, M., Férard, C., Skouri-Panet, F., Guigner, J.-M., Posth, N., Galvez, M., Brown, Jr. G. E., Guyot, F. 2009. Iron biomineralization by anaerobic neutrophilic iron-oxidizing bacteria. Geochim Cosmochim Acta 73(3): 696–711.

Mishra, V., Balomajumder, C., Agarwal,V.K. 2010. Biosorption of Zn (II) onto the surface of non-living biomasses: A comparative study of adsorbent particle size and removal capacity of three different biomasses. Water, Air, and Soil Pollution 211: 489-450.

Missiaen, L., Raeymaekers, L., Dode, L., Vanoevelen, J., Baelen, K.V., Parys, J.B., Callewaert, Miyata, N., Tani, Y., Iwahori, K., Soma, M. 2004. Enzymatic formation of manganese oxides by an Acremonium-like hyphomycete fungus, strain KR21-2. FEMS Microbiol Ecol 47:101-109.

Montanini, B., Blaudez, D., Jeandroz, S., Sanders, D., Chalot, M. 2007. Phylogenetic and functional analysis of the Cation Diffusion Facilitator (CDF) family: improved signature and prediction of substrate specificity. BMC Genomics 8: 107.

Moraleda, M.A., Pérez, J., Fontes, M., Muñoz-Dorado, F.J.M. 2005. Copper induction of carotenoid synthesis in the Bacterium *Myxococcus Xanthus*. Mol Microbiol 56 (5):1159–1168.

Morgan, B., Lahav, O. 2007. The effect of pH on the kinetics of spontaneous Fe(II) oxidation by O_2 in aqueous solution – basic principles and a simple heuristic description. Chemosphere 68 : 2080–2084.

Mosley, S. 2009. A network of trust: Measuring and monitoring air pollution in British cities, Environment and history 15(3): 273-302.

Muhammad, I., Ashiru, S., Ibrahim I., Salawu, D.K., Muhammad, T.D., Muhammad, A.N. 2013. Determination of some heavy metals in wastewater and sediment of artisanal gold local mining site of Abare area in Nigeria. Enviro Treat Tech 1(3): 174-182.

Mukhopadhyay, R., Rosen, B.P., Phung, L.T., Silver, S. 2002. Microbial arsenic: from geocycles to genes and enzymes. FEMS Microbiol Rev 26(3): 311–325.

Nadadur, S.S., Srirama K., Mudipalli, A. 2008. Iron transport & homeostasis mechanisms: Their role in health and disease. Indian J Med Res 128: 533-544.

Nagatomo, S., Umehara, F., Hanada, K., Nobuhara, Y., Takenaga, S., Arimura, K., et al. 1999. Manganese intoxication during total parenteral nutrition: Report of two cases and review of the literature. J Neurol Sci 162: 102-5.

Naik, S., Furtado, I. 2013. Equilibrium and kinetics of adsorption of Mn^{2+} by Haloarchaeon *Halobacterium* sp. GUSF (MTCC3265). Geomicrobiology Journal DOI:10.1080/01490451.2013.859769

Nair, S., Finkel, S.E. 2004. Dps protects cells against multiple stresses during stationary phase. J Bacteriol. 186(13): 4192–4198.

Nairz, M., Schroll, A., Sonnweber, T., Weiss, G.2010.The struggle for iron – a metal at the host-pathogen interface. Cell Microbiol (12):1691–1702.

Naja, G., Mustin, C., Berthelin, J., Volesky, B. 2005. Lead biosorption study with *Rhizopus arrhizus* using a metal-based titration technique. J Colloid Interface Sci. 292: 537–43.

Naja, G.M., Volesky, B. 2011. The mechanism of metal cation and anion biosorption. In: Kotrba, P., Mackova, M., Macek, T., (Eds.), Microbial biosorption of metals Springer –Verlog, pp. 19-58.

Nakajima, A., Yasuda, M., Yokoyama, H., Ohya-Nishiguchi, H., Kamada, H. 2001. Copper biosorption by chemically treated *Micrococcus luteus* cells. World J Microbiol Biotechnol. 17:343–7.

Nealson, K. 2006. The manganese-oxidizing bacteria. In: Dworkin Metal (eds) The prokaryotes. Springer, New York, pp 222–231.

Nealson, K., Myers, C. 1992. Microbial reduction of manganese and iron: new approaches to carbon cycling. Applied and Environmental Microbiology 58:439-443.

Nealson, K.H., Saffarini, D. 1994. Iron and manganese in anaerobic respiration environmental significance, physiology, and regulation. Annual Review of Microbiology 48: 311-343.

Neilands, J.B. 1995. Siderophores: structure and function of microbial iron transport compounds. J Biolog Chem 270(45): 26723–26726.

Nelson, M. Y., Lion, L.W., Ghiorse, W.C., Shuler, M.L. 1999. Production of biogenic Mn oxides by *Leptothrix discophora* SS-1 in a chemically defined growth medium and evaluation of their Pb adsorption characteristics. Appl Environ Microbiol 65(1):175-180.

Nelson, N. 1999. Metal ion transporters and homeostasis. EMBO Journal 18: 4361- 4371.

Nies, D. H. 1999. Microbial heavy-metal resistance. Appl Microbiol Biotechnol 51**:**730-750.

Nies, D. H. 2003. Efflux-mediated heavy metal resistance in prokaryotes. FEMS Microbiol Rev 27(2-3): 313–339.

Nies, D.H., Koch, S., Wachi, S. 1998. CHR, a novel family of prokaryotic proton motive force-driven transporters probably containing chromate/sulfate antiporters. Journal of Bacteriology 180: 5799-5802.

Nieto, J. J., Ventosa, A., Ruiz-Berraquero, F. 1987. Susceptibility of halobacteria to heavy metals. Applied and environmental microbiology. 53(5):1199-1202.

Nieto, J.J., Fernandez-Castillo, R., Marquez, M.C., Ventosa, A., Quesada, E., Ruiz-Berraquero, F. 1989. Survey of metal tolerance in moderately halophilic eubacteria. Appl Environ Microbiol 55: 2385–2390.

Niu. H., Xu, X.S., Wang, J.H., Volesky, B. 1993. Removal of lead from aqueous solutions by *Penicillium* biomass. Biotechnol Bioeng. 42:785–7.

Nourbakhsh, M., Sag, Y., Ozer, D., Aksu, Z., Kutsal, T., Caglar, A. 1994. A comparative study of various biosorbents for removal of chromium(VI) ions from industrial wastewaters. Process Biochem. 29:1–5.

O'Loughlin, E. J., 2008. Effects of electron transfer mediators on the bioreduction of Lepidocrocite (γ-FeOOH) by *Shewanella putrefaciens* CN32. Environ Sci Technol 42(18):6876–6882.

Oberdoerster, G., Cherian, G. 1988. Manganese. Biological monitoring of toxic metals. Rochester series on environmental toxicity 283-301.

Orange, F., Jean-Robert D.S., Westall ,F., Prieur , D., Baillif, P. 2011. Metalcation binding by the hyperthermophilic microorganism, archaea Methanocaldococcus jannaschii, and its effects on silicification. Palaeontology 54(5): 953-964.

Orell, A., Navarro, C.A.,Rivero, M., Aguilar, J.S., Jerez, C. A. 2012. Inorganic polyphosphates in extremophiles and their possible functions. Extremophil. DOI 10.1007/s00792-012-0457-9.

Oren, A. 2012. Taxonomy of the family *Halobacteriaceae*: a paradigm for changing concepts in prokaryote systematic. Int J Syst Evol Microbiol 62(2): 263–271.

Osborn, A.M., Bruce, K.D., Strike, P., Ritchie, D.A. 1997. Distribution, diversity and evolution of the bacterial mercury resistance (mer) operon. FEMS Microbiol Rev 19(4): 239–262.

Oshiki, M., Ishii, S., Yoshida, K., Fujii, N., Ishiguro, M., Satoh, H., Okabe, S. 2013. Nitrate-dependent ferrous iron oxidation by anaerobic ammonium oxidation (Anammox) bacteria. Appl Environ Microbiol 79(13):4087-4093.

Ozbahce, A., Zengin, M. 2010. Effects of manganese fertilizers on yield and yield components of dwarf dry bean. J Plant Nutr 34(1):127-39.

Ozdemir, G., Ceyhan, N., Ozturk, T., Akirmak, F., Cosar, T. 2004. Biosorption of chromium (VI), cadmium (II) and copper (II) by Pantoea sp. TEM18. Chemical Engineering Journal 102: 249-253.

Ozer, A., Ozer, D. 2003. Comparative study of the biosorption of Pb(II), Ni(II) and Cr(VI) ions onto S. cerevisiae: determination of biosorption heats. J Hazard Mater 100: 219–29.

Ozturk, A. 2007. Removal of nickel from aqueous solution by the bacterium *Bacillus thuringiensis*. J Hazard Mater 147:518–23.

Pagnanelli, F., Esposito, A., Veglio, F. 2002. Multi-metallic modeling for biosorption of binary systems. Water Res 36:4095–105.

Pal, A., Paul, A.K. 2008. Microbial extracellular polymeric substances: central elements in heavy metal bioremediation. Indian J Microbiol 48: 49-64.

Pal, P.K., Samii, A., Calne, D.B. 1999. Manganese neurotoxicity: A review of clinical features, imaging and pathology. Neurotoxicology 20: 227-38.

Pardo, R., Herguedas, M., Barrado, E., Vega, M. 2003. Biosorption of cadmium, copper, lead and zinc by inactive biomass of *Pseudomonas putida,* Anal Bioanal Chem 376: 26–32.

Parikh, S., Chorover, J. 2005. FTIR spectroscopic study of biogenic Mn-oxide formation by *Pseudomonas putida* GB-1. Geomicrobiol J 22:207-218.

Parisa, T.M.G., Saeid, G.M. 2009. Effect of salinity on vanadate biosorption by *Halomonas* sp. GT-83: Preliminary investigation on biosorption by micro-PIXE technique. Bioresour Technol 100: 2361–2368.

Park, D., Yun, Y.S., Jo, J.H., Park, J.M. 2005. Mechanism of hexavalent chromium removal by dead fungal biomass of Aspergillus niger. Water Research 39: 533–540.

Parker, C.W., Wolf, J.A., Auler, A.S., Barton, H.A., Senko, J.M. 2013. Microbial reducibility of Fe(III) phases associated with the genesis of iron ore caves in the iron quadrangle, Minas Gerais, Brazil. Minerals 3:395-411.

Parmar, N., Warren, L.A., Roden, E.E., Ferris, F.G. 2000. Solid phase capture of strontium by the iron reducing bacteria *Shewanella* alga strain BRY. Chem Geo169: 281–288.

Parvathi, K., Nareshkumar, Nagendran R. 2007. Biosorption sites of *Saccharomyces cerevisiae*. Environ Technol 28(7):779-84.

Parvathi, K., Nareshkumar, R., Nagendran, R.2007. Biosorption of manganese by *Aspergillus niger* and *Saccharomyces cerevisiae*. World J Microbiol Biotechnol 23:671–676.

Patil, S., Fernandes, J., Tangasali, R., Furtado, I. 2013. Exploitation of *Haloferax alexandrinus* for biogenic synthesis of silver nanoparticles antagonistic to human and lower mammalian pathogens. Journal of Cluster Science doi: 10.1007/s10876-013-0621-0.

Paulsen, I.T., Saier Jr., M.H. 1997. A novel family of ubiquitous heavy metal ion transport proteins. J Mem Biol 156 (2) 99–103.

Payne, S.M.1994. Detection, isolation, and characterization of siderophores. Methods Enzymol 235:329-44.

Peacock, C.L., Sherman, D.M., 2004. Vanadium (V) adsorption onto goethite at pH 1.5 to 12: a surface complexation model based on ab initio molecular geometries and EXAFS spectroscopy. Geochim. Cosmochim Acta 68: 1723– 1733.

Pearson, G.F., Greenway, G.M. 2005. Recent developments in manganese speciation. Trends in Analyt Chem 24: 803-809.

Pereira, F, Kerkar, S., Krishnan, K.P. 2012. Bacterial response to dynamic metal concentrations in the surface sediments of a solar saltern (Goa, India). Environ Monitor Assess. 185(5):3625-36.

Perl, D.P., Olanow, C.W. 2007. The neuropathology of manganese-induced parkinsonism. J Neuropath Experimental Neurolog 66(8) pp. 675–682.

Pinsino, A., Matranga, V., Roccheri, M.C. 2012. Manganese: A new emerging contaminant in the environment, environmental contamination, Dr. Jatin Srivastava (Ed.), ISBN: 978-953-51-0120-8.

Poli, A., P. Di Donato, G. R. Abbamondi, Nicolaus, B. 2011. Synthesis, production and biotechnological applications of exopolysaccharides and polyhydroxyalkanoates by archaea. Archaea article id 693253:13.

Pollmann, K., Matys, S. 2007. Construction of an S-layer protein exhibiting modified self-assembling properties and enhanced metal binding capacities. Appl Microbiol Biotechnol 75:1079–1085.

Popescu, G., Dumitru, L. 2009. Biosorption of some heavy metals from media with high salt concentrations by halophilic archaea. Biotechnology and Biotechnological Equipment 23:sup1 791-795.

Popova, O. B., Sanina N. M., Likhatskaya G. N., Bezverbnaya I. P. 2008. Effects of copper and cadmium ions on the physicochemical properties of lipids of the marine bacterium Pseudomonas *putida* IB28 at different growth temperatures. Russian Journal of Marine Biology 34(3): 179-185.

Pósfai, M., Buseck, P.R., Bazylinski, D.A., Frankel, R.B. 1998a. Reaction sequence of iron sulfide minerals in bacteria and their use as biomarkers. Science 280: 880–883.

Pósfai, M., Buseck, P.R., Bazylinski, D.A., Frankel, R.B. 1998b. Iron sulfides from magnetotactic bacteria: structure, compositions, and phase transitions. Am Mine 83: 1469–1481.

Prakash, W.G., Gnanadesigan, M., Ravikumar, S., 2012a. Biosorption and bio-kinetic properties of solar saltern halobacterial strains for managing Zn^{2+}, As^{2+} and Cd^{2+} metals. Geomicrobiol J doi:10.1080/01490451.2012.732663.

Prakash, W.G., Gnanadesigan, M., Ravikumar, S., 2012 b. Biosorption and bio-kinetic studies of halobacterial strains against Ni^{2+}, Al^{3+} and Hg^{2+} metal ions. Bioresour Technol 107: 526-529.

Prospero JM, Lamb PJ. 2003. African droughts and dust transport to the Caribbean: climate change implications. Science 302:1024–1027.

Puranik., R., P., Paknikar., M., K. 1999. Biosorption of lead, cadmium and zinc by *Citrobacter* strain MCM B181:characterisation studies. Biotechnol Prog 15: 228-237.

Puranik, P.R., Paknikar, K.M. 1997. Biosorption of lead and zinc from solutions using *Streptoverticillium cinnamoneum* waste biomass. J Biotechnol. 55:113–24.

Puri, S., Hohle, T.H., O'Brian, M.R. (2010) Control of bacterial iron homeostasis by manganese. PNAS doi/10.1073/pnas.1002342107.

Quan, H., Bai, H., Han, Y., Kang, Y., Sun, J. 2013. Removal of Cu(II) and Fe(III) from aqueous solutions by dead sulfate reducing bacteria. Frontiers of Chemical Science and Engineering 7(2): 177-184.

Raghavan, T.M., Furtado, I. 2005. Expression of carotenoid pigments of haloarchaeal cultures exposed to aniline. Environmental Toxicology 20: 165-169.

Raghavan, T.M., Furtado, I. 2000. Tolerance of an estuarine halophilic archaebacterium to crude oil and constituent hydrocarbons. Bull of Environ Contam Toxicol 65:725-731.

Raimunda, D., Gonz´alez-Guerrero, M., Leeber III, B.W., Arg¨uello, J.M. 2011.The transport mechanism of bacterial Cu^{+}-ATPases: distinct efflux rates adapted to different function. Biometals 24(3): 467–475.

Raiswell, R., Canfeild, D.E. 1998. Sources of iron for pyrite formation in marine sediments. Am J Sci 298:219-245.

Rashmi, R., Yuti, A.M., Basavaraj, K.H. 2012. Enhanced ferritin/iron ratio in psoriasis. Indian J Med Res 135(5)662-665.

Ratledge, C. and Dover, L.G. 2000. Iron metabolism in pathogenic bacteria. Annu Rev Microbiol 54:881-941.

Ravenscroft, P., McArthur, J.M., Hoque, M.A. 2013. Stable groundwater quality in deep aquifers of Southern Bangladesh: The case against sustainable abstraction. Sci Tot Environ 454-455: 627–638.

Razmovski, R., Sciban, M. 2008. Iron (III) biosorption by *Polyporus squamosus*. African Journal of Biotechnology 7: 1693-1699.

Rea, P. A., Li, Z. S., Lu, Y. P., Drozdowicz, Y. M., Martinoia, E. 1998. From vacuolar GS-X pumps to multispecific ABC transporters. Annl Rev Plant Biol 49: 727– 760.

Refat, M.S., Al-Qahtani, M.M. 2011. Unusual route for preparation of manganese(II), cobalt(II), zinc(II) and cadmium(II) carbonate compounds: synthesis and spectroscopic characterizations. Bull Mater Sci 34(4):853-857.

Reid, E., Xingrong, Liu., Judd, S.J. 2006. Effect of high salinity on activated sludge characteristics and membrane permeability in an immersed membrane bioreactor. Journal of Membrane Science 283: 164–171.

Reimann, C.,de Caritat P. 1998. Chemical elements in the environment—Factsheets for the geochemist and environmental scientist. Springer-Verlag, Berlin-Heidelberg, 398.

Reimann,C., Siewers, U., Tarvainen, T., Bityukova, L., Ericksson, J., Gilucis, A. 2003. Agricultural soils in Northern Europe. A Geochemical Aspect. Geologisches Jahrbuch, Stuttgart, Germany.

Reindel, S., Schmidt, C.L., Anemuller, S., Matzanke, B.F. 2005. Expression and regulation pattern of ferritin-like DpsA in the Archaeon *Halobacterium salinarum*. BioMetals. 18(4): 387–397.

Rensing, C., Mitra, B., Rosen, B. P. 1997. Insertional inactivation of *dsbA* produces sensitivity to cadmium and zinc in *Escherichia coli*. J Bacteriol 179:2769-2771.

Roh, Y., Chon, C.-M., Moon, J.-W. 2007. Metal reduction and biomineralization by alkaliphilic metal reducing bacterium, *Alkaliphilus metalliredigens* (QYMF). Geosciences Journal 11(4): 415–423.

Roh, Y., Gao, H., Vali, H. et al. 2006. Metal reduction and iron biomineralization by a psychrotolerant Fe(III)-reducing bacterium, Shewanella sp. strain PV-4. Appl Environ Microbiol 72(5): 3236–3244.

Roh, Y., Liu, S.V., Li, G., Huang, H., Phelps, T.J., Zhou, J. 2002. Isolation and characterization of metal-reducing *Thermoanaerobacter* strains from deep subsurface environments of the Piceance Basin, Colorado. Appl Environ Microbiol 68: 6013–6020.

Roh, Y., Zhang, C.L., Vali, H., Lauf, R.J., Zhou, J., Phelps, T. J. 2003. Biogeochemical and environmental factors in Fe biomineralization: magnetite and siderite formation. Clays and Clay Minerals 51(1): 83–95.

Romera, E., Gonzalez, F., Ballester, A., Blazquez, M.L., Munoz, J.A. 2006. Biosorption with algae: a statistical review. Crit Rev Biotechnol. 26:223–35.

Rosenberg, M. 1991. Basic and applied aspects of microbial adhesion at the hydrocarbon: water interface. Crit Rev Microbiol 18: 157-173.

Ross, S. M. 1994. Retention, transformation and mobility of toxic metals in soils. In: Toxic Metals in Soil-Plant Systems, S.M. Ross, Ed., pp. 63–152, JohnWiley & Sons, Chichester, UK.

Roth, J.R., Lawrence, J.G., Rubenfield, M., Kieffer-Higgins, S., Church, G.M. 1993. Characterization of the cobalamin (vitamin B12) biosynthetic genes of *Salmonella typhimurium*. J Bacteriol 175(11): 3303–3316.

Sabrina, H., Michaeal, S., Barrie, J.D. 2011. The iron oxidizing proteobacteria. Microbiology 157: 1551-1564.

Safavi, A., Abdollahi, H. 1999. Speciation of Fe(II) and Fe(III) with chromagenic mixed reagents by principal-component regression. Microchem J 63: 211–217.

Saier Jr., M. H. 1994. Computer-aided analyses of transport protein sequences: gleaning evidence concerning function, structure, biogenesis, and evolution. Microbiol Rev 58(1): 71–93.

Salehi, P., Tajabadi, F.M., Younesi, H., Dasht, Y. 2013. Optimization of lead and nickel biosorption by *Cystoseira trinodis* (brown algae) using response surface methodology. Clean. DOI: 10.1002/clen.201100429.

Salehizadeh, H., Shojaosadati, S.A. 2003. Removal of metal ions from aqueous solution by polysaccharide produced from *Bacillus firmus.* Water Res. 37:4231–5.

Salt, D.E., Wagner, G.J. 1993. Cadmium transport across tonoplast of vesicles from oat roots. Evidence for a Cd^{2+}/H^{+} antiport activity. J Biolog Chem 268(17) 12297–12302.

Salto, T., Ohyama, Y., Ide, H., Ohta, S., Yamamoto, O. 1998. A carotenoid pigment of the radioresistant bacterium Deinococcus radiodurans. Microbios 95: 79-90.

Sambrook, J., Fritsch, E.F., Maniatis, T. 1989. Molecular cloning: a laboratory manual, edn. Cold Spring Harbor Laboratory, New York. 177.

Sanchez, D.J., Domingo, J.L., Llobet, J.M., Keen, C.L. 1993. Maternal and developmental toxicity of manganese in the mouse. Toxicol Lett 69(1): 45-52.

Sandy, M., Butler, A. 2009. Microbial Iron Acquisition: Marine and Terrestrial Siderophores. Chem Rev 109(10):4580-4595.

Santamaria, A.B. 2008. Manganese exposure, essentiality and toxicity. Indian Journal of Medical Research. 128(4):484–500.

Sara, M., Sleytr, U.B. 2000. S- layer Proteins. Journal of Bacteriology 182: 859-868.

Saric, M. 1996. Manganese. Handbook on the toxicology of metals, vol. II: Specific metals. New York: Elsevier Science Publishing Co: 354-86.

Sasaki, K., Matsuda, M., Hirajima, T., Takano, K.,Konno, H. 2006. Immobilisation of Mn(II) ions by Mn-oxidising fungus Paraconiothyrium sp. like strains at neutral pH. Mater Trans 47:2454-2461.

Say, R., Yilmaz, N., Denizli, A. 2003. Biosorption of cadmium, lead, mercury, and arsenic ions by the fungus *Penicillium purpurogenum*. Sep Sci Technol. 38:2039–53.

Sayyed, R.Z, Chincholkar, F.B. 2010. Growth and siderophores production in *Alcaligenes faecalis* is regulated by metal ions. Indian J Microbiol 50(2):179–182.

Scăeţeanu, G.V, Ilie, L., Calin, C. 2013. An overview on manganese in nature. American Chemical Science Journal 3(3): 247-263.

Schelert, J., Drozda, M., Dixit, V., Dillman, A., Blum, P. 2006. Regulation of mercury resistance in the crenarchaeote *Sulfolobus solfataricus*. J Bacteriol 188(20): 7141– 7150.

Schneider, S., Paoli, M. 2005. Crystallization and preliminary Xray diffraction analysis of the haem-binding proteinHemS from *Yersinia enterocolitica*. Acta Crystall 61(8): 802–805.

Schreiber, D.R., Millero, F.J., Gordon, A.S. 1990. Production of an extracellular copper-binding compound by the heterotrophic marine bacterium *Vibrio alginolyticus*. Mar Chem 28: 275-284.

Schroder, I., Johnson, E., Vries, de S. 2003. Microbial ferric iron reductases. FEMS Microbiology Reviews 27:427-447.

Schulte, E.E. 2004. Soil and applied iron. In: Understanding Plant nutrients. A3554.

Schultze-Lam, S., Thompson, J.B., Beverdige, T.J. 1993. Metal ion immobilization by bacterial surfaces in freshwater environments. Water Pollution Research Journal of Canada 28:51–81.

Schwyn, B., Neilands, J.B. 1987. Universal chemical assay for detection and determination of siderophore. Annal Biochem 160:47.

Sehgal, S.N., Gibbons, N.E .1960. Effect of some metal ions on the growth of Halobacterium cutirubrum. Can J Microbiol 6:165–169.

Selatnia, A., Boukazoula, A., Kechid, N., Bakhti, M.Z., Chergui, A., Kerchich, Y. 2004a. Biosorption of lead (II) from aqueous solution by a bacterial dead *Streptomyces rimosus* biomass. Biochem Eng J 19:127–35.

Selatnia, A., Boukazoula, A., Kechid, N., Bakhti, M.Z., Chergui, A. 2004b. Biosorption of Fe3+ from aqueous solution by a bacterial dead *Streptomyces rimosus* biomass. Process Biochem. 39:1643–51.

Selatnia, A., Madani, A., Bakhti, M.Z., Kertous, L., Mansouri,Y., Yous, R. Biosorption of Ni^{2+} from aqueous solution by a NaOH-treated bacterial dead Streptomyces rimosus biomass. Mine Eng 2004c.17:903–11.

Sequiera, F. 1992. Microbiological study of saltpans in Goa. [Master's Thesis]. Department of microbiology, Goa University, Goa, India.

Sevgi, D., Beyza, U., Belma, A., Zekiye, S., 2009. Toxicity and uptake of iron ions by *Synechocystis* sp. E35 isolated from Kucukcekmece Lagoon, Istanbul. Journal of Hazardous Materials.171, 710-716.

Sierra, P., Chakrabarti, S., Tounkara, R., Loranger, S., Kenned,Y.G., Zayed, J. 1998. Bioaccumulation of manganese and its toxicity in feral pigeons (Columba livia) exposed to manganese oxide dust (Mn_3O_4). Environ Res 79: 94-101.

Silva, M.F., Winkler, H.A.A., de Oliveira, D.M., Agüeros, M., Peñalva, R., Irache, J.M., Pineda, E.A. 2013. Optimization of maghemite-loaded PLGA nanospheres for biomedical applications. Eur J Pharm Sci 49:343-51.

Silva, P.R.M., Rodriguez, A.A., De Oca, J.M.G.M. Moreno, D.C. 2009. Biosorption of chromium, copper, manganese and zinc by *Pseudomonas aeruginosa* AT18 isolated from a site contaminated with petroleum. Bioresour technol 100:1533-1538.

Silveira, C.B., Cardoso, A.M., Coutinho, F.H., Lima, J.L., Pinto, L.H., *et al*. 2013. Tropical aquatic archaea show environment-specific community composition. PLoS ONE 8(9): e76321.

Silver, S., Phung, L. T. 2005. Genes and enzymes involved in bacterial oxidation and reduction of inorganic arsenic. Appl Environ Microbiol 71(2): 599-608.

Silver, S., Phung, L.T. 1996. Bacterial heavy metal resistance: new surprises. Annu Rev Microbiol 50: 753±789.

Singh, J., Carlisle, D. L., Pritchard, D. E., Patierno, S. R**.** 1998. Chromium-induced genotoxicity and apoptosis: relationship to chromium carcinogenesis. Oncol Rep 5**:**1307-1318.

Sintuprapa, W., Thiravetyan, P., Tanticharoen, M. 2000. A possible mechanism of Zn2+ uptake by living cells of Penicillium sp. Biotechnol Let. 22 (21): 1709-1712.

Slobodkin, A.I., Jeanthon, C., Haridon, S.L., Nazina, T., Miroschnichenko, M., Bonch-Osmolovskaya, E. 1999. Dissimilatory reduction of Fe^{3+} by thermophilic bacteria and archaea in deep subsurface petroleum reservoirs of western Siberia. Curr Microbiol 39: 99–102.

Smedt, G., Segaert, H.D., Wuytack, F. 2004. SPCA1 pumps and Hailey- Hailey disease. Biochemical and Biophysical Research Communications. 322 (4):1204–1213.

Snavely, M. D., Florer, J. B., Miller, C. G., Maguire, M. E. 1989. Magnesium transport in Salmonella typhimurium: $28Mg^{2+}$ transport by the CorA, MgtA, and MgtB systems. J Bacteriol 171(9):4761–4766.

Solioz, M., Stoyanov, J. V. 2003. Copper homeostasis in *Enterococcus hirae*. FEMS Microbiol Rev 27(2-3):183–195.

Solomon, E.I., Sundaram, U.M., Machonkin, T.E. 1996. Multicopper oxidases and oxygenases. Chem Rev 96:2563–2605.

Southam, G. 2000. Bacterial surface-mediated mineral formation. In: Environmental Microbe-Mineral Interactions. Lovley DR (ed) ASM Press, Washington, DC, p 257-276.

Spanelova, M., Machovic, V., Brezina, M. 2003. Characterization and sorption properties of *Aspergillus niger* waste biomass. Cent Eur J Chem. 1:192–200.

Spark, K. M., Wells, J. D., Johnson, B. B. 1997. The interaction of a humic acid with heavy metals. Aust J Soil Res 35:89-101.

Sparks, D. L. 2005. Toxic metals in the environment: the role of surfaces. *Elements* 1(4): 193-197.

Srinath, T., Verma, T., Ramteke, P.W., Garg, S.K. 2002. Chromium (VI) biosorption and bioaccumulation by chromate resistant bacteria. Chemosphere. 48:427–35.

Srivastava, P., Kowshik, M. 2013. Mechanisms of metal resistance and homeostasis in haloarchaea. Archaea. 13. http://dx.doi.org/10.1155/2013/732864.

Srivastava, S., Goyal, P. 2010. Decontamination of toxic metals from waste water. In: Allan, R., Forstner, U., Salomons, W., (SubEds.), Novel biomaterials, pp. 1-147. Environmental Science and Engineering.

Steele, R.A., Opella, S. J.1997. Structures of the Reduced and Mercury-Bound Forms of MerP, the Periplasmic Protein from the Bacterial Mercury Detoxification. Sys *Biochem* 36(23): 6885–6895.

Stumpe, S., Bakker, E.P. 1997. Requirement of a large K^+-uptake capacity and of extracytoplasmic protease activity for protamine resistance of *Escherichia coli*. Arch Microbiol 167(2-3): 126–136.

Sunda, W.G. 2012. Feedback Interactions between Trace Metal Nutrients and Phytoplankton in the Ocean. Front Microbiol. 3: 204.

Sunda, W.G., Huntsman, S.A. 1998. Processes regulating cellular metal accumulation and physiological effects: Phytoplankton as model systems. Sci Total Environ, 219(2-3): 165–181.

Suresh, S. 2005. Characteristic of soils prone to iron toxicity and management: A review. Agricultural Reviews 26, 50-58.

Suzuki, T., Miyata, N., Horitsu, H., Kawai, K., Takamizawa, K., Tai, Y., Okazaki, M. 1992. NAD(P)H-dependent chromium(VI) reductase of *Pseudomonas ambigua* G-1: a Cr(V) intermediate is formed during the reduction of Cr(VI) to Cr(III). J Bacteriol. 174**:**5340-5345.

Suzuki, Y., Matsushita, H. 1968.Interaction of metal ions and phospholipids monolayers as a biological membrane model. Industrial Health 6(3):128–133.

Sweet, C.W., Vermette, S.J., Lansberger, S. 1993. Sources of toxic trace elements in urban air in Illinois. Environ Sci Technol 27: 2502-2510.

Tabak, H. H., Lens, P., Hullebusch V.E.D., Dejonghe W. 2005. Developments in bioremediation of soils and sediments polluted with metals and radionuclides-1. Microbial processes and mechanisms affecting bioremediation of metal contamination and influencing metal toxicity and transport. Rev Environ Sci Biotechnol. 4(3): 115–156.

Takeno, N. 2005 Atlas of Eh-pH diagrams. Intercomparison of thermodynamic databases. National Institute of Advanced Industrial Science and Technology, Japan. 146.

Tame, J. R. H., Murshudov, G. N., Dodson, E. J. *et al.* 1994. The structural basis of sequence-independent peptide binding by OppA protein. Science 264: 1578–1581.

Tamura, K., Peterson, D., Peterson, N., Stecher, G., Nei, M., Kumar, S.2011: MEGA5: Molecular Evolutionary Genetics Analysis using maximum likelihood, evolutionary distance, and maximum parsimony methods. Mol Biol Evol 28:2731–2739.

Tan, T.W., Cheng, P. 2003. Biosorption of metal ions with *Penicillium chrysogenum*. Appl Biochem Biotechnol.104:119–28.

Taylor, S.R. 1964. Abundance of chemical elements in the continental crust: a new table. Geochimica et Cosmochimica Acta 28:1273-1285.

Tebo, B.M, Johnson, H.A., McCarthy, J.K., Templeton, A.S. 2005. Geomicrobiology of manganese (II) oxidation. Trend Microbiol 13:421-428.

Tebo, B.M., Bargar, J.R., Clement, B.G., Dick, G.J., Murray, K.J., Parker, D., Verity, R., Webb, S.M. 2004. Biogenic manganes oxides: properties and mechanisms of formation. Annual Review of Earth and Planetary Sciences, 32:287–328.

Tewari, N., Vasudevan, P., Guha, B.K. 2005. Study on biosorption of Cr (VI) by Mucor Hiemalis. Biochemical Engineering Journal 23:185–192.

Tindall, B.J. 1992. The Prokaryotes: A handbook of Bacteria. 2nd Edition, Volume 4. Springer

Ton, V., Mandal, D., Cordelia, V., Rao, R. 2002. Functional expression in yeast of the human secretory pathway Ca^{2+}, Mn^{2+}-ATPase defective in Hailey-Hailey disease. J Biol Chem 277:6422–6427.

Toner, B., Fakra, S., Villalobos, M., Warwick, T., Sposito, G. 2005. Spatially resolved characterization of biogenic manganese oxide production within a bacterial biofilm. Appl Environ Microbiol 71:1300–1310.

Tottey, S., Rich, P.R., Rondet, S.A.M., Robinson, N.J. 2001. Two menkes-type ATPases supply copper for photosynthesis in Synechocystis PCC6803. J Biolog Chem 276(23) 19999–20004.

Trenberth, K.E. 2011. Changes in precipitation with climate change. Clim Res. 47: 123–138.

Tsezos, M. 2007. Biological Removal of Ions: Principles and Applications. Adv Mat Res. 20-21: 589-596.

Tunali, S., Cabuk, A., Akar, T. 2006. Removal of lead and copper ions from aqueous solutions by bacterial strain isolated from soil. Chem Eng J, 115:203–11.

Turner, J.S., Glands, P.D., Samson, A.C.R., Robinson, N.J., 1996. Zn+2-sensing by the cyanobacterial metallothionein repressor SmtB: different motifs mediate metal-induced protein-DNA dissociation. Nucleic acids Res 24: 3714-3721.

U.S. Geological Survey. 2011. Mineral commodity summaries 2011: U.S. Geological Survey.198.

US EPA Wastewater Technology Fact Sheet 2000. Chemical Precipitation. US EPA Washington. DC: 832-F-00-018.

USEPA. 2008. Final 2008 Effluent Guidelines Program Plan [Online]. Available at http://www.epa.gov/guide/304m/2008.

Uslu, G., Tanyol, M. 2006. Equilibrium and thermodynamic parameters of single and binary mixture biosorption of lead(II) and copper(II) ions onto *Pseudomonas putida*: effect of temperature. J Hazard Mater. 135:87–93.

Uversky, V.N., Li, J., Fink, A.L. 2001. Metal-triggered structural transformations, aggregation, and fibrillation of human α-synuclein. A possible molecular link between Parkinson's disease and heavy metal exposure. J Biol Chem 276:44284-44296.

Uyar, G., Oren, M., Yildirim, Y., Oncel, S. 2008. Biomonitoring of metal deposition in the vicnity of Eregli steel plant in Turkey. Environmental Forensics 9:350–363.

Valko, M., Morris, H., Cronin, M.T. 2005. Metals, toxicity and oxidative stress. Curr Med Chem 12 (10): 1161–1208. doi:10.2174/0929867053764635.

Van Veen, H.W., Margolles, A., M¨uller, M., Higgins, C.F., Konings, W.N. 2000. The homodimeric ATP-binding cassette transporter LmrA mediates multidrug transport by an alternating two-site (two-cylinder engine) mechanism. EMBO J 19(11): 2503–2514.

Van Waasbergen, L.G., Hildebrand, M., Tebo, B.M. 1996. Identification and characterization of a gene cluster involved in manganese oxidation by spores of the marine *Bacillus* sp. strain SG-1. J. Bacteriol. 12:3517–3530.

Van, H.A., Ward, D.M, Kaplan, J. 2002. Transition metal transport in yeast. Annu Rev Microbiol 56:237–261.

Vandieken, V., Finke, N., Thamdrup, Bo. 2013. Hydrogen, acetate, and lactate as electron donors for microbial manganese reduction in manganese-rich coastal marine sediment. FEMS Microbiol Ecol :1-13.

Veglio, F., Beolchini, F. 1997. Removal of metals by biosorption: a review. Hydrometallurgy. 44:301–16.

Ventosa, A. 2004. Halophilic Microorganisms. Springer, Berlin Heidelberg, NewYork.

Ventosa, A., Nieto, J.J., Oren, A.1998. Biology of moderately halophilic aerobic bacteria Microbiol. Mol Biol Rev 62(2):504.

Villalobos, M., Toner, B., Bargar, J., Sposito, G. 2003. Characterization of manganese oxide prduced by Pseduomonas putida. Geochim Cosmochim Act 67(14): 2649–2662.

Vogel, A.L., Mendham, J. 2000. Vogel's textbook of quantitative chemical analysis. Mendham J (ed). Prentice Hall. 6th edition.

Volesky, B. 1994. Advances in biosorption of metals — selection of biomass types. FEMS Microbiol Rev.14:291–302.

Volesky, B. 2007. Biosorption and me. Water Res 41:4017–4029.

Vuori, K. M. 1995. Direct and indirect effects of iron on river ecosystems. Annal Zool Fennici 32: 317-329.

Waasbergen van, L.G., Hildebrand, M.,Tebo, B.M. 1996. Identification and characterization of a gene cluster involved in manganese oxidation by spores of the marine *Bacillus* sp. strain SG-1. J Bacteriol 178: 3517–3530.

Waldron, H.A.: Metals in the environment. Academic Press, London, 1980, 333 p.

Wang, G., Kennedy, S.P., Fasiludeen, Rensing, S.C., DasSarma, S. 2004. Arsenic resistance in *Halobacterium* sp. strain NRC-1 examined by using an improved gene knockout system. J Bacteriol 186(10): 3187–3194.

Wang, J.L., Chen, C. 2006. Biosorption of heavy metals by *Saccharomyces cerevisiae*: a review. Biotechnol. Adv. 24:427–51.

Wang, W., Shao, Z., Liu Y., Wang, G. 2009. Removal of multi-heavy metals using biogenic manganese oxides generated by a deep-sea sedimentary bacterium – *Brachybacterium* sp. strain Mn32. Microbiol 155: 1989–1996.

Wang, X., Gan, L., Wiens, M., Schloßmacher, U., Schröder, H.C., Müller, W.E. 2012. Distribution of microfossils within polymetallic nodules: biogenic clusters within manganese layers. Mar Biotechnol (NY) 14(1):96-105 ISSN 1436-2236.

Wedler, F. 1994. Biochemical and nutritional role of manganese: an overview. In: Manganese in health and disease, D. Klimis-Tavantzis (ed), CRC Press, 1–38, ISBN: 9780849378416, Boca Raton, Florida.

Wehrli, B., Friedl, G., Manceau, A. 1995. Reaction rates and products of manganese oxidation at the sediment-water interface, In: Aquatic Chemistry: principles and applications of interfacial and inter-species interactions in aquatic systems, C.P. Huang, C. O' Melia, J.J. Morgan (eds), Washington, 111-134.

Weiss, G. 2005. Modification of iron regulation by the inflammatory response. Best Pract Res Clin Haematol 18: 183-201.

Wells, M.L., Smith, G.J., Bruland, W.K. 2000 The distribution of colloidal and particulate bioactive metals in Narragansett Bay, RI. Mar Chem 71:143-163.

Whittaker, J.W. 2000. Manganese superoxide dismutase. Met Ions Biol Syst 37: 587-611.

WHO. 2004. Manganese and its compounds: environmental aspects. Geneva: World Health Organization.

Williams, M., Todd, G.D., Roney, N. 2012. Toxicological profile for manganese. ATSDR (Agency for Toxic Substances and Disease Registry) Atlanta, GA: US Department of Health and Human Services, Public Health Service. 539-550.

Winkelmann, G. 2001. Microbial transport systems. Wiley-VCH, Weinheim.

Wu, J., Boyle, E.A., Sunda, W., Wen, L., 2001. Soluble and colloidal iron in the oligotrophic North Atlantic and North Pacific. Science 293:847-849.

Wu, J., Luther, G. W. 1995. Complexation of iron(III) by natural organic ligands in the Northwest Atlantic Ocean by a competitive ligand equilibration method and a kinetic approach. Mar. Chem. 50: 159–177.

Xiang, M., Mohamalawari, D., Rao R. 2005. A novel isoform of the secretory pathway Ca^{2+}, Mn^{2+}-ATPase, hSPCA2, has unusual properties and is expressed in the brain. J Biol Chem 280:11608–11614.

Yaman, M. 2012. Comprehensive comparison of trace metal concentrations in inhaled air samples, air pollution - monitoring, modelling, health and control, Dr. Mukesh Khare (Ed.). Science Communication Unit, University of the West of England, Bristol. 2013. Science for Environment Policy In-depth Report: Soil Contamination: Impacts on Human Health. Report produced for the European Commission DG Environment.

Yang, W., Zhang, Z., Zhang, Z., *et al*. 2013. Population structure of manganese-oxidizing bacteria in stratified soils and properties of manganese oxide aggregates under manganese–complex medium enrichment. PLoS ONE 8(9): e73778.

Ybarra, G.R., Webb, R.1999 Effects of divalent metal cations and resistance mechanisms of the cyanobacterium *Synechococcus* sp. strain PCC7942. J Hazard Sub Res 2:1-5.

Yildirim, K., Karatay, S., Melikoglu, M.A., Gureser, G., Ugur, M., Senel, K. 2004. Associations between acute phase reactant levels and disease activity score (DAS28) in patients with rheumatoid arthritis. Ann Clin Lab Sci 34:423-426.

Yilmaz, E. I., Ensari, N. Y. 2005. Cadmium biosorption by *Bacillus circulans* strain EB1, World J Microbiol Biotechnol 21: 777–779.

Yoshida, H., Yamamoto, K., Murakami, Y., Katsuta, N., Hayashi, T., Naganuma, T. 2008. The development of Fe-nodules surrounding biological material mediated by microorganisms. Environmental Geology 55:1363–1374.

Yuan, C., Lu, X., Jie, Q., Rosen, B. P., Le, X.C. 2008.Volatile arsenic species released from Escherichia coli expressing the aslll S-adenosylmethionine methyltransferase gene. Environ Sci Technol 42 (9): 3201–3206.

Yuan, J., Zhu, J., Bi, H., Zhang, Z., Chen, S., Liang, S., Wang, X. 2013. Self assembled hydrothermal synthesis for producing a MnCO3/ graphene hydrogel composite and its electrochemical properties. RSC Adv 3:4400-4407.

Zafrilla, B., Mart´ınez-Espinosa, R.M., Alonso, M.A, Bonete., M.J. 2010. Biodiversity of Archaea and floral of two inland saltern ecosystems in the Alto Vinalop´o Valley, Spain. Sal Sys 6(1) 10.

Zegeye, A., Huhuet, L., Abdelmoula, M., Carteret, C., Mullet, M., Jorand, F. 2007. Biogenic hydroxysulfate green rust, a potential electron acceptor of SRB activity. Geochimica et Cosmochimica Acta 71: 5450–5462.

Zhang, C., Liu, S., Phelps, T. J., Cole, D.R., Horita, J., Fortier, S.M., Elless, M., Valley, J. 1997. Physiochemical, mineralogical, and isotopic characterization of magnetite-rich iron oxides formed by thermophilic iron-reducing bacteria. Geochim Cosmochim Acta 61(21): 4621–4632.

Zhang, G., Jiang, H., Kukkadapu, R.K., Kim, J., Dennis, E., Zhiqin, X. 2009. Biomineralization associated with microbial reduction of Fe3+ and oxidation of Fe^{2+} in solid minerals. American Mineralogist 94: 1049–1058.

Zhang, J., Lion, L.W., Nelson, Y.M., Shuler, M.L., Ghiorse, W.C. 2002. Kinetics of Mn (II) oxidation by *Leptothrix discophora* SS1. Geochimic Cosmochim Act, 65(5):773–781.

Zhou, M., Liu, Y.G., Zeng, G.M., Li, X., Xu, W.H., Fan. T. 2007. Kinetic and equilibrium studies of Cr (VI) biosorption by dead *Bacillus licheniformis* biomass. World J Microbiol Biotechnol. 23:43–8.

Zhu, H., Stein, W.E., Lu, Z., Lvov, Y.M., McShane, M.J. 2005. Synthesis of size-controlled monodisperse manganese carbonate microparticles as templates for uniform polyelectrolyte microcapsule formation. Chem Mater 17:2323-2328.

Ziagova, M., Dimitriadis, G., Aslanidou, D., Papaioannou, X., Tzannetaki, E.L., Liakopoulou-Kyriakides, M. 2007. Comparative study of Cd(II) and Cr(VI) biosorption on *Staphylococcus xylosus* and *Pseudomonas* sp. in single and binary mixtures. Bioresour Technol. 98:2859–65.

Zouboulis, A.I., Loukidou, M.X., Matis, K.A. 2004. Biosorption of toxic metals from aqueous solutions by bacteria strains isolated from metal-polluted soils. Process Biochem. 39:909-916.

Zumft, W. G., Viebrock-Sambale, A., Braun, C. 1990. Nitrous oxide reductase from denitrifying *Pseudomonas stutzeri*. Genes for copper-processing and properties of the deduced products, including a new member of the family of ATP/GTP-binding proteins. Eur J Biochem 192(3): 591–599.

Appendix

a) NTYE (Tryptone Yeast Extract medium containing 25 % Solar salt)

$MgSO_4.7H_20$ 20.0 g

KCI 5.0 g

$CaCl_2.2H_20$ 0.2 g

Yeast Extract 3.0 g

Tryptone 5.0 g

Crude salt 250.0 g

Distilled water 1000.0 ml

Adjust pH to 6.5-7 with 1 M NaOH

For solid media: (Agar) 20.0 g

Digest for 30 minutes, sterilise at 121 °C and 15 lbs pressure for 20 min.

b) NGSM (Mineral salt medium containing 20 % NaCI and 0.2 % Glucose)

NaCI 200.0 g

$MgC1_2.6H_20$ 13.0 g

$CaCl_2.6H_20$ 1.0 g

KCI 4.0 g

$NaHCO_3$ 0.2 g

NH_4CI 2.0 g

$FeC1_3.6H_20$ 0.005 g

KH_2PO_4 0.5 g

Distilled water 1000.0 ml

*Glucose solution 100.0 ml

Adjust pH with 1 M KOH

For solid media: (Agar) 20.0 g

Digest for 30 minutes, sterilise at 121 °C and 15 lbs pressure for 20 min.

0.2 % Glucose solution:

Glucose solution is separately sterilised at 121 °C and 15 lbs pressure for 10 min. This is then added to sterilised liquid medium or solid medium. In NASM, sodium acetate was used instead of glucose.

Protein estimation

Reagent A

2 % (w/v) Sodium carbonate in 0.1 N Sodium hydroxide

Reagent B

0.5 % (w/v) Copper sulphate in1 % (w/v) Sodium potassium tartarate

Reagent C

Reagent A 50 m1 + Reagent B 1 ml

Reagent D

Folin- Ciocalteaux solution: Distilled water (1:3)

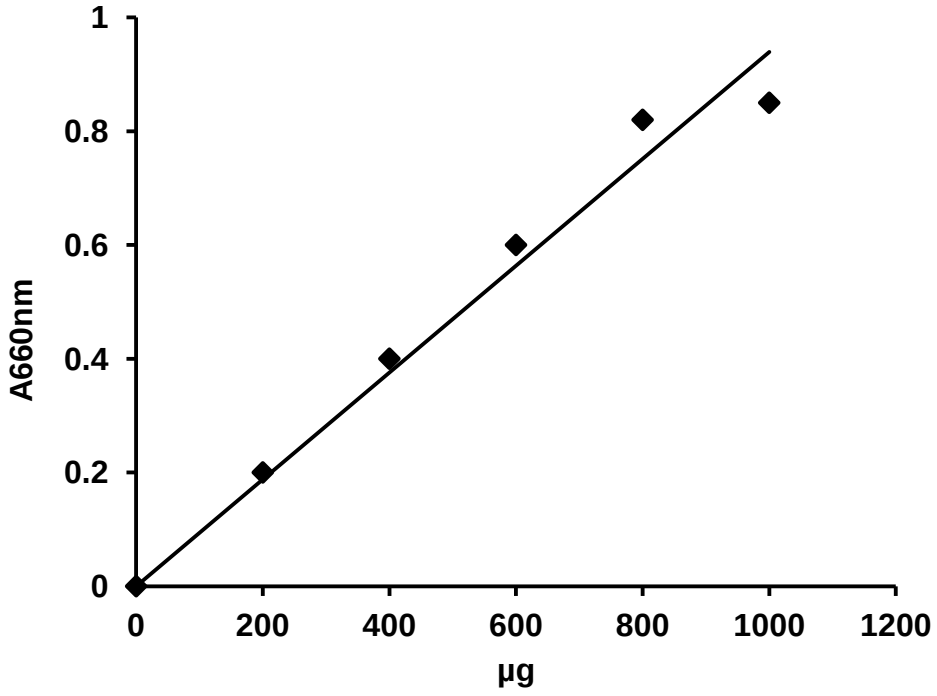

Standard graph for protein estimation

Grams stains

i) Crystal violet

Dissolve 20 g of crystal violet in 200 ml of methylated (rectified) spirit. Dissolve 8 g of ammonium oxalate in 800 ml of D/W mix both together to make 100ml

ii) Gram's iodine

Iodine	10 g

K1 20 g

Mix well and dissolve in 100 ml D/W

iii) 70% alcohol

Absolute alcohol 700 ml

D/W 300 ml

iv) Saffranine (0.5%)

saffranine 500 mg

D/W 100 ml

Grind the stain with pestle and motor with 10ml and make to 100ml

1 Molar stock solution of Metal salts

a) $FeSO_4.7H_20$ 278.01 g

D/W 1000 ml

b) $MnSO_4.7H_2O$ 277.10 g

D/W 1000 ml

c) $MnCl_2.6H_20$ 233.93 g

D/W 1000 ml

d) $FeCl_3.6H_2O$ 270.29 g

D/W 1000 ml

Reagents

1,10- phenanthroline for estimation of iron

Heat the D/W to 70 ^{o}C. Dissolve 0.5 g of phenanthroline in 100 ml D/W. Stir till compound totally dissolves with clean glass rod.

Standard curve graph for estimation of iron using 1, 10 –phenanthroline method.

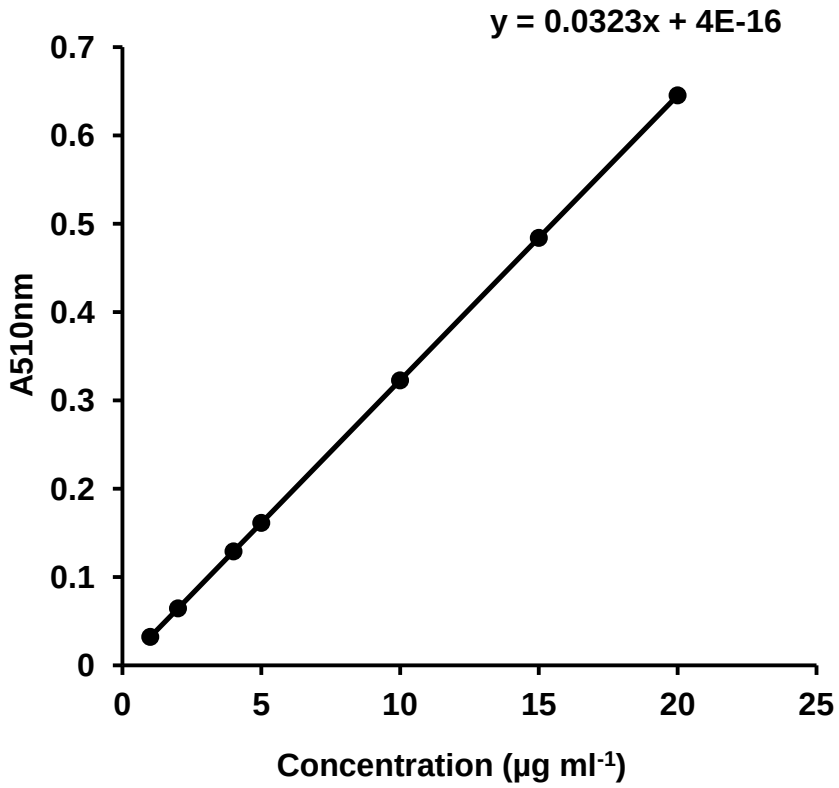

Reagents for Polyacrylamide Gel electrophoresis (SDS — PAGE)

a) Upper Tris (0.1N)

Tris base 3.03 g

SDS 0.2 g

D/W 40 ml

pH adjusted to 6.8 with conc. HCI. Final volume to 50 ml. Keep at 0-4°C

b) Lower Tris (1. 5M)

Tris base 18.15 g

SDS 0.4 g

D/W 90 ml

pH adjusted to 8.8 (conc. HCl). Final volume to 100 ml.

c) Acrylamide

Acrylamide 29.2 g

Bisacrylamide 0.8 g

D/W 100 ml

Filter through whatman filter paper

d) Sample buffer (Laemmli, 1970)

Upper tris (pH 6.8) 1.25 ml

10% SDS 3.0 ml

glycerol 1.0 ml

mercaptoethanol 0.50 ml

D/W 4.75 ml. Freeze.

e) Running buffer

Tris base	3.03 g
SDS	1.0 g
Glycine	14.4 g
pH to 8.3	
Final volume 1L.	

f) Staining solution

Coomasie brilliant blue	1.0 g
Methanol	500 ml
Acetic acid	100 ml
D/W	40 ml
Filter	

g) Destaining soin I / II

Methanol	500 ml / 70 ml
Acetic acid	100 ml/ 50 ml
D/W	1 L/1 L

h) Tracking dye

Bromophenol blue	0.1 g
50 % sucrose	100 ml

i) Fixative for coomassie

Methanol	50 ml
Glacial acetic acid	5 ml
Distilled water	45 ml

Composition for preparation of gel

	Separating gel (10 %) ml	**Stacking gel (5 %) ml**
Monomer solution	2.5	0.33
Separating gel buffer (pH8.8)	1.875	-
Stacking gel buffer (pH 6.8)	-	0.625
10% SDS	0.075	0.025
Water	3	1.525
APS	0.0375	0.025
TEMED	0.005	0.005

APS - Ammonium per sulfate

TEMED - Tetra ethylene methyl ethylene diamine

Reagents for plasmid DNA isolation by alkaline lysis method

i) Solution I (pH 8.0)

Glucose	0.9 g
Tris-HC1	0.394 g
EDTA	0.292 g
D/W	100 ml

ii) Solution II

SDS	1.0 gm
0.2 N NaOH	100 ml

iii) Solution III (pH 5.2)

5 M Potassium acetate	60 ml
Glacial acetic acid	11.5 ml
D/W	28.5 ml

Resulting solution is 3 M w.r.t pottasium acetate and 5 M acetic acid

d) DNA loading dye

Glycerol	2.7 ml
(5X) TAE	0.3 ml
SDS (1%)	1.0 ml
EDTA	0.5 M
Bromothymol Blue :	0.25%

e) TE Buffer

10mM Tris chloride (pH 8)

1mM EDTA (pH 8)

f) 40X TAE buffer

Tris base (1.6 M)	193.6 g
Na acetate .3H0_2 (0.8 M)	108.9 g
EDTA-Na2. 2$H_2$0 (40 mM)	15.2 g

pH to 7.2 with CH_3COOH

water to make to I L

g) Agarose gel

Agarose	0.8 g
TAE (IX)	100 ml
Ethidium Bromide :	2-3 µl
(10mg / ml stock)	

h) Lysing solution

SDS	3%

50 mM Tris pH 12.6

adjust volume to 100 ml with D/W.

Inhibitors

a) DCCD (1 M stock)

DCCD	1.031 g
methanol	5 ml

30 µI of stock added to 30 ml cell suspension to obtain a concentration of 1 mM

b) Sodium azide (1M stock)

Sodium azide	0.13 g
Distilled water	2 ml

c) 2, 4 – dinitrophenol (1M stock)

2,4 – dinitrophenol	0.184 g
Distilled water	10 ml

Preparation of Thin layer chromatography plates

Thin layer silica gel plates were prepared by dissolving silica gel G / H / 60F250, (Acme / Qualigens / Merck, India) in distilled water to obtain slurry of desired thickness. The slurry was spread evenly using a clean glass rod on to grease free glass plates placed side by side and fixed using leucoplast. The air dried plates were then activated in the oven at 110°C for 30 to 40 min and used as and when needed.

PUBLICATIONS

1. Naik S. & Furtado I. (2014) Equilibrium and kinetics of adsorption of Mn^{2+} by Haloarchaeon GUSF (MTCC3265). Geomicrobiology Journal. DOI:10.1080/01490451.2013.859769.
2. Naik S. & Furtado I. (2014) Formation of rhodochrosite by the haloarchaeon *Haloferax* sp. GUSF-1. FEMS Letters in Microbiology (Under review).
3. Naik S. & Furtado I. (2014) Biomineralisation of iron (III) to nanosized γFe_2O_3 by *Haloferax* sp. GUSF-1. (Communicated).
4. Naik S. & Furtado I. (2014) Adsorption of Fe (II) from saline systems by dry cells of *Haloferax* sp. GUSF-1 involving S-layers. (Communicated).

Manuscripts under preparation

1. Naik S. & Furtado I. (2014) Interaction of Haloarchaeon *Haloferax* sp. GUSF-1with Fe and Mn (Under Preparation).
2. Naik S. & Furtado I. (2014) Fe^{2+} uptake by Haloarchaeon *Haloferax* sp. GUSF-1from saline system (Under Preparation).
3. Naik S. & Furtado I. (2014) Uptake kinetics of Mn^{2+} ions by Haloarchaeon *Haloferax* sp. GUSF-1 (Under Preparation).

Papers presented in conferences

1. I.Furtado[1] & S. Naik (2009) Tolerance and Sorption of Metal-ions by Haloarchaea International Symposium on Advanced Inorganic Biological Chemistry (SABIC 2009) Tata Institute of Fundamental Research Centre. Mumbai held from 4th Nov – 7th Nov 2009.
2. S. Naik[1], R. B. Tangsali[2] & I. Furtado[1] (2011) Interaction of Haloarchaea GUSF/MTCC3265 with Fe^{+2}/Fe^{+3} ions. Association of Microbiologists of India International conference organized by Punjab University Chandigarh held from Nov 3rd- Nov 6th 2011.